



The  
University  
Of  
Sheffield.

**Modelling and Control of Lower Limb  
Exoskeletons and Walking Aid for  
Fundamental Mobility Tasks**

by

**Daniela Miranda Linares**

A thesis submitted to the University of Sheffield  
for the degree of Doctor of Philosophy

Department of Automatic Control and Systems Engineering

**November 2016**



# Abstract

In the last five decades, exoskeletons have emerged as a solution to assist paraplegic and elderly patients perform fundamental mobility tasks. The main challenge nowadays, is to develop a device that is safe, power sufficient, seamlessly integrates with the user, while being affordable. Several solutions have been proposed, and controllers have been identified as the only component which can enhance integration with the user without adding weight to the system, or increasing energy consumption. Moreover, a software platform where the mechanical design and control techniques can be assessed, prior to experimental trials, could save resources and decrease costs.

In this thesis, the development of humanoid and exoskeleton models, within the SimWise virtual environment, to perform an initial validation of controllers proposed without the need of a physical prototype, is performed. Furthermore, the selected platform is evaluated regarding its fitness for this application.

The methodology used to generate CAD models of a humanoid, exoskeletons and a wheel walker within the SimWise virtual environment is described, along with its integration with MATLAB Simulink. Two exoskeleton models with their corresponding controllers were developed, firstly, a hybrid exoskeleton with a wheel walker for restoration of walking in paraplegic patients. And secondly, an actuated exoskeleton for assistance in standing-up and sitting-down motions in both the elderly and paraplegic patients.

The hybrid exoskeleton uses functional electrical stimulation as actuation for knee joints and a frame with brakes mounted at hip, knee and ankle joints to generate the walking cycle. The wheel walker is used for support and equilibrium. A fuzzy controller for the low level and a finite state controller for the middle level is developed. Validation of the system over repeated walking cycles, including external disturbances, and simulation of use by humanoids of different dimensions, is performed within the virtual environment and results discussed.

PID low level control of hip and knee joints is used to analyse standing-up and sitting-down motions, and incorporated with an actuated exoskeleton for assisting elderly people on performing the aforementioned tasks. A finite state middle level control is developed to generate reference trajectories at variable velocities for the restoration of these motions for paraplegic patients. An optimisation algorithm is used to identify low level controller parameters for ankle joints. Finally, offline and online calculation and incorporation of zero moment point in the control loop is performed to assess equilibrium of the system.

# Acknowledgements

Firstly I thank God for allowing me to accomplish this goal, and giving me health and strength to do so. I am immensely grateful with Him for each, and every blessing I have received during the course of my life, and especially in the last 4 years.

I also wish to express my most sincere gratitude to my supervisor Dr. Osman Tokhi for his guidance, patience, and encouragement throughout this research. For his trust, kind commitment to his students, and for sharing his valuable experience and knowledge with all of us.

I am grateful as well to Professor Juan Coronado, Carlos Díaz and all the guys from the Polytechnic University of Cartagena for their collaboration, teachings and warm hospitality during my stay.

I gratefully acknowledge the National Council for Science and Technology and the Automatic Control and Systems Engineering Department for sponsoring my research studies. As well as the ACSE staff, whom I have had the opportunity to meet during these years, for their valuable advice and enthusiasm towards research.

I am indebted to all those who throughout my education life, have taught me important lessons: lecturers at ACSE, at the ITESM-CEM and CEMA, in México, particularly those who, beyond academic knowledge, have taught me valuable life lessons.

I am thankful to all the colleagues who have in one way or another helped ignite my scientific curiosity, given support, advice and researched and worked by my side, especially Normaniha, Siti Khadijah, Asnor, Ghasaq, Norafizah, Omar, Hyreil, Nafri, Abdullah, Ahmad and all the guys from 307.

On the personal side I would like to thank my parents Alberto and Emma, to whom I am indebted for their devotion to our family wellness and education. For teaching me so much, challenging me to dream big, and especially for their help and understanding during the pursue of this degree, and for being such working and loving parents and grandparents. I am grateful too to my sister Verónica and my brother Luis for so many childhood memories, for their love, support and inspiration.

I am also thankful to my Mexican, Brazilian, Malaysian, Nigerian, Chinese and English friends at Sheffield and at home, for sharing your knowledge, culture and special moments with me. Thanks especially to Nora and Janet, for their support and company during these years.

I want to express my outmost gratitude to my husband José de Jesús for being my colleague, my friend, and an amazing father. For providing prised advice and help in the writing of this thesis. For being always loving and supportive, particularly during the research journey we have gone through together, for being at my side in the past to face every challenge, and for the hope of adventures that we are yet to share.

Finally I am thankful to my little José Alberto, since even without knowing it, he has been my inspiration and has brighten my days with his sole existence and cute innocence. It has been a blessing being able to witness every minute of his life.

# Table of contents

<b>ABSTRACT</b> .....	<b>I</b>
<b>ACKNOWLEDGEMENTS</b> .....	<b>II</b>
<b>TABLE OF CONTENTS</b> .....	<b>III</b>
<b>LIST OF FIGURES</b> .....	<b>VI</b>
<b>LIST OF TABLES</b> .....	<b>X</b>
<b>LIST OF ACRONYMS</b> .....	<b>XI</b>
<b>CHAPTER 1 MOBILITY IMPAIRMENTS AND EXOSKELETONS: PARAPLEGIC AND ELDERLY PEOPLE</b> .....	<b>1</b>
1.1 BACKGROUND AND MOTIVATION .....	1
1.2 THE SOLUTION TO IMMOBILITY: EXOSKELETONS .....	3
1.3 MAIN CHALLENGES .....	9
1.4 AIM AND OBJECTIVES .....	12
1.5 MAIN CONTRIBUTIONS .....	13
1.6 THESIS OUTLINE .....	14
1.7 PUBLICATIONS .....	16
<b>CHAPTER 2 MODELLING OF HUMANOID, EXOSKELETON AND WHEEL WALKER</b> .....	<b>17</b>
2.1 INTRODUCTION .....	17
2.2 MOBILITY ISSUES .....	18
2.2.1 Spinal cord injury and paraplegia .....	18
2.2.2 Elderly muscle weakening .....	19
2.3 EXOSKELETONS REVIEW .....	20
2.3.1 Sensors .....	24
2.3.2 Actuators .....	25
2.3.3 Power supplies .....	27
2.3.4 Control techniques .....	27
2.4 MODELLING OF HUMANOID, EXOSKELETON AND WALKING AID .....	33
2.4.1 Software .....	33

2.4.2	Humanoid modelling.....	36
2.4.3	Exoskeleton for paraplegic patients.....	38
2.4.4	Exoskeleton for elderly and paraplegic patients assistance.....	42
2.4.5	Integration of models in SimWise 4D and MATLAB Simulink.....	45
2.5	SUMMARY.....	47

**CHAPTER 3 LOW AND MIDDLE LEVEL CONTROL OF HYBRID EXOSKELETON AND WHEEL WALKER FOR PARAPLEGIC GAIT IN STRAIGHT LINE .....49**

3.1	INTRODUCTION.....	49
3.2	WALKING CYCLE.....	50
3.3	MUSCLES OPERATION.....	52
3.4	FUNCTIONAL ELECTRICAL STIMULATION OF PARAPLEGIC MUSCLES.....	53
3.5	CONTROL OF PARAPLEGIC WALKING WITH HYBRID ORTHOSIS.....	58
3.5.1	Fuzzy control of knee joints torque.....	59
3.5.2	Finite State Control.....	64
3.6	VALIDATION TESTS.....	73
3.6.1	Repeatability tests.....	76
3.6.2	Stability.....	78
3.6.3	Range.....	81
3.6.4	Torque and energy consumption.....	82
3.7	SUMMARY.....	85

**CHAPTER 4 PID CONTROL OF HUMANOID AND EXOSKELETON FOR ELDERLY ASSISTANCE ON STANDING-UP AND SITTING-DOWN TASKS.....87**

4.1	INTRODUCTION.....	87
4.2	ASSISTIVE DEVICES FOR ELDERLY MOBILITY.....	88
4.3	ELDERLY STANDING-UP AND SITTING-DOWN.....	90
4.4	OPEN-LOOP SIMULATIONS OF STANDING-UP AND SITTING-DOWN MOTIONS.....	94
4.5	PID CONTROL OF HUMANOID FOR TORQUE PROFILES ASSESSMENT.....	95
4.5.1	PID Control.....	95
4.5.2	Closed-loop PID control scheme.....	97
4.5.3	Tests with different gains.....	98
4.5.4	Tests with different saturation levels.....	102
4.5.5	Tests with different velocities.....	105
4.6	PID CONTROL OF EXOSKELETON FOR STANDING-UP ASSISTANCE.....	107
4.6.1	Standing-up with unactuated exoskeleton.....	107
4.6.2	Exoskeleton assistance.....	110
4.6.3	Reaction force with seat and ground.....	115
4.7	SUMMARY.....	116

<b>CHAPTER 5 ONLINE TRAJECTORY TRACKING CONTROL OF EXOSKELETON FOR PARAPLEGIC ASSISTANCE ON STANDING-UP AND SITTING-DOWN TASKS .....</b>	<b>117</b>
5.1 INTRODUCTION.....	117
5.2 EQUILIBRIUM OF MOBILE SYSTEMS.....	118
5.2.1 Static equilibrium and-centre of mass.....	118
5.2.2 Dynamic equilibrium and zero moment point .....	121
5.3 METHODOLOGY FOR ONLINE TRAJECTORY TRACKING CONTROL.....	126
5.3.1 Control scheme .....	126
5.3.2 Finite state controller for standing-up and sitting-down .....	127
5.4 OFFLINE VERIFICATION OF DYNAMIC STABILITY .....	137
5.5 IMPLEMENTATION OF ONLINE TRAJECTORY TRACKING CONTROL WITH FSC .....	140
5.6 SUMMARY .....	148
<b>CHAPTER 6 PARTICLE SWARM OPTIMISATION OF ANKLE JOINT CONTROL PARAMETERS FOR DYNAMIC EQUILIBRIUM DURING STANDING-UP AND SITTING-DOWN TASKS .....</b>	<b>149</b>
6.1 INTRODUCTION.....	149
6.2 PARTICLE SWARM OPTIMISATION ALGORITHM .....	150
6.3 PARTICLE SWARM OPTIMISATION OF ANKLE JOINT CONTROL PARAMETERS .....	155
6.3.1 Optimisation of ankle joint PID controller gains .....	155
6.3.2 Optimisation of feet orientation PID controller gains.....	158
6.3.3 Optimisation of feet orientation fuzzy control parameters .....	159
6.4 ONLINE TRACKING OF ZMP .....	160
6.5 IMPLEMENTATION OF ANKLE JOINT CONTROL .....	162
6.6 SUMMARY .....	167
<b>CHAPTER 7 CONCLUSIONS AND RECOMMENDATIONS FOR FUTURE WORK.....</b>	<b>169</b>
7.1. SUMMARY OF CONTRIBUTIONS .....	169
7.2. CONCLUSIONS .....	171
7.3. CHALLENGES.....	174
7.4. RECOMMENDATIONS FOR FUTURE WORK.....	176
<b>REFERENCES.....</b>	<b>179</b>
<b>APPENDICIES.....</b>	<b>191</b>
APPENDIX A .....	191
APPENDIX B .....	192
APPENDIX C .....	195
APPENDIX D .....	196
APPENDIX E.....	197

# List of figures

Figure 2.1 Cord Injury levels and effects, modified from (Harrison, 2006). .....	19
Figure 2.2 Lower limb orthosis (Hsu et al., 2008) .....	21
Figure 2.3 Exoskeletons control structure, modified from (Tucker et al., 2015) .....	29
Figure 2.4 Humanoid model: a) Isometric, b) frontal and c) lateral views .....	38
Figure 2.5 a) Initial (zero) position and ranges of motion for b) hip, c) knee and d) ankle. ..	38
Figure 2.6 Exoskeleton model: a) Isometric, b) frontal and c) lateral views.....	40
Figure 2.7 Wheel Walker: a) Isometric, b) frontal and c) lateral views .....	41
Figure 2.8 Humanoid wearing exoskeleton and wheel walker: a) Isometric, b) frontal and c) lateral views.....	42
Figure 2.9 EXO LEGS exoskeleton: a) Isometric, b) frontal and c) lateral views .....	43
Figure 2.10 Humanoid wearing exoskeleton: a) Isometric, b) frontal and c) lateral views..	44
Figure 2.11 SimWise Plant.....	46
Figure 2.12 Example of Simulink implementation of SW Plant.....	46
Figure 3.1 Phases of gait cycle, modified from (Hsu, et al., 2008) .....	50
Figure 3.2 Joint trajectories in normal adult walking modified from (Okamoto and Okamoto, 2007).....	51
Figure 3.3 a) Motor unit diagram b) Motor unit activation sequence, modified from (Dictionary, 2009) .....	52
Figure 3.4 FES parameters .....	54
Figure 3.5 Control scheme for simulation of paraplegic walking with FES and hybrid orthosis. ....	58
Figure 3.6 Control scheme of experimental validation of paraplegic walking with FES and hybrid orthosis.....	59
Figure 3.7 Fuzzy membership function.....	60
Figure 3.8 Simple fuzzy control system (Ross, 2010).....	61
Figure 3.9 Control loop of fuzzy controller for one leg from (Jailani, 2011) .....	63
Figure 3.10 Knee joint references considered in a) Jailani's work, b) Winter's work, c) reference proposed. ....	64
Figure 3.11 Simple finite state machine .....	65
Figure 3.12 Finite state controller of walking motion.....	68
Figure 3.13 Switching period of brakes and FES for both legs with knee orientation for reference. ....	72
Figure 3.14 a) Exoskeleton angles and distances to floor b) Exoskeleton link lengths.....	73
Figure 3.15 Knee joint actual orientation and reference during a complete walking cycle ...	74
Figure 3.16 Comparison of paraplegic walking with FES and hybrid orthosis vs normal walking joints trajectories .....	75

Figure 3.17 a) Repeatability test run with incomplete step b)Zoom in of incomplete step ...	77
Figure 3.18 Repeatability test run starting step with left leg a) Complete simulation run b) Zoom in initial steps.....	78
Figure 3.19 a) Representation of disturbances applied .....	79
Figure 3. 20 System reaction to external disturbances a) Complete simulation b) Zoom in affected time slot.....	79
Figure 3.21 Travelled distance with disturbances.....	80
Figure 3.22 Test 2: System reaction to external disturbances a) Complete simulation b) Zoom in affected time slot .....	81
Figure 3.23 Test 2: Travelled distance with disturbances.....	81
Figure 3.24 Knee joint torques a) 10 seconds segment b) Zoom in initial step .....	83
Figure 3.25 Torque-Time integral of knee joints a) Complete simulation b) Zoom in initial step .....	84
Figure 4.1 Standing-up motion phases (Kralj and Bajd, 1989).....	91
Figure 4.2 Sitting-down motion phases (Kralj and Bajd, 1989) .....	92
Figure 4.3 Standing-up and sitting-down lower limbs joints orientations .....	92
Figure 4.4 Simulation of standing-up and sitting-down motions.....	94
Figure 4.5 Simulink control diagram of humanoid hip joints .....	97
Figure 4.6 Simulink control diagram of humanoid hip and knee joints.....	99
Figure 4.7 Orientation, torque and TTI of a) hip and b) knee joints with gain combination for minimum RMSE .....	99
Figure 4.8 Orientation, torque and TTI of a) hip and b) knee joints with gain combinations for minimum TTI .....	100
Figure 4.9 Relation between TTI and $Kd$ gain for a) hip joints and b) knee joints .....	101
Figure 4.10 Relation between RMSE and a) $Ki$ gain and b) $Kp$ gain for knee joints.....	101
Figure 4.11 Orientation, torque and TTI of a) hip and b) knee joints with lowest torque saturation values.....	102
Figure 4.12 Relation between RMSE and saturation torque for a) hip and b) knee joints...	103
Figure 4.13 Relation between TTI and saturation torque for a) hip and b) knee joints .....	104
Figure 4.14 Relation between TTI and RMSE for a) hip and b) knee joints .....	104
Figure 4.15 a)Orientation, b)torque and c)TTI of hip joints for three different velocities ..	106
Figure 4.16 a)Orientation, b)torque and c)TTI of knee joints for three different velocities	107
Figure 4.17 Exoskeleton joints.....	108
Figure 4.18 a)Orientation, b)torque and c)TTI of hip joints with unactuated exoskeleton for different velocities .....	109
Figure 4.19 a)Orientation, b)torque and c)TTI of knee joints with unactuated exoskeleton for different velocities .....	110
Figure 4.20 Simulink control diagram of hip and knee joints of humanoid and exoskeleton .....	111
Figure 4.21a)Orientation, b)torque and c)TTI of hip joints with actuated exoskeleton for different velocities .....	112

Figure 4.22 a)Orientation, b)torque and c)TTI of knee joints with actuated exoskeleton for different velocities.....	113
Figure 4.23 Standing-up and sitting-down motion with exoskeleton assistance.....	113
Figure 4.24 a) RMSE and b) TTI of with actuated exoskeleton, unactuated exoskeleton and humanoid alone .....	114
Figure 4.25 Reaction force with a) ground and b) seat with knee orientation as reference .	115
Figure 5.1 a) Humanoid and wheel walker CoM b) CoM and centroids diagram c) CoM during standing-up motion .....	120
Figure 5.2 Middle and low level control scheme .....	127
Figure 5.3 Finite state controller of standing-up and sitting-down motions .....	129
Figure 5.4 Feet and joints angles and distances between joints .....	134
Figure 5.5 Finite State Machine of fundamental mobility tasks .....	136
Figure 5.6 Robotic arm representing lower limbs .....	138
Figure 5.7 Orientation, angular velocity and angular acceleration during standing-up motion .....	139
Figure 5.8 Orientation, angular velocity and angular acceleration during sitting-down motion .....	139
Figure 5.9 Standing-up and sitting-down joints trajectories divided by state .....	141
Figure 5.10 Normalised orientation of a) hip joint and b) knee joint at different velocities	141
Figure 5.11 Hip joint orientation, torque and torque time integral at different velocities....	142
Figure 5.12 Knee joint orientation, torque and torque time integral at different velocities .	143
Figure 5.13 Hip joint orientation and torque after error.....	144
Figure 5.14 Knee joint orientation and torque after error.....	144
Figure 5.15 Stick diagram of standing-up motion.....	145
Figure 5.16 ZMP and CoM during standing-up motion at average velocity compared to the support area .....	146
Figure 5.17 Zoom in view of ZMP and CoM during standing-up motion at average velocity .....	147
Figure 5.18 ZMP and CoM during sitting-down motion at average velocity a) compared to the support area b) zoom in view .....	147
Figure 6.1 Particle swarm optimisation algorithm .....	152
Figure 6.2 PID low level control scheme for ankle joint.....	156
Figure 6.3 Control scheme with feet orientation PID controller .....	158
Figure 6.4 Control scheme with feet orientation fuzzy controller.....	160
Figure 6.5 Middle and low level control scheme with ZMP calculation and PSO optimisation .....	161
Figure 6.6 Hip, knee and ankle joints orientation, torque and TTI, with feet fixed to ground .....	162
Figure 6.7 Hip, knee and ankle joints orientation, torque and TTI, of control scheme with feet orientation PID and feet unfixed from ground, .....	164
Figure 6.8 Hip, knee and ankle joints orientation, torque and TTI, of control scheme with feet orientation FLC and feet unfixed from ground, .....	165

Figure 6.9 Hip, knee and ankle joints orientation, torque and TTI, of control scheme with ZMP fuzzy controller.....	166
Figure A.1 Winter's human proportions.....	191
Figure B.1 Same orientations, starting with left step.....	192
Figure B.2 Same orientations, starting with right step.....	192
Figure B.3 Different Orientation, starting with left step .....	193
Figure B.4 Different Orientation, starting with right step .....	193
Figure B.5 Tall humanoid.....	194
Figure B.6 Short humanoid.....	194
Figure C.1 Kinematic diagram for Denavit Hartenberg parameters.....	195
Figure D.1 Humanoid and exoskeleton during standing-up and sitting-down motions.....	196
Figure E.1 Robotic arm during standing-up and sitting-down motions.....	197

# List of tables

Table 1.1 Comparison of commercial exoskeletons for paraplegics .....	6
Table 1.2 Comparison of exoskeletons for elderly people .....	8
Table 2.1. Human body lower limbs kinematic specifications (Low, 2011) .....	23
Table 2.2 Winter's humansegment's mass percentage (Winter, 2009).....	37
Table 2.3 Humanoid model dimensions (Winter, 2009) .....	37
Table 2.4 Humanoid model joints .....	37
Table 2.5 Exoskeleton joints .....	40
Table 3.1 Fuzzy rules for knee joint flexion and extension.....	62
Table 3.2 Walking cycle of paraplegic walking with FES and hydrid orthosis: Right swing	67
Table 3.3 Maximum and average gait speeds. ....	76
Table 5.1 Standing-up motion biomechanics including phases and characteristic actions/postures .....	128
Table 5.2 Denavit Hartenberg parameters.....	138
Table 6.1 Fuzzy rules for knee joint flexion and extension.....	160

# List of acronyms

CoM	Centre of Mass
SCI	Spinal Cord Injury
ZMP	Zero Moment Point
EMG	Electromyography
EEG	Electroencephalography
FES	Functional Electrical Stimulation
FSC	Finite State Controller
PSO	Particle Swarm Optimisation
FLC	Fuzzy Logic Controller
TTI	Torque Time Integral
RMSE	Root Mean Squared Error
DoF	Degree of Freedom
CAD	Computer Aided Design
RoM	Range of Motion
CoP	Centre of Pressure
SBO	Spring Brake Orthosis

*Para mis padres, Emma y Alberto,*

*para mi esposo José de Jesús*

*y para mi hijo José Alberto*

# CHAPTER 1

## Mobility impairments and exoskeletons: Paraplegic and elderly people

### 1.1 Background and motivation

Human mobility is defined as the ability to change body position to manipulate objects or move about the environment, including home and regions beyond (Webber et al., 2010; WHO, 2015a). Mobility is one of the most important abilities that a human possesses, as simple as it appears, being able to move from place to place allows the preservation of independence, enables societal interaction, and enhances general health, among many other benefits (Webber et al., 2010).

Although mobility is no longer an ability on which survival is dependent on, as it was in the past (Tan, 2004), it is an enormously determinant factor on patients' physical and mental health. By being able to walk around, the musculoskeletal system is kept strong, and cardiovascular and digestive systems working appropriately. Furthermore, patients' psychological health is more stable while they are able to move around (Webber et al., 2010).

Mobility impairment is a category of disability which includes various types of physical disabilities that affect upper or lower limbs. It comprehends the loss of the limbs or their incapacity, as well as decreased or complete absence of manual dexterity and disability in coordination of different organs of the body. They can be categorised as congenital, acquired with age, or consequence of disease or injury (Disabled World, 2015).

This research is focused on those impairments that prevent people from performing basic mobility tasks such as walking, standing-up, sitting-down, and climbing and descending stairs. Although it is difficult to find an exact number of people with these limitations, it is known that in the UK, there are around 6.5 million people with mobility impairments, excluding dexterity issues (Office of disability issues, 2014; Department of Work and Pensions, 2015),

and around 1.2 million wheelchair users, approximately 2 per cent of the UK population (EFDS, 2016).

Limited mobility tends to affect older people in a higher proportion than younger people; in the UK, 72 per cent of wheelchair users, around 864,000 people, are 60 years old or over (Papworth Trust, 2016; Department of Work and Pensions, 2015). However, there are also other causes for mobility limitations from which the most sudden is Spinal Cord Injury (SCI). It is estimated that 50,000 people in the UK and Ireland, and 2.5 million people globally, are paralysed due to SCI (Spinal Research, 2011).

Considering that in the world there are around 630 million people aged 65 or older (International Data Base, 2016), and that it is estimated that mobility limitations affect between one third to half of adults above this age (Webber et al., 2010), it is possible to affirm that at least 211 million elderly people globally have some sort of mobility issues, this is 2.9 per cent of the total population. Moreover, extrapolating the fact that in the UK at least 1.4 per cent of the population are elderly wheelchair users (Papworth Trust, 2016; EFDS, 2016), it can be estimated that globally, at least 102 million people above 65 years old need a wheelchair, although not all of them have access to one, especially in underdeveloped countries. If we consider elderly people with mobility difficulties that need an assistive device as crutches, cane or walker to ambulate, the number of assistive technology users for mobility purposes could duplicate according to the United States Census Bureau, (2012). Adding to this amount those paralysed due to SCI, the number would equal over 206 million people in the world who could be benefited by this area of research.

For many years researchers were focused on restoring walking for people with paraplegia and similar diseases, especially in the last five decades (Hsu, Michael and Fisk, 2008). However, nowadays, a good proportion of the research in this area is focused on elderly assistance due to the increasing rate of older people in the world (WHO, 2015b). In addition, they are prone to enter into a vicious cycle in which they develop gait or balance disorders due to arthritis, orthostatic hypotension, obesity, diabetes mellitus, gout, osteoarthritis, osteoporosis, multiple sclerosis, Parkinson disease, stroke, visual impairments, among many others, and then, these disorders increase their risk of falls.

When falls do occur, the result is inevitably injury or disability. These could, in turn, expose the elderly to further falls or injuries, damaging their confidence, independence and at the end, limiting their life quality (Salzman, 2010).

Brown and Flood, (2013), concur that although the causes of mobility limitation are multifactorial, the most common risk factors are low physical activity, obesity, strength or balance impairments, and chronic diseases like diabetes and arthritis. Considering the fact that the group of people 65 or older is growing every year; devices that provide assistance to enable them to preserve their lifestyle and overall health, are an imperious need nowadays.

Unlike aging, a progressive process that, although hard to face, allows the body to adapt to weakened capacities, injury is usually a sudden loss of the ability to move due to communication breakage between the brain and muscles. SCI, happens when damage is done to the spinal cord, thus affecting its normal functions (Barr, 1979). Even when musculoskeletal system works properly by itself, it cannot be activated without an electrical signal from the brain. Such signal travels through the spinal cord to specific nerves that generate muscle contraction and thus, body motion. Unfortunately, when that channel is broken, it is impossible to restore it, even with the great leaps that medicine and technology have had in recent years.

Unlike sixty years ago, when 80 per cent of SCI patients died in the first two years after the injury, nowadays, the survival rate is above 93 per cent (Tan, 2004). However, people with SCI are still two to five times more likely to die prematurely than people without SCI since it is associated with a risk of developing secondary conditions which can be life-threatening (WHO, 2013).

After the injury, patients loose sensation and wilful movement in varying degrees that depend on the level of the injury (Harrison, 2006). When the injury affects lower limbs, as it is the case of paraplegia, the loss of mobility, independence and autonomy is inevitable, excluding the patient from full participation in society. Unfortunately, patients' general health is also threatened, sooner or later, by conditions such as deep vein thrombosis, urinary tract infections, muscle spasms, osteoporosis, pressure ulcers, chronic pain, and respiratory complications, as well as depression (WHO, 2013). For this reason, one of the main objectives of many researchers has become the restoration of human locomotion after SCI using any means available.

## **1.2 The solution to immobility: Exoskeletons**

When immobility is not attended, it can initiate a chain reaction that generates or greatly boosts other health risks. Assistive technology devices as crutches, orthoses, wheelchairs and scooters intend to maintain functional capabilities of people with mobility impairments (WHO, 2011).

However, restoration to their original condition had not been possible until the emergence of exoskeleton devices. Exoskeletons are thought as an assistive technology with the benefits of all the above: provide support while standing, enable displacement, usable in limited spaces and energy efficient. Overall, they aim to restore and, in some cases, increase lost mobility capabilities. Moreover, by increasing user's mobility, exoskeletons can decrease health issues such as cardiovascular diseases, providing enhanced general health, independence and self-sufficiency to users.

In the context of this research, an exoskeleton can be defined as a robotic orthosis. According to ISO 8549-1:1989 and 8551:2003, an orthosis is an externally applied mechanical device, encompassed to the body to aid or modify the structural and functional characteristics of the neuromuscular and skeletal system; a deeper description of orthoses is carried out in chapter 2 (Hsu et al.,2008).

Orthoses, combined with actuators, sensors and other electronic equipment are called active orthoses, robotic orthoses or exoskeletons. They prevent or increase range of motion of specific joints, thus, enabling a person to accomplish a mobility task (Pons, 2008)

Research on exoskeletons started in the 1960's almost in parallel at the United States and the former Yugoslavia; although the purpose of the U.S. researchers was to augment capabilities of soldiers, whereas Yugoslavian researchers aimed to restore walking in paraplegic and other disabled patients (Dollar and Herr, 2007).

Neil Mizen from Cornell Aeronautical Labs designed the Man-Amplifier in 1961-1962. It was planned to be a wearable suit attached closely to the body to follow its motion and adjustable for various wearer's dimensions; it included adjustable stops to limit the range of motion and was instrumented to record joints positions through time. It was designed to be actuated by hydraulic motors but only mock-up tests were performed (Mizen,1964).

One of the first actuated wearable robots was the Hardiman, created by General Electric in conjunction with the U.S. military between 1965 and 1971. It was a full body master-slave exoskeleton composed by 30 hydraulically powered, servo-controlled joints which used force-feedback control. It was designed to amplify human force in a 25:1 scale (Makinson and General Electric, 1971).

In 1971, Seireg and Grundmann from the University of Wisconsin-Madison created an exoskeleton to help disabled people rehabilitate and walk, it was powered by AC current and operated by a "puppet system". Cables extended from cams located in a backpack to transmit the motion to each joint in order to generate forward walking. It incorporated plastics and fiberglass materials to minimise weight as well as electronic servomechanisms (Seireg and Grundman, 1981).

Meanwhile, in 1969, Vukobratovic, along with the Mihailo Pupin Institute, in Yugoslavia, created an active exoskeleton, pneumatically powered and partly kinematically programmed for producing near-anthropomorphic gait for handicapped people. A more successful version of the exoskeleton for rehabilitation of paraplegics and similar disabled persons was a pneumatically powered and electronically programmed device, developed and tested at a Belgrade Orthopedic Clinic in 1972. In 1974, the first active exoskeleton with electromechanical drives and electronically programmed was built and tested (Vukobratovic, 2007).

Combination of functional electrical stimulation (FES) with orthoses to be used by disabled patients was also developed and tested in the 1980's in the University of Belgrade with Dejan Popovic as leader, these devices were called hybrid orthoses (Dollar and Herr, 2007).

Research on exoskeletons for mobility restoration and rehabilitation of disabled and elderly people, as well as strength and resilience augmentation for military, industrial and even nursing care applications continued through the following decades. These included full body devices, single joint orthoses for correcting gait abnormalities such as foot drop, and also modular exoskeletons, thought to include only the necessary and particular components that each patient need to restore his ambulation capabilities. Apart from accomplishing these purposes, exoskeletons must be designed to be portable, which means they should be lightweight and power independent, and to seamlessly integrate with the user, allowing them to move without restrictions.

This research is focused on orthotic lower limb exoskeletons to aid elderly and paraplegic people to perform fundamental mobility tasks. During recent years, various exoskeletons of this kind have been designed and even released for sale or rent to either rehabilitation clinics or private users. Some examples of commercial exoskeletons for paraplegic people are Rewalk by Argo Medical Technologies, Ekso by Ekso Bionics and HAL by Cyberdyne (Kazerooni, 2013; EksoBionics, 2013; Cyberdyne, 2015). These have proved to be effective in restoring walking motion and other mobility tasks with help of walking aids such as crutches; whereas REX, by Rex Bionics, carries the user around by itself (RexBionics, 2011; Schütz, 2012). These devices use novel techniques for sensing, actuation and control, Table 1.1 shows a comparison between these 4 commercial exoskeletons. It enlists their main capabilities, dimensions, configuration and requirements.

The interest on exoskeletons for the elderly is more recent. One of the first ones to embark on elderly assistance was Sogang University with its EXPOS, whose focus was to minimize weight carried by the user as much as possible in order to maximize the level of assistance (Kong and Jeon, 2006). From then on, due to the realisation of the magnitude and impact of the growing old population in modern society, several universities and organisations have been working on the development of devices to aid elderly people continue being mobile, although most are still in clinical trials stage. Examples of these devices are Honda's Stride Management Assist (SMA) (Buesing et al., 2015), EXPOS, mentioned above, the exoskeleton with flexible shafts by Ikehara et al., (2011), and the Harvard Wyss Institute soft exosuit whose purpose is to reduce the net metabolic cost of walking, either for healthy people or those with light impairments such as the elderly (Asbeck et al., 2015). A comparison of these devices is shown in Table 1.2, although many others have been developed.

Table 1.1 Comparison of commercial exoskeletons for paraplegics (Cyberdyne, 2015; EksoBionics, 2013; Kazerooni, 2013; RexBionics, 2011)

Characteristics	HAL-5	Ekso	Rewalk	Rex
<b>Design</b>				
<b>Company</b>	Cyberdyne	Ekso Bionics	Argo Medical Technologies	Rex Bionics
<b>DoF Hip</b>	1 actuated, 2 sprung	1 actuated	1 actuated, 1 sprung	3 actuated
<b>Knee</b>	1	1 actuated	1	1
<b>Ankle</b>	1	1 sprung	1 actuated and sprung	2
<b>Sensors</b>	Potentiometers, accelerometer, pressure	Angle, 2 DoF accelerometers, foot pressure, foot contact, crutch pressure with ground.	Angle, ground force wireless tilt, accelerometer, touch sensitive mode selector	Position and velocity, pressure and distance in feet, accelerometers, inclinometers, HMI with joystick
<b>Actuators</b>	DC motors with harmonic drive	DC motors	DC motors	DC motors
<b>Control system</b>	Finite State Machine	Finite State Machine	Finite State Machine	Positioning control
<b>Weight</b>	12 kg	23 kg	15 kg	38 kg
<b>Approx. Cost</b>	Rent £1,300 per month	£75,000	£70,000	£118,000
<b>Max Speed</b>		0.9 m/s	0.83 m/s	0.05 m/s
<b>Battery</b>	1 hour	3 to 6 hours	2 hours 40 min	2 hours walking

<b>Characteristics</b>	<b>HAL-5</b>	<b>Ekso</b>	<b>Rewalk</b>	<b>Rex</b>
<b>Aid. Support</b>	Crutches	Crutches	Crutches	None
<b>Motions performed</b>	Sit Stand Walk in straight line Ascending and descending stairs Hold and lift heavy objects	Sit Stand Walk on flat surfaces	Sit Stand Walking on flat surfaces Walking on sloping surfaces Ascending and descending stairs	Sit Stand Walking on flat surfaces Turning Walking on sloping surfaces Ascending and descending stairs
<b>Abilities needed</b>		Self-transfer from a wheelchair to a chair	Ability to use hands and crutches	Self-transfer from a wheelchair to a chair.
<b>Users range</b>	Between 4'9" – 6'1" tall and weigh 220 lbs or less	Between 5'2" – 6'4" tall and weigh 220 lbs or less	Between 5'3" – 6'3" tall and weigh 220 lbs or less	Between 4'8" – 6'4" tall and weigh 220 lbs or less

Table 1.2 Comparison of exoskeletons for elderly people (Buesing et al., 2015; Ikehara et al., 2011; Kong and Jeon, 2006; Asbeck et al., 2015)

Characteristics	Stride Management Assist	Ikehara et al.	EXPOS	Soft Exosuit
<b>Design</b>				
<b>Company</b>	Honda	NA	Sogang University	Harvard U./Wyss IBIE/Boston U.
<b>DoF</b>	1 in hip	1 in knee and 1 in ankle	1 in hip and 1 in knee	1 for ankle and hip
<b>Sensors</b>	Angle and current	Encoders and sole pressure	Potentiometers and pressure	Force and foot switches
<b>Actuators</b>	Brushless DC motors	DC geared motors with flexible shafts and worm gears	Servomotors for joints Pneumatic actuators for walker	DC motor with pulley and bowden cable, exosuit
<b>Control system</b>		Torque, angle control through PD	Fuzzy control	Position controlled motor, trajectory activated after heel strike
<b>Weight</b>	2.7 kg		Frame 3 kg	10 kg
<b>% of assistance</b>		~10%	32%	~6%
<b>Battery</b>	Lithium-ion 60 min	Lithium-ion		
<b>Aid. Support</b>	NA	Cane	Actuated caster walker	NA
<b>Motions performed</b>	Walking in flat surfaces	Walking	Walking, standing up/sitting down.	Walking
<b>Users range</b>	Size of hip frame M-size (hip width: 340 mm) L-size (hip width: 380 mm)	+/- 15 mm adjustment at thigh and +/- 30 mm at calf		Tested in 5 individuals with height 183.8 +/- 6.1 cm and weight 85.6 +/- 12.1 kg.

### 1.3 Main challenges

Ideally, exoskeletons should be designed to be portable, meaning self-contained, lightweight and power independent, in addition to seamlessly integrating with the user without restricting motion. Moreover, in order to commercialize them, they should be easy to wear, low cost, and overall, safe.

Although the development of exoskeleton devices has been going on for decades, Goldfarb and Durfee mentioned in 1996 that, due to the size and weight of current actuators, fully powered orthoses were not feasible yet. In 2008 Kazerooni confirmed that the main limitation for exoskeleton technologies was still the power supply (Kazerooni, 2008). However, according to Tucker et al., (2015), nowadays exoskeleton research is entering an age in which both hardware and software technologies are mature enough to develop lower limb exoskeletons that are practical and safe for real-world use.

Even though current exoskeleton devices are now in the market and are capable of restoring basic mobility tasks, thus enabling users' independence and improving their health, the most "durable" device is probably Ekso's that can stay powered on for up to 6 hours, due to the lower amount of actuated motors and decreased weight (Gofeer and Zilberstein, 2013). However, in order to accomplish the portability objective, exoskeletons should be able to work for at least 16 hours, which represents a normal day journey.

Apart from the lack of a sufficient power supply, many challenges still need to be overcome in order to successfully restore mobility in activities of daily life without being a burden to the user. Considering that, currently, available portable power supplies that could provide energy for a longer time are still heavy and voluminous, researchers need to look for smaller actuators, more efficient transmissions, and lighter materials for the frame in order to reduce energy requirements.

When considering seamless integration with the user, it must be noted that there are many areas where issues can arise from. Regarding the frame, misalignments of human and exoskeleton joints can generate motions different from the target as well as injuries in the user's limbs since they may be forcing joints. Over-restricting motion might make the user feel clumsy and more prone to tip over, while under restricting motion, could end up in hyperextension of joints. It is also important to consider that when users have mobility impairments, their range of motions might be reduced and joints stiffened, therefore an analysis of the user's motion capabilities should be taken into consideration beforehand.

Related with the latter, another challenge is the variation of physical characteristics of users. Not only in height but in weight, width, muscular tone, joints stiffness, among other individual characteristics. Therefore, exoskeletons' mechanical design must include sliding

components to adjust to different dimensions not only in the vertical axis but in the horizontal one as well, to ensure that the exoskeleton is as close as possible to the body without restricting motion. This is usually taken care of by interface components; however they do not always have the required range to cover the varying dimensions.

All the components should be thought-up to make the system “transparent”, so that the user does not find it hard to move while wearing the exoskeleton if not actuated, nor need more energy to move with it when actuated, compared to performing the same tasks without it. Considering that users have different levels of injury or impairment, ideally, exoskeletons should be able to firstly assess their condition and automatically update its control parameters and techniques to ensure safety and efficiency in aiding or restoring mobility tasks.

Another issue with the current devices is the elevated cost of exoskeletons which is between £55,000 and £100,000 (Marinov, 2015). According to the Income, Poverty, and Health Insurance Coverage in the United States, (2011), only 12% of the population earns more than that quantity per year. Therefore, only this small percentage would be capable of purchasing one of this exoskeletons after saving money over several years (DeNavas-Walt, 2011). There are several reasons behind these high costs, the first of them is that not only the exoskeletons themselves are being developed, but also specialized hardware and materials, including biomechanical frames, actuators and sensors. Although these components increase the uniqueness of the system, they often sacrifice the target market that exoskeletons have, considering the price they must be sold for.

A second reason for the high cost of exoskeletons is that unlike other complex systems, significant testing for function, comfort, and safety is still performed in physical labs since there are not many software available to simulate the conceptual and detailed design of exoskeletons and their controllers. Therefore, many researchers are forced to move almost directly from the initial idea to prototype, spending high amounts of money when flaws are found once the device is constructed (AnyBodyTechnology, 2016)

It is important to consider that the difficulty to produce a software for this application is due to the interaction of humans with the exoskeletons, which is much more complicated than in the case of other products, since they need to be closely attached to the body. Considering that interface components and the human body are composed of non-rigid segments, the simulation of the interaction between them is even more challenging.

A third reason for the high costs of exoskeletons is that while doing research in this area, motion data, as well as force and torque measurements are often considered essential for the understanding of the mobility tasks and the developments of controllers. However, the hardware required to obtain these is expensive. Although it is true that the availability of these data is desired, there are studies that describe the biomechanics of fundamental tasks which

can be used to simulate the motions without the need to spend in sophisticated equipment and marker-less techniques which are less expensive (Kerr et al., 1994; Mundermann et al., 2006).

Even though there would still be a need to verify the functionality of exoskeletons after using software simulation alternatives, it is clear that both the mechanic components and control scheme would be more robust before prototype construction since design flaws could be found in earlier stages.

In order to produce affordable exoskeletons, researchers have the challenge of looking for novel but cost effective software alternatives both for the design stage and for the product itself, and finding new ways of minimising the amount and weight of hardware used to decrease costs and unnecessary complexity.

In the case of exoskeletons being used to restore motion for paralysed patients as it is the case of paraplegics, there are other actuation alternatives that can be considered, such as FES. When external actuators generate the motions, even though users' legs move along with the device, their muscles do not contract because all the effort is done by the exoskeleton itself. As stated by (Kralj and Bajd, 1989), blood circulation is closely related to muscle contraction, so external actuation is not the best option if a general health improvement is sought.

Actuating muscles through electrical stimulus would help enhance circulation in SCI patients which would result in numerous benefits. However it should be noted that the main issue with FES is the rapid muscle fatigue when the stimuli are applied for long periods of time (Kralj and Bajd, 1989). Orthoses have helped to reduce this problem by supporting the limbs between one stimulation cycle and the next, extending the time that FES can be applied. Developing hybrid orthoses, which are frames with FES employed as actuation, help enhance patient's general health while restoring mobility tasks. Moreover, these devices are lighter and less expensive than their traditionally actuated counterparts.

Finally, but not less importantly, control techniques could be used to tackle some of the main challenges of exoskeletons. In order to decrease power consumption, the controller could ensure that the device is actuated precisely and only when needed. Complex sensors could even be supplanted by simpler sensors which along with algorithms could produce nearly the same result, helping to decrease cost. Moreover, parameters could be automatically optimised or different control techniques selected based on users' characteristics and capabilities, making the system adaptable. Controllers must also be programmed to include fail safe mechanisms and redundancy.

## 1.4 Aim and objectives

This research embarks on the development and evaluation of control approaches of robotic assisted mobility for disabled and elderly people. Lower-extremity exoskeleton control mechanisms are proposed to help individuals towards up-right standing and overall mobility. It involves theoretical work and verification through simulated exercises.

The main aim of this project is to develop humanoid and exoskeleton device models within a virtual environment, capable of communicating with software where middle and low level control strategies for the performance of fundamental mobility tasks can be implemented and assessed. This project is composed of two main applications, with the specific objectives described below. The first application aims on restoring walking for paraplegic patients where the objectives are:

- Develop a simplified CAD model of a human that performs realistically in terms of kinematics and dynamics within a virtual environment.
- Design a CAD model of a simplified hybrid lower limb exoskeleton frame, which can be attached to the humanoid body and perform motions for simulation purposes, in addition to a CAD model of a walking aid which provides equilibrium to the humanoid wearing the exoskeleton device.
- Investigate FES as an actuation technique that allows for the maximisation of paraplegic patients' lower-limbs locomotion in order to enhance their blood circulation while minimising power consumption.
- Develop low and middle level exoskeleton controllers to perform the different stages of paraplegic walking, and validate their functionality by simulating the humanoid, exoskeleton and walking devices in the selected virtual environment.

For the second application which aims to assist and restore standing-up and sitting-down motions for the elderly and paraplegic patients, objectives are:

- Adapt a CAD model of an actuated lower limb exoskeleton frame which can be coupled to the humanoid body and receive commands from a controller to simulate motions in the selected virtual environment.
- Perform an analysis of joints torque profiles required for standing-up and sitting-down tasks at different velocities with the aid of low level exoskeleton controllers for hip and knee joints
- Develop low and middle level exoskeleton controllers for ankle, hip and knee joints exoskeleton that performs the different stages of standing-up and sitting-down tasks while maintaining dynamic stability, and validate their functionality through

simulation of the exoskeleton and humanoid while performing the aforementioned tasks within a virtual environment.

## 1.5 Main contributions

Main contributions of this thesis are:

- Modelling in SolidWorks and SimWise of a humanoid with dimensions and mass parameters based on Winter's diagram and joints in anatomically correct positions. Modelling of a hybrid exoskeleton device based on existing products, and an actuated exoskeleton device adapted from the EXO-LEGS device. The resulting models behave realistically in terms of kinematics and dynamics, and are integrated with MATLAB Simulink, providing a platform in which exoskeleton controllers can be assessed without the need of a physical prototype.
- Development of a finite state middle level controller based on the biomechanics of the walking cycle, and fuzzy low level controllers for a hybrid exoskeleton. These controllers enable paraplegic walking in straight line with the use of a wheel walker. Controllers in Simulink, integrated with the models proposed in SimWise, enabled the testing of the full system, which proved to be capable of generating continuous walking motion at an average velocity of 0.3 meters per second. The device was able to withstand external disturbances and was capable of starting the walking motion from different initial conditions. All of the above with acceptable torque profiles and energy consumption.
- Simulation of the humanoid performing standing-up and sitting-down motions to perform an analysis of torque requirements. Through the use of PID controllers, it was possible to analyse relationships between gains, maximum torque, error and velocity of the motion. These were useful to acknowledge the limits of the system in terms of velocity, and to enable manual adjustment of the exoskeleton controller parameters when required. The posterior coupling of exoskeleton and humanoid enabled the evaluation of their interaction, the level of assistance that the latter provides, and the energy expenditure of the system. It was found that the exoskeleton was able to sharpen motion while decreasing energy expenditure when used by elderly people.
- Development of a finite state middle level exoskeleton controller to assist paraplegic patients to perform standing-up and sitting-down motions. This controller is based on the biomechanics of the aforementioned motions and enables assistance at different velocities. It also allows the system to return to initial conditions when a manoeuvre is not completed. Additionally, the FSC simplifies the connection with other

controllers to perform further motions and eases the fine tuning of parameters to adjust the device to different users.

- Calculation of the zero moment point offline and online to evaluate the dynamic equilibrium of the system and to include it as a parameter in the closed loop controller.
- Implementation of particle swarm optimisation algorithm to find the best combination of controller parameters for ankle joint. PID and fuzzy control techniques were assessed for feet and ankle joint orientations. Additionally, a fuzzy controller of ZMP was also included in the control loop. With the aforementioned strategies, standing-up motion could be partially completed.
- Initial validation of the proposed controllers was possible with the humanoid and exoskeleton models developed. Although tests performed are only an initial validation of the system, they help to decrease costs eliminating the need of a physical prototype in early design stages.

## 1.6 Thesis outline

This thesis presents the results obtained throughout this PhD research programme and is divided in two sections. The first section, comprised of chapters 2 and 3, describes the modelling of humanoid and exoskeletons and the development of low and middle level controllers for a hybrid exoskeleton and walker for paraplegic assistance on walking motion. The second section, comprised of chapters 4, 5 and 6, describes the development of an actuated exoskeleton middle and low level controllers for assistance on standing-up and sitting-down motions. A more detailed description of the contents in every chapter is included below.

Chapter 2 presents the background of mobility issues that paraplegic and elderly people face along with their causes and consequences. Additionally, a full exoskeleton review is presented, including the main components, such as orthotic frames, actuators, sensors and control techniques, as well as existing developments and challenges. Finally, the methodology used to generate CAD models of a humanoid, exoskeletons and a wheel walker within the SimWise virtual environment is described, along with its integration with MATLAB Simulink.

Chapter 3 presents the design of a control scheme applied to an assistive device for the restoration of walking motion in paraplegic patients. The hybrid device used to simulate the aforementioned motion is composed of an exoskeleton and FES. Firstly, an analysis of the walking cycle is presented to understand the biomechanics behind walking motion, then, the fundamentals of muscles operation are described in order to better explain the details of FES. Afterwards, a brief review of applications utilising FES for the restoration of mobility tasks is presented. The proposed control scheme for the assistive device is depicted, including a fuzzy

controller for the lower layer and a finite state controller for the middle layer. Additionally, the theory behind these control techniques is briefly discussed. Finally, results of the simulation and various tests performed to validate the functionality of the system such as repeatability, stability and range are described and discussed.

Chapter 4 introduces the investigation through simulation, of a humanoid and exoskeleton within the Simwise virtual environment for assisting the elderly during standing-up and sitting-down motions. A brief review on the existing exoskeleton technology for the elderly is presented, together with an analysis of the aforementioned motions to better understand the actions needed to complete them. A low level control of the exoskeleton's hip and knee joints is addressed through the use of PID controllers. Several combinations of gains and torque saturation values are tested to assess the feasibility of the system, focusing on obtaining standing-up and sitting-down motions with low root mean squared error and using the minimum amount of energy. The latter is measured through torque time integral. Additionally, simulations are performed at three different velocities to assess the impact on torque profiles. Relations between gains, torque saturation values and motion velocities are investigated in order to better characterise the system. And finally, estimations of ground and seat reaction forces are obtained.

Chapter 5 describes a middle level control system able to generate exoskeleton standing-up and sitting-down reference trajectories, at variable velocities through the online tracking of joints orientations with a finite state controller. Additionally, equilibrium of the system is assessed offline. Firstly, the fundamental concepts of static and dynamic equilibrium in mobile systems, including centre of mass and zero moment point are described and the methodology to calculate them is explained. Then, the middle level control scheme is presented, including the finite state controller that is based on the biomechanics of standing-up and sitting-down motion and additional tools. Afterwards, the calculation of the zero moment point is performed to evaluate the dynamic stability of the system. Finally, results obtained with the developed control scheme are presented and discussed.

Chapter 6 describes the use of an optimisation algorithm to identify low level exoskeleton controller parameters for the ankle joints, to enable paraplegic assistance during standing-up and sitting down tasks. Firstly, the particle swarm optimisation algorithm is described, secondly, two control techniques are considered with the purpose of controlling ankle joint flexion and extension while maintaining dynamic equilibrium of the system. In order to achieve this, the calculation of the zero moment point is performed online and included in the control loop. Finally a comparison of both control techniques is presented and results are discussed.

Chapter 7 presents a summary of the main contributions and general conclusions of this research, including a description of the main issues faced and proposals for future work.

## 1.7 Publications

D. Miranda-Linares and M. O. Tokhi. (2014) Finite state control of exoskeleton and wheel walker for gait restoration. 17th International Conference on Climbing and Walking Robots and the Support Technologies for Mobile Machines. p. 77  
DOI: 10.1142/9789814623353\_0009

D. Miranda-Linares, J. Lopez-Coronado, C. A. Diaz-Hernandez, Ishak A.J and M. O. Tokhi. (2015) Modelling and simulation of assistive exoskeleton for elderly mobility. 18th International Conference on Climbing and Walking Robots p. 95-102 DOI: 10.1142/9789814725248\_0015

D. Miranda-Linares, G. Alrezage, M.O.Tokhi . (2015) Control of lower limb exoskeleton for elderly assistance on basic mobility tasks. 19th International Conference on System Theory, Control and Computing . p . 441-446. DOI: 10.1109/ICSTCC.2015.7321333

Asnor J. Ishak , M O. Tokhi , Maged S. Al-Quraishi , Daniela M. Linares, Siti K. Ali. (2016) Modelling and Control of Standing Up and Sitting Down Manoeuver. International Conference on Electrical & Electronic Technology 2016. Malaysia, August 2016

# CHAPTER 2

## Modelling of humanoid, exoskeleton and wheel walker

### 2.1 Introduction

The purpose of generating a humanoid and exoskeleton model in a simulation environment, is to have a platform to test controllers developed while avoiding the complications and costs that building a prototype would represent. Modelling through computer aided design (CAD) has been adopted since a mathematical representation of both humanoid and exo would signify a great difficulty. It would be necessary to include legs' muscle models which are time varying, nonlinear complex dynamical systems, as well as mechanical and electrical models of the components of the exoskeleton, in addition to the kinematics of the full system.

A review of the available muscle models revealed that several coefficients are required to calculate muscles' behaviour, and these can only be obtained experimentally. Furthermore, these constraints are specific for every person, therefore, if a different user was to be wearing the exoskeleton, a new model would need to be defined and implemented (Jailani, 2011; Riener and Edrich, 1999).

CAD models can be created with the same mechanical properties as real prototypes, therefore, through the selection of the appropriate materials, properties, dimensions, masses, friction, and restitution coefficients, it is possible to ensure that their kinematic and dynamic behaviour is realistic.

In this research, CAD models are developed in SOLIDWORKS and each part is then exported to SimWise, which is a virtual environment where the characteristics previously mentioned can be configured for every part. Assemblies can be created through specific constraints, making this software suitable for the present application. Additionally, Simulink enables the connection of SimWise with MATLAB, where the control strategy is developed.

## 2.2 Mobility issues

As mentioned in Chapter 1, mobility is one of the most important abilities that humans possesses, and exoskeletons are the most complete solution for elderly and disabled people's mobility issues. However, in order to propose appropriate control techniques for exoskeletons, it is important to understand the basis and origin of the mobility issues which they are required to solve.

### 2.2.1 Spinal cord injury and paraplegia

The spinal cord is responsible for the innervation or activation of the nerves of the body, as well as the transmission of sensory information. It has a very complex internal arrangement, it is composed of nervous tissue inside a cylindrical structure, which is slightly flattened and located within the spinal canal of the vertebral column. It extends from the brain to the peripheral nervous system, and is formed by 31 pairs of spinal nerves: 8 cervical, 12 thoracic, 5 lumbar, 5 sacral and one coccygeal (Barr, 1979).

SCI occurs when the spinal cord is damaged in such a way that its normal functions are affected. There are two classifications to determine the degree of disability caused by SCI. The first one is based on the completeness of the lesion; in complete transection, all voluntary movement and sensibility is lost below the lesion, and in hemi-section, a partial transection of the spinal cord, the sensory and/or motor functions of one of the sides of the body are preserved below the injury (Barr, 1979).

The second classification depends on the site of the injury. Cervical injury causes paralysis of the four limbs and torso, in that case, it is also called tetraplegia. Thoracic or lumbar injury results in paralysis of both legs and torso and is often called paraplegia. This is better illustrated in Figure 2.1, which shows lesions at different levels of the spine and the loss of mobility that each of them causes.

There are many causes for SCI. These can be divided into traumatic and non-traumatic. The latter includes degenerative disorders, tumours and infections (Barr, 1979), while the former, being the most common, comprise motor vehicle accidents, falls, bullet or stab wounds, diving and other sport accidents (elearnSCI.org, 2012).

In the US, of the total patients with SCI, around 42 per cent are paraplegic (National Spinal Cord Injury Statistical Center, 2016). The meaning of the word paraplegia itself is paralysis of the lower limbs, though in most cases it also includes part of, or the whole trunk (Walsh, 1964). As mentioned before, paraplegia occurs when there is a transection of the spinal cord between the cervical and lumbosacral sections. As a result one or both legs lose all

the voluntary movement and sensibility (Barr, 1979). In addition, paraplegia has other implications such as loss of normal bladder and bowel function (Rogers, 1986).

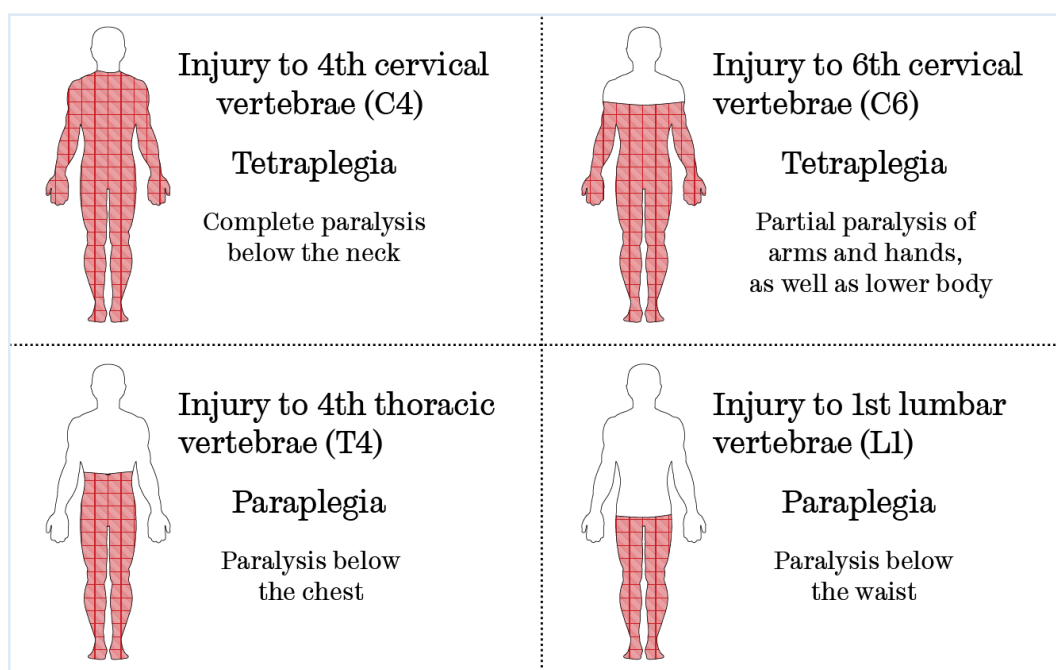


Figure 2.1 Cord Injury levels and effects, modified from (Harrison, 2006).

Paraplegia has existed since the beginning of mankind; the first registered case dates from 3000 year ago by an Egyptian physician who described it as “an ailment not to be treated”. It was until the second world-war that this belief began to change and treatments were developed, resulting in an improvement of the survival rate to almost 92 per cent (Walsh, 1964).

Unfortunately, paraplegia still means loss of independence and autonomy for the patient. In most cases, the lesion is permanent and patients experience a total life change, having to adhere to strict medical advice to survive, due to the increased risk that something as simple as staying in bed implies on their health.

Many efforts have been made to restore paraplegic patients’ lifestyle to normality. Rehabilitation techniques and devices have been created to control organ functions and restore basic mobility tasks in paraplegic people. This group has been chosen above tetraplegics in many studies, since it is necessary to have some control in the upper body to enable the use of most assistive devices.

### 2.2.2 Elderly muscle weakening

Apart from the multiple diseases that generate gait and balance disorders in elderly people, there is a slow, progressive and inevitable loss of muscle mass and strength that occur with

advancing age. This reduction of muscle mass seems to be responsible for the decrease in muscle strength and power, as well as the loss of functional mobility in the elderly. There is around 20 and 40 per cent diminution in muscle strength and power between 70 and 80 years of age, and around 50 per cent over 90 years of age (Garcia et al., 2011).

Although it is difficult to quantify the decrease of strength that occurs in old age, Schultz, (1995) estimated that between ages 25 and 65 the decline in muscle strength is one third. Additionally, it was found through isokinetic tests of muscle strength and power of hip and knee extensors that peak torque capacities were around 35 per cent less in a group of people 80 or over, as compared to a group of 65 to 69 years old (Garcia et al. , 2011).

Moreover, gait disorders are present in around 25 per cent of people between 70 and 74 years old, and in almost 60 per cent of those 80 to 84 years old. Mobility impairments in the elderly are usually identified by a variety of symptoms, like dyspnea, imbalance, diminished strength, limited range of motion, and poor posture, among others (Salzman, 2010).

Some researchers suggest that maximum torque is not completely associated with mobility impairments, since, to perform most motions, the required torque is lower than available torque. On the other hand, the decrease in ability to develop joint torques rapidly seems to be more associated with age decline, e.g. older adults took 161 milliseconds more than younger adults to develop 60 Newton meters of plantar flexor torque (Schultz, 1995).

Even though the specific reason for elderly mobility impairments is not clear, it is certain that they are forced to modify the way they perform basic mobility tasks, making them slower and insecure, as well as more vulnerable to falls. In many cases becoming dependent on other people, disabling them to perform daily life activities and ending up isolated from society, boosting other physical or psychological conditions.

### **2.3 Exoskeletons review**

As mentioned, exoskeletons offer a solution to mobility issues of both paraplegic patients and the elderly. This section presents the basic terminology used in this research discipline, in addition to a review of the main exoskeleton components and accomplishments in this area during the last decades, from the incorporation of closed loop control strategies.

Exoskeletons can be defined as robotic orthoses. According to ISO 8549-1:1989 and 8551:2003, an orthosis is “an externally applied device” that has traditionally been used as a mechanical aid, to modify the structural and functional characteristics of the neuromuscular and skeletal system. They are usually attached to the body to manage abnormalities in length, shape or function, as well as to prevent or increase the range of motion of specific joints, modify the length or shape of a segment, protect tissues by reducing or redistributing loads,

compensate muscle weakness, and to control muscle hyperactivity, among others (Hsu et al., 2008).

Orthoses are made up of the following components according to ISO 13404:2005:

- **Interface components:** Those in contact with the wearer, they transmit forces between the user and the orthosis, thus resulting in the desired function as well as keeping the orthosis in place. Some examples are shells, pads, straps, foot orthoses, and shoes (Hsu et al., 2008).
- **Articulating components:** Control the motion of anatomical joints, their description should include the anatomical joint they are paired to, the residual motions of the joint after it is connected to the orthosis, the form of the articulation, e.g. prismatic, revolute, or spherical, the axis of rotation, and finally, the type of controls it uses. Examples for these components are locks and limiting mechanisms.
- **Structural elements:** Those which connect interface and articulating components maintaining the alignment of the orthosis, these are commonly lightweight metallic bars.
- **Cosmetic components:** As their name implies, provide shape, colour and texture to the orthosis (Hsu et al., 2008).

Figure 2.2 shows an example of lower limb orthosis and its interface, articulating and structural components.

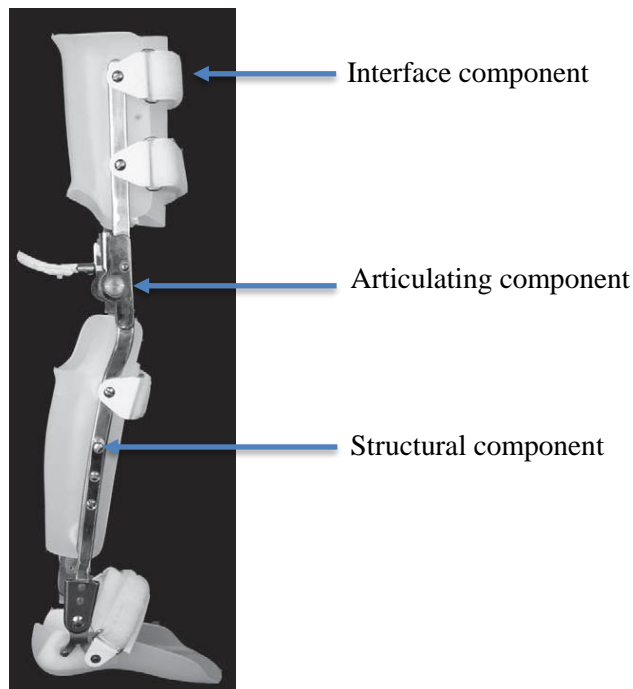


Figure 2.2 Lower limb orthosis (Hsu et al., 2008)

For many years, orthoses have evolved from simple mould shapes to complex mechanical devices with movable joints, springs, brakes, pulleys, stoppers and actuators of different natures. Orthoses, combined with actuators, sensors and other electronic equipment are called active or robotic orthoses, they prevent or increase range of motion of specific joints, thus, enabling the user to accomplish a mobility task. Furthermore, making use of the available technology, this kind of hybrid orthosis have been programmed to perform specific tasks transforming them into wearable robots (Hsu et al., 2008; Pons, 2008)

Exoskeletons have also been defined as wearable robots, these being person-oriented robots that a human can put on to aid the function of a limb or to substitute it entirely This classification is more adequate and inclusive of those devices which have as purpose the augmentation of human capabilities. Apart of differentiating exoskeletons according to their function, they can be classified based on the way they interact with humans and the limb they are attached to, as empowering robotic exoskeletons, orthotic robots and prosthetic robots (Pons, 2008):

- Empowering robots are also called augmentation exoskeletons since they are robotic structures that when assembled to the human body, increase the strength of limbs. These usually work under a master-slave configuration.
- Robotic orthoses are those coupled to human limbs to restore and enhance functions, such as walking or standing, after a trauma or disease like SCI.
- Prosthetic robots are those electromechanical structures that replace a lost limb (Pons, 2008).

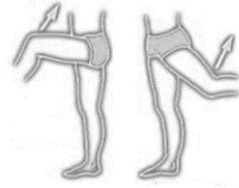
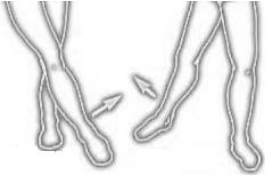
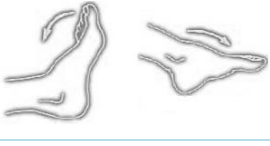
Another classification is simply based on the limb to which the robot will be attached. They can be “upper limb” which are used for manipulation and require low force and torque, but high kinematic compatibility with human limbs. Or “lower limb”, used for support, mobility and stability, and whose kinematic compatibility can be slightly less complex than upper limb exoskeletons, but require higher force and torque (Pons, 2008).

In the case of single joint devices, they are called after the name of the joint and/or the segment of the body they aid or are attached to, examples of these are Active Ankle Foot Orthosis (AFO) and Active Knee Orthosis (AKO) (Dollar and Herr, 2007).

In order to properly understand the operation of exoskeletons, they are often classified based on their kinematic specifications compared to the human body. Some of these specifications are: type of motion, degrees of freedom (DoF), range of motion (RoM) and torque (Low, 2011).

Table 2.1 shows the kinematic characteristics of the human body’s lower limbs which are useful for the description and classification of lower limb exoskeletons. These characteristics are used to compare existing exoskeleton designs throughout this research.

Table 2.1. Human body lower limbs kinematic specifications (Low, 2011)

Joints	DoF		Motion	Axis/Plane Of motion	RoM	Average Torque
<b>Hip</b>	3		Flexion	Y or transverse axis/ Sagittal plane	100°-140°	140 Nm
			Extension		15°-30°	120 Nm
			Adduction	X or sagittal axis/ Frontal plane	20°-40°	
			Abduction		30° - 40°	
			Internal	Z or vertical axis/ Transverse plane	15°-30°	
			External		60°	
<b>Knee</b>	1		Flexion	Y or transverse axis/ Sagittal plane	120°-150°	140 Nm
			Extension		0°-10°	15 Nm
<b>Ankle and Foot</b>	2		Flexion	Y or transverse axis/ Sagittal plane	40°-50°	165 Nm
			Extension		20°	
			Inversion	X or sagittal axis/ Frontal plane	30°-35°	
			Eversion		15°-20°	

The majority of the exoskeleton systems are conformed by a mechanical frame, actuators, sensing equipment, a controller and a portable power supply. The former are attached to the body in a similar manner as an orthosis. The functions of the mechanical components are to: act as interface between exoskeleton and wearer, restrict, or even block motion in specific axes, maintain alignment of the exoskeleton, and support actuators, sensors and controllers in place. Materials used for frames are usually metallic like aluminium, carbon steels, and titanium and its alloys. The use of thermoplastics and carbon composites have increased due to the need to create light, strong and biomechanically effective devices (Hsu et al., 2008).

Recently, wearable soft robotics have been used instead of rigid frames to try to reduce weight and to better integrate actuation with the human body. Some examples are Soft Suits developed at Harvard (Asbeck, De Rossi, Holt and Walsh, 2015) and the Superflex exosuit by SRI Robotics. The latter is an ankle joint exomuscle/exotendon which, when actuated, can

help reduce fatigue and give an extra “boost” to complete the walking motion. The whole system is less than 4 kilograms but can generate more than 200 pounds of force (Hernandez, 2015; Next big future, 2016). An advantage of soft suits, apart from being lightweight, is that they distribute the load comfortably over the wearer’s limbs, and users have stated that they can barely feel them when inactive.

There is a wide variety of power supplies, sensors, actuators and control strategies that have been used for exoskeletons, they are presented in the following subsections.

### **2.3.1 Sensors**

Sensors are used to know the conditions of systems at every moment to control devices accordingly. They serve various purposes in lower limb exoskeletons, such as reading orientation of different joints through encoders, goniometers and potentiometers, and measuring distances or detecting contact between the user’s feet and ground.

They can also be used to determine if a load has been applied in a certain area by means of force sensors at feet and/or crutches, as well as in interface components for detecting intention or estimating torque. Additionally, they can read position, velocity and acceleration of segments of the body, including trunk by means of accelerometers and gyroscopes, and are even used to detect EMG or EEG signals through implanted or surface electrodes in order to trigger specific actions, measure the level of required assistance, or evaluate the performance of exoskeleton devices.

HAL 5 by Cyberdyne uses potentiometers to measure relative joint angles, and semiconductor type pressure sensors installed in shoes, together with a tri-axial accelerometer to obtain absolute angles of the user’s trunk (Tsukahara et al., 2010). BLEEX uses hip and knee angle sensors, switches at each foot to get the location of the centre of pressure, and a rubber pressure tube filled with hydraulic oil to measure the user’s load distribution. Crutches used along with the exoskeleton employ pressure sensors and a 2 DoF accelerometer at the arm (Kazerooni et al., 2005). Rewalk uses sensors to measure hip and knee angle, ground force, and wireless tilt of the upper body, as well as a touch sensitive mode selector (Gofeer and Zilberstein, 2013).

All the aforementioned devices are aimed to sense the paraplegic patients’ intention and conditions of the system, in order to start predefined manoeuvres, since the exoskeleton is the one leading the motion. However, to be able to aid elderly people or those with mild mobility impairments, exoskeletons must be able to follow their motion and complete it when necessary. Therefore, apart from the aforementioned measurements, specific torque requirements for every joint must be acquired or estimated with the use of sensors.

EXPOS uses potentiometers located in pulleys to measure angle and calculate joints velocities, as well as pressure sensors installed at thigh braces and shoes. Changes in pressure of an air bladder which contracts just before the motion is initiated are measured to estimate torque requirements, therefore, the exoskeleton can anticipate the motion and actuate its joints along with the wearer's joints (Kong and Jeon, 2006). Soft exosuits use encoders at motors, force sensors in the upper and lower part of Bowden cables, and foot switches to detect heel strike (Asbeck et al., 2015).

Honda's SMA includes angle and current sensors at actuators to monitor the range of motion of the user's hip joints and torque generated by the SMA (Buesing et al., 2015). Ikehara's exoskeleton system uses pressure sensors in soles, located at thenar muscles and heels of feet, to determine walking phases based on variations in voltage. Torque is estimated through the twisting angles of flexible shafts and angles of the motors, and joint angles are measured through encoders (Ikehara et al., 2011).

EMG and EEG signals have been used to detect user's intention when they are not able to activate a joystick, button or another human machine interface (HMI) to generate a direct command. An example of this is HAL, which uses knee flexor EMG signals to detect user's motion intentions (Kawamoto et al., 2010). EMG signals are also used to better integrate exoskeletons with users taking advantage of the remaining electrical pulses to calculate the level of assistance required (He and Kiguchi, 2007). Another alternative is to use EMG signals of upper body to trigger lower body exoskeleton motions (Sylos-Labini et al., 2014).

It has been demonstrated that it is also possible to obtain signals directly from the brain; a 64 Channel electrode cap placed on the head along with a wireless interface, were used to detect and transmit EEG data to a controller in order to command the start and stop of walking motion using a REX exoskeleton (Kilicarslan et al., 2013).

An enormous amount of sensors are readily available for exoskeleton applications. Most of them are already compact and some are even capable of wirelessly communicating with controllers. This results useful considering that portability is one of the main goals of exoskeletons.

### **2.3.2 Actuators**

Compact actuators are what enabled the genesis of exoskeletons, these are usually attached to the frame and their purpose is to generate the functional movement of the device according to signals sent by the controller. A huge variety of actuators have been used in exoskeletons and are summarised below.

Electric actuators, specifically DC motors are the most common, although researchers have looked for different mechanical alternatives to make systems as compact as possible in order to even fit exoskeletons beneath clothes such as the device by Ikehara et al., (2011) which is actuated by DC motors connected through flexible shafts to worm gears for knee and ankle joints. Similarly, the newly developed soft suits use DC motors coupled with a pulley and a Bowden cable, which along with a strap system, generate ankle and hip joints motion (Asbeck et al., 2015; Hernandez, 2015). For these two systems, motors are located at the backpack to reduce adding weight to the user's legs.

Actuators are usually aligned with human joints as is the case of the following exoskeletons. DC motors with harmonic drives are used in HAL exoskeleton's knees and hips (Tsukahara et al., 2010), whereas Vanderbilt exoskeletons uses brushless DC motors for the same joints (Quintero et al., 2012). Honda uses two DC motors for SMA, a hip single joint exoskeleton (Buesing et al., 2015), while REX uses ten DC RE 40 ironless rotor motors manufactured by Maxon (Schütz, 2012). Practically, nowadays, all the commercial exoskeletons use DC motors.

However, researchers have been looking for other alternatives; servomotors coupled to pulleys were used to actuate hip, knee and ankle joints in EXPOS (Kong and Jeon, 2006). Yamamoto used pneumatic actuators for knee and hip joints for his patient handling exoskeleton device (Yamamoto et al., 2003), Seireg used hip and knee hydraulic actuators with servo valves (Siciliano and Khatib, 2008) similarly to Kazerooni's BLEEX (2005), which included hydraulic actuators located at thigh for knee joint flexion and extension, and at calf for ankle joint actuation (Zoss et al., 2006). Pratt, on the other hand, used linear series-elastic actuators for a knee brace (Pratt et al., 2004).

In EXPOS, actuators are not directly attached to the exoskeleton frame. The exoskeleton is coupled to a smart actuated caster walker, which as well as assisting the user's stable posture, contains a pneumatic up and down mechanism, and encloses the servomotors that actuate the frame (Kong and Jeon, 2006).

In exoskeletons for paraplegic patients, actuators can be replaced by user's legs, which, although cannot be activated by brain signals, can be externally stimulated using FES with the help of electrodes located near specific nerves and muscles. In that way, muscle contraction and consequently, functional movement of joints is generated.

FES used in combination with orthoses, to provide support and decrease stimulation application time has been tested through the creation of hybrid orthoses by Miyamoto et al., (1999), as well as Jailani et al., (2011), and others. Even though there are several options for exoskeleton actuation, they either consume such a big amount of energy that current power supplies are not capable of satisfying them for more than 6 hours, or are still too bulky to make exoskeleton systems portable and transparent.

### 2.3.3 Power supplies

Another important component for making exoskeletons portable is power supply, which is what actually allowed them to become autonomous devices and enabled companies to commercialize them for personal use. Most commonly used power supplies in current devices are lithium ion batteries, although there is interest on utilizing fuel cells.

A feasibility study conducted by Jansen and colleagues, (2000), pointed out that fuel cell might be the best options for exoskeleton devices because of their quiet operation, relatively low temperatures, and benign emissions. However, concerns were mentioned regarding the hydrogen source (Jansen et al., 2000).

In 2010 Lockheed Martin, developer of HULC, a battery-powered hydraulic exoskeleton, announced that fuel cell batteries were being considered for their next prototype although it was never completed since the company opted in 2012 for unpowered exoskeletons (DailyTech, 2014; Kopp, 2011). Although fuel cell might still be a feasible alternative, it will not be a solution for exoskeletons until a suitable hydrogen source is available.

Sarcos XoS 2 by Raytheon, is an augmentation exoskeleton which weighs about 95kg and through a combination of controllers, sensors, high-strength aluminium and steel along with hydraulic actuators, is able to carry 100 kilograms for prolonged periods. However, it requires a tethered high-pressure hydraulic engine. For the succeeding prototype, a fuel-carrying backpack with hydraulic servos is being developed to enable it to recover autonomy, while powering the system for at least eight hours. The advantage of using hydraulics instead of lithium ion batteries is that the risk of breach and explosion is eliminated (Armytechnology.com, 2016).

Nowadays, lithium ion batteries are still the most common and safest for civil applications. Depending on the system's efficiency, these can provide a runtime of up to 6 hours without recharging. Undoubtedly, the development of a power supply which allows exoskeleton systems to run for more time is still one of the biggest challenges of this technology (Dollar and Herr, 2007). For this reason, researchers are focusing on minimising the weight of frame through the use of novel materials, as well as miniaturising sensors and actuators in order to reduce weight and dimensions, thus increasing exoskeletons' efficiency.

### 2.3.4 Control techniques

Early versions of exoskeletons for paraplegics used predetermined or pre-programmed periodic motions (Siciliano and Khatib, 2008). Trajectories were obtained from healthy subjects and processed to generate standard references that were sent to actuators; hence,

exoskeletons' control was open loop until the inclusion of sensors to these systems enabled the use of feedback techniques.

The next big step was to use sensor measurements to close the control loop, enabling communication between the user and the exoskeleton device. Contact of feet with ground and joint angles were obtained in the first developments as conditions to be met to initiate pre-programmed motions. The use of force sensors or remaining EMG signals has also been used as input from the user to generate proportional exoskeleton actuation, or detect user's intention. Nowadays, even electroencephalographic (EEG) signals have been used to activate different mobility tasks using the steady state visual evoked potential (Kwak, Muller and Lee, 2015). However, in order to control an exoskeleton device which integrates seamlessly with its user, a combination of complex control systems is needed.

At the beginning of this research, few studies on the whole control schemes for exoskeleton systems were found in the literature. Papers often included details on hardware used, as well as mechanical design descriptions of the devices. In the cases where details regarding the control scheme were included, they would only expand on a particular control level, or two at the most, especially the upper levels. This made the understanding of the functionality of the whole system complicated and hardened the task of comparison between devices to find the best direction to take. Nowadays there is more information available and it is possible to make a more complete review on the advances of control techniques for exoskeletons.

According to Tucker et al., (2015), control of exoskeletons should be hierarchical and consider not only the user and the exoskeleton, but also the environment in which both of them move. Therefore, communication from the user to the exoskeleton and the environment, from the environment to the user and the exoskeleton, and from the exoskeleton to the user and the environment should be incorporated into the design. This communication can be in the form of physical or signal interactions.

Figure 2.3 shows these interactions as well as the three control levels needed for active lower limb exoskeletons. This research is focused on developing low and middle level control schemes.

The highest level called perception layer should recognise the user's intention, his current state, i.e. his pose, which includes his position and orientation, as well as that of the device and the environment. It can be either direct volitional or voluntary control, incorporate some mode recognition system, or a combination of both.

The mid-level control or translation layer, interprets the directions from the high-level controller into device states and therefore, desired outputs. And the low-level control or execution layer contains the feedback loop that computes the error for each specific device.

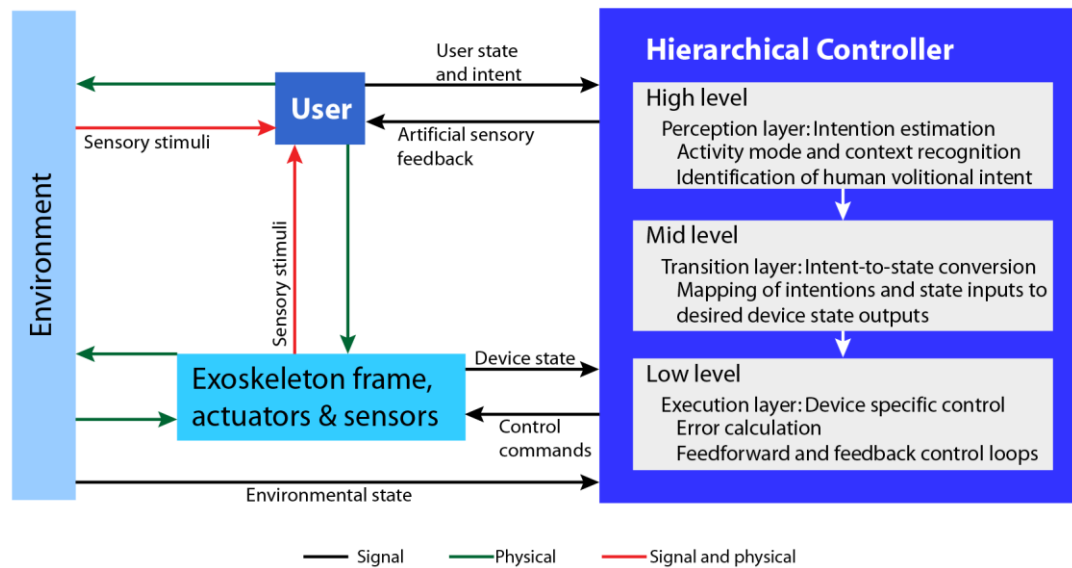


Figure 2.3 Exoskeletons control structure, modified from (Tucker et al.,2015)

In the case of a lower limb exoskeleton, a complete controller example using this configuration would, in the highest level, detect or receive directions from the user, device and/or environment to send indication to the mid-level controller to either walk, climb stairs, sit down or perform other fundamental mobility tasks. The mid-level controller for e.g. walking, would then decide, based on the state of the system and the indications from the high-level controller, when and which low-level controllers must be used for each part of the cycle such as the swing motion of left leg, and provide them with joints references to be followed. Finally, the low-level controllers for that specific action would activate motors of the different joints of the left leg based on the received references, updating the pose of the user and device, and therefore closing the control loop. It is important to consider, as well, the inclusion of algorithms to ensure safety of the user and the device.

Most commercial exoskeletons use manual mode switching as high-level controller to change between different tasks such as standing-up, walking, stair climbing, and sitting-down, among others. This manual control can be done through a remote control, pushing a button, pressing a lever or executing a particular sequence with a finger (Tucker et al., 2015). However, as it was mentioned in section 2.3.1, many different sensing techniques have been used to detect users' intention, such as switches and pressure sensors in feet, EMG signals from upper body or remaining signals from lower limbs, or even EEG signals, specifically through steady state visual evoked potential (Kwak, et al., 2015). Moreover, some algorithms have been developed to identify user's intention to perform specific actions through the measurement of the position or shift of measured or calculated Centre of Mass (CoM) or Pressure (CoP).

The most popular mid-level controller is the finite state controller (FSC) used in Ekso, Rewalk, HAL and many others (Tucker et al., 2015). FSCs are highly suitable for control of gait due to its sequential operation (Sweeney et al., 2000). However, the first to present a description of finite automata, in 1943, were neurophysiologists McCulloch and Pitts. Later on, computer scientists, Mealy and Moore, generalized the theory to more powerful machines in 1955 and 1956 (Dar Aziz et al., 2004). FSCs have been used for applications such as telephone systems, vending machines, traffic lights, bar code readers, and gasoline pump dispensers, among others (Keller, 2001)

A finite state machine or finite automaton is a conceptual model which involves states with corresponding outputs or actions to be performed, and the transitions between them (Hopcroft et al., 2007). Transitions depend on the actual state and the input, which control if the system will be moved to the next state. It is also necessary to indicate the initial state in which the system will be placed and the final or accepting state (Hopcroft et al., 2007).

In the mid-level control layer, Ekso's uses a FSC that includes different states as "Start Walk", "Walking", "End Walk", "Standing", "Sit Down", "Seated" and "Stand Up". To activate any of them, the system needs input from sensors. When the user requires a state change, the system determines, based on those sensors' readings, if it is possible and safe to trigger it. Each state contains instructions that are later send to the actuators controllers to accomplish the desired motion. In the higher-level, the user can also regulate the walking speed by the means of a button, a thumbwheel, or other signal generator; by voice command or by brain signals obtained using an Artificial Neural Network, among other tools and techniques (Kazerooni et al., 2013)

A FSC is also used in Rewalk exo where states as "Sitting", "Standing", "Walking", "Climb stairs" and "Descend stairs", are available to be selected in the portable control panel by the user. Depending on the selection, a different algorithm will be executed. The user needs to lean forward to initiate the action, however, this is only performed when the stance is adequate for the action required basing on the measured load in each leg. When all conditions are met, an algorithm is executed to e.g. extend the leg and step. The system also includes an alert system which, based on the loadings and the upper body tilting, can tell if the person is at risk of falling (Gofeer and Zilberstein, 2013)

Meanwhile, HAL exoskeleton uses an algorithm in the form of a FSC in which inequalities must be accomplished to activate phases. Two phases are used for walking and five phases to sit-to-stand and stand-to-sit. Inequalities are based on the calculation of centre of pressure and floor reaction force (Tsukahara et al., 2010).

Finite state control has also been used in neural prostheses in conjunction with FES. The system detects subject's intentions and processes measurement from sensors, so that when conditions are met, the trigger of FES activation state is performed (Sweeney et al., 2000).

Jailani (2011) programmed an FSC to control a hybrid exoskeleton which used FES to restore walking in paraplegic people with the aid of a spring brake orthosis (SBO) and a walker. The SBO was created with a modified reciprocating gait orthosis. Its function was to generate flexion through application of FES to hamstrings, and to quadriceps to generate extension (Gharooni et al., 2001). Jailani modelled the SBO system as well as a simplified humanoid model and a wheel walker in Visual Nastran 4D, and created a FSC to activate FES and brakes to generate a walking cycle (Jailani et al., 2011).

Most of the FSCs, require a heuristic tuning of parameters in order to ensure user's comfort and device's efficiency. However, due to the fact that there must be a FSC for each mobility task, that each of them involve variables regarding the activation of transitions between states, and inputs detailing the pose of the system, as well as outputs for actuating each joint; the number of tuneable parameters quickly increases (Tucker et al., 2015).

Low-level control is highly device specific but it is usually a type of feedback or feedforward controller. Methods commonly used are fuzzy control and proportional, integral, derivative (PID) control, although there is not much documentation regarding this control level.

Another review on exoskeletons control by Yan et al., (2015), classified full body and single joint exoskeletons in nine assistive strategies; where two of them, muscle stiffness control and proportional myoelectrical control, apply only to single joint devices. The first strategy, sensitivity amplification control is mainly used for load-carrying augmentation exoskeletons, devices that use this strategy are Berkeley Lower Extremity Exoskeleton (BLEEX), and Naval Aeronautical Engineering Institute Exoskeleton Suit (NAEIES), among others (Yan et al., 2015).

Predefined gait trajectory control is another strategy in which joint reference trajectories are obtained from a healthy person or from gait analysis. It is used mainly in applications for patients with lost or partially lost voluntary movement, as it is the case of SCI. Exoskeletons such as ATLAS, ReWalk, sLEGS, IHMC, MINDWALKER, walking assistance device by Ikehara, Vanderbilt lower-limb orthosis, Powered Knee Orthosis (PKO) and Stance control knee–ankle–foot orthoses (SCKAFOs), use this strategy (Yan et al., 2015).

In model based control strategy, the desired actuation of joints is calculated based on a human-exoskeleton model. They usually consider gravity compensation and Zero Moment Point (ZPM) for balance. ABLE, Body Extender (BE), Nurse Robot Suit, Wearable Walking Helper (WWH), Walking Power Assist Leg (WPAL), XoR, Robo Knee, Technische Universität Berlin Powered Lower Extremity Exoskeleton (TUPLEE), IPECAFO and the Stewart-platform-type AFO, are examples of this strategy. These exoskeletons are mainly aimed at disabled and elderly people (Yan et al., 2015).

Adaptive oscillators-based control captures periodic locomotion-related signal features during rehabilitation exercises, and calculates desired joint trajectories based on those features. This strategy is mainly used to reduce efforts in healthy subjects or those with weakened muscles. It is utilised in the Robot Suit, LOPES, ALEX II, and the One-DOF exoskeleton device by G. Aguirre-Ollinger (Yan et al., 2015).

Predefined action based in gait pattern control has been used for load carrying augmentation devices such as the MIT exoskeleton; for assistance of healthy subjects using the Soft Exosuit, the Power Assist Wear, the knee extension assist device (KEA), and the MIT knee exoskeleton. And for weak or disabled walking, this strategy has been used for the pneumatic active gait orthosis by Belforte and MIT active ankle-foot orthosis (AAFO), among others. In this strategy, actuators such as passive springs or pneumatic cylinders are activated or deactivated depending on the current walking phase (Yan et al., 2015).

Hybrid assistive strategy as its name implies, involves the use of more than one strategy in different phases of the mobility task. Examples of this strategy are BLEEX and AIT leg exoskeleton, which establish a predefined gait trajectory offline and afterwards, uses a fuzzy controller to modify it online (Yan et al., 2015).

In most cases, muscle stiffness and proportional myoelectric strategies measure muscle action to control actuation of pneumatic actuators. They differentiate only by the kind of sensor used to estimate the muscular action. Examples of muscle stiffness control can be found in the knee orthosis by K. Kim et al., (2010) while the Powered Ankle-Foot Orthoses (PAFOs) employ proportional myoelectric control (Yan et al., 2015).

Lastly, fuzzy control is used when it is complicated to generate an accurate dynamic model, therefore, it is appropriate for exoskeleton's control and is typically used for physically weak patients such as elderly people. Although it is a practical way to control this kind of devices, manual tuning of variables is needed (Yan et al., 2015).

Numerous control techniques have been used since the appearance of exoskeletons. Although there are no rules or conventions for their application, some generalities have been noted:

- High-level control is mainly subject on resources available, especially sensors.
- Mid-level control has to be designed considering the objective of the device, considering if it will lead the motion, as is the case of paraplegic patients, or if the user will lead the exoskeleton movement, as with augmentation devices or those for elderly people.
- Low level control is generally dependent on the type of actuators used.

Controllers are the only component which can help enhance integration of the device with the user without adding weight to the system. By using appropriate control techniques, it could even be possible to save energy. Controllers are the most flexible component in exoskeleton

devices, therefore various control techniques can be explored to obtain the best possible results with the least amount of resources. However, to do this in a cost-effective manner, it is necessary to have a software platform that allows for the simulation of different controllers.

Exoskeletons are thought as an assistive technology that provide support while standing, enable displacement, usable in limited spaces and energy efficient. Their purpose is to restore and, in some cases, increase lost mobility capabilities, providing enhanced general health, independence and self-sufficiency to users. These devices have been aimed for paraplegic patients to recover lost mobility capabilities, however, recently, elderly people have also been considered as beneficiaries of this technology

Hardware and software have been developed to achieve the aforementioned goals, and although a variety of sensors and actuators are readily available, materials are still not light enough and power supplies are still not sufficient to make exoskeletons portable for a whole day journey. Moreover, although several control techniques have been tested and developed, integration between user and device is still not enough to smoothly support or produce motions and to avoid being a burden for the user when the device is not powered.

Control strategies still need to be explored to eliminate these issues, however, in many cases, it is difficult to assess controllers without a physical prototype. Therefore, a software platform that allows a realistic integration of humanoid and exoskeleton models, and the communication with controllers in order to perform the necessary tests to validate the exoskeleton design, would be primordial to decrease their cost.

## **2.4 Modelling of humanoid, exoskeleton and walking aid**

### **2.4.1 Software**

SOLIDWORKS is a Computer Aided Design software by Dassault Systemes that delivers robust 3D design capabilities performance. It allows the user to create detailed 3D parts, complex surfaces and assemblies based on 2D sketches, among other numerous facilities (Dassault Systems, 2016). This software was selected for this research due to the ease of generating complex parts that can be easily exported to other software as is the case of SimWise. It was also selected since it was available for this project. SOLIDWORKS was used to design realistic limbs and segments of the body according to Winter's anthropometric parameters of weight and height, at the same time of keeping them simple enough for simulations to run in the virtual environment without generating a large computational burden. It was also used to design the exoskeletons that are attached to the humanoid to support the lower body; and finally, to design the wheel walker and additional supports such as crutches that are necessary for gait stability.

Selection of a software to perform the humanoid and exoskeleton models was performed looking for a user friendly interface that allows the creation of joints, actuators, controllers and sensors, simulations of kinematics and dynamics of the system, and the easy integration with MATLAB. Some of the available software included the possibility of modelling musculoskeletal systems, however, this was not the focus of this research and would considerably increase the complexity of the system.

	SimWise	OpenSim	Simechanics	ADAMS
Possibility to import CAD parts	X	X	X	X
Graphic user interface to create joints, actuators, controllers and sensors	X		X	
Possibility to communicate with MATLAB	X	X	X	X
Musculoskeletal modelling		X		
Kinematic and dynamic simulations	X	X	X	X
Interaction with ground	X			X

SimWise 4D was chosen since it complies with the requirements mentioned and includes a friendly graphic user interface. It is a virtual environment created by MSC Software Corporation for the design and engineering of 3D parts and assemblies. It is possible to generate and simulate systems which react in a realistic way to external forces such as gravity and contact forces with other elements. This is done through the simulation of kinematic and dynamic motion of the system. Additionally, different actuators can be represented through constraints with the possibility of configuring them with specific characteristics, such as joint limits and axis rotation. Further, it allows for changes in height or weight of parts, to test a range of systems in a straightforward manner, whereas if a mathematical model was used, calculations for different coefficients would be needed every time there is a change in the design.

SimWise also calculates accurate, physics based, engineering data which can be used to verify the operation of the system while displaying animations to provide visual feedback, useful to understand how the design works. Finally, but most importantly, SimWise can be

integrated effortlessly with MATLAB Simulink through a pre-defined block which represent the mechanical system (Design Simulation Technologies, 2016).

In this project, SimWise was used for three main purposes, to assemble the human like model from the segments created in SOLIDWORKS and couple them with appropriate kinematic characteristics. Further, to measure torques, orientations and positions of the joints and links, these values can be sent to MATLAB to perform the necessary computations to control the exoskeleton and humanoid. And lastly, to visualize the motion of the humanoid, exoskeleton and wheel walker, interacting with external forces and disturbances in a realistic environment.

SimWise simulation settings like tolerance and integration time can be configured according to user's need. In this project, tolerance for position was set to 1 millimetre for orientation to 0.5 degrees, for overlap to 1 millimetre, and for assembly and bond to 0.1 millimetre. Regarding time integration, a fixed step Kutta-Merson integrator with a step size of 0.001 seconds was selected, while animation frame time is 0.01 seconds. These parameters were selected after several tests trying to maximise performance while minimising simulation time.

MATLAB is an environment created by MathWorks for interactive programming using high-level language, engineering numerical computations, graphics and tools for data visualisation, and add-on toolboxes for a wide range of engineering and scientific applications. Simulink is the block diagram environment integrated with MATLAB, useful for model-based design. It enables the communication with SimWise and includes tools such as Stateflow, user defined embedded functions, and integration with other add-on toolboxes such as the control systems one, which includes the Fuzzy Logic toolbox (The MathWorks Inc, 2016c).

Simulink Library Browser includes continuous and discrete dynamics blocks, algorithmic blocks and structural blocks. It is also possible within Simulink to build customized functions by using blocks or incorporating hand-written MATLAB functions, or other languages code into the model. It is also possible to include add-on products with components for PID control and fuzzy logic control (The MathWorks, Inc, 2016b). The Simulink environment was used in this research to connect all the control elements such as the finite state machines created in a state-flow form, fuzzy controllers, and embedded MATLAB functions; and incorporate them with the plant in SimWise. The main advantage of using this software is that the communication channel with SimWise is already built-in and easy to use.

Stateflow is an environment included in Simulink useful for modelling and simulating combinatorial and sequential decision logic, based on state machines. Within this environment it is possible to model how the system reacts to events, time-based conditions, or external input signals, therefore, designing logic for supervisory control, task scheduling, and fault management applications is straightforward. Stateflow includes the animation of state machine

as well as static and run-time checks to test design consistency and completeness (The MathWorks, Inc 2016c).

In this research, Stateflow was used to program the finite state machines to coordinate the activation of different states; each state is a portion of a fundamental motion task such as walking, standing, and sitting, among others. During each state, lower level controllers in the form of PID, or fuzzy controllers received different inputs to be used as references.

The Fuzzy Logic Toolbox contains applications and a Simulink blocks for the analysis, design and simulation of systems based on fuzzy logic. It includes functions such as fuzzy clustering and adaptive neurofuzzy learning (The MathWorks, Inc, 2016a). It was used in this research to represent fuzzy controllers to generate the necessary torque to produce joints rotation according to a desired trajectory.

## 2.4.2 Humanoid modelling

For the purpose of this research, a humanoid of 80 kilograms and 1.7 meters in weight ( $W$ ) and height ( $H$ ), respectively, was considered. The length of each segment of the humanoid model was calculated basing on human average dimensions given by Winter, (2009), as shown in the diagram in Appendix A, and by segments' mass percentages in Table 2.2. Several humanoid models were created, where all of them complied with dimensions stated above. In the first stage of this research; a simpler humanoid model, whose segments were considered as truncated cones, was developed. However, in order to have a more realistic model, the different segments of an existing humanoid model (Cordero, 2012), were modified in SOLIDWORKS. The modifications were performed to create solid parts from the existing surfaces, to align each part origin to the 'world' origin in order to ease the creation of joints in the next stage, and finally, to amend their magnitudes according to Winter, (2009). Final dimensions for the humanoids are shown in Table 2.3.

Once each segment was generated, they were exported to the SimWise virtual environment and constraints were created, considering the anatomical position of joints, e.g. hip, knee and ankle constraints were aligned in the frontal plane. For simplification purposes, humanoid models created in this project have 14 joints of the 32 major degrees of freedom (DoF) of the human body, when considering rigid toes and fingers. This number of joints allows the assembled humanoid to move in the sagittal and frontal planes,  $y$  axis and  $x$  axis respectively; while transversal plane,  $z$  axis, is blocked. The  $x$  axis is represented in red,  $y$  axis in green, and  $z$  in blue throughout this thesis. From the 14 joints, 6 of them are free to move.

SimWise has multiple options for constraint creation, those used in this research are revolute motors, revolute joints, and rigid joints. Table 2.4 shows the humanoid joints along

with the body segments connected through them, the number of joints in the humanoid, and the axes on which they rotate.

Table 2.2 Winter's humansegment's mass percentage (Winter, 2009)

Body Segment	Mass Percentage
Hands	1.2%
Forearms	3.2%
Upper arms	5.6%
Feet	2.9%
Lower legs	9.3%
Upper legs	20%
Head and neck	8.10%
Trunk	49.70%

Table 2.3 Humanoid model dimensions (Winter, 2009)

Body segment	Mass(kg)	Length(m)
Hand	0.48	0.202
Forearm	1.28	0.36
Upper arm	2.24	0.295
Foot	1.16	0.12
Lower leg	3.72	0.48
Upper leg	8	0.54
Head and neck	6.64	0.35
Trunk	28	0.575
Pelvis	11.6	0.25

Table 2.4 Humanoid model joints

Joint name	Link between	Quantity	Axis of rotation
Shoulder	Trunk - Forearm	2	Y ( flexion / extension)
Elbow	Forearm – Arm	2	X ( flexion / extension)
Wrist	Arm - Hand	2	X ( flexion / extension)
Neck	Head-Trunk	1	Y ( flexion / extension)
Waist	Trunk-Pelvis	1	Y ( flexion / extension)
Hip	Pelvis - Thigh	2	Y ( flexion / extension)
Knee	Thigh - Calf	2	Y ( flexion / extension)
Ankle	Calf- Foot	2	Y (dorsiflexion / plantar flexion)

Figure 2.4 shows the frontal and lateral views of the humanoid model developed and used throughout this research. Humanoid model is presented in a swinging posture, showing the 3 DoFs per leg that can be actuated.

It is important to mention that SimWise also allows the user to select joint limits, which in this case were set according to human restrictions as in Low, (2011). Hip joint is able to flex from -30 to 120 degrees, knee joint from 0 to -135 degrees and ankle from -50 to 20 degrees, as shown in Figure 2.5. Also, as mentioned before, friction and restitution coefficients are enforced for parts which are set to collide within the virtual environment, as it is the case of shoes and the ground, or pelvis and seat.

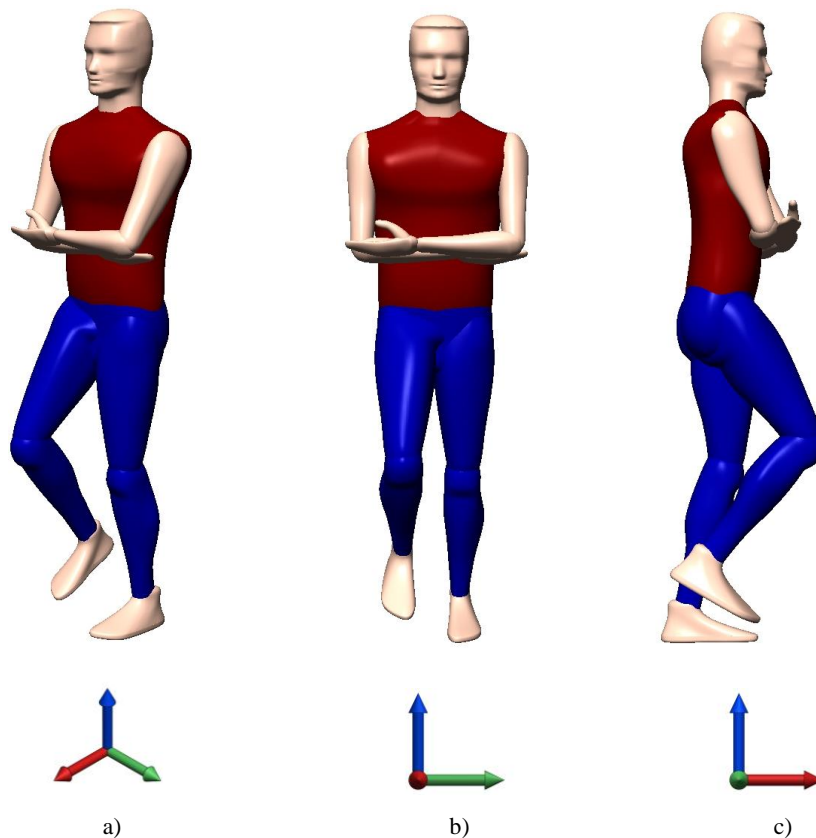


Figure 2.4 Humanoid model: a) Isometric, b) frontal and c) lateral views

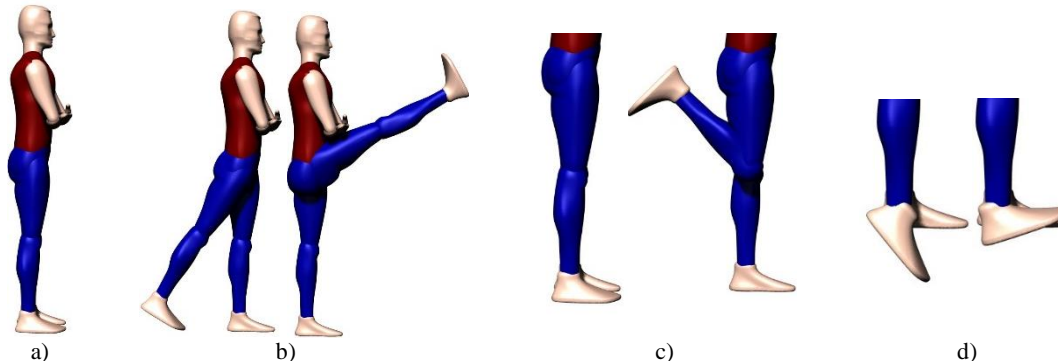


Figure 2.5 a) Initial (zero) position and ranges of motion for b) hip, c) knee and d) ankle.

## 2.4.3 Exoskeleton for paraplegic patients

### 2.4.3.1 CAD modelling of hybrid orthosis exoskeleton

For the first part of this research an exoskeleton was designed such that, in combination with FES, can enable the restoration of gait in paraplegic people. The purpose of the exoskeleton frame was to follow the flexion and extension motions of the legs in the admissible range, i.e. the motion in the sagittal plane. Also, it was required to prevent rotation in the frontal and horizontal planes to simplify the control of the system. Finally, to stop joint motion in the

sagittal plane through the use of brakes during specific phases to generate different postures needed to complete the walking cycle, and decrease muscle fatigue. This exoskeleton was therefore considered semi-passive, since it does not generate motion but restrain it as needed.

In this case, the exoskeleton frame does not include conventional actuators since the patient's legs were used to generate the motion with the help of FES. Actuation is to be provided by electrodes placed in the skin on top of the main muscles of the thigh hamstrings muscles which when activated by FES, generate flexion of knee and in turn of the exoskeleton itself. Motion of hip joint is a consequence of knee flexion as in the Spring Brake Orthosis; and the ankle joint is free to move in the admissible range.

For the purposes stated above, off the shelf orthoses were modelled in SOLIDWORKS. Four components were designed for each leg and modifications such as the addition of both structural and articulation components were done so that they could be assembled to the rest of the exoskeleton. Interface elements were also added to enable the frame to be fastened to the chest and lower segments of the humanoid body. Dimensions of these components correspond to those of the humanoid, and polymers and aluminium comprise the materials used to ensure the mass is kept as low as possible.

The parts were exported to SimWise, and constraints were created, firstly to generate 6 revolute joints free to move in the sagittal plane within the admissible limits, and secondly, to create 6 rigid joints that act as brakes to stop motion when needed. Finally, to generate 2 revolute motors for knee joints to be actuated by torque representing the electrical stimulation. The first 12 joints were created in pairs, one revolute joint and one rigid joint, for each hip, knee and ankle joint.

Brakes considered for this exoskeleton model are Electro Release Brakes by Warner Electric. This type of brakes provides braking action with the removal of electrical power. They are ideal for this application since this capability ensures that the brakes are always active and are deactivated only when the controller sends the appropriate signal, once all the safety conditions are met. In order to release the brakes, a direct current must be applied to generate a magnetic force which will attract the moving armature and allow the free rotation of the axis in the required instant, e.g. after the hip is moved by the inertia generated by knee rotation during the swing phase (Gharooni et. al., 2001).

Table 2.5 shows the different components of the exoskeleton including constraints used in SimWise to represent them, the structural parts to which they were assembled to, the quantity of joints in the lower body exoskeleton, and the weight of each part.

Figure 2.6 shows frontal and lateral views of the exoskeleton model developed and used for this stage during right leg swing.

Table 2.5 Exoskeleton joints

Exoskeleton component	Constraint type	Between	Quantity	Weight (kg)
<b>Hip Joint</b>	Revolute joint	Walker - Thigh Support	2	1.75
<b>Hip Brake</b>	Rigid joint	Walker - Thigh Support	2	
<b>Knee Joint</b>	Revolute joint	Thigh Support - Calf Support	4	1.57
<b>Knee Brake</b>	Rigid joint	Thigh Support - Calf Support	2	
<b>Knee Motor</b>	Revolute motor	Thigh Support - Calf Support	2	
<b>Ankle Joint</b>	Revolute joint	Calf Support – Shoe	4	0.3
<b>Ankle Brake</b>	Rigid joint	Calf Support – Shoe	2	

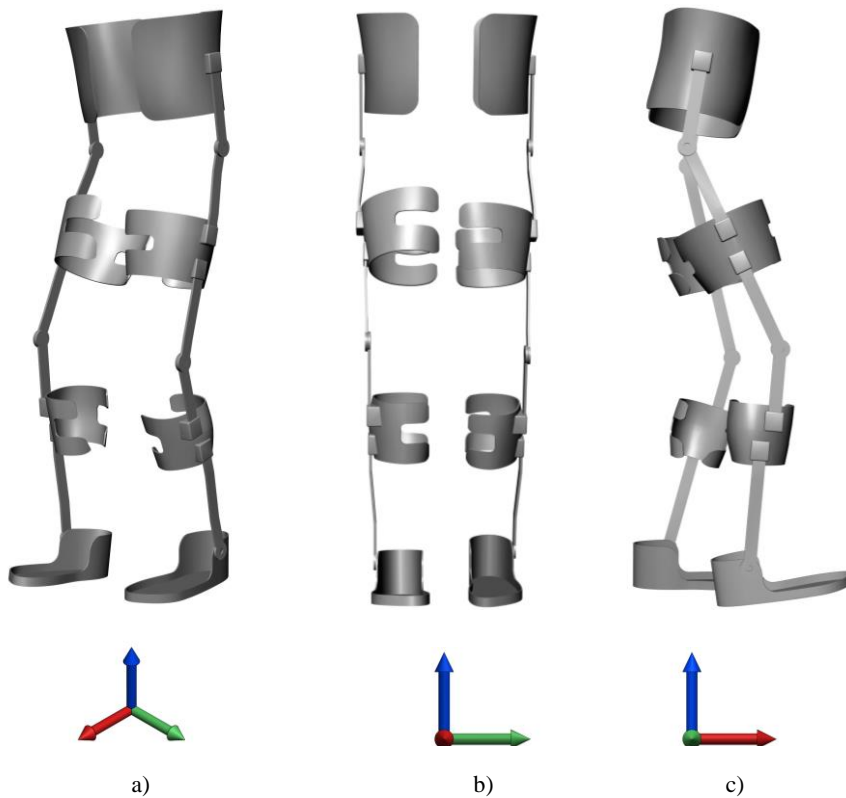


Figure 2.6 Exoskeleton model: a) Isometric, b) frontal and c) lateral views

In the virtual environment, the exoskeleton was attached to the humanoid at waist and feet through rigid joints representing belt and shoe straps, while leg interface systems were set to collide with the humanoid legs to simulate straps, but allowing the legs and support to move independently.

### 2.4.3.2 CAD modelling of wheel walker

A wheel walker was drawn in SOLIDWORKS based on the design of a Rifton Pacer Gait Trainer to provide support to the user, in addition to producing the motion that a healthy person would generate by leaning forward. This walker is based on the concept of a baby walker since it partially carries the body and the exoskeleton using a harness while standing or walking. The height of the wheel walker is selected depending on the length of the user's lower body. In this design, the upper body is held fixed in a constant angle, so the forward movement, normally generated by the tilting of the upper body during the walking cycle, is constrained with this configuration (Rifton, 2014).

The walker is equipped with actuators at the wheels, which generate the necessary forward motion to complete the walking manoeuvre. To represent these, revolute motors in the sagittal plane were created in SimWise at each of the 4 wheels. These constraints were actuated by angular velocity during specific phases of the gait cycle. The weight of the wheel walker is 24 kilograms according to Rifton manufacture specifications. Figure 2.7 shows the wheel walker model and Figure 2.8 shows the humanoid wearing the exoskeleton and the wheel walker.

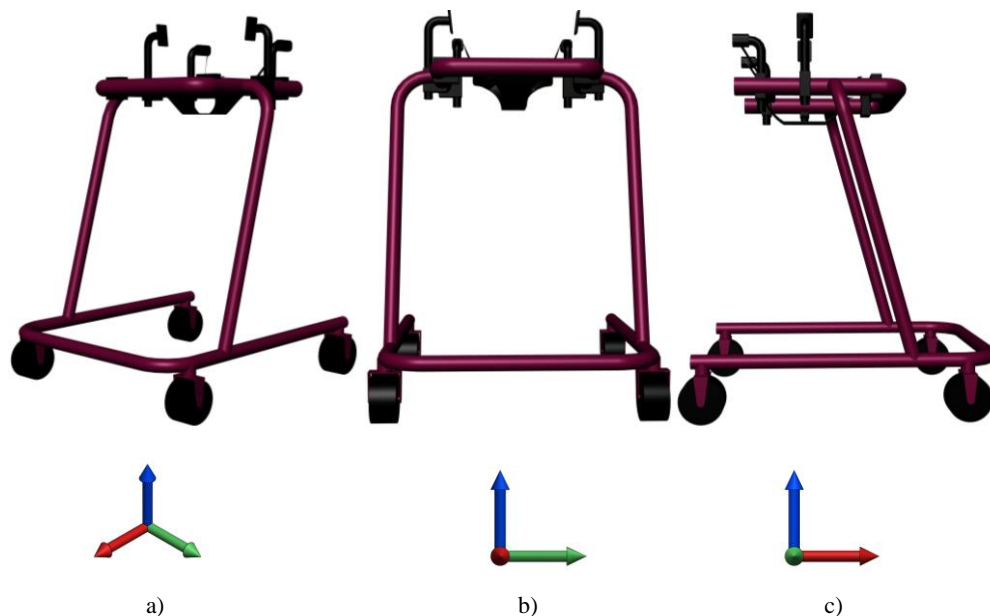


Figure 2.7 Wheel Walker: a) Isometric, b) frontal and c) lateral views

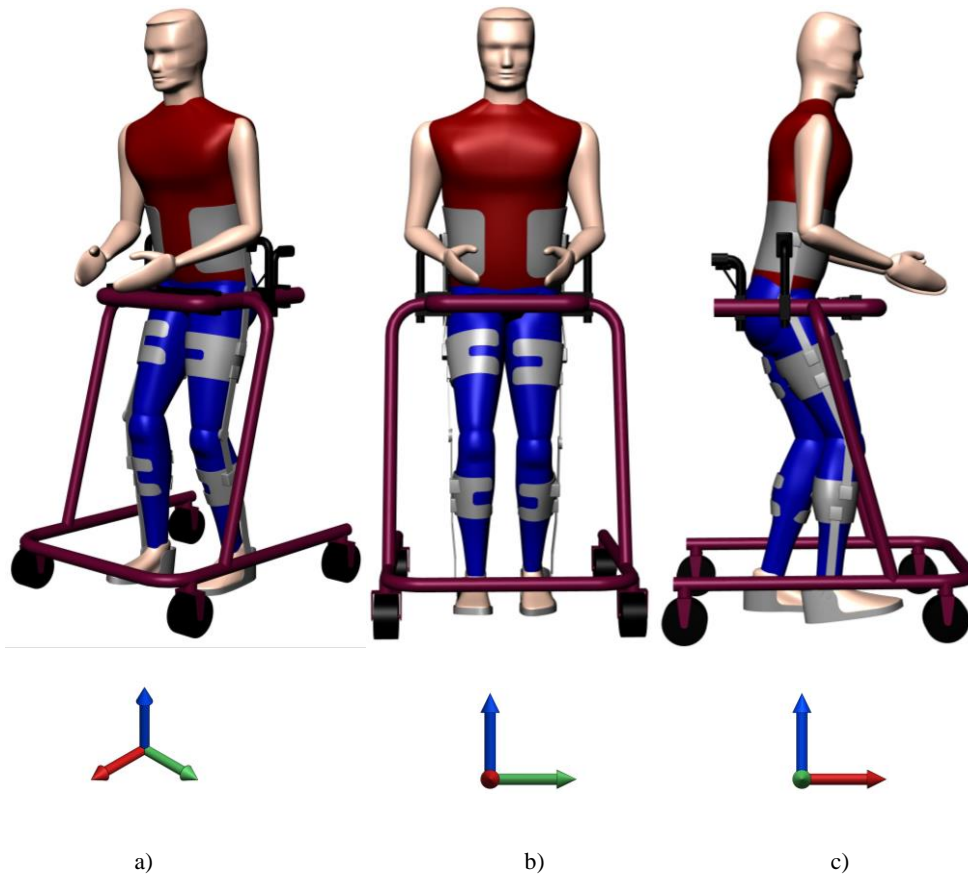


Figure 2.8 Humanoid wearing exoskeleton and wheel walker: a) Isometric, b) frontal and c) lateral views

#### 2.4.4 Exoskeleton for elderly and paraplegic patients assistance

The second section of this research contemplates the use of an actuated exoskeleton to assist the elderly in basic mobility tasks. Such exoskeleton needs to be lightweight and “transparent”, meaning that it should be able to follow the motion of the user smoothly when not actuated, and additionally complete the motions properly when actuated, by supplying the necessary torque. The exoskeleton model used for this section was designed by PCM, Proyecto Control Montaje, S.L. as part of the EXO LEGS project (Virk, 2014, Miranda-Linares and Tokhi, 2015).

The CAD model was modified using SOLIDWORKS to simplify it; the resulting system has 16 parts per leg, 3 parts for the belt, 4 for the thigh component, 5 parts for the leg component and 4 for the shoe. These parts were later exported to SimWise and linked by 3 actuated revolute motors (A) and 3 passive (P) revolute joints per leg, as well as 2 prismatic (Pr) joints per leg used to adapt the exoskeleton to humanoid dimensions, specifically, length of thigh and calf. These prismatic joints were configured offline, which means that they were

set in the necessary length before the simulation. The assembled exoskeleton is shown in Figure 2.9.

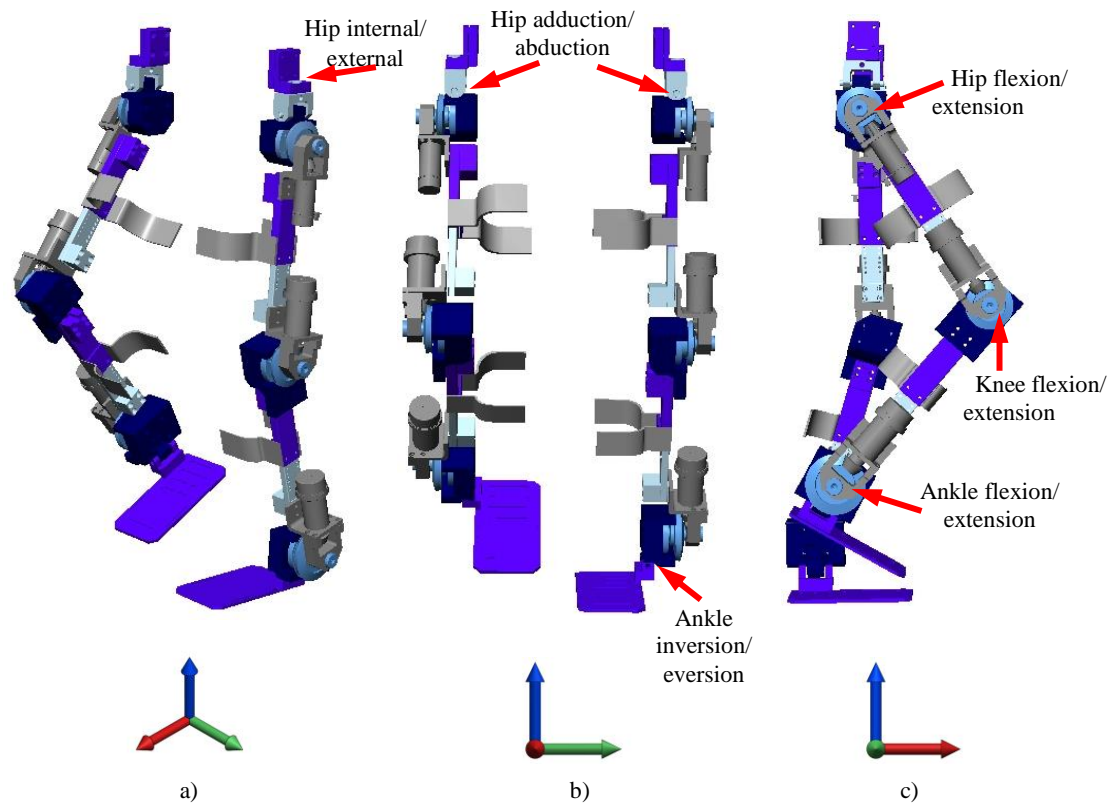


Figure 2.9 EXO LEGS exoskeleton: a) Isometric, b) frontal and c) lateral views

Actuated joints are hip, knee and ankle, in the sagittal plane, while passive joints include hip in frontal and horizontal plane, and ankle in frontal plane. Joints can be set to be actuated by orientation or torque, meaning that either orientation or torque trajectories can be sent to each of them in SimWise. For the passive joints, a fixed orientation value was sent in order to keep a constant angle. The rest of the parts were kept together through rigid joints.

Each component mass was specified in SimWise so that each leg weights 15 kilograms, the same as the experimental prototype. Total weights per exoskeleton section, e.g. thigh support, shoe, leg support, were indicated by the designers, and respected in this research, although some smaller component's weights may vary since the individual weight was not indicated by PCM.

In the virtual environment, the exoskeleton was attached to the humanoid at waist and feet through rigid joints representing belt and shoe straps, while legs interface systems were represented by bars which were attached to the thigh and leg supports, these were set to collide with the humanoid legs, similarly to the previous exoskeleton.

Motors considered for the prototype, and represented by actuated revolute joints in SimWise, were selected by PCM based on torque requirements to provide 30% support while performing basic mobility tasks. For hip joints, motors used are Maxon flat brushless, 70 watt,

EC45 while for knee and ankle joints four motors used are Maxon flat brushless, 100 watt, EC60. These are coupled with planetary gearheads to reduce velocity and increase torque.

For hips, GP52C gearboxes with reduction of 19:1 (3-15 Nm) were selected, while for knee and ankle joints, GP42C gearboxes with reduction of 53:1 (4-30 Nm) were chosen. Additionally, bevel gears are used at each joint to further reduce velocity with a gear ratio of 3:1, but mainly, to decrease the lateral protrusion of the motors. With this reduction and motor characteristics, hip joints are able to generate a maximum nominal torque of 17.97 Nm and knee and ankle joints 20.38 Nm.

All motors have an integrated incremental encoder MILE with 1024 counts per turn, 2 channels, maximum operating frequency of 500 kHz and maximum speed of 6000 rpm. Controller cards EPOS2 50/5 are also integrated in the system to be able to send and receive data from the encoder and to the motor as well as from the computer through USB port, to ease experimental tests (Maxon, 2016). Figure 2.10 shows the humanoid wearing the EXO - LEGS exoskeleton.

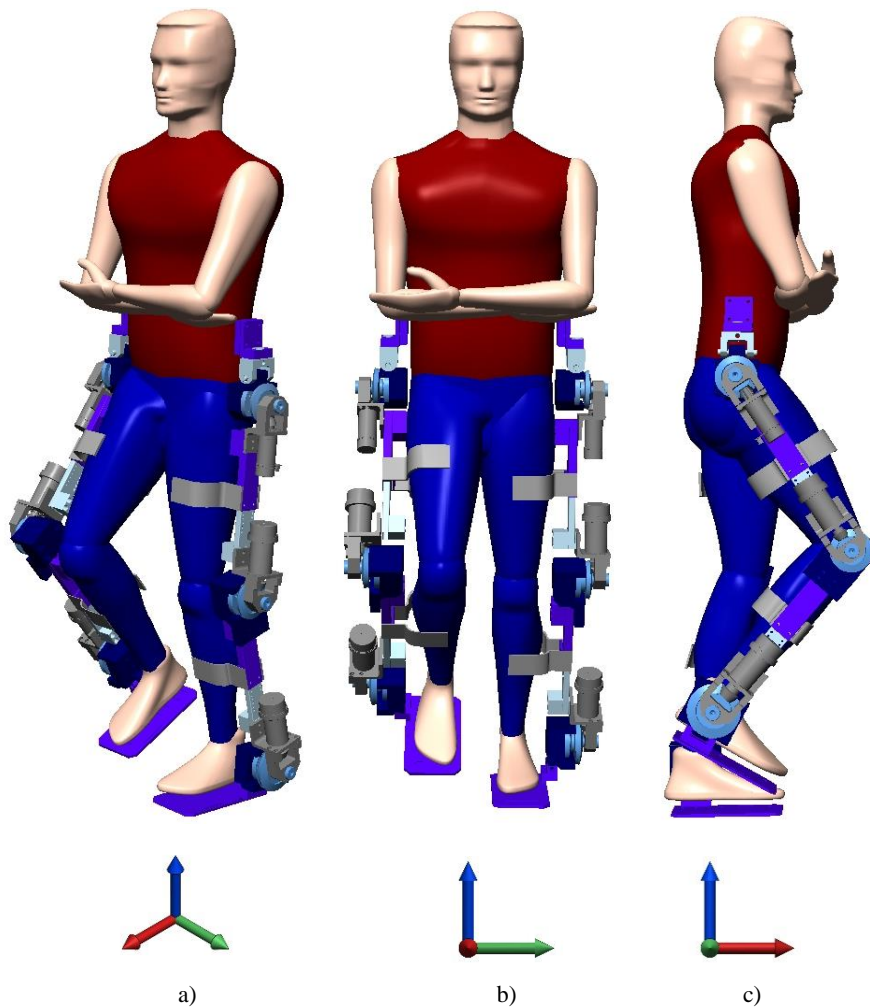


Figure 2.10 Humanoid wearing exoskeleton: a) Isometric, b) frontal and c) lateral views

In the virtual environment, orientation meters were added at each hip, knee and ankle joint to get feedback from the system and send it to the controller. Additionally, position meters are added at each segment and contact force with ground and seat were also monitored.

It is important to mention that for part of this research, feet are free to move, therefore they are able to interact with the ground. Considering the latter, balance had to be observed and control techniques were used to maintain equilibrium. Friction parameters were set according to the corresponding materials.

### 2.4.5 Integration of models in SimWise 4D and MATLAB Simulink

Being able to communicate the humanoid and exoskeleton model in SimWise, with MATLAB, was of outstanding importance for this research, since it enabled the possibility of having a closed-loop control system. Moreover, with the variety of tools that MATLAB possesses, it is possible to evaluate different control techniques and validate their functionality using SimWise without the need to build a prototype in the early design phases.

SimWise software was selected mainly because it has the capability of sending and receiving data to and from MATLAB Simulink, with just inserting one block called SWPlant. Within this block, it is possible to browse and select the SimWise file with .WM3 extension. The controls of revolute motors created in SimWise appear as inputs, and meters that represent sensors as outputs, therefore the necessary items can be easily selected.

As mentioned in previous sub-sections, actuated joints are represented by revolute motors; these can be actuated by orientation, torque, angular velocity or angular acceleration. For most cases in this research, the torque option is selected, hence, when inserting a control for the joint, a slider named “Torque of Joint *Name*” is created. This control then appears as input in the SWPlant Simulink block.

Likewise, when selecting any joint, a meter of orientation, angular velocity, angular acceleration, force, torque or displacement, can be inserted. When selecting a part, a meter of position, velocity, acceleration, linear momentum, orientation, angular velocity or angular acceleration can be inserted. And when selecting two parts, it is possible to insert a meter of contact force, contact impulse, friction force, closest distance and interference. For all these, it is possible to select the  $x$ ,  $y$  or  $z$  component in the SWPlant Simulink Block, while for velocities, accelerations, forces and torque, the resultant or magnitude is also available.

Once the inputs and outputs have been selected, it is necessary to connect the SWPlant Simulink block to a demux at the output and a mux at the input with the correct number of signals. Once the signals are available in Simulink, it is possible to link them to scopes or controllers in the form of stateflow charts, fuzzy controllers or embedded MATLAB functions.

Figure 2.11 shows the SWPlant and the way in which the SimWise file and input and output signals can be selected. Figure 2.12 shows a simple example of how the SWPlant can be connected to a stateflow chart in Simulink.

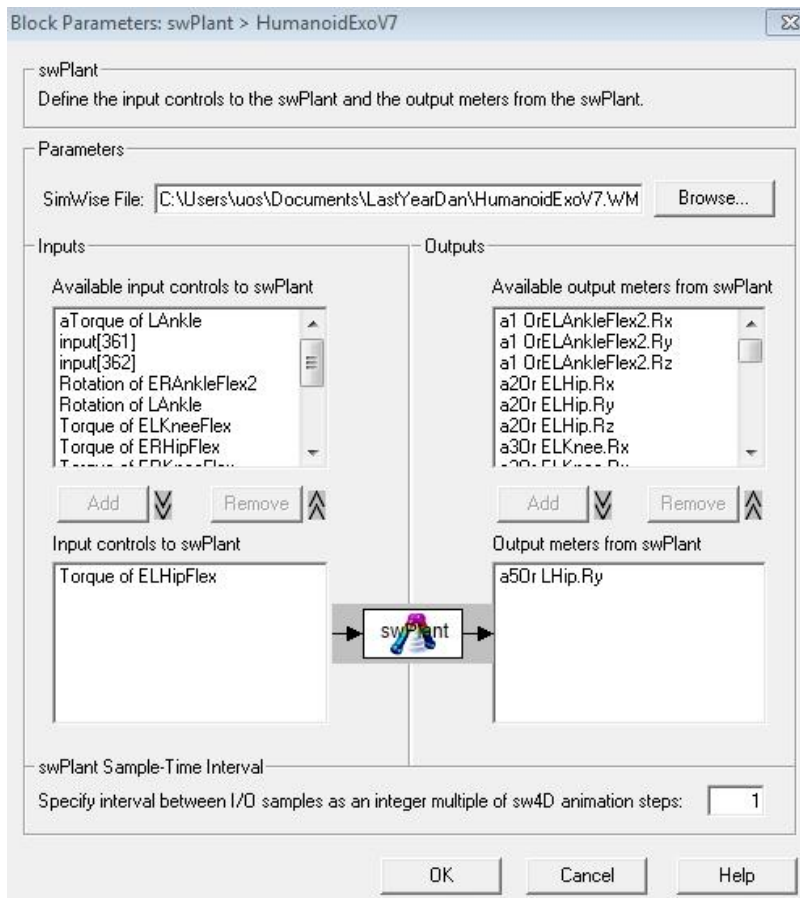


Figure 2.11 SimWise Plant

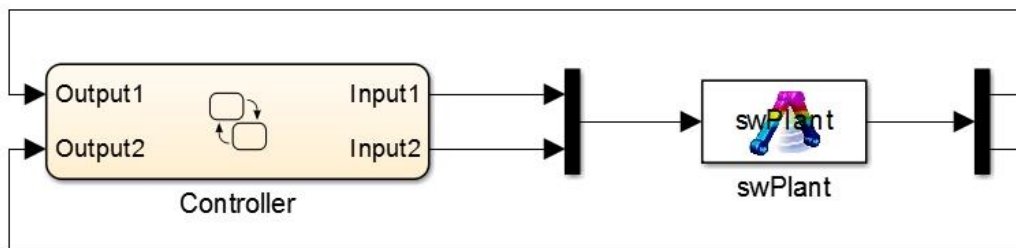


Figure 2.12 Example of Simulink implementation of SW Plant

## 2.5 Summary

This chapter has presented a background on mobility issues and a detailed review of the main components of exoskeletons including frame, sensors, actuators, power supplies and control techniques, along with the main challenges that this research area faces nowadays.

The methodology used to develop CAD models of a humanoid, a hybrid orthosis exoskeleton, an actuated exoskeleton and a wheel walker, to be used in this research, was presented. These elements will be used to simulate in the most realistic manner, the behaviour of the models while being controlled, with the objective of restoring or aiding fundamental mobility tasks in paraplegic or elderly people. Additionally, the components of the EXO-LEGS prototype, whose CAD model is used in part of this research, have been introduced.

A description of the capabilities of the software used for the aforementioned purpose was included, along with the justification of the selection of the exoskeleton components such as frame, strapping components, actuators and sensors, which are represented in the virtual environment.

Finally, the basis of the methodology used to integrate SimWise virtual environment to MATLAB Simulink is presented. It is important to mention that the developments portrayed in this chapter are of utmost importance for this research since they provide the platform on which the controllers could be tested.



# CHAPTER 3

## Low and middle level control of hybrid exoskeleton and wheel walker for paraplegic gait in straight line

### 3.1 Introduction

The assistive system generated in this research and presented in this chapter, is comprised of a computer aided design of an orthotic frame, and a wheel walker, coupled with a dimensionally correct humanoid model within a virtual environment. The purpose of the exoskeleton is to follow the flexion and extension motions of the lower limbs in the sagittal plane, and use brakes aligned with each joint to generate specific postures. These are needed to produce a continuous walking cycle. The wheel walker provides support for patients that are unable to shift their centre of mass from one leg to the other.

The system is controlled using fuzzy logic for the low level or execution control layer, which provides the necessary torque to generate knee joints flexion and extension. In simulation, these motions are generated by revolute motors at humanoid model knees, whereas experimentally, the system could be complemented by a controller whose input is torque and outputs are parameters to develop a signal for application of functional electrical stimulation (FES) through surface electrodes to hamstrings and quadriceps muscles.

The development of a finite state controller (FSC) is included as middle level or translational control layer to coordinate the activation of brakes, wheel walker and FES/torque. States in this FSC are based on the phases of the walking cycle, therefore, an analysis of this motion is performed. Simulations are run as initial validation of the system and several tests are carried out including repeatability, stability and range.

The advantage of this device is that it would not only support paraplegic patients in a walking task, but would use their own muscles as actuation. Therefore, contraction of their lower limbs muscles could be maximised as compared with commonly actuated exoskeletons. Consequently, patients would obtain benefits such as enhancement of blood circulation and general health. Additionally, exoskeleton weight would be reduced, hence, the power requirements would be lower than usual.

### 3.2 Walking cycle

In order to design a controller which is capable of restoring the walking motion in paraplegic people, it is necessary to understand how healthy walking is performed. This section explains the basics of the walking cycle, phases, duration and muscles involved.

The normal walking cycle is composed by 2 phases. Swing phase, also called short phase, and stance phase, called long phase. The former refers to the actual stepping, while the latter refers to the phase in which the foot is in contact with the floor, supporting the opposite leg while swinging. As shown in Figure 3.1, stance is divided into four sub-phases: loading response, mid-stance, terminal stance and pre-swing. The starting position for each sub-phase is right heel or initial contact, left toe off, right heel off and left initial contact respectively (Hsu et al., 2008).

The swing phase, in turn, is divided into initial swing, mid-swing and terminal swing. These phases start with right toe off, both feet aligned, and when right tibia is vertical but not touching the ground (Hsu et al., 2008).

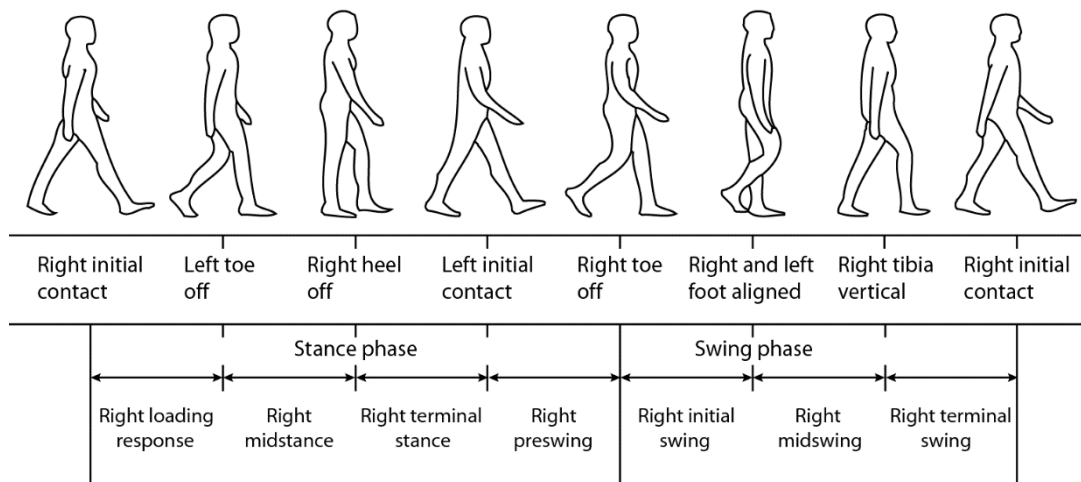


Figure 3.1 Phases of gait cycle, modified from (Hsu, et al., 2008)

During the walking cycle, six major movements can be observed: ankle plantar flexion and dorsiflexion, knee joint extension and flexion, and hip extension and flexion. For ankle movement, the lateral gastrocnemius muscle is responsible for the plantar flexion motion

performed during the last part of the stance phase, while the tibialis anterior muscle is in charge of the dorsiflexion executed during most of the swing phase, and in the first part of the stance phase (Okamoto and Okamoto, 2007).

Biceps femoris, which is part of the hamstring muscle group, is responsible for knee flexion during initial swing, while rectus femoris and vastus medialis, both part of the quadriceps muscle group, perform knee extension during midswing and terminal swing. Gluteus maximus and biceps femoris are responsible for hip extension during stance phase, and rectus femoris contracts to generate hip flexion during swing phase. Finally, vastus medialis, rectus femoris, biceps femoris and gluteus maximus muscles are also responsible for shock absorption during the transition from swing phase to the stance phase (Okamoto and Okamoto, 2007).

Figure 3.2 shows orientation trajectories of ankle, knee and hip joints, as well as the positions of toes and heels in different instants of the walking cycle. This information was of particular importance for the development of the finite state controller.

A complete walking cycle for one leg, i.e. one step with each leg, lasts around 1.1 seconds on average, considering a velocity of 5 km per hour and a stride length of 76 cm. Swing phase usually lasts around 40% of the cycle (Physiopedia, 2016).

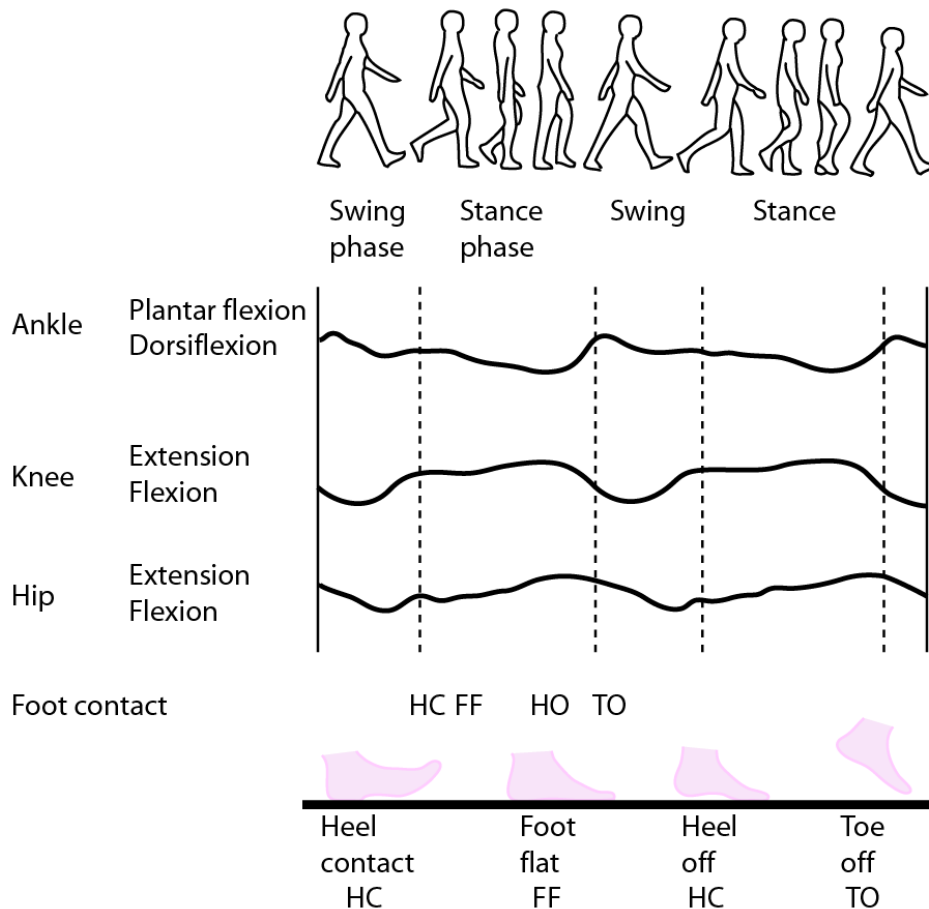


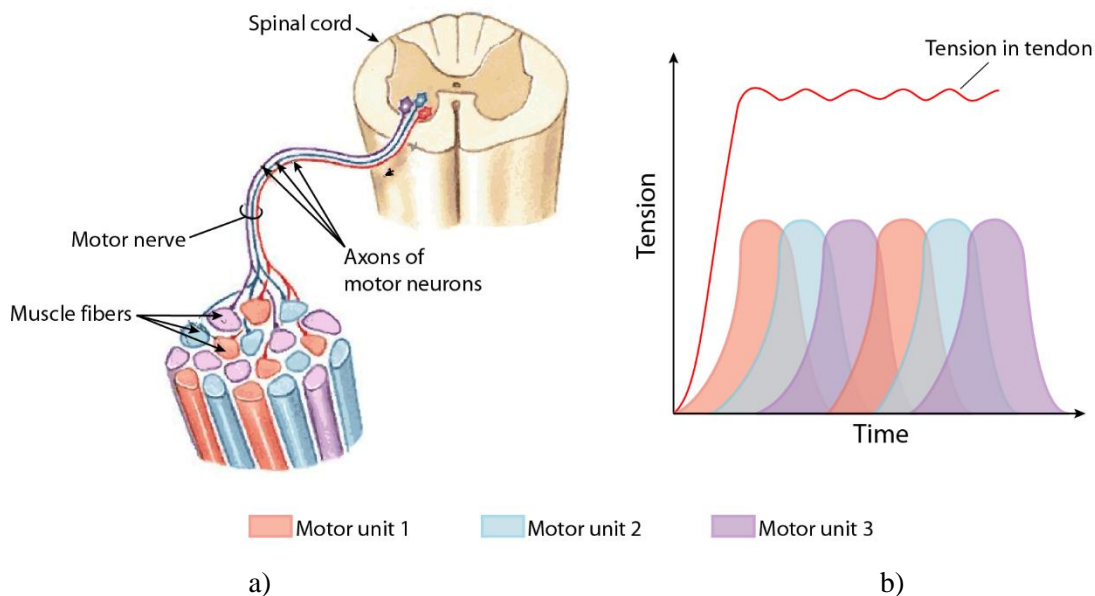
Figure 3.2 Joint trajectories in normal adult walking modified from (Okamoto and Okamoto, 2007).

### 3.3 Muscles operation

To better understand the biomechanics of human body and specifically of basic mobility tasks, as well as techniques such as FES, it is important to understand the function of muscles. Skeletal muscles are formed by thin fibres, around 0.01 millimetres wide and of different lengths, which can reach up to 30 millimetres according to the function they perform. Each fibre is connected to a motor neuron axon by a neuromuscular junction, but not all the fibres are connected to the same motor neuron as can be observed in Figure 3.3 a). The reason is that each motor neuron with the fibres connected to it, constitutes a motor unit, and each of them is activated at different moments of time as shown in Figure 3.3 b) (Basmajian, 1978)

The number of fibres attached to each motor neuron is indirectly proportional to the fineness of the movement. For example, for the human extra-ocular muscles which perform fine motions, each motor unit is composed of 5 or 6 fibres, while for the gastrocnemius medial head which is involved in gross motions, each motor unit is composed of 2000 fibres (Basmajian, 1978).

When a voluntary contraction is triggered, the force produced is directly proportional to the number of motor units recruited and their firing frequency (Merletti and Parker, 2004). To generate a small contraction, only a few motor units are recruited, but while the force that needs to be overcome is augmented, additional motor units are activated by the neurons (Basmajian, 1978).



The number of motor units recruited and their mean discharge frequency of excitation also define the electrical activity in a muscle. Therefore, there is a direct relationship between

the electromyogram (EMG) and the applied force. Electromyography is a graphical representation of the electric potential field that is generated in muscle fibres when a depolarisation occurs at the outer muscle membrane during a contraction.

The depolarisation process is called action potential and is activated when a threshold value is reached, generating a transient voltage phenomenon in a muscle cell membrane. The action potential is activated naturally when the neurotransmitter acetylcholine triggers a change in sodium (Na) conductance. It can also be activated by an external stimulation (Merletti and Parker, 2004)

Electromyography enables the study of muscle function and their exact activation time-sequences in different postures and movements. However, it is important to know that EMG signal's amplitude is affected by muscle parameters such as force and closeness to the source, in addition to fatigue, muscle length, and even temperature (Merletti and Parker, 2004).

Fatigue is defined as a sensation of weakness, pain and decrease in performance. The instant when fatigue is reached is generally associated with the moment in which a task can no longer be performed, an effort sustained, or a contraction force achieved. However, fatigue is a process that develops in time, which changes the motion function temporally. In EMG signals, fatigue can be observed as a progressive slowing during voluntary sustained contractions with the same magnitude (Merletti and Parker, 2004).

### **3.4 Functional electrical stimulation of paraplegic muscles**

Functional Electrical Stimulation (FES), as its name implies, is the application of low electrical stimulation to muscles deprived of nervous control, as it is the case of patients after spinal cord injuries. When applied to a muscle or nerve, FES generates a muscular contraction which may be used to produce a functional movement. This technique has been applied since the 1960's to patients with diverse motor system lesions or diseases like SCI, cerebral palsy, and multiple sclerosis, among others (Kralj and Bajd, 1989).

FES is also used as treatment or therapy to restore or improve mobility in several conditions, some examples are patients with foot drop, or patients who suffered a stroke and lost the capacity to perform the grasping motion. For FES to be effective, peripheral nerves must be intact as, although signals from the brain can be "replaced" by FES, the communication between nerves, and the muscles they activate, is still necessary to perform the motion (Multiple Sclerosis Trust, 2016; Ostock Medical Limited, 2011).

FES is generated by a series of rectangular electrical pulses, which can be symmetric or asymmetric. These pulses are characterised by parameters such as amplitude, pulse width, period, and duration of the pulse train, they are illustrated in Figure 3.4 (Kralj and Bajd, 1989).

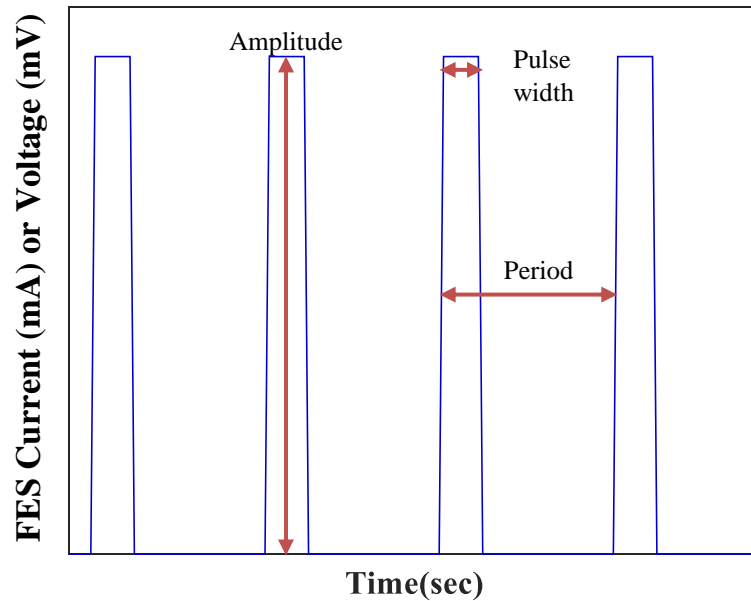


Figure 3.4 FES parameters

Muscle response depends on FES signal parameters. If amplitude of the signal is increased, muscle joint torque increases since new fibres are activated. However, the response is not linear and after a certain range, the muscle is saturated and joint torque no longer increases. The saturation value varies among different muscles and people (Kralj and Bajd, 1989).

Muscle response also depends on the frequency of the signal, if a single pulse is applied, it generates a short twitch of the muscle; if the same pulse is applied once per second, the twitches will repeat and between each twitch the muscle will try to relax. Finally, if the frequency is increased to ten pulses per second, for example, the muscle twitch but it does not have enough time to relax so the joint torque remains almost constant until the muscle is fatigued (Kralj and Bajd, 1989).

FES is transmitted to the human body via a pair of electrodes, there are three main types of electrodes: surface, percutaneous and implanted. Surface electrodes are attached over the skin using an aqueous electrolyte, they can be made of rubber or different metals. Their main benefit is that they are non-invasive, which makes them convenient during evaluation of patient's abilities, training or strengthening of muscles. They are also convenient when it is necessary to adjust their position to find the best response (Kralj and Bajd, 1989).

Due to the skin's high electrical resistance, the stimulus voltage while using surface stimulation must be higher and electrodes must be larger to overcome the barrier to get to the muscle, making the whole system voluminous. Furthermore, the positioning of the electrodes takes time, that could otherwise be used for tests or training. Additionally, the best location of the electrodes varies from person to person; therefore, the positioning process cannot be easily optimized. Finally, when using surface electrodes, deep nerves and muscles are unreachable,

and those which can be stimulated produce a lower force than those activated by other electrode types (Rushton, 1997).

Percutaneous electrodes are placed close to motor nerves using a hollow needle. There are different shapes and materials that can be used, multi-stranded stainless steel conductors are preferred. The main benefit of this electrode type is that, as they are close to the nerve, the stimulation current can be small and is not likely to alter any other muscle function, and they can stay in place from a few weeks to a couple of years depending on the location. The main disadvantage is that movement of the electrode can occur during muscle contraction, thus changing the results of the same stimulus, additionally, it is not possible to see if they are located precisely where they are needed (Rushton, 1997).

Finally, there is the option of implanting electrodes; although their placement is complicated due to the need of surgery. Unlike the other two options discussed above, they can be placed in the exact position where they are needed. Additionally, stimulation using implanted electrodes can be small and controlled. There are disadvantages of this kind of electrodes such as the scarring due to the surgery, as well as risks such as constriction of nerves or other damages that can take place during a procedure (Rushton, 1997).

For engineering research, surface electrodes are the most common since they can be placed with minimum knowledge of nervous and musculoskeletal system, and most importantly, they are non-invasive and rarely produce side effects. However, once it has been demonstrated that the stimulation is good for the patient, implanted electrodes can be considered.

FES' main issue is muscle fatigue, which although is a natural response, appears much faster when a muscle is electrically stimulated than when moved voluntarily (Kralj and Bajd, 1989). The reason for this is that the work needed to generate joint torque is normally divided among motor units, and force is generated in an asynchronous sequence. However, when an electrical stimulus is applied to generate the motion, the same motor units are constantly stimulated instead of the non-simultaneous manner of natural movement (Kralj and Bajd, 1989). Further, when FES is applied to paralysed muscles, these become fatigued quicker since they are different from muscles in a healthy person, due to their reduction in capillary density and their loss of fatigue resistant fibres (Rushton, 1997).

The use of FES to restore standing up motion and gait restoration started around 1960's, relying on the blocking and activation of joints using multiple muscle stimulation, and open loop control strategies (Goldfarb and Durfee, 1996). The main problems with this kind of stimulus were rapid muscle fatigue, falling risk due to lack of stability and support, and variation in stride length due to the inadequate control of joint torque. In order to avoid or lessen these problems, sensors were added to the systems to close the control loop (Goldfarb and Durfee, 1996).

FES standing was possible for a patient by applying bilateral electrical stimulations to the quadriceps muscle for locking the knee (Kralj and Bajd, 1989). Gluteus maximus and medius muscles were used to assist with hip extension, and soleus and gastrocnemius muscles helped for intermittent toe standing, which is beneficial for muscle strengthening. In their system, Kralj and Bajd (1989) included a switch-on command to be activated by the patient, a delay to enable hands placement after the activation, and an auditory signal to indicate the start of a gradual rising of the quadriceps stimulation.

Some FES systems use remaining EMG signals of patients with incomplete SCI to generate the proper stimulus to activate motion. An example of this is a system developed for gait restoration for a 23-year-old individual with C7 motor, and C6 sensory incomplete SCI, who was able to stand but could not initiate a step. The system used voluntary surface EMG signals to activate FES and assist the walking movement during the swing phase. Electrical stimulation was generated using intramuscular electrodes to activate quadriceps, iliopsoas, tensor fascia latae and tibialis anterior. Surface EMG signals were taken from the erector spinae, medial gastrocnemius, gluteus medius, rectus femoris and tibialis anterior; and were later processed using a classifier to generate the activation (Dutta et al., 2008).

A similar system was generated using intramuscular EMG electrodes. Two different kinds of EMG classifiers were used, the first one was based on thresholding, and the second used a pattern recognition algorithm. Although results achieved were better than previous studies, these systems depended on detection of remaining EMG signals. These can easily be obtained from healthy subjects, however, in patients with complete SCI, the signals are non-existent (Dutta et al., 2008).

Another strategy to solve FES issues is to combine it with lower limb orthoses to provide support and decrease the electrical stimulation application time. In addition, the use of orthoses reduces the kinematic complexity of lower limbs by blocking motion in the frontal and horizontal planes (Miyamoto et al., 1999). In 1999 standing-up motion was restored for a patient with complete paraplegia. To achieve this, it was necessary to use an ankle foot orthosis (AFO). The stimulated muscles were gluteus maximus, iliopsoas, rectus femoris, the long head of the biceps femoris and vastus lateralis and medialis. It was also needed to stimulate femoral and superior gluteal nerves using subcutaneous electrodes. Stimulation was applied based on stimulation patterns generated by measuring EMG signals during standing up motion of healthy subjects using the AFO. The stimulation patterns were later formed by rectangular pulse trains of -15V at 20 Hz and 0.2ms pulse width to generate the movement. The result was a smooth standing up motion with a duration of 2 s (Miyamoto et al., 1999).

Another example of hybrid orthosis is the work by Jailani et al., (2011). Hamstrings and quadriceps muscle models were developed using an adaptive neuro-fuzzy inference system (ANFIS), to avoid the difficulty of using a mathematical model due to the complexity, time

varying and non-linear dynamics of muscles. Fuzzy muscle models were inferred through a 5 layer Sugeno ANFIS architecture. Data used was obtained by placing a paraplegic subject in a semi-upright sitting position with the thighs hanging. Electrical stimulation was delivered via two MultiStick™ gel surface electrodes with the cathode positioned over the upper thigh, and anode over the lower aspect of thigh, for quadriceps muscle experiments. And for hamstrings muscle trials, cathode was positioned at the lower thigh, and anode between the tendons of the biceps femoris and semimembranosus.

The isometric force output of the quadriceps muscle was recorded through a force transducer aligned with the anterior aspect of the leg. The position of the leg was recorded instantaneously using MATLAB through an analogue to digital converter (ADC) card. Force and torque were also recorded.

The network architecture for both muscle models consists of three inputs and one output. The parameters of choice as inputs must have an influence on the desired output, therefore, for these models, stimulation frequency, pulse width and stimulation time were selected as model inputs. Time was included since stimulation time has a significant influence on muscle torque, and muscle fatigue occurs when the stimulation time increases.

These muscle models were later integrated with fuzzy controllers and PIDs to determine the pulse width and obtain the torque needed to perform knee flexion and extension. To test the controllers, they were connected to a humanoid model and wheel walker in Visual Nastran 4D (VN4D) software, the predecessor of SimWise. The humanoid received torque of knee joint to generate flexion and extension. Orientation and angular velocity were measured and sent as inputs to the controllers, closing the control loop.

Finally, a Spring Brake Orthosis (SBO) was incorporated to the system to support the user during the swing phase of walking motion, and decrease FES application time to the quadriceps muscles, which generate knee extension. Springs were used for knee and hip flexion, together with brakes at knees and hips, to stop motion in specific stages of the walking cycle. A finite state control (FSC) was used to synchronize the application of FES and activation of brakes, achieving two full steps (Jailani, 2011). The current research uses part of Jailani's work, includes some modifications in the hybrid exoskeleton, and an augmented FSC, in order to test the system for longer periods and under different circumstances. Moreover, the muscle models described above can be used in future work when testing the system experimentally, to generate the necessary FES signal to actuate knee joints.

### 3.5 Control of paraplegic walking with hybrid orthosis

Control of the SimWise humanoid, exoskeleton and wheel walker in this project is mainly based on fuzzy, and a finite state controllers. The control loop can be observed in Figure 3.5, where the CAD design of humanoid, exoskeleton and walker described in Chapter 2, is represented by the SimWise block, the plant to be controlled.

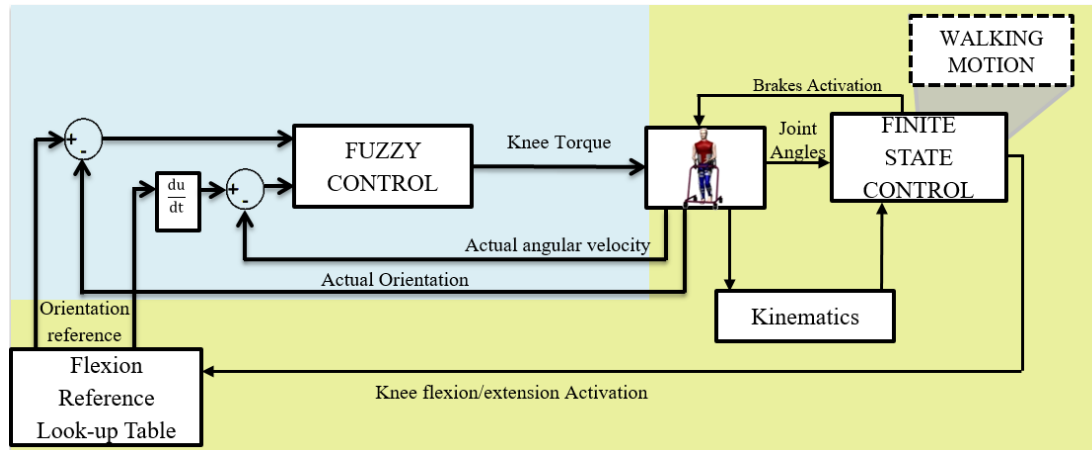


Figure 3.5 Control scheme for simulation of paraplegic walking with FES and hybrid orthosis.

The area in blue includes a fuzzy controller that generates the necessary torque to activate knee flexion and extension of the SimWise humanoid. Its inputs are based on the error and the change of error between the actual knee orientation and angular velocity from the plant, and the orientation reference from the look-up table. These elements were developed by previous researchers and are explained in detail in the following section (Jailani, 2011).

The yellow area outlines contributions of the present work, described in this chapter. Control in this area is performed by a finite state controller, which generates outputs based on inputs such as hip, and knee joint angles from the plant. It also requires information of foot contact with the ground, which can be obtained through kinematics. In turn, the finite state controller is in charge of activating brakes in the exoskeleton to maintain the necessary postures during the walking cycle, as well as generating the inputs for the flexion reference look-up table. The latter provides the reference that the fuzzy controller must follow. A detailed description of the blocks in Figure 3.5 can be found in the following sections.

Figure 3.6 shows the control scheme needed for experimental validation. A fuzzy controller whose output is a specific pulse width would be needed. Along with it, pulse duration and frequency would need to be selected to construct a FES signal to be sent to the user through surface electrodes. These stimuli would generate torque needed to flex and extend the knees.

In order to obtain appropriate FES parameters, the muscle models of hamstrings and quadriceps would be needed to assess the system through simulation. The resulting torque could then be connected to a humanoid model and sensors deliver knee joint orientation and angular velocity as input to the fuzzy controller, thus, closing the control loop.

It is important to mention that Jailani's, (2011) muscle models of hamstrings and quadriceps, and the fuzzy controller which provides pulse width to generate the necessary torque to flex and extend knee joints of a humanoid model in VN4D, were only tested through simulation of one walking cycle, therefore, further validation of the system is required.

Although experimental validation of this system is not part of the scope of this research, it was considered necessary to include a possible solution in this thesis to highlight that the FSC scheme proposed is feasible.

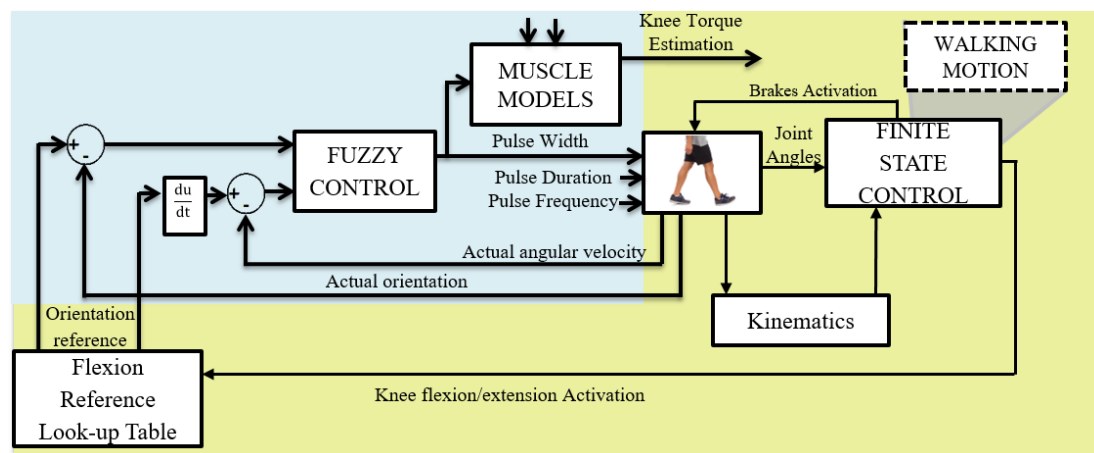


Figure 3.6 Control scheme of experimental validation of paraplegic walking with FES and hybrid orthosis

### 3.5.1 Fuzzy control of knee joints torque

Fuzzy theory is based on the idea that no real system or behaviour is entirely white or black, but a shade of colour in between them. When there is a need to categorise a grey colour, it is characterised as *blacker* or *whiter*, so it still belongs in some degree to both categories. The degree assigned to it will depend on previous experiences on categorisation of colours, and different categorisers will give a different degree of black and white to each grey colour.

Control is the area in which fuzzy logic has had the greatest success since it can be used in applications in which classic control has not been effective or efficient. Many consumer products, including washing machines and rice cookers, as well as industrial applications, involve fuzzy control (Ross, 2010).

The first step in designing a fuzzy controller is to identify variables of the plant such as inputs, outputs and states. Then, it is necessary to partition the universe of discourse into a number of fuzzy sets, and assign a linguistic label to each, such as small, black and quick. The

next step is fuzzification, which is the process of making a crisp quantity fuzzy, i.e. translate it into a membership function (Ross, 2010).

Membership functions are defined to measure the degree to which a numeric data  $u$  belongs to a certain universal set  $U$ . A fuzzy set  $X$ , can then be defined as a set of ordered pairs of  $u \in U$  and its membership degree  $\mu_X(u)$ , where  $\mu_X$  determines if an element of  $U$  belongs to  $X$  and to what degree.

Figure 3.7 shows a triangular membership function as well as the crossover point in which  $\mu_X(u)=0.5$ . Membership functions can be trapezoidal, Gaussian or take several other forms. Scaling factors must be assigned to inputs and outputs to normalise the variables to  $[0,1]$  or  $[-1,1]$  interval (Mahfouf, 2013)

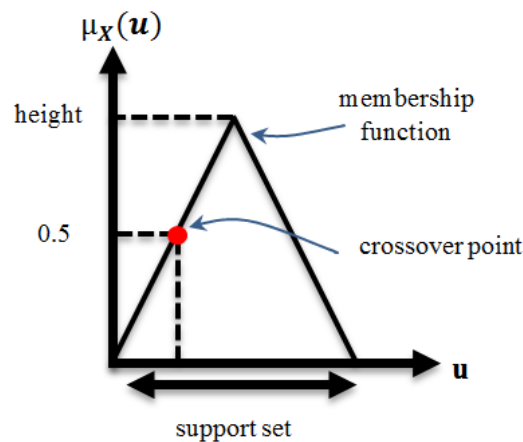


Figure 3.7 Fuzzy membership function

The next step in designing a fuzzy controller is called inference, which involves the mapping or definition of fuzzy relations between inputs and outputs through deductive, if-then rules, based on heuristics. The number of rules depends on the amount of inputs and the number of linguistic variables assigned to each input. Therefore, fuzzy control can handle single input single output (SISO), or multiple input multiple output (MIMO) systems. Each combination of inputs must generate a determined fuzzy output.

If-then rules can be presented in different formats, however, the standard system is composed of inputs, outputs and linguistic variables of the form IF *premise*, THEN *conclusion/restriction*. Rules can also be connected by linguistic connectives such as “and”, “or”, “else”, e.g. IF  $x$  is  $A$  and  $y$  is  $B$ , THEN  $z$  is  $C$  where,  $x$  and  $y$  are inputs,  $z$  is output and  $A, B$  and  $C$  are linguistic variables.

There are two main methods of deductive inference for fuzzy systems based on linguistic rules. Mamdani and Sugeno models. Mamdani method, as described above is formed of linguistic variables in the premises and in the conclusion/restriction:

$$\text{IF } x_1 \text{ is } A_1^k \text{ and } x_2 \text{ is } A_2^k \text{ THEN } y^k \text{ is } B^k$$

Sugeno method or TSK (Takagi, Sugeno and Kang) was created when trying to develop a systematic way to generate fuzzy rules from input-output data. The output in the Sugeno method is not a linguistic variable but a crisp function of the inputs. A typical Sugeno rule has the form:

$$\text{IF } x_1 \text{ is } A_1^k \text{ and } x_2 \text{ is } A_2^k \text{ THEN } y^k \text{ is } y^k = f(x_1, x_2)$$

In order to be able to use the output in any application, linguistic variables must be defuzzified, that is, to convert them to crisp values. Methods such as Centroid of Gravity, Max-Membership, Middle of Maxima, among others, can be used depending on the requirements of the system. In the Sugeno method, the output of each rule is already a crisp value, but the overall output has to be obtained through weighted average defuzzification. Figure 3.8 shows a simple fuzzy control system, where the different steps described above can be seen (Ross, 2010)

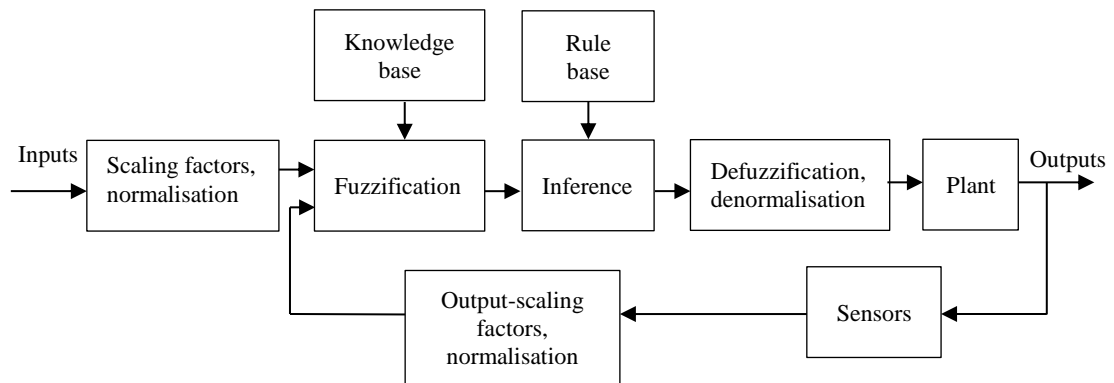


Figure 3.8 Simple fuzzy control system (Ross, 2010)

Hellendoorn and Thomas, (1993), proposed five criteria to evaluate defuzzification methods. The first is continuity, this states that a small change in the input of a fuzzy process should not produce a large change in the output. Secondly, a defuzzification method should result in a unique value for the defuzzified value, which means it should not be ambiguous. The third criterion is plausibility, the defuzzified value should lie approximately in the middle of the support region of the union of the membership functions and have a high degree of membership in it. The fourth criterion refers to computational simplicity, the less time consuming the method is, the more value it has in a computation system. Finally, the last criterion is called the weighting method, which weights the output fuzzy sets, however, this criterion is considered problem dependent (Hellendoorn and Thomas, 1993)

In applications such as the current project, fuzzy theory is useful since the human body is a precise machine, but works inherently with fuzzy phenomena (Belohlavek and Klir, 2011). Therefore, mathematical models would be a very complex option since the system is time-

varying nonlinear. Fuzzy models, on the other hand, can be generated in a relatively easier manner from data, using an inference system like ANFIS.

Moreover, fuzzy systems can better represent human intuition than other techniques, due to its quicker response. Since for this application, the priority is to produce a good response to disturbances than have an extremely precise control action, fuzzy control is an ideal alternative.

Fuzzy control can be used without having a model, and even nonlinear and uncertain systems can be handled using this method. It was also chosen for this research since an accurate control strategy was needed, but only heuristic data was available on the desired behaviour of the controller. Finally, fuzzy logic controllers can be blended in a straightforward manner with other control techniques such as finite state control.

Fuzzy controllers for hamstrings and quadriceps muscle models were developed in previous research by Jailani, (2011). The error between knee orientation ( $\beta$ ), measured between the plant and a knee reference orientation trajectory; as well as the derivative of the error, obtained through the calculation of the difference between knee angular velocity ( $\beta'$ ), measured from the plant, and the derivative of the reference, were used as inputs. The output is the torque necessary to generate knee flexion and extension motions that perform swing phase of the walking cycle, and is sent to the humanoid model in SimWise. These models were not included in this research.

For each controller, five Gaussian type membership functions, normalised from 0 to 1, were designed for each input and output. Gaussian membership functions are used for smoothness. Linguistic variables used are NB: Negative Big, NS: Negative Small, Z: Zero, PS: Positive Small, and PB: Positive Big. In order to control both inputs, 25 rules had to be determined and are shown in Table 3.1. This set of rules allow the activation of one rule with any combination of inputs, they are consistent, continuous and with no contradictions.

Table 3.1 Fuzzy rules for knee joint flexion and extension

$e \backslash \Delta e$	NB	NS	Z	PS	PB
NB	NB	NB	NS	NS	Z
NS	NB	NS	NS	Z	PS
Z	NS	NS	Z	PS	PS
PS	NS	Z	PS	PS	PB
PB	Z	PS	PS	PB	PB

Finally, centroid of gravity method was used for defuzzification to obtain the crisp torque values. Due to the normalisation of inputs and output membership functions, scaling factors were added to adapt the controllers to the different inputs and outputs. Gains used were 0.055 for the error and 0.0025 for the change of error. The fuzzy control scheme is shown in Figure 3.9 where a control loop is used for each leg.



seconds, but the final reference was shortened to compensate for the longer extension time. However, this still would need to be evaluated experimentally to assess if this shortening has any negative effects on joints or muscles.

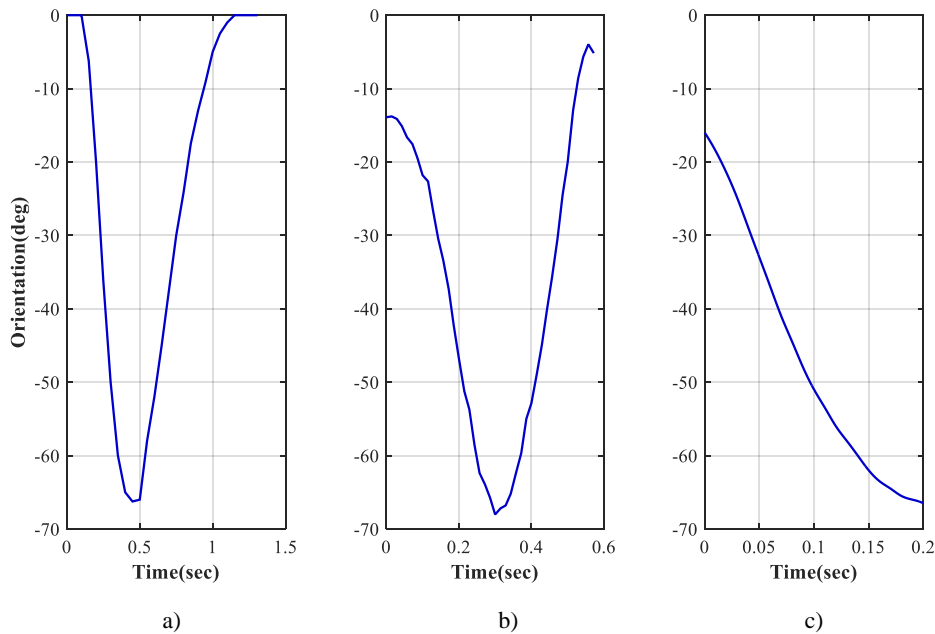


Figure 3.10 Knee joint references considered in a) Jailani's work, b) Winter's work, c) reference proposed.

### 3.5.2 Finite State Control

Automata theory is the study of abstract computing devices or machines. A finite state machine or finite automaton is a conceptual model that involves states with corresponding outputs or actions to be performed, as well as the transitions between them. Conditions to trigger transitions depend on the current state and the input, thus controlling if the system will be taken to the following state. It is also necessary to indicate the initial state in which the system will be placed, and the final or accepting state. One of the advantages of having a finite number of states is that it is possible to implement the system based only on a limited amount of data (Hopcroft et al., 2007).

There are two types of automaton, deterministic and nondeterministic. The first one refers to a system where the transition function specifies only one future state for a combination of current state and inputs. The latter refers to an automaton in which none, one or more future states can be activated with a specific combination of current state and inputs. A finite machine can be represented graphically as in Figure 3.11, where the initial state is indicated by an arrow, other states are represented by circles and the transitions functions are represented by arcs. The latter are activated by the inputs (Hopcroft et al., 2007).

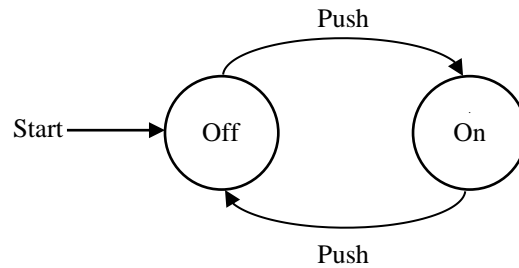


Figure 3.11 Simple finite state machine

A finite state controller (FSC) can be described by the sextuplet  $\{S, I, O, n(s, i), o(s, i), s_0\}$  where  $S$  is the set of states,  $I$  is the set of inputs, also called input vocabulary,  $O$  is the set of outputs or output vocabulary,  $n(s, i)$  is the next-state function,  $o(s, i)$  is the current output function, and  $s_0$  is the set of initial states (MIT, 2011). Where,  $n(s, i)$  maps the current state and inputs to the state in the next sample time  $s(t + 1)$ , and  $o(s, i)$  depends on the current state and input.

As mentioned in Chapter 2, the most popular mid-level controller is by far the FSC, used in Ekso, Rewalk, HAL and many other exoskeleton devices now in the market (Tucker et al., 2015). The reason for this is that FSCs are highly suitable for control of gait due to its sequential operation (Sweeney et al., 2000).

Ekso uses a FSC which includes different states, such as “Start Walk”, “Walking”, “End Walk”, “Standing”, “Sit Down”, “Seated” and “Stand Up” (Kazerooni et al., 2013). Rewalk exo uses states as “Sitting”, “Standing”, “Walking”, “Climb stairs” and “Descend stairs” (Gofeer and Zilberstein, 2013). HAL exoskeleton uses an algorithm in the form of a FSC in which inequalities must be accomplished to activate phases. Two phases are used for walking and five phases to sit to stand and stand to sit (Tsukahara et al., 2010).

Finite state control has also been used in neural prostheses in conjunction with FES. In a past application, the system detects subject’s intention and reads measurement from sensors, so that when conditions are met, the trigger of the FES activation state, is performed (Sweeney et al., 2000).

Most of the FSCs, require a heuristic tuning of parameters to ensure user’s comfort and device’s efficiency. However, one of its disadvantages is that considering that an FSC is required for each mobility task, and each of them involve variables dependant on the activation of transitions between states, inputs detailing the pose of the system, as well as outputs for actuating each joint; the number of tuneable parameters quickly increases (Tucker et al., 2015). However, this issue could be minimised using optimisation algorithms.

In MATLAB, finite state machines can be programmed in the Stateflow environment, graphically, or in Table representation. Stateflow is also capable of displaying state machine animations, and includes static and run-time checks useful for testing design consistency and completeness. Using Stateflow, it is possible to model system's modes of operation as states

and represent the logic for switching between modes using transitions and junctions. There is also the option to model states that execute exclusively or in parallel, in other words, as deterministic or non-deterministic automaton.

A stateflow chart can be added in Simulink and inputs and outputs can be created through the model explorer. In that way, the FSC can be easily connected to the plant in SimWise to get information from the meters. It is also possible to send signals to the flexion reference generator, so that the fuzzy controller starts the motion and send information back to the plant to activate and deactivate brakes.

Programming of the FSC to enable paraplegic walking with the aid of FES and a hybrid orthosis was based on the normal walking cycle. Taking walking cycle phases and sub-phases as reference, a FSC was built using 21 states to activate or deactivate FES/torque, wheel walker actuation, and hip, knee and ankle brakes; depending on the position of feet and orientation of joints, thus generating the necessary postures to produce a walking cycle.

Half of the states activate one leg while the second half activates the opposite one. Differently from the normal walking cycle, in the proposed controller, swinging starts until both feet are flat in the ground, therefore, double support is longer in this configuration for stability purposes.

Table 3.2 shows as reference the normal walking cycle phases and sub-phases along with the actions which delimitate them, it also shows the finite states programmed to coordinate the motion of left and right legs, in addition to the duration of each state during a paraplegic walking cycle. A diagram of the FSC developed in the present work is depicted in Figure 3.12 and can be described by the sextuplet  $\{S, I, O, n(s, i), o(s, i), s_0\}$ , each of these sets are explained below:

The 21 states are represented by the set:

$$S = \{0,1,2,3,4,5,6,7,8,9,10,11,12,13,14,15,16,17,18,19,20\}$$

In order to trigger transitions, and to calculate some of the output functions, eight inputs are required as shown in the input set:

$$I = \{i_{L\ heel\ z}, i_{L\ toe\ z}, i_{LK\ or}, i_{LH\ or}, i_{R\ heel\ z}, i_{R\ toe\ z}, i_{RK\ or}, i_{RH\ or}\}$$

where

- $i_{L\ heel\ z}$  and  $i_{R\ heel\ z}$  are left and right heel positions in the vertical axis
- $i_{L\ toe\ z}$  and  $i_{R\ toe\ z}$  are left and right toe positions in the vertical axis
- $i_{LK\ or}$  and  $i_{RK\ or}$  are left and right knee orientations in the sagittal plane
- $i_{LH\ or}$  and  $i_{RH\ or}$  are left and right hip orientations in the sagittal plane

Heel and toe positions can be either measured or calculated as mentioned in subsequent sections, whereas knee and hip orientations are measured from encoders coupled to the exoskeleton frame joints.

Table 3.2 Walking cycle of paraplegic walking with FES and hybrid orthosis: Right swing

<b>Phase</b>	Stance						Swing							
<b>Sub-phase</b>	Loading Response	Mid-stance				Terminal Stance	Pre-swing	Initial Swing	Mid-swing	Terminal Swing				
<b>Activated by:</b>	Right heel contact	Right foot flat				Heel off		Toe off	Both feet aligned/	Right tibia vertical, no ground contact				
<b>Leg</b>	Right	Left				Right								
<b>State</b>	Release ankle	FK	BA	BH	EK	SK	RH	RA	Flex Knee	Brake ankle	Brake hip	Extend knee	Stop knee	Release hip
<b>Duration</b>	8.9%	50%				5.8%	5.3%		0.1%	29.7%		0.1%	0.1%	
		70%							30%					

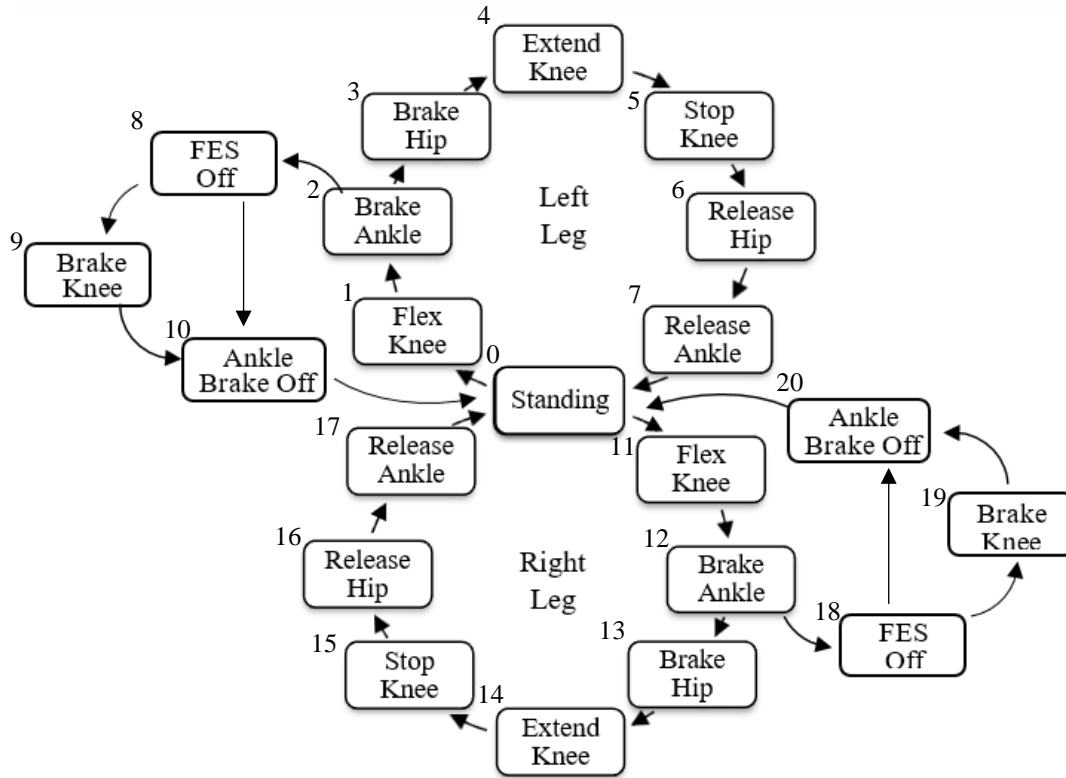


Figure 3.12 Finite state controller of walking motion

The next state or transitions function for the FSC controller is:

$$n(s, i) = \left\{ \begin{array}{l} 1 \text{ if } s = 0, \quad i_{L\text{heel}z} = 0 \text{ mm and } i_{L\text{toe}z} = 0 \text{ mm} \\ 2 \text{ if } s = 1, \quad i_{LKor} \leq -30 \text{ deg} \\ 3 \text{ if } s = 2, \quad i_{LHor} \geq 17 \text{ deg} \\ 4 \text{ if } s = 3, \quad i_{LKor} < -30 \text{ deg} \\ 5 \text{ if } s = 4, \quad i_{LKor} \geq -17 \text{ deg} \\ 6 \text{ if } s = 5, \quad i_{LHor} \geq 17 \text{ deg} \\ 7 \text{ if } s = 6, \quad i_{Lheelz} \leq 6 \text{ mm} \\ 0 \text{ if } s = 7, \quad i_{Ltoez} \leq 6 \text{ mm} \\ 8 \text{ if } s = 2, \quad \text{error} \\ 9 \text{ if } s = 8, \quad i_{LKor} \geq -10 \text{ deg} \\ 10 \text{ if } s = 9, \quad i_{Lheelz} \leq 6 \text{ mm} \\ 0 \text{ if } s = 10, \quad i_{Ltoez} \leq 6 \text{ mm} \\ 11 \text{ if } s = 0, \quad i_{Rheelz} = 0 \text{ mm and } i_{Rtoez} = 0 \text{ mm} \\ 12 \text{ if } s = 11, \quad o_{RKor} \leq -30 \text{ deg} \\ 13 \text{ if } s = 12, \quad o_{RHor} \geq 17 \text{ deg} \\ 14 \text{ if } s = 13, \quad o_{RKor} < -30 \text{ deg} \\ 15 \text{ if } s = 14, \quad o_{RKor} \geq -17 \text{ deg} \\ 16 \text{ if } s = 15, \quad o_{RHor} \geq 17 \text{ deg} \\ 17 \text{ if } s = 16, \quad o_{Rheelz} \leq 6 \text{ mm} \\ 0 \text{ if } s = 17, \quad o_{Rtoez} \leq 6 \text{ mm} \\ 18 \text{ if } s = 12, \quad \text{error} \\ 19 \text{ if } s = 18, \quad o_{RKor} \geq -10 \text{ deg} \\ 20 \text{ if } s = 19, \quad o_{Rheelz} \leq 6 \text{ mm} \\ 0 \text{ if } s = 20, \quad o_{Rtoez} \leq 6 \text{ mm} \end{array} \right.$$

Four outputs are generated for each leg and one for wheel walker motor, therefore the output set is:

$$O = \{o_{LKF}(t), o_{LHB}(t), o_{LKB}(t), o_{LAB}(t), o_{RKf}(t), o_{RHB}(t), o_{RKB}(t), o_{RAB}(t), o_{WW}(t)\}$$

where  $o_{LKF}(t)$  is FES signal activation for knee flexion,  $o_{LHB}(t), o_{LKB}(t), o_{LAB}(t)$  are hip, knee and ankle brakes of left leg respectively,  $o_{RKf}(t)$  is FES signal activation for right flexion,  $o_{RHB}(t), o_{RKB}(t), o_{RAB}(t)$  are hip, knee and ankle brakes of right leg respectively and  $o_{WW}(t)$  is wheel walker activation. The initial state set is  $s_0 = \{0\}$

Each state with its input sets and output functions are described below:

**0 STANDING:** This is the initial state in which the humanoid is in standing position, therefore hip, knee and ankle brakes are on to support this posture. The next state is activated when both feet are touching the ground, and a signal is received from the upper level to start walking. This can be detected in a practical manner with the use of simple contact or force sensors, or through kinematics. The wheel walker is deactivated in this state. Corresponding input set and output functions are:

$$i_0 = \{i_{L\text{ heel } z}, i_{L\text{ toe } z}\}$$

$$\begin{array}{lll} o_{LKF}(t) = 0 & o_{LAB}(t) = 1 & o_{RHB}(t) = 1 \\ o_{LHB}(t) = 1 & o_{WW}(t) = 0 & o_{RKB}(t) = 1 \\ o_{LKB}(t) = 1 & o_{RKf}(t) = 0 & o_{RAB}(t) = 1 \end{array}$$

**1 FLEX KNEE:** In this state, FES is applied to hamstrings and quadriceps to generate flexion of knee. In SimWise, this is simulated through the activation of a revolute motor in the humanoid's knee which receives torque input from the fuzzy controller. Hip and knee brakes are not activated; therefore, knee and hip joints are free to move. Knee flexion causes hip to flex due to the acceleration of the lower leg, this is an adaptation of the working principle of the spring brake orthosis (SBO) (Gharooni et al., 2001). The wheel walker starts moving forward during this state. Input set and output functions for this state are:

$$i_0 = \{i_{LKor}\}$$

$$\begin{array}{lll} o_{LKF}(t) = 1 & o_{LAB}(t) = 0 & o_{RHB}(t) = 0 \\ o_{LHB}(t) = 0 & o_{WW}(t) = 1 & o_{RKB}(t) = 1 \\ o_{LKB}(t) = 0 & o_{RKf}(t) = 0 & o_{RAB}(t) = 0 \end{array}$$

**2 BRAKE ANKLE:** Flexion of knee causes the ankle to flex, generating heel off. It has been estimated that it occurs when the knee is 30 degrees flexed. At this instant, the brake in ankle is activated. Meanwhile FES is still active, causing knee joint to keep flexing towards toe off posture. Brakes are represented by rigid joints in SimWise that can be activated or deactivated through the communication with Simulink. Corresponding input set and output functions for this state are:

$$i_0 = \{i_{LHor}\}$$

$$\begin{array}{lll}
 o_{LKF}(t) = 1 & o_{LAB}(t) = 1 & o_{RHB}(t) = 0 \\
 o_{LHB}(t) = 0 & o_{WW}(t) = 1 & o_{RKB}(t) = 1 \\
 o_{LKB}(t) = 0 & o_{RKF}(t) = 0 & o_{RAB}(t) = 0
 \end{array}$$

3 BRAKE HIP: After toe off, brake in hip is activated along with brake in knee to stop its flexion. FES signal is deactivated to avoid muscle fatigue. This state is active for a single sample time. Input set and output functions for this state are:

$$\begin{array}{l}
 i_0 = \{ i_{LKor} \} \\
 \begin{array}{lll}
 o_{LKF}(t) = 0 & o_{LAB}(t) = 1 & o_{RHB}(t) = 0 \\
 o_{LHB}(t) = 1 & o_{WW}(t) = 1 & o_{RKB}(t) = 1 \\
 o_{LKB}(t) = 1 & o_{RKF}(t) = 0 & o_{RAB}(t) = 0
 \end{array}
 \end{array}$$

4 EXTEND KNEE: In this state, brake in knee is released and as FES is deactivated, and as the knee joint is free to move, extension of knee joint occurs due to gravity. This is simulated in Simwise as the activation of a revolute joint in the humanoid knee, and the deactivation of the revolute motor that simulates muscle activation through FES. Hip and ankle brakes are activated. Corresponding input set and output functions for this state are:

$$\begin{array}{l}
 i_0 = \{ i_{LKor} \} \\
 \begin{array}{lll}
 o_{LKF}(t) = 0 & o_{LAB}(t) = 1 & o_{RHB}(t) = 0 \\
 o_{LHB}(t) = 1 & o_{WW}(t) = 1 & o_{RKB}(t) = 1 \\
 o_{LKB}(t) = 0 & o_{RKF}(t) = 0 & o_{RAB}(t) = 0
 \end{array}
 \end{array}$$

5 STOP KNEE: Once knee extension is complete, the brake in knee is activated again to stop extension and wheel walker is stopped since forward motion interferes with leg extension. This state is active for a single sample time. Input set and output functions for this state are:

$$\begin{array}{l}
 i_0 = \{ i_{LHor} \} \\
 \begin{array}{lll}
 o_{LKF}(t) = 0 & o_{LAB}(t) = 1 & o_{RHB}(t) = 0 \\
 o_{LHB}(t) = 1 & o_{WW}(t) = 0 & o_{RKB}(t) = 1 \\
 o_{LKB}(t) = 1 & o_{RKF}(t) = 0 & o_{RAB}(t) = 0
 \end{array}
 \end{array}$$

6 RELEASE HIP: In this state brake in hip is released causing the leg to drop to the floor, towards heel contact, which is detected using kinematics of heel position in the vertical axis. The duration of this state depends on the height of the foot at the end of the swing phase. Corresponding input set and output functions for this state are:

$$\begin{array}{l}
 i_0 = \{ i_{L\ heel\ z} \} \\
 \begin{array}{lll}
 o_{LKF}(t) = 0 & o_{LAB}(t) = 1 & o_{RHB}(t) = 0 \\
 o_{LHB}(t) = 0 & o_{WW}(t) = 0 & o_{RKB}(t) = 1 \\
 o_{LKB}(t) = 1 & o_{RKF}(t) = 0 & o_{RAB}(t) = 0
 \end{array}
 \end{array}$$

7 RELEASE ANKLE: Once heel contact occurs, the brake in ankle is released, causing the foot to drop to floor, causing ankle extension. When the toe touches the ground, the cycle starts

again with the opposite leg, and wheel walker actuation is activated. Input set and output functions for this state are:

$$\begin{aligned}
 i_0 &= \{ i_{L\ toe\ z} \} \\
 o_{LKF}(t) &= 0 & o_{LAB}(t) &= 0 & o_{RHB}(t) &= 0 \\
 o_{LHB}(t) &= 0 & o_{WW}(t) &= 1 & o_{RKB}(t) &= 1 \\
 o_{LKB}(t) &= 1 & o_{RKF}(t) &= 0 & o_{RAB}(t) &= 0
 \end{aligned}$$

A secondary loop was created that includes 3 additional states to ensure that the system is capable of recovering after an incomplete step. This happens when the knee flexion does not generate sufficient hip flexion to reach the trigger condition for the “BRAKE HIP” state.

8 FES OFF: This state is triggered by a time out and as its name implies, deactivate FES signal, this is simulated in Simwise as the deactivation of the revolute motor and the activation of a revolute joint, allowing knee joint to extend. Wheel walker is stopped while the system recovers

$$\begin{aligned}
 i_0 &= \{ i_{LKor} \} \\
 o_{LKF}(t) &= 0 & o_{LAB}(t) &= 1 & o_{RHB}(t) &= 0 \\
 o_{LHB}(t) &= 0 & o_{WW}(t) &= 0 & o_{RKB}(t) &= 1 \\
 o_{LKB}(t) &= 0 & o_{RKF}(t) &= 0 & o_{RAB}(t) &= 0
 \end{aligned}$$

9 BRAKE KNEE: This state can be skipped if heel ground contact occurs, and knee rotation is more than 10 degrees. However, if it is less than 10 degrees, the state is activated and knee brake is switched on to avoid hyperextension.

$$\begin{aligned}
 i_0 &= \{ i_{L\ heel\ z} \} \\
 o_{LKF}(t) &= 0 & o_{LAB}(t) &= 1 & o_{RHB}(t) &= 0 \\
 o_{LHB}(t) &= 0 & o_{WW}(t) &= 0 & o_{RKB}(t) &= 1 \\
 o_{LKB}(t) &= 1 & o_{RKF}(t) &= 0 & o_{RAB}(t) &= 0
 \end{aligned}$$

10 ANKLE BRAKE OFF: This state is activated when the knee has extended enough for heel to touch the ground but knee flexion is still more than 10 degrees. As its name implies, during this state ankle brake is deactivated to allow ankle joint extension in order to achieve toe contact with the ground, which is a condition to move to FLEX KNEE state and start the walking cycle again.

$$\begin{aligned}
 i_0 &= \{ i_{L\ toe\ z} \} \\
 o_{LKF}(t) &= 0 & o_{LAB}(t) &= 0 & o_{RHB}(t) &= 0 \\
 o_{LHB}(t) &= 0 & o_{WW}(t) &= 0 & o_{RKB}(t) &= 1 \\
 o_{LKB}(t) &= 1 & o_{RKF}(t) &= 0 & o_{RAB}(t) &= 0
 \end{aligned}$$

States 11 to 20 perform the same actions as states 1 to 10 but with the opposite leg. The description, input set, and output functions are not presented here to avoid repetitiveness. Figure 3.13 shows the period in which brakes at hip, knee and ankle joints, as well as FES are active during a complete walking cycle. Red dashed lines show knee joints trajectories for reference. It can be seen that FES is active only for a short period of time, during knee flexion,

this was set in that manner with the purpose of minimising muscle fatigue. Brakes compensate the lack of actuation, keeping the system in the desired postures, and ensuring safe standing and walking motion.

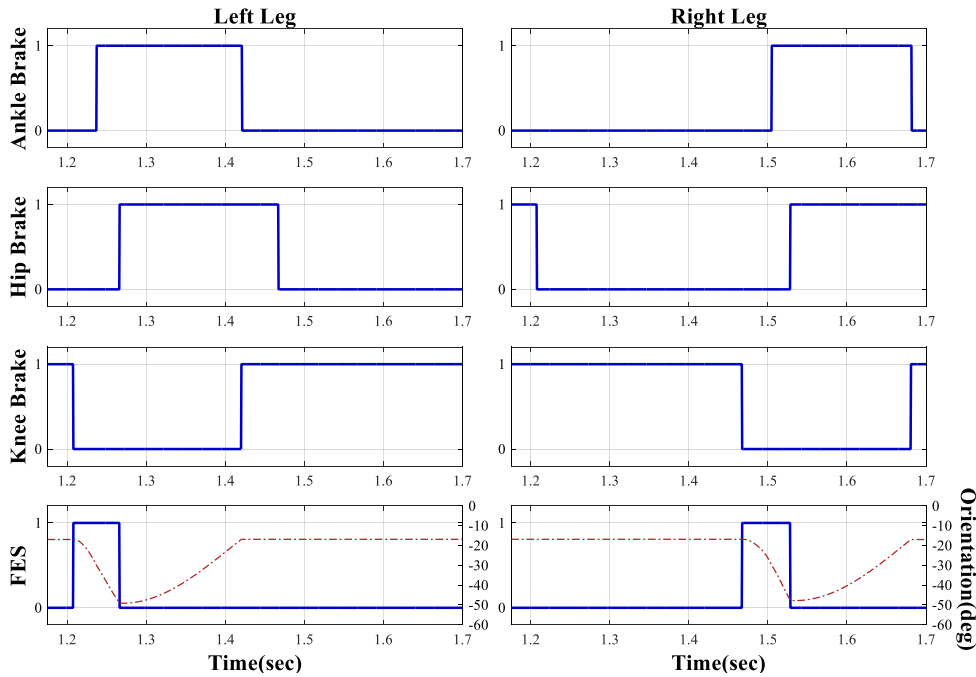


Figure 3.13 Switching period of brakes and FES for both legs with knee orientation for reference.

### 3.5.2.1 Kinematics of heel and toe

In order to recognise specific postures, such as heel- and toe-ground contact without sensors in the soles, it was necessary to measure the angles between links. These measurements can be done through encoders at hip, knee and ankle joints. Then, distance from ankle and toe to the floor can be computed through kinematics. Resulting angles and distances are shown in Figure 3.14 (a). The benefit of using kinematics is that it is possible to replace readings from distance or contact sensors, thus avoiding unnecessary costs as well as additional maintenance while the system is being experimentally tested.

It is possible to use kinematics because the lengths of links shown in Figure 3.14 (b) are always known. Then, using lengths and measured angles, and, considering that the wheel walker position in the vertical axis is constant during the walking motion, it is simple to calculate any point in the kinematic chain. In this case, the points of interest are the distances between heel and toe to floor, which will be used to identify heel and toe contact and off instants in the gait cycle. Equations (3.1) and (3.2) show how these distances are calculated.

$$Heel_z = T \cos(\gamma) + C \cos(\gamma + \beta) + F_1 \cos\left(\gamma + \beta - \alpha + \frac{\pi}{2}\right) - A \cos(\gamma + \beta - \alpha) \quad (3.1)$$

$$Toe_z = T \cos(\gamma) + C \cos(\gamma + \beta) + F_2 \cos\left(\gamma + \beta - \alpha + \frac{\pi}{2}\right) + A \cos(\gamma + \beta - \alpha) \quad (3.2)$$

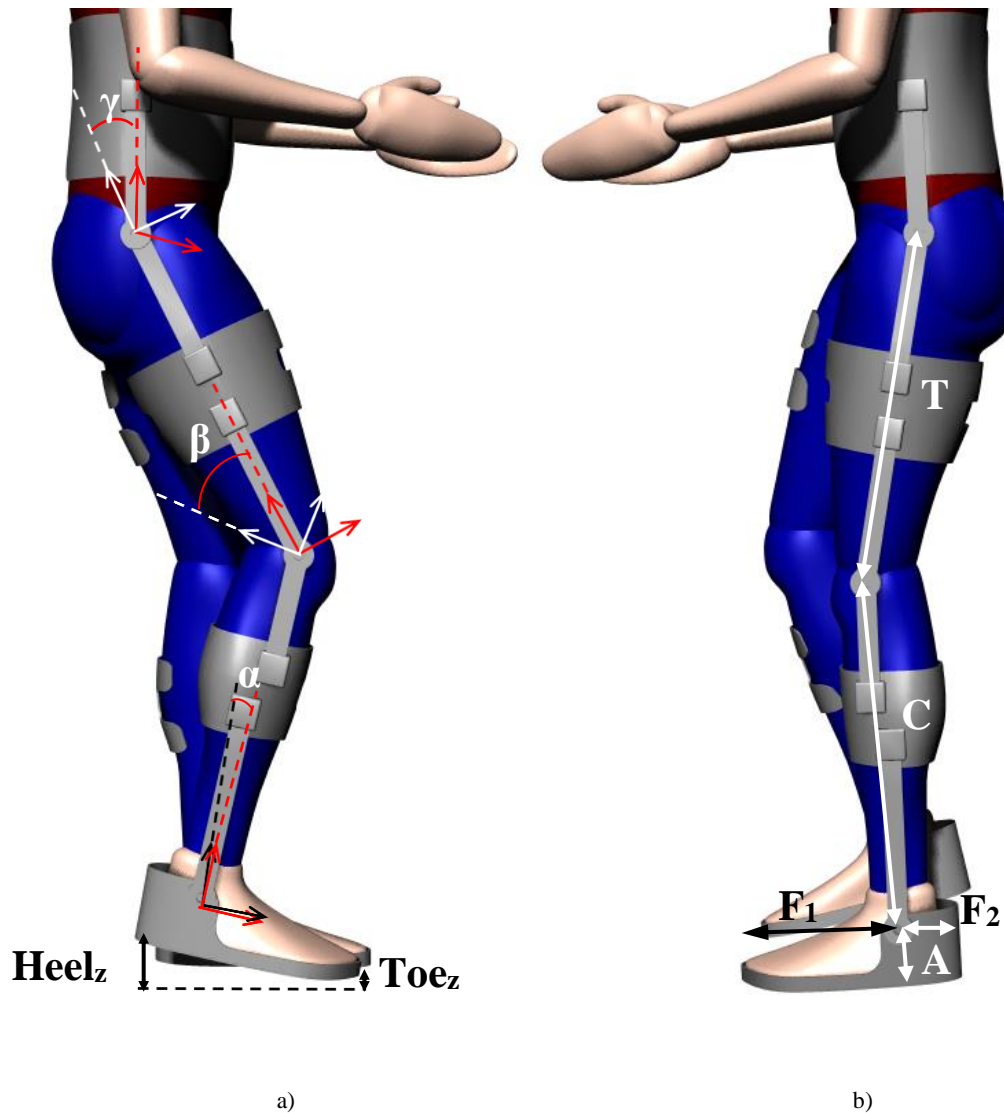


Figure 3.14 a) Exoskeleton angles and distances to floor b) Exoskeleton link lengths

### 3.6 Validation tests

After the humanoid, exoskeleton and wheel walker models were assembled in SimWise, and controls configured in MATLAB Simulink, tests were done to assess different trigger parameters for the FSC to generate successful steps. That is, generate swing of knee joints and achieve required orientations of hip and ankle joints, while maintaining balance. The analysis of the normal walking cycle served as reference, although manual tuning of the trigger conditions was necessary. Figure 3.15 shows acceptable results of knee flexion, it is possible to see the reference sent to the system and the actual knee joint trajectory during two steps.

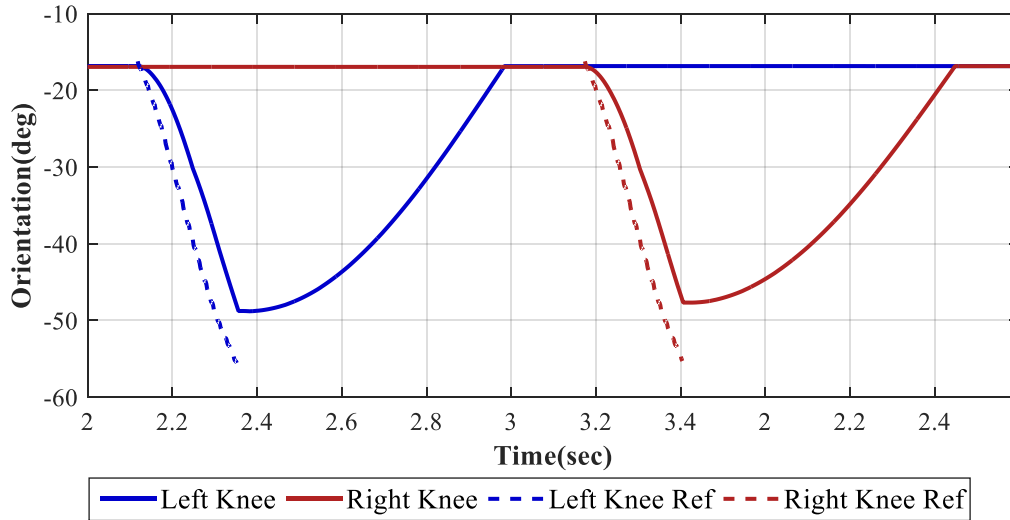


Figure 3.15 Knee joint actual orientation and reference during a complete walking cycle

The root mean squared error (RMSE) between the knee orientation reference and the actual value was calculated using equation (3.3), only while FES was activated.  $\hat{\theta}$  is the desired orientation, in this case, knee reference, and  $\theta$  is the actual orientation, in this case knee orientation measured from SimWise;  $n$  is the number of time steps.

$$\text{RMSE} = \sqrt{\frac{\sum_{t=1}^n (\hat{\theta} - \theta)^2}{n}} \quad (3.3)$$

RMSE was 7.1 for left knee and 7.3 for right knee during a 60 second simulation. Although these values are still high, it was demonstrated that even with this error, it was possible to generate an acceptable walking cycle. Moreover, an optimisation algorithm can be used to reduce RMSE further, however, this is not in the scope of the current chapter.

Taking as reference the normal walking cycle, joint trajectories obtained through measurements performed by the Polytechnic University of Cartagena (UPCT), in addition to values calculated from Winter's Tables, a comparison was done with measurements taken from SimWise during the simulation and control of paraplegic walking with FES and hybrid orthosis. These three trajectories for each joint are shown in Figure 3.16.

Results show that there are slight differences between UPCT's and Winter's trajectories. This is expected, and can be due to variations in subject's, height, health conditions or even walking styles (Hsu et al., 2008). Additionally, differences could be caused by variations in motion speed in the three trajectories. These are not noticeable in the  $x$  axis because trajectories were normalised in time to enable comparison.

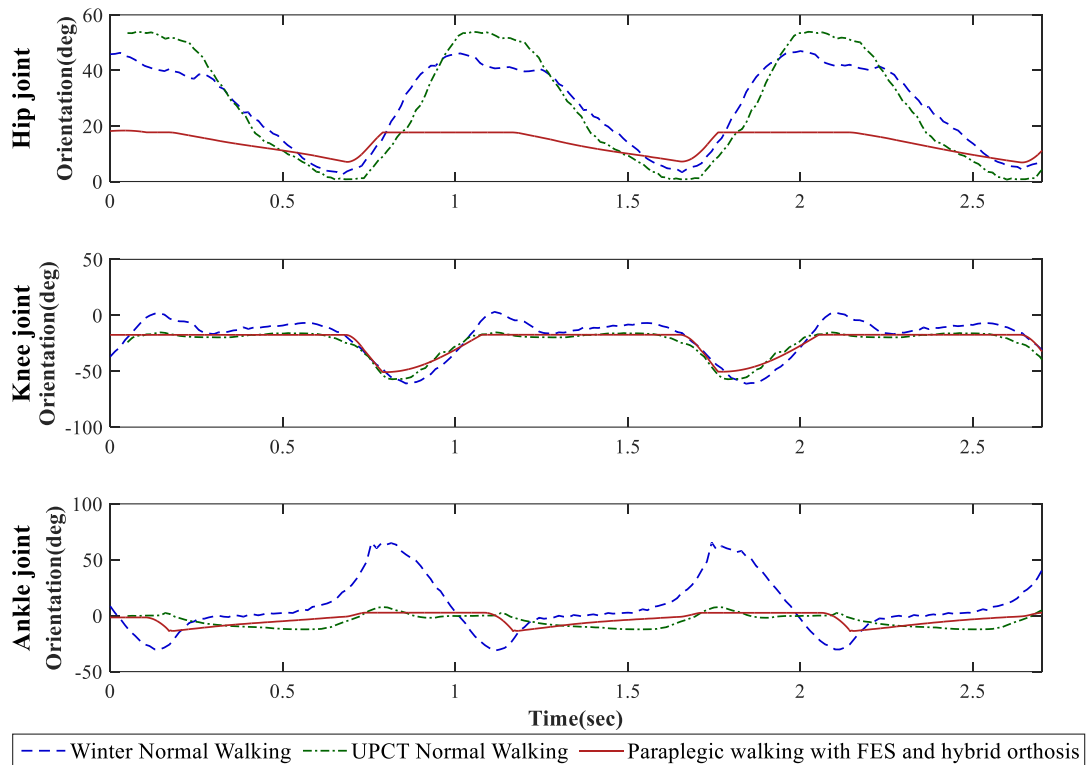


Figure 3.16 Comparison of paraplegic walking with FES and hybrid orthosis vs normal walking joints trajectories

The trajectories of joints during paraplegic walking with FES and hybrid orthosis, on the other hand, present several discrepancies with the normal walking cycle. The hip joint moves within a limited range, the reason for this is the lack of actuation in this joint. However, this range is enough for maintaining ground clearance during the swing phase. It is also clear that there is a flat region that corresponds to brake activation which shows some similarity to the normal walking cycle, which also presents a flat region.

Knee joint motion during the swing phase is slightly reduced in the vertical axis, and knee flexion and extension motions, do not have the same duration as in normal walking cycle. This is because FES is used only for a limited amount of time, to generate knee flexion and therefore, the necessary hip flexion. During the stance phase, a constant angle is kept due to the activation of brakes, this is not very different from the UPCT normal walking cycle, as shown in Figure 3.16. In Winter's trajectories, it is possible to see more oscillations. This could be attributed to variations of knee joint motion from person to person.

Ankle joint motion varies significantly from normal walking cycle, due to the activation of brakes in hip, knee and the ankle joint themselves. The ankle joint usually compensates the motion of the other two joints, in the sagittal and frontal planes, to keep balance. However, in this case, motion in the latter is blocked, movement in the sagittal plane is reduced, and wheel walker is responsible for balancing the system. Therefore, the ankle joint during paraplegic walking performs very limited motion.

After a pair of steps were successfully completed, longer simulations were ran finding that the walking cycle was adequate for paraplegic patients. Further trials were done to validate the system, where these tests include repeatability, stability and range. The torque of knee joints was assessed, as well as the amount of energy produced by user's muscles with the aid of FES. These tests were also useful to determine the capabilities of the system, such as the maximum speed, in addition to verifying if it could withstand external disturbances.

### 3.6.1 Repeatability tests

To test the repeatability of the system, validation simulations were run during 60 seconds using different wheel walker's angular velocities, these were also useful to calculate the maximum walking velocity. As mentioned, the wheel walker provides the forward motion since the user's upper body is constrained, and cannot lean to accomplish it.

Table 3.3, shows that the maximum gait speed obtained was 0.3 meters per second, with a wheel walker angular velocity of 280 degrees per second. This maximum linear gait speed is superior to that of REX system, 0.05 meters per second, which is due to its heavy weight and short stride. However, other commercial exoskeletons like Ekso can reach a speed of up to 0.9 meters per second, which is just below the human average gait speed (1.3 m/s); this is due to the long stride, achievable by its capacity to both flex and extend hip, unlike the configuration used in this research. By only actuating the knee joint, the system generates a limited hip flexion, resulting in a short stride. Nevertheless, this gait speed is enough for users to receive the benefits of upright mobility without forcing their joints.

Table 3.3 Maximum and average gait speeds.

Wheels angular velocity (deg/sec)	Maximum gait speed (m/sec)	Average Gait Speed (m/sec)	Unsuccessful steps (#)
255	0.27	0.26	0
260	0.28	0.27	1
265	0.28	0.26	3
280	0.3	0.26	5

Results shown in Table 3.3 indicate that when wheel walker's angular velocity is increased, the number of unsuccessful steps increases. However, in all the cases, the system managed to recover and continue with the gait cycle until the end of the test, with no other inconvenience than time lost to repeat the step. If the wheel walker's velocity were further augmented, incomplete steps would result in a more important decrease of the average velocity. In an experimental application, the user could choose the wheel walker speed that better satisfies his needs within a certain range

Joint trajectories during the 60 second test with wheels' angular velocity of 260 degrees per second and average gait speed of 0.27 meters per second are shown in Figure 3.17 a) though only 30 seconds are shown to improve visibility. In Figure 3.17 b) it is possible to observe the unsuccessful step at time  $t = 22$  seconds, which occurred because the required hip flexion of left leg was not achieved. The step was reinitiated twice, however, the system recovered after less than 2 seconds.

Additionally, simulations were done to test repeatability under different initial conditions. Two of those simulations were run for 10 seconds with same initial conditions for both legs, i.e. same joint angles, but starting the walking cycle with a different leg each time. Initial angles for the joints were:  $\gamma = 11$  degrees for hip joints,  $\beta = -16$  degrees for knee joints, and  $\alpha = -5$  degrees for ankle joints. During these two simulations, there were no unsuccessful steps.

Another pair of validation simulations were run for 10 seconds, but with different initial conditions for each leg and initiating the walking cycle with a different leg each time. Initial angles for the joints were  $\gamma_L = -0.45$  degrees for left hip joint,  $\beta_L = -12.75$  degrees for left knee joint,  $\alpha_L = -12.67$  degrees for left ankle joint,  $\gamma_R = 7.34$  degrees for right hip joint,  $\beta_R = -15.88$  degrees for right knee joint, and  $\alpha_R = -7.78$  degrees for right ankle joint. Joint trajectories of both legs during the simulation started with left leg, are shown in Figure 3.18. It is possible to observe that once again there were no unsuccessful steps. Results of all the simulations described above are shown in Appendix B.

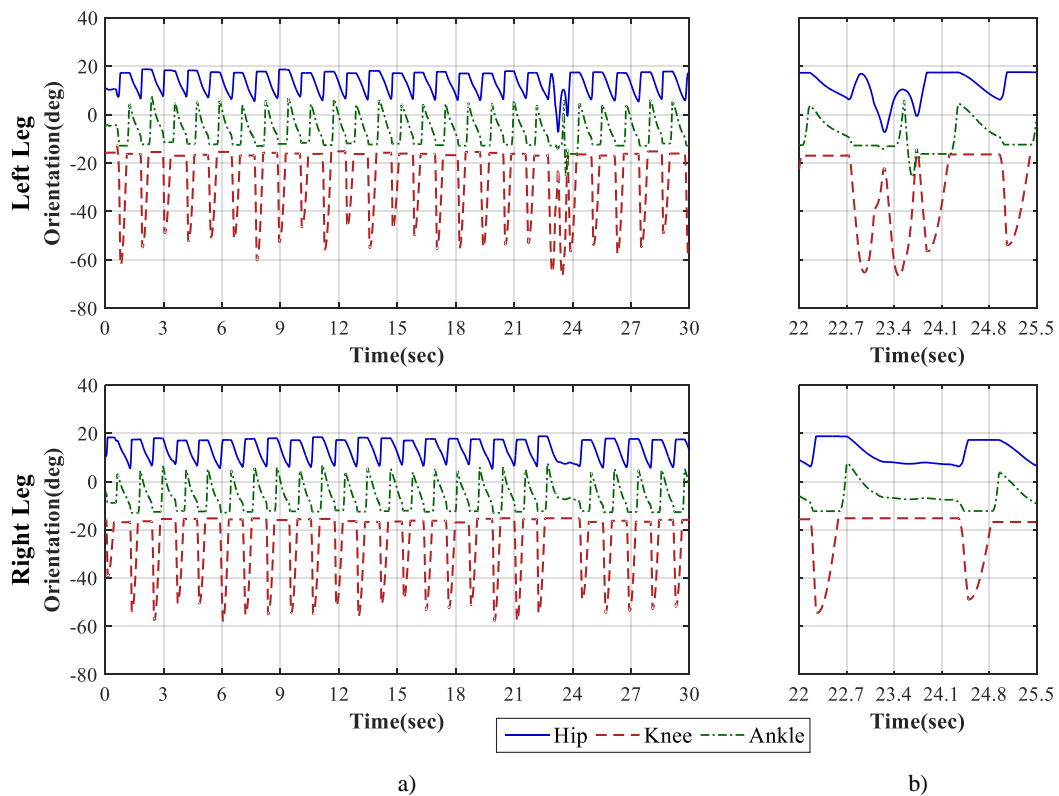


Figure 3.17 a) Repeatability test run with incomplete step b)Zoom in of incomplete step

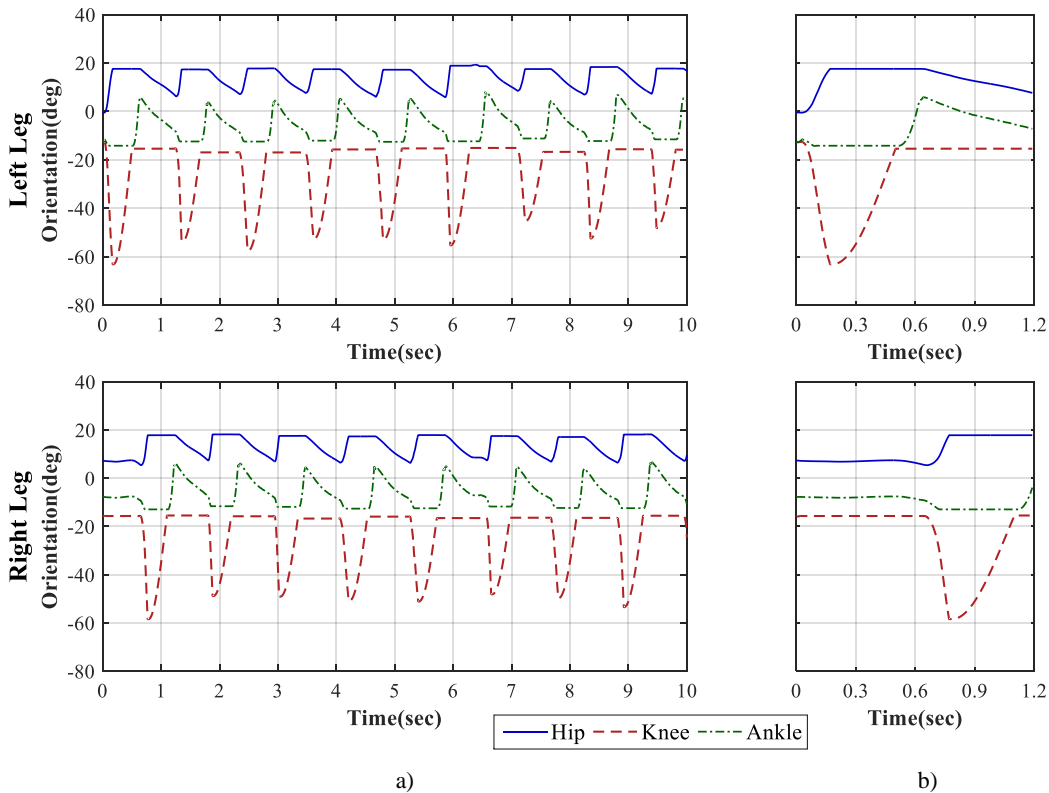


Figure 3.18 Repeatability test run starting step with left leg a) Complete simulation run b) Zoom in initial steps

With these validation simulations, it was possible to demonstrate that system can perform as expected, even from varying initial conditions. That is, complete steps can be achieved through the adequate guidance of the user by the exoskeleton, generating the required postures to complete the walking task. It was also possible to observe that the walking cycle can be repeated for long periods of time without presenting cumulative errors or other system malfunctions.

### 3.6.2 Stability

In order to validate stability of the system, external forces were applied during 0.2 seconds in frontal ( $x$ ) and lateral ( $y$ ) directions as shown in Figure 3.19. The force in lateral direction was 500 Newtons and was applied from time 1.8 seconds. In the frontal direction, 1000 Newtons were applied from time 3.8 sec, obtaining the results shown in Figure 3. 20. These magnitudes were selected considering a collision with another person moving towards the user.

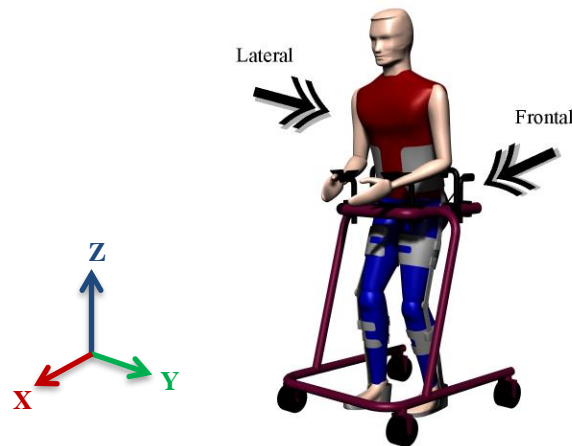


Figure 3.19 a) Representation of disturbances applied

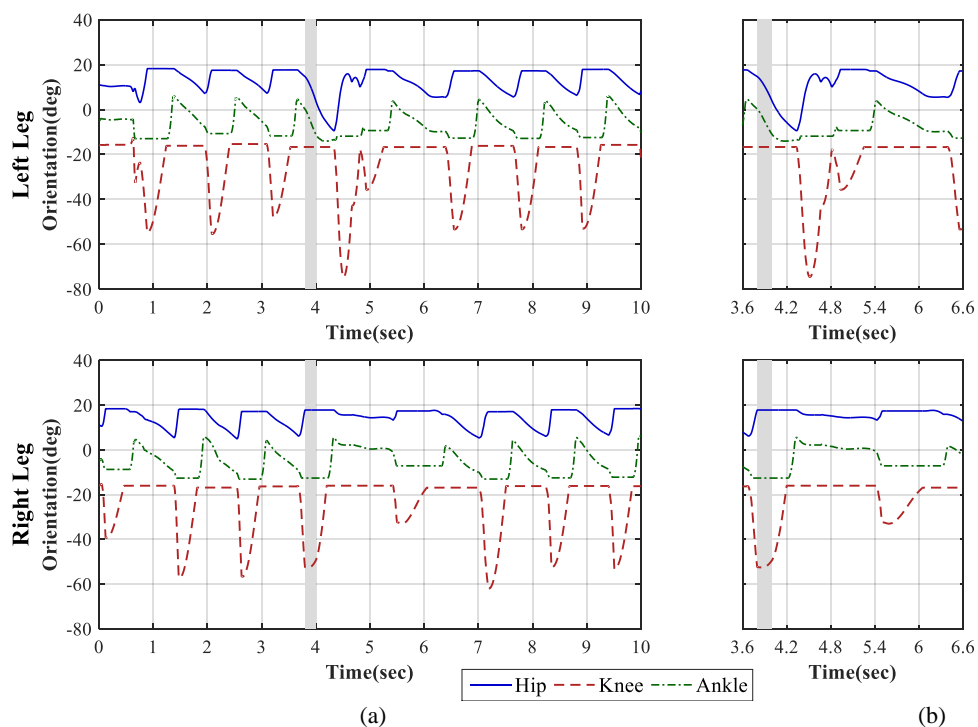


Figure 3.20 System reaction to external disturbances a) Complete simulation b) Zoom in affected time slot

It is possible to observe that the force applied in lateral direction does not affect the trajectories due to the stability that the wheel walker provides, only a small tilting could be observed during the simulation. However, force applied in frontal direction generated an important disturbance. In this case, the force was applied during the swing phase, resulting in a longer stride of the right leg that, in turn, caused an incomplete left step. It had to be repeated until the desired hip angle was reached and the gait cycle could be restarted normally, in this case, it took less than 2 seconds after the force was applied.

In Figure 3.21 it is easy to observe that the forward force momentarily augmented the speed in the highlighted zone; it is also possible to see that the wheel walker stopped during the stabilisation period. Afterwards the speed returned to an average of 0.24 meters per second.

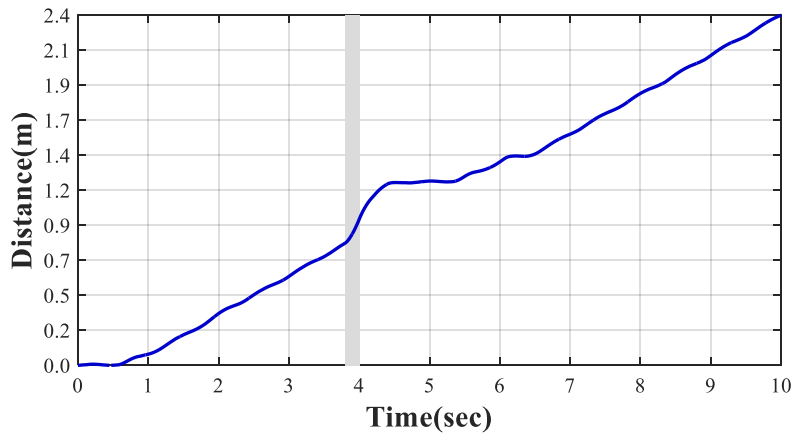


Figure 3.21 Travelled distance with disturbances

The same methodology was followed with forces applied during 0.2 seconds in frontal and lateral directions but in different moments of the gait cycle. Similarly, the force applied in the lateral direction was 500 N from time 1 second, and in the frontal direction force applied was 1000 N from time 3 seconds, obtaining the results shown in Figure 3.22.

Similar results as those of the previous simulation were obtained. In this case, force was applied before initiating a step, therefore, there was a slight sliding of the walker which can be observed as a more pronounced slope in the highlighted area in Figure 3.23. Due to this displacement, the first step after the disturbance could not be completed and had to be repeated, the second step after the disturbance was also incomplete, and therefore, the system took around 2.5 seconds to stabilize. Average speed during this test was 0.23 meters per second.

These validation tests were useful to know if the system and controller were robust enough to withstand external disturbances. In future work, this test could be performed more extensively to find the maximum forces that the system can withstand.

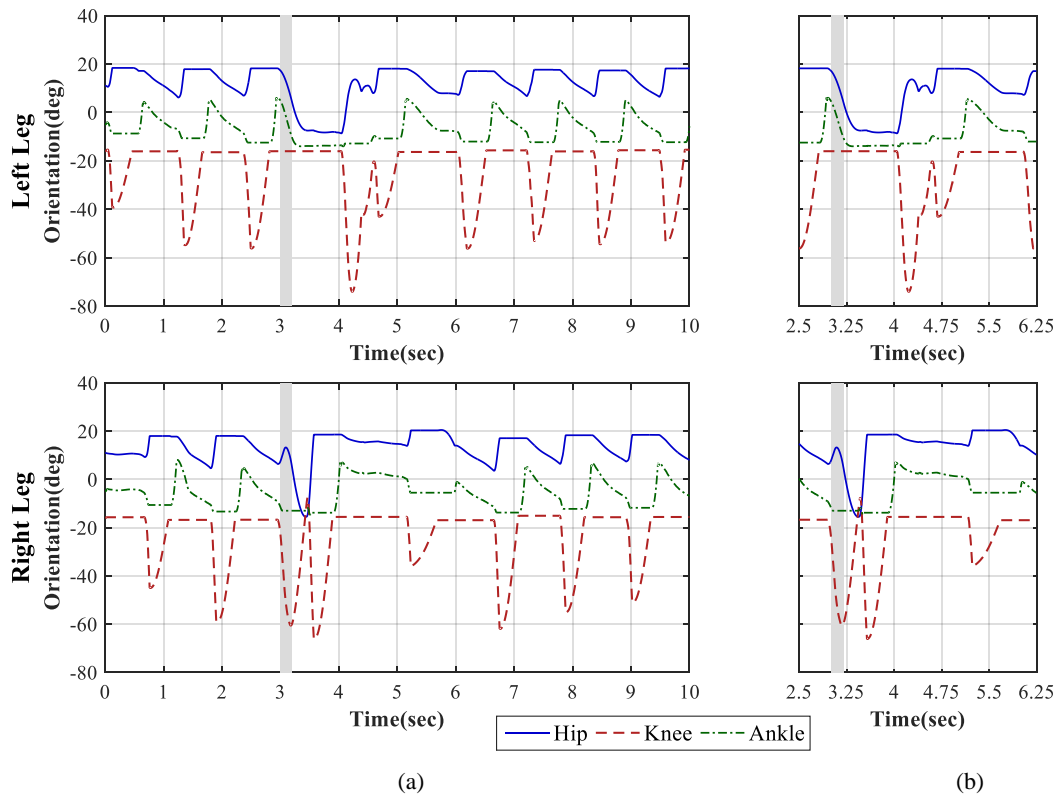


Figure 3.22 Test 2: System reaction to external disturbances a) Complete simulation b) Zoom in affected time slot

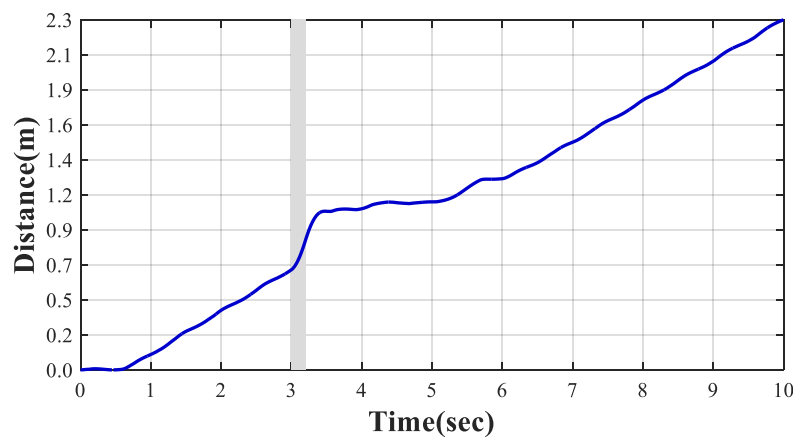


Figure 3.23 Test 2: Travelled distance with disturbances

### 3.6.3 Range

The objective of this simulation is to determine if the same exoskeleton system and controller can be used with humanoids of different dimensions. Additionally, to define what modifications would be required to maintain adequate performance of the system. The first step was to create two additional humanoids, one shorter and lighter and one taller and heavier than the original model. Dimensions were based on the ranges of height that commercial exoskeletons claim to have. The humanoids used for range validation were 1.85, 1.7 and 1.5 meters in height.

Slight modifications had to be made to the dimensions of the exoskeleton links to be properly fitted to each humanoid segment. Based on those changes, the relevant parameters were updated so that kinematics calculations were correct.

After the implementation of these changes, simulations were run for 60 seconds, finding that humanoids were capable of walking with the same system, that is, using the same controllers and wheel walker speed. Moreover, the 1.5-meter humanoid was found to be able to walk at an average gait speed of 0.3 meters per second, with a wheel walker angular velocity of 280 degrees per second.

Considering that the exoskeleton's segments lengths were superior for the 1.85 meter humanoid and, consequently, the stride achieved was longer, it was possible to increase wheel walker angular velocity to 350 degrees per second, generating a gait speed of 0.35 meters per second.

Range simulations were performed as described previously, to demonstrate that the system could be adapted to different users without altering controllers. Another important observation after the range test, is that reference trajectories and controller gains generated successful walking cycles, however, they could be further optimised, and adapted to each humanoid to obtain a higher speed. Although maximising speed is not one of the purposes of this research, optimisation can be done to better determine the limits of the system.

### **3.6.4 Torque and energy consumption**

Torque in knee joints was measured during a 60 second simulation to ensure that the system was not forcing the user beyond natural limits. Figure 3.24 shows the resulting torque in both legs with knee joint orientation as reference although only 10 seconds of the simulations are shown to ease visualisation. Torque is only applied during the knee extension state, which corresponds to the application of FES. This state is active for approximately 0.2 seconds every walking cycle.

Maximum torques for both knee joints are well below 120 Newton-metre ( $N \cdot m$ ), which is the maximum torque during walking motion according to Low (2011). Although the duration of the stimulation time is small, it is possible to observe that the torque provided through the fuzzy controller is not smooth, and presents peaks which could expose the user to muscle fatigue. This can be avoided through the optimisation of gains.

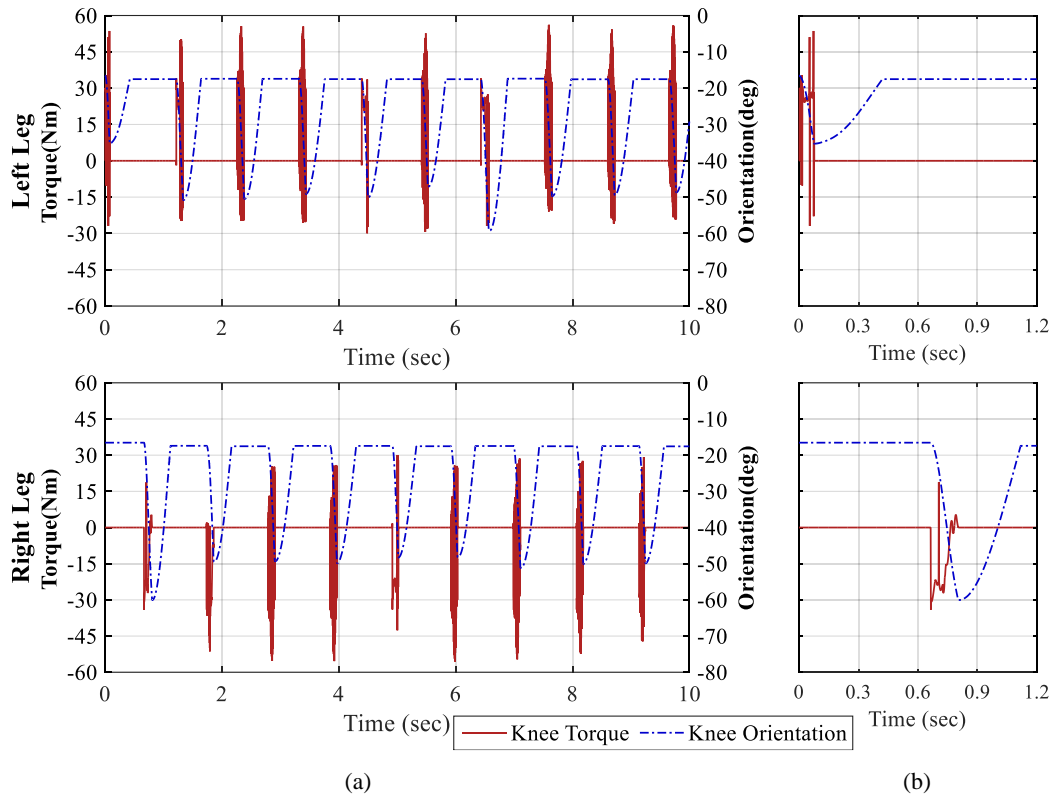


Figure 3.24 Knee joint torques a) 10 seconds segment b) Zoom in initial step

Torque-Time Integral was computed using equation (3.4), where  $\tau$  is torque in  $N \cdot m$ , and  $n$  is the number of time steps.  $TTI$  refers to the amount of torque needed to perform a motion. In this research, the integral was calculated using trapezoidal numerical integration for a 60 seconds run resulting in  $TTI = 333 N \cdot m \cdot s$ .

$$TTI = \int_{t=0}^n \tau dt \quad (3.4)$$

Figure 3.25 shows the amount of torque required for both legs during the 60 seconds simulation independently, and jointly. In Figure 3.25a), it is possible to see that both legs require almost the same amount of torque, and in Figure 3.25b), it is evident that torque is applied only during a short time, therefore generating the stepped  $TTI$ .

Power generated by FES during every instant of the simulation was also calculated as the product of torque and angular velocity. The amount of energy generated by FES during the 60 seconds simulation was later obtained through trapezoidal numeric integration of power with respect to time. The result obtained for each knee joint was very similar at 13.8 Joules. Therefore, the total amount of energy generated through FES by the system was 27.6 Joules.

This is very low compared with other devices, however, in order to compute the real consumed energy, it would be necessary to obtain the FES signal necessary to produce the torque output and consider the amount of energy employed to activate brakes and wheel

walker. Although this calculation is out of the scope of the project, it is possible to affirm that this system would still consume less energy than conventional exoskeletons since motors are only included in the wheel walker and not in the frame, materials used are light, and because human muscles are used as actuation.

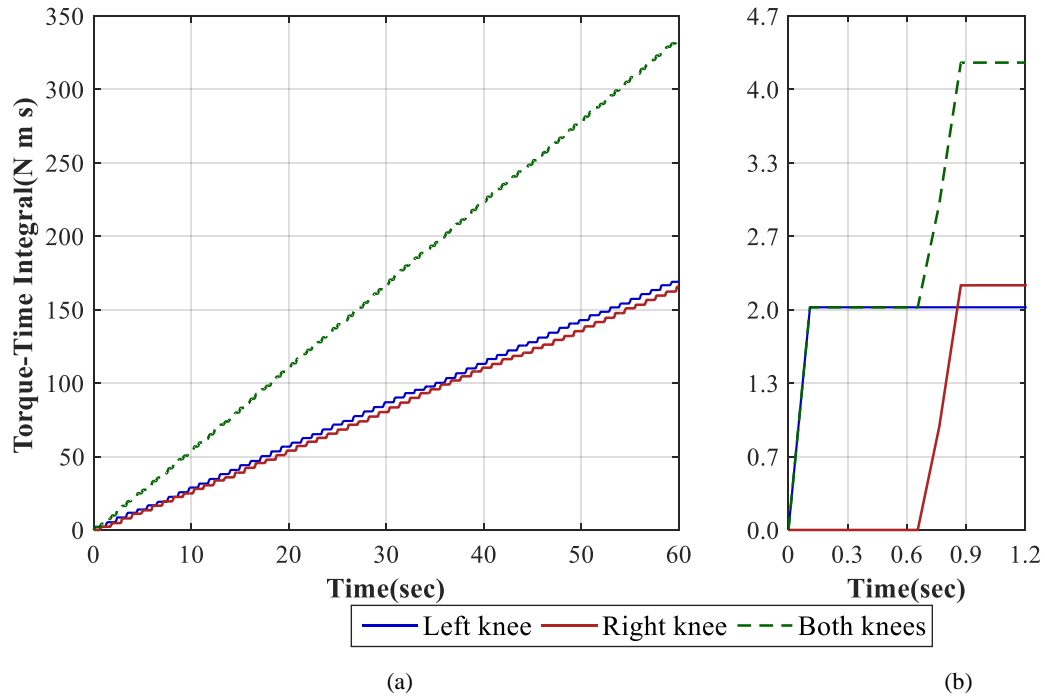


Figure 3.25 Torque-Time integral of knee joints a) Complete simulation b) Zoom in initial step

### 3.7 Summary

In this chapter, a CAD humanoid, a hybrid exoskeleton device, and a wheel walker model, were controlled using fuzzy and finite state control mechanisms. These are adequate for this application due to the complexity of the system and because FSCs are highly suitable for gait control due to its sequential operation (Sweeney et al., 2000).

It has been shown through simulations that the device is capable of generating a continuous walking manoeuvre using a fuzzy control of knee joints torque as low-level controller. Although in simulation, torque is sent to a revolute motor, in an experimental set up, these would be replaced by the FES applied to quadriceps and hamstrings.

Flexion and extension of the knee joints is the only means of active actuation. It is combined with brakes mounted on a frame in a similar arrangement to that of the Spring Brake Orthosis, to produce postures needed to complete walking cycles in paraplegic patients. The wheel walker is used for stability purposes, additionally, to support some of the weight of the system and help the user generate the forward motion. A FSC was used as midlevel controller to coordinate the activation of knee motors/FES, brakes at joints, and wheel walker actuation.

Alternative tests can be performed, starting from different initial conditions, running for longer simulation times, with external disturbances of different magnitudes, durations and locations. However, those described in this chapter demonstrate that the control system is adequate to generate continuous walking cycles in straight line, while there is enough power and no obstacles. The results were satisfactory, although optimisation techniques could be used to enhance the fuzzy control gains, as well as the conditions to trigger state changes in the finite state controller. This would help to increase speed of the system and smoothness of torques sent to joints, which in turn, could help to save energy.



# CHAPTER 4

## **PID control of humanoid and exoskeleton for elderly assistance on standing-up and sitting-down tasks**

### **4.1 Introduction**

According to the World Population Ageing 2013 report, the global share of older people, those aged 60 years or over, will grow 9.4 per cent by 2050, summing more than 2 billion, and representing 21.1 per cent of the total world population. Moreover, the older population is itself ageing, by 2050, there will be three times more people 80 years or over in the world. The issue which emerges, is that those additional years are not always lived in good health, but threatened by diseases as memory loss, urinary incontinence, depression, falls or immobility (United Nations, 2013)

Standing-up motion is one of the most important tasks to enable mobility. Not being able to stand may hinder elderly independence due to the lack of mobility, damaging life quality. According to Alexander, et al., (1991), 8 per cent of people over 65 years old, have difficulty standing-up from a sitting position, while 3 per cent of them requiring assistance. Moreover, of people 85 years old or over, 9 per cent require assistance to complete these tasks.

It is through rising that one can perform activities that make musculoskeletal and cardiorespiratory systems stronger, more agile and improve cognitive and motor competencies (Sveistrup et al., 1999). Being able to stand also enables interaction with the environment, and it is through this interaction, that it is possible to get sensory feedback and develop motion control. Standing-up is also important as a precursor of other activities such as walking, reaching objects above ground level, one to one conversations, among others (Sveistrup, et al., 1999). For all these reasons, standing-up motion is considered one of the most important, if

not the most important, carried out by a human. Devices that provide assistance for standing-up to enable the elderly to preserve their lifestyle, and overall their health, are an imperious need nowadays.

The current chapter presents investigation, through simulation of a humanoid and exoskeleton within SimWise, of the necessary torque profiles for assisting the elderly during standing-up and sitting-down motions. Assistance is provided by an exoskeleton, described in Chapter 2, which was designed as part of the EXO LEGS project (Virk et al., 2013). Low level control of the exoskeleton's hip and knee joints are addressed in this chapter using PID controllers.

Several combinations of gains and torque saturation values are tested to assess the feasibility of the system. This is done focusing on obtaining standing-up and sitting-down motions with low error, compared to the reference sent, and using the minimum amount of energy possible.

Relations between the RMSE, gains, torque saturation values and TTI are investigated to better characterise the system. Additionally, tests are done at three different speeds to assess the effect on torque profiles. Finally, estimations of ground and seat reaction forces are obtained to be used as input parameters for the exoskeleton upper level control in future research.

## **4.2 Assistive devices for elderly mobility**

According to the WHO, (2016), assistive technology is an umbrella term which covers the systems and services delivered by assistive products, and services to maintain or improve users functioning and independence, and as a result, promote their well-being.

Assistive technology offer users the possibility to live healthier, more productive, independent and dignified lives through their participation in education, labour market and social life. It also reduces the users' need for formal health services or long-term care. Additionally, it is often created to avoid exclusion, isolation and poverty of disabled people, or those with long-term diseases, and their families. However, nowadays only 1 in 10 people in need have access to the assistive technology they require for reasons such as high costs, lack of awareness, and availability of both, the technology and specialised trainers (WHO, 2016).

Those in most need of assistive technology include people with disabilities, the elderly, and people with gradual functional decline, among others. In the case of older people, assistive technology can enable them to continue living at home and delay, or prevent, their need for long-term care (WHO, 2016)

Although there is not enough data to quantify the global number of assistive technology users, it is estimated that mobility limitations affect between one third and 50 per cent of adults above 65 years old (Webber et al., 2010). Therefore, around 2.9 per cent of the global population, 211 million elderly people, have some sort of mobility issue. From those, at least 102 million need a wheelchair (Papworth Trust, 2016; EFDS, 2016), while the rest need an assistive device such as crutches, cane or walker to ambulate (United States Census Bureau, 2012).

Common assistive technology for the elderly can be classified in 4 categories as follows.

1. Products to support them in the standing position while maintaining or even improving their health like standing frames, and standing wheelchairs.
2. Walking products for those who are able to walk or stand with assistance such as canes, crutches, walkers, and gait trainers.
3. Wheeled mobility products that enable users with reduced mobility to move indoors and outdoors, like wheelchairs and scooters.
4. Advanced technology such as exoskeletons, conceived initially to aid people with disabilities such as paraplegia or cerebral palsy that impede standing and walking tasks (Disabled World, 2016).

Exoskeletons are the most recent addition to mobility assistive technology and as already mentioned, some devices for paraplegic patients are now on the market. However, considering the growing elderly population and the lengthening of life expectancy, research is being focused on the design of exoskeletons for elderly people who can stand or even walk, although require some degree of support to perform those motions.

As mentioned above, assistive technology devices intend to maintain functional capabilities of people with mobility impairments (WHO, 2011). Exoskeletons are thought as assistive technology with the benefits of common devices such as canes, crutches, standers, walkers, wheelchairs and scooters, integrated into a single device that provides support while standing, enables displacement, is usable in limited spaces, and energy efficient. Overall, exoskeletons aim to restore and, furthermore, increase previously lost mobility capabilities (Disabled World, 2016).

In recent years, various studies have been carried out regarding exoskeletons for the elderly, EXPOS, a light exoskeletal device from Sogang University was one of the first devices developed. Combined with a smart caster walker that carries most of equipment, the exoskeleton provides the additional support that older people need to stand and walk (Kong and Jeon, 2006). This device is still at the research stage, such as the prototype from Saga University that uses EMG-based control methods to activate the exoskeleton (Kiguchi and Imada, 2009).

Honda has been developing and testing a walking assistive device, which provides support at hip joint while lifting legs when walking, thus lengthening stride to cover longer distances at higher speeds (Honda, 2015). Cyberdyne has now launched into the market the living support for lower limbs Hybrid Assistive Limb (HAL), among other products. HAL is a full robotic lower limb exoskeleton capable of assisting the wearer to walk, stand-up and sit-down by sensing bioelectric signals to follow user's motion (Cyberdyne, 2015). It is now available for rent to institutions for an initial installation cost of around £3000, and a monthly fee of £1000.

The newest trend are exoskeletons with flexible shafts such as the one developed by Ikehara et al., (2011), and the Harvard Wyss Institute 'soft exosuit', whose purpose is to reduce the net metabolic cost of walking, either for healthy people or those with light impairments such as the elderly (Asbeck et al., 2015). More details on exoskeletons for the elderly can be found in Chapter 1 and 2.

Considering that nowadays, about two thirds of the world's older persons live in developing countries, and by 2050, 8 in 10 of them will live in under-developed countries (United Nations, 2013), there is an imminent need to generate an exoskeleton device for the elderly that is sufficiently complex to safely assist them in everyday activities, but at the same time as being simple enough to be affordable and manageable.

The EXO-LEGS project for the elderly focuses on creating and commercializing an affordable exoskeleton device which assists the elderly on a set of tasks defined by its end users group (Virk, et al., 2013). Several European universities and companies are involved in the EXO-LEGS project, different mobility tasks have been assigned to each group. The research group at the University of Sheffield, working in collaboration with the Polytechnic University of Cartagena in Spain, were assigned the standing-up and sitting-down tasks.

### **4.3 Elderly standing-up and sitting-down**

In healthy adults, the standing-up motion takes between 1.5 and 2 seconds to complete (Nuzik et al., 1986; Kralj and Bajd, 1989, Schenkman et al., 1990). During this motion, the whole-body posture is changed through the coordinated movement of several of its segments, which follow a forward and upward movement, taking the body from a large stable base formed by buttocks and feet, to a smaller and less stable base formed of the feet only.

Several biomechanical studies related to the standing-up and sitting-down motions have been developed. An example is the work developed by Kralj and Bajd, (1989) which describes a standing-up manoeuvre divided in 4 phases. Figure 4.1 shows a timeline with each phase.

The first phase called initiation or flexion-momentum, mainly consists of a forward upper body movement during which hip flexion increases, to generate a momentum that enables the

transition from sitting support to leg support. This motion also pushes the CoM forward and downwards, increasing stability in preparation for the next phase. The lower body remains in a static position during initiation.

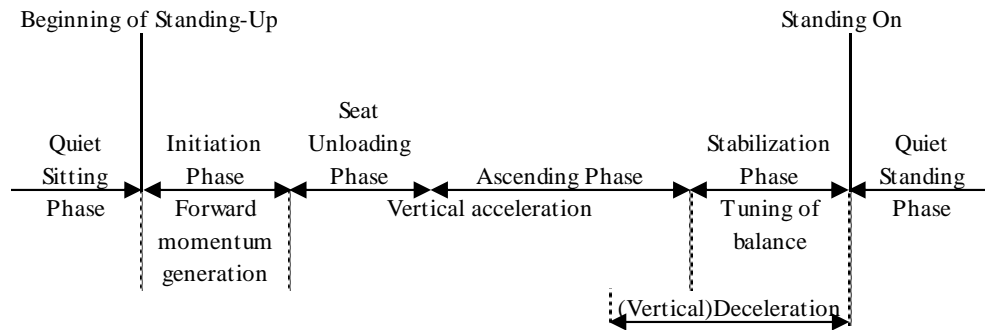


Figure 4.1 Standing-up motion phases (Kralj and Bajd, 1989)

The next stage, seat unloading or momentum-transfer, begins when vertical acceleration starts, therefore, it is in this moment that there is an apparent sudden increase of body weight. Upper body forward momentum decreases and extension velocity of hip, knee and ankle joints increase, pushing CoM upwards. The body rotates forward with ankle joints as pivot points. This is the shortest phase but also the most demanding and least stable.

The third phase, called ascending or extension phase, starts when ankle is at its maximum flexion and the CoM reaches its maximum forward position. Extension velocity of hip and knee joints decreases during this phase, and vertical deceleration begins towards the end of this phase.

The last phase, stabilisation, starts when hip and knee joints are fully extended and finishes when a stable standing position is reached. During this stage, small anteroposterior and lateral movements are used to achieve balance, these motions mainly involve hip and ankle joints (Karl and Badj, 1989, Svestrup et al., 1999).

There are fewer studies on sitting-down motion, Figure 4.2 shows a timeline in which the sitting-down motion is divided in 4 phases (Kralj and Bajd, 1989). The first phase is initiation or forward lean which is achieved through flexion of hips; it is during this stage that the upper body moves forward to lower the CoM and transition body erect posture into a stooping posture. The second stage, descending, also called vertical displacement, involves firstly a vertical downward acceleration while the trunk starts to move down through flexion of hip and knee joints, and then, a deceleration motion. The next phase is seat loading which starts at the first contact with the seat; in this stage, weight is transferred from the legs to the seat. The last phase is stabilisation or recovery, in which trunk moves backwards through hip extension to obtain a balanced sitting posture (Kralj et al., 1990, Kerr et al., 1997)

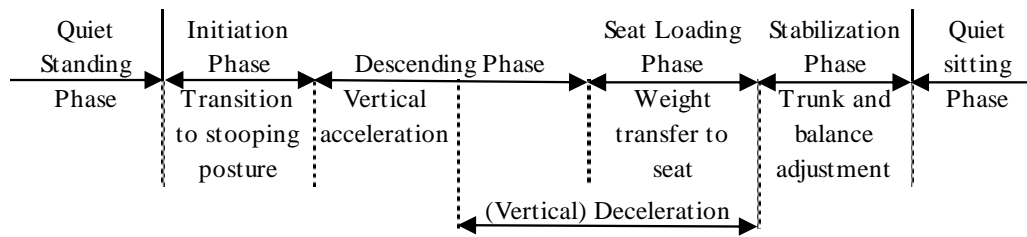


Figure 4.2 Sitting-down motion phases (Kralj and Bajd, 1989)

Orientation of hip, knee and ankle joints during standing-up and sitting-down motions are shown in Figure 4.3. According to a research where EMG signals were used to extract behaviour primitives during standing-up motion, the main muscles used are quadriceps, tibialis anterior, latissimus dorsi and gastrocnemius (An et al., 2009). It was found that the motion is divided mainly in two different contributions. The first one makes dynamics of the movement, and the second controls posture (An, et al., 2009)

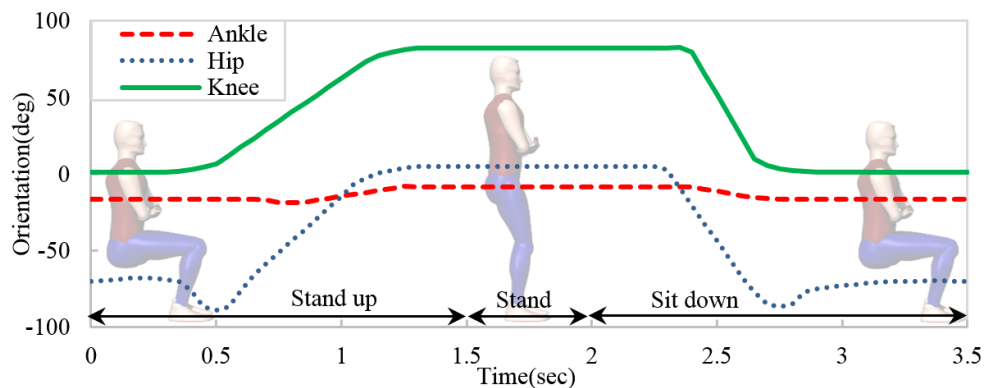


Figure 4.3 Standing-up and sitting-down lower limbs joints orientations

It has been found that joints trajectories and muscle activity tend to remain relatively constant even when arms are used for support or seat height is different (Munton et al., 1984). However, the initial position of head, arms, pelvis, buttocks and feet, affect the ease of standing-up due to their influence on force and momentum, as well as in balance (Sveistrup et al., 1999). The velocity in which the motion is performed also influences the difficulty to complete it.

There are some changes that occur while aging such as slowness, hesitancy, unsteadiness and increased tendency to fall, which affect the way in which the elderly perform mobility tasks. These changes have been attributed to insufficiencies in the musculoskeletal and sensory systems like muscle weakening (Sveistrup et al., 1999).

Muscle strength gradually declines from 25 to 60 years old, around one third of peak capacity (Schultz, 1995), and declines more sharply after that (Wheeler et al., 1985, Faulkner, 1995). It is estimated that there is between 20 and 40 per cent diminution in muscle strength

and power at 70 to 80 years of age, and around 50 per cent over 90 years of age (Garcia et al., 2011).

Muscle weakness is also more pronounced in women and in the muscles of the lower limbs for both men and women, which results more problematic than weakness in the upper body (Sveistrup et al., 1999). The effects of muscle weakness varies for different types of muscle contraction involved in motion. A contraction is the generation of tension within a muscle fibre; eccentric muscle contractions, which result in elongation of the muscles, are stronger and better preserved at older age than concentric muscle contractions, those in which the muscles shorten while generating force (Boundless, 2016, Sveistrup et al., 1999).

The main reasons for muscle weakness are decreased innervation, due to the loss of motor units, decreased muscle activity, and decreased nutrition due to loss of interest in food at older age (Faulkner, 1995). Muscle weakness can also cause muscle stiffness and shortening, or even physical blockage or pain, which reduces the range of motion of joints. Therefore, the elderly often modify their movements to avoid pain or compensate deficiencies, resulting in inefficient manoeuvres that might even complicate the activity (Sveistrup et al., 1999).

Another important change that occurs with ageing is that, the ability of the central nervous system to integrate information from multiple sensory modalities, is reduced (Faulkner, 1995). This causes an increase in reaction times, as well as a generalised slowing of motor activities. Redundancy of information and peripheral sensory input are also reduced as consequence of ageing (Sveistrup et al., 1999). The ability to develop joint torques rapidly has also been found to be associated with age decline. Older adults take 161 milliseconds more than younger adults, to develop 60 Nm of plantarflexor torque (Schultz, 1995).

Taking more time to perform the standing-up motion is a strategy commonly adopted to overcome the reduced sensory capabilities. However, momentum is decreased under this circumstance, and strength requirements, together with instabilities, increase (Kotake et al., 1993).

Alexander et al., (1991), found that positions of segments and orientations of joints during the standing-up motion of young and healthy elderly people are relatively consistent. However, elderly people aged 75 to 92 years old, who need arm assistance to perform the standing-up motion, use a different strategy to complete it. Differences include a doubled duration of the tasks, changes in alignment of segments and a shift backwards of the position of CoM for stability (Schultz et al., 1992), in addition to the aforementioned arm and hands support. For this research, healthy standing-up and sitting-down motions are considered, although different durations of these motions are assessed, to understand the impact of velocity in torque profiles.

## 4.4 Open-Loop simulations of standing-up and sitting-down motions

The purpose of this chapter is to analyse standing-up and sitting-down manoeuvres, and design a low level controller for hip and knee exoskeleton joints to aid the elderly in these activities of daily life. One of the main goals is to get torque profiles to ease actuator selection when the system has been analysed sufficiently to carry out experimental trials. In order to do so, simulations of the humanoid performing sitting-down and standing-up motions were performed in SimWise software.

Data from Figure 4.3 was used to generate the standing-up and sitting-down references through an open-loop control. The plant consists of a humanoid and an exoskeleton models. Hip, knee and ankle joints in both, exoskeleton and humanoid, were represented by revolute motors actuated by orientation. Meters were added to monitor angular velocity, orientation and torque at the three joints.

For this open-loop simulation, a block diagram was created in Simulink and connected to the plant in SimWise. Inputs were three sets of data, one per joint where the first column was time in seconds, and the second column, the desired orientations in degrees of each joint. Outputs were actual joints orientations, velocities, accelerations and torques.

Figure 4.4 shows the humanoid during the different stages of the complete standing-up and sitting-down manoeuvre. Snapshots are equally spaced and it is possible to observe that trajectories followed are not perfect since some postures seem unbalanced, however, no further offsetting of references was performed to avoid time delays.

From the simulation, it was possible to measure torques of the different joints. However, since the magnitudes were not restricted, the system could use an unlimited amount of torque to follow the desired orientations as closely as possible. This resulted in some torques being above human limits. This simulation was useful to assess the trajectories used before closing the control loop.

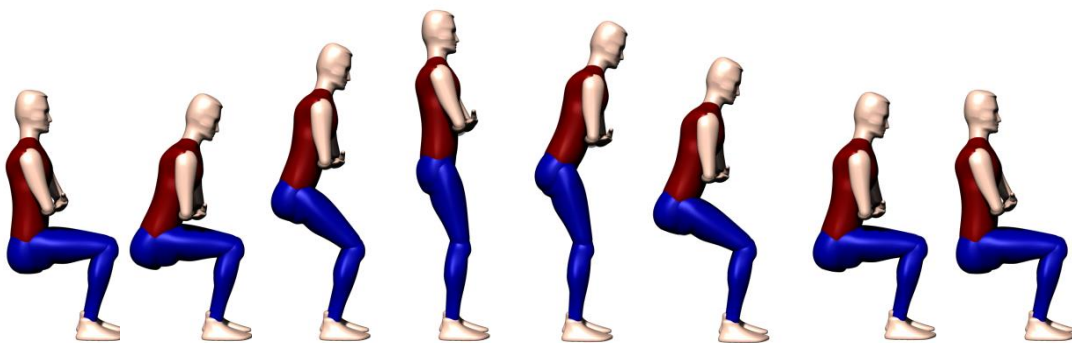


Figure 4.4 Simulation of standing-up and sitting-down motions

## 4.5 PID control of humanoid for torque profiles assessment

Following the definition of the orientation profiles, controls were added to the system with orientation error as reference, and torque as output. These were added with the purpose of providing only the necessary amount of torque to the system. Proportional Integral Derivative (PID) controllers were used due to their ease of implementation when the mathematical model of the plant is unknown, since analytical design methods cannot be used (Sung, Lee and Lee, 2009). PID control is ideal in this case in which the plant is a CAD model since several tests can be made with different gains and torque saturation values, to find the minimum necessary torque to perform standing-up and sitting-down motions.

### 4.5.1 PID Control

Proportional Integral Derivative (PID) controllers, or modified versions, are used in more than half of industrial applications, due to its general applicability on most control systems (Sung, et al., 2009). PID controllers have proved to be useful even when the mathematical model of the plant is not available, providing satisfactory results with robustness to uncertainties through relatively simple strategies. However, in most cases, results are not optimal (Ogata, 2010).

PID controllers are a type of automatic controllers. These compare the actual value of the plant output against the desired value, determine the difference, and produce a control signal to reduce the difference, taking it to zero or close to zero. The manner in which the automatic controller produces the control signal is called a control action (Ogata, 2010).

PID controllers are conformed of three terms, a proportional, an integral, and a derivative term.

Proportional (P) term:  $u(t) = K_p e(t)$  in Laplace-transformed:  $U(s) = K_p E(s)$

Integral (I) term:  $u(t) = K_i \int_0^t e(t) dt$  in Laplace-transformed:  $U(s) = K_i \frac{1}{s} E(s)$

Derivative (D) term:  $u(t) = K_d \frac{de(t)}{dt}$  in Laplace-transformed:  $U(s) = K_d s E(s)$

The complete PID controller has the form:

$$u(t) = K_p e(t) + \frac{K_p}{T_i} \int_0^t e(t) dt + K_p T_d \frac{de(t)}{dt}$$

and in Laplace-transformed:

$$U(s) = K_p \left( 1 + \frac{1}{T_i s} + T_d s \right) E(s)$$

In digital form:

$$U(z) = K_p E(z) \left[ 1 + \frac{T}{T_i(1 - z^{-1})} + T_d \frac{(1 - z^{-1})}{T} \right]$$

Where  $T_d$  is the derivative time and  $T_i$  is the integral time (Ogata, 2010)

The proportional term is essentially an amplifier with an adjustable gain, which aims to stabilize the system. A merely proportional control results in a steady state error or offset with a step input. This offset can be decreased if the proportional gain  $K_p$  is increased, however, it could cause the system response to be more oscillatory (Ogata, 2010).

The integral term is used to eliminate or reduce that offset, however, it may lead to oscillatory responses of either, slowly decreasing or increasing amplitude. Both of these are undesired in the process. Adding an integral term to the system increases its order therefore the system might become unstable (Ogata, 2010).

The derivative term anticipates the actuating error and initiates an early corrective action before the error becomes too large, increasing the stability of the system. Therefore, when a derivative term is added to a controller, a controller with high sensitivity is obtained. Although the derivative part does not decrease the offset directly, it adds damping to the system which in turn, enables the increase of gain  $K_p$ , resulting in a steady state error decrease (Ogata, 2010).

Trial-and-error tuning is frequently used to determine the gains of a PID controller, by inspecting the dynamic behaviour of the controlled process output (Sung, et al., 2009). For successful tuning, it is very important to understand the effects of each parameter on the behaviour of the process. PID controllers show the following dynamic behaviours after a step set-point change:

1. If the process output shows a big oscillation, then the proportional gain  $K_p$ , is too large.
2. If the controlled process output shows an overdamped response, then the proportional gain  $K_p$  of the PID controller is too small.
3. For a positive step set-point change, if the process output oscillates and stays above the set-point longer than under it, then, the integral time  $T_i$  is too small, meaning that the integral control action is too strong.
4. For a positive step set-point change, if the process output oscillates and stays under the set-point longer than above the set-point, then, the integral time  $T_i$  is too large, meaning that the integral control action is too weak.
5. If the process output shows a high-frequency oscillation from the start to the steady state, then the derivative time  $T_d$  is too large. This is due to the amplification of a high frequency signal by the overly strong derivative term.

For successful trial-and-error tuning, it is important to maintain the proportional gain  $K_p$  as large as possible, since closed-loop dynamics usually become slower when the focus is the removal of the five dynamic behaviours mentioned (Sung, et al., 2009)

### 4.5.2 Closed-loop PID control scheme

Following the definition of orientation profiles in the previous section, constraints in the lower limbs of the humanoid model were changed to revolute motors actuated by torques, and a closed-loop set-point tracking digital PID control was designed for hip and knee joints. The diagram in Figure 4.5 shows the implementation in Simulink for hip joint. In this scheme, the reference orientation or desired trajectory of the hip joint is compared with the corresponding measured hip orientation of the plant. The error obtained is input to the PID controller, which generates the necessary control action in the form of torque to actuate the hip joint.

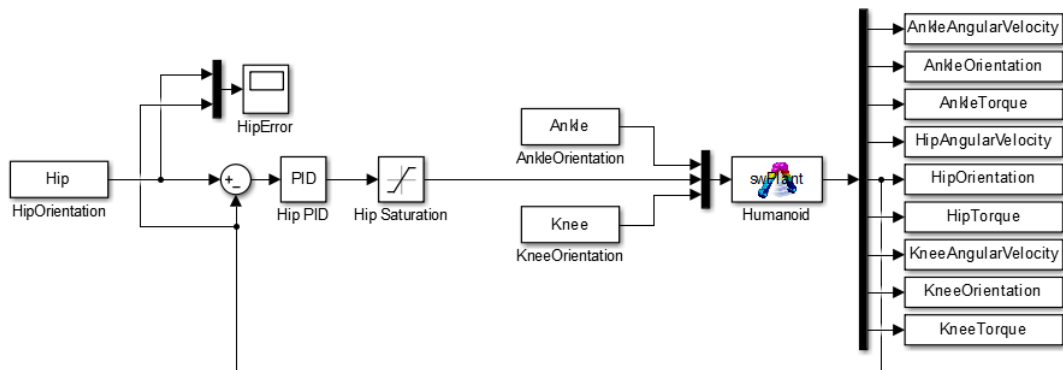


Figure 4.5 Simulink control diagram of humanoid hip joints

A saturation block of 160 Nm was added at the output of the hip joints PID controllers and of 210 Nm at the output of the knee joints PID controllers. Several simulations were run without the saturation block with different combinations of gains to try to obtain trajectories with torque below 160 Nm and acceptable MSE. However, the torque obtained was constantly over 350 Nm. For that reason, saturation blocks were added to restrict the amount of torque sent to the system in order to avoid peaks in the control signal.

For this research, the same reference was sent to both legs, therefore, it is assumed that right and left legs move synchronously. Another assumption made is that balance is sustained throughout the motion. To simulate this in SimWise, feet were attached to the ground with a rigid joint. In Chapter 6, balance is not assumed and the control scheme is updated to address it.

It is important to mention that when the hip joint was controlled, knee and ankle joints were set as revolute motors actuated by orientation in SimWise in order to simplify the process and to evaluate the behaviour of one joint at a time. The same procedure was repeated with knee joints, having hip and ankle revolute motors actuated by orientation. Ankle was not controlled in this section but its controller is described in Chapter 6.

### 4.5.3 Tests with different gains

To evaluate the behaviour of the system with different gains, a script was created in MATLAB to run simulations with several  $K_p$ ,  $K_i$  and  $K_d$  gains for the controller of hip revolute motor. Gains were evenly distributed from 2 to 20 for  $K_p$ , from 1 to 10 for  $K_i$  and from 0.1 to 10 for  $K_d$ . Most tests with  $K_p$  smaller than 10 were unstable, unless  $K_i$  had a large value as well.

The root mean squared error between the hip orientation reference and the actual value was calculated as in equation 3.1. Torque-Time Integral was also calculated as in equation 3.2. A comparison of the resulting RMSE and TTI was performed.

The same process was repeated to determine the  $K_p$ ,  $K_i$  and  $K_d$  gains for knee, sending the reference orientation profiles of ankle and hip directly to the humanoid. Simulations were performed with gains evenly distributed from 2 to 20 for  $K_p$ , from 1 to 10 for  $K_i$  and from 0.1 to 10 for  $K_d$ . After obtaining the best sets of gains for both hip and knee PID controllers separately, a new Simulink diagram was created with PID torque controllers for both hip and knee joints, whereas ankle reference orientation profiles were sent directly to the plant as shown in Figure 4.6.

A minimum RMSE of 2.48 for hip joint orientation and 3.11 for knee joint orientation were achieved with  $K_p = 20$ ,  $K_i = 2$  and  $K_d = 2$  for hip joints, and  $K_p = 20$ ,  $K_i = 10$  and  $K_d = 4$  for knee joints, with saturation values of 160 Nm for hip joints, and 210 Nm for the knee joints.

On the other hand, a minimum TTI of 119 Nms for hip joint and 193 Nms for knee joint were achieved with  $K_p = 12$ ,  $K_i = 1$  and  $K_d = 0.6$  for hip joints, and  $K_p = 12$ ,  $K_i = 6$  and  $K_d = 1.2$  for knee joints, and saturation values of 160 Nm and 210 Nm, respectively.

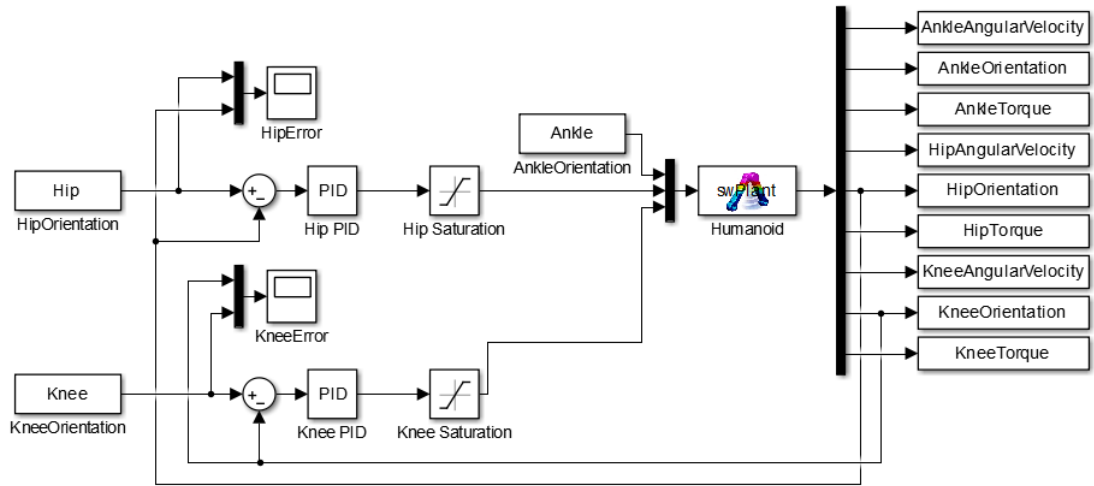


Figure 4.6 Simulink control diagram of humanoid hip and knee joints

Figure 4.7 shows that for the set of gains which had the smallest RMSE, the torque is less smooth and TTI is larger, 138 Nms and 228 Nms for hip and knee joints, respectively, compared to the results with the second set of gains shown in Figure 4.8.

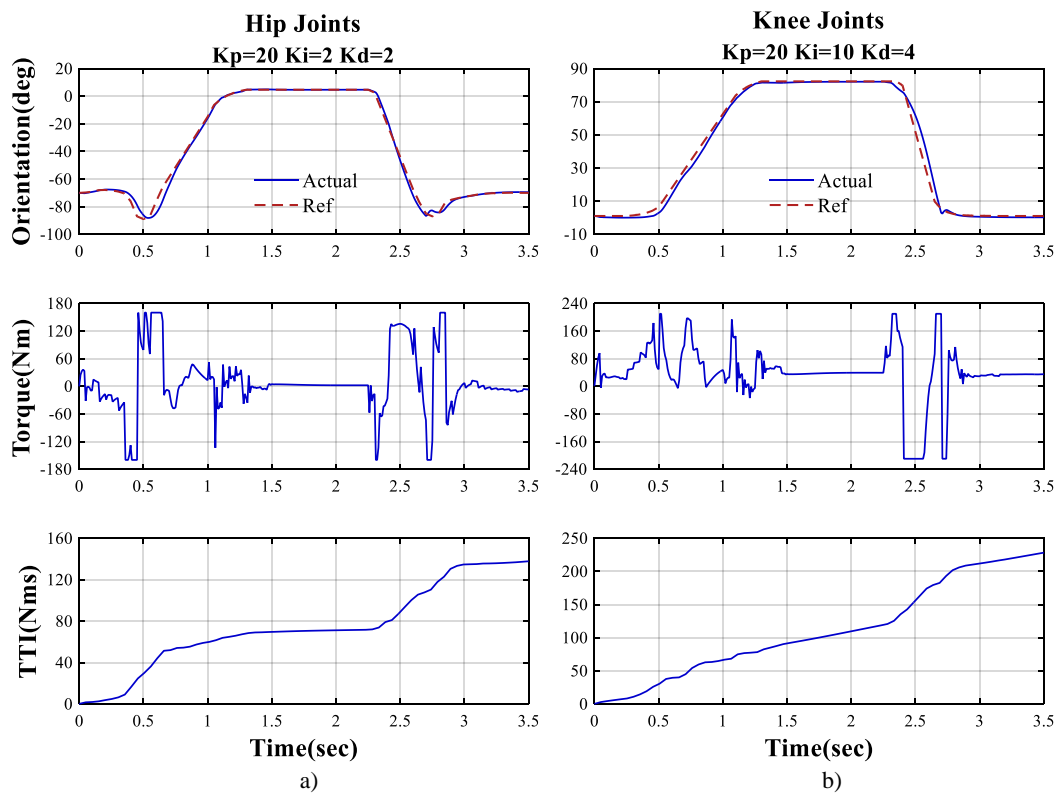


Figure 4.7 Orientation, torque and TTI of a) hip and b) knee joints with gain combination for minimum RMSE

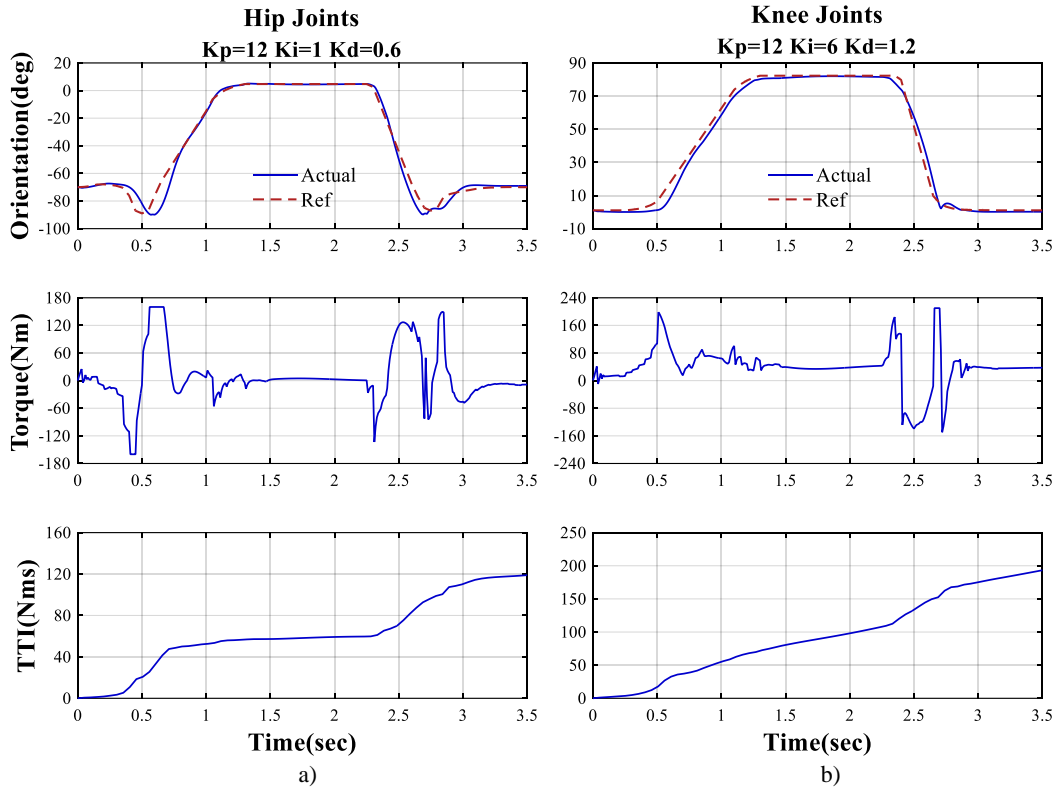


Figure 4.8 Orientation, torque and TTI of a) hip and b) knee joints with gain combinations for minimum TTI

For the set of gains with the lowest TTI, RMSE was higher, 4.56 and 3.34 for hip and knee joints, respectively. Although for hip joint, it is twice the value than that with the first set of gains, RMSEs are still well below the 10% of the amplitudes of the references, and therefore they are acceptable. Moreover, in this case, torque is smoother, resulting in a lower TTI, which in the long term would represent savings in energy expenditure and less damage to the actuators.

It was observed that a relation existed between the PID gains and the TTI. Scatter plots of trajectories with an acceptable RMSE for both joints were used to further analyse the relations between PID gains with RMSE and TTI, in addition to those of RMSE and TTI, for both joints. Gain combinations considered were those with RMSE smaller than 10% of the orientation range, which is less than 9 degrees and 8 degrees for hip and knee joints, respectively.

Data with RMSE higher than 10% was discarded since the behaviour is not acceptable and some trajectories are even unstable. This was the case for all the combinations with  $K_p$  of 4 or less, and about half of those with  $K_p$  of 6. The reason for this being that low  $K_p$  gain controllers do not provide the necessary control action to stabilize the system.

Results were presented in scatter plots and a polynomial of 4<sup>th</sup> degree was fitted to the data. A proportional relation was found between  $K_d$  gains of both joints and TTI as shown in

Figure 4.9. This is reasonable since it is known that when PIDs have a strong derivative control action, the system is too sensitive, therefore oscillations occur. In this case, those oscillations increase the TTI because the system is attempting to minimise the error as much as possible, thus using all the available torque.

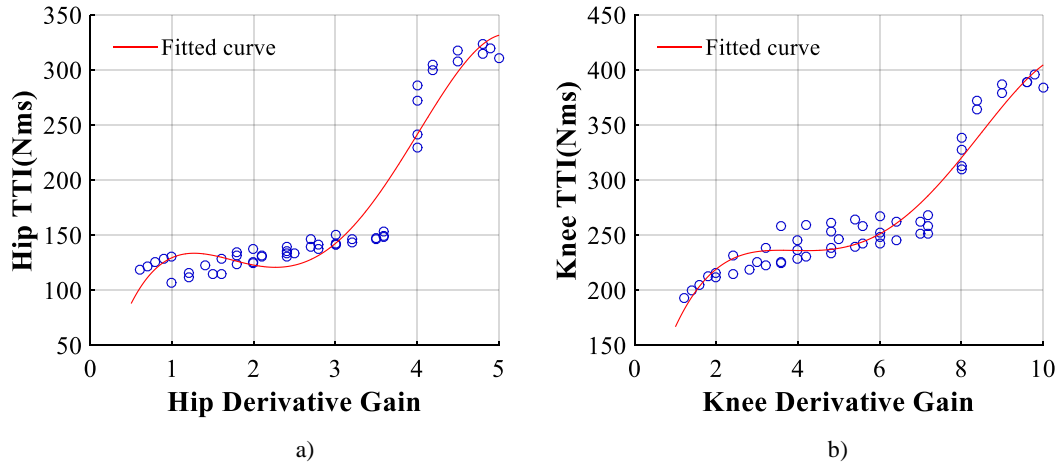


Figure 4.9 Relation between TTI and  $K_d$  gain for a) hip joints and b) knee joints

Additionally, it was also found, as shown in Figure 4.10 a) and b), that RMSE decreased when proportional and integral gains were higher, although the increase in RMSE is not significant. In summary, from the analysis, it was observed that  $K_d$  gain should not be very high to avoid increasing TTI unnecessarily, while  $K_i$  and  $K_p$  should be as large as possible if the focus is on minimising RMSE, however as it is below 10% even with small integral gains,  $K_i$  could take a wider range of values in the second half preferably to avoid instability.

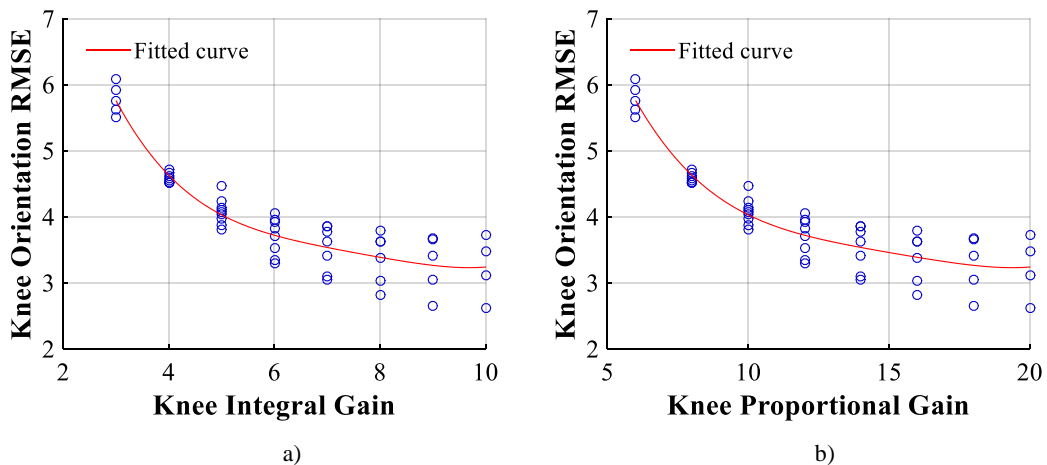


Figure 4.10 Relation between RMSE and a)  $K_i$  gain and b)  $K_p$  gain for knee joints

#### 4.5.4 Tests with different saturation levels

Hip joint PID gains of  $K_p = 14$ ,  $K_i = 1$  and  $K_d = 1.4$ , and knee joints PID gains of  $K_p = 14$ ,  $K_i = 7$  and  $K_d = 2.8$  were selected after the analysis of behaviour with different gains. As mentioned above, saturation blocks were added at the output of each PID controller to ensure that the torque value was not above human limits, however, in this subsection, the system was tested with several combinations of saturation levels to assess if it was possible to achieve the same trajectories with a lower amount of torque and TTI.

Saturation torques for hip joint were evenly distributed in the range of 60 to 150 Nm and for knee joint from 120 to 210 Nm. Figure 4.11 shows the best results obtained with saturation limits of 100 Nm for hip joint and 120 Nm for knee joint. RMSE in this case was 4.2 for the former and 5.2 for the latter, where both are well below 10%. Moreover, TTI was 109 Nms and 183 Nms for hip and knee joints respectively, lower than in the previous section.

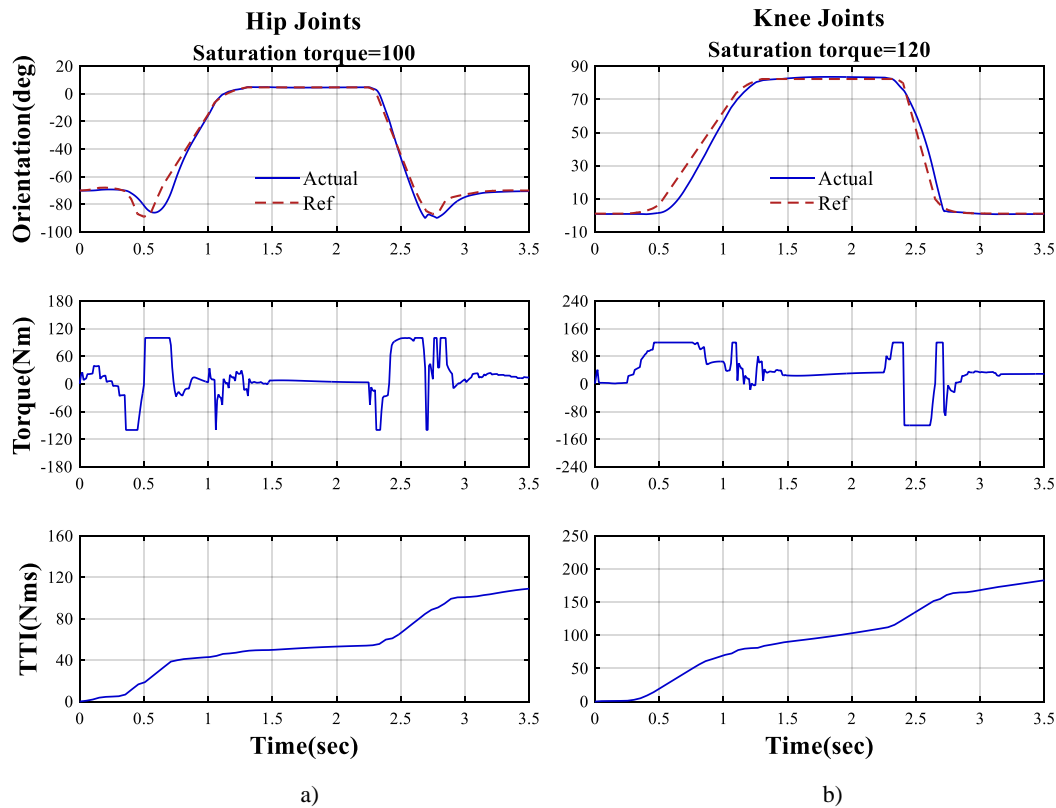


Figure 4.11 Orientation, torque and TTI of a) hip and b) knee joints with lowest torque saturation values

It was also observed that a relation exists between the torque saturation values and the TTI. Scatter plots of trajectories with an acceptable RMSE were used to further analyse the relations between torque saturation values and RMSE, saturations and TTI, and RMSE and TTI for both joints.

Similarly with the previous approach, data with RMSE higher than 10% was excluded due to instability. This was the case for all the hip saturations of 90 Nm or less, many of those of 100 Nm and some of 110 Nm. The reason for this is that excessively limiting torque, generates a low control action, which prevents the system to reach the desired position.

Once again, a polynomial of 4<sup>th</sup> degree was fitted to data and an inversely proportional relation was found between saturation torques and RMSE for both joints. If saturation torque is higher, that is, the system is allowed to use more torque, the error is lower. However, as seen in Figure 4.12, the decrease in RMSE is not very significant for either of the joints.

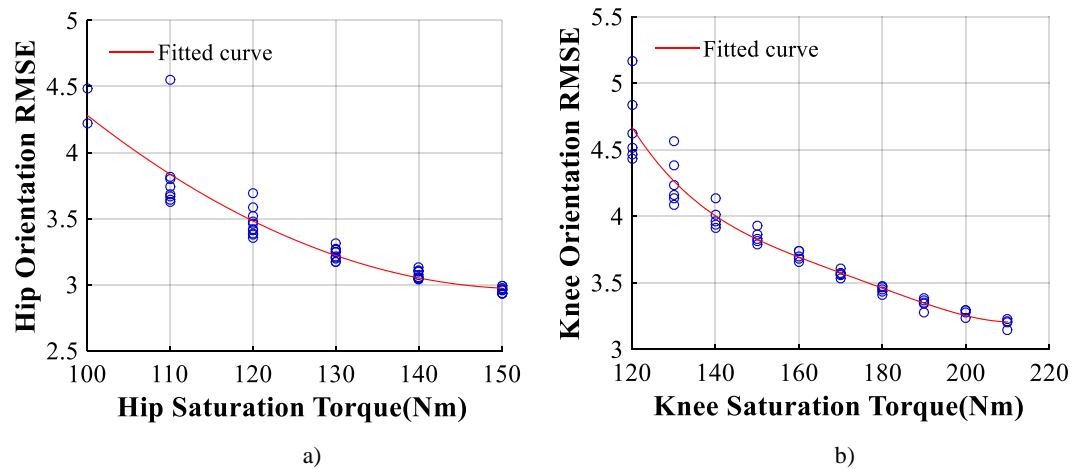


Figure 4.12 Relation between RMSE and saturation torque for a) hip and b) knee joints

A proportional relationship was also found between saturation torques and TTI as shown in Figure 4.13, this was expected since limiting of torque leads to a reduction of the TTI. However, it was observed that, for knee, data was more concentrated over the fitted curve whereas hip data is more dispersed. This means that same saturation values for knee joint produced same TTI for this joint, however, some saturation values for hip joint, produced different TTI for hip. Therefore, it is possible to observe that another factor affects hip joint TTI behaviour. Since the only additional changing parameter is knee saturation, it is possible to conclude that changes in knee saturation affect hip TTI whereas changes in hip saturation does not affect knee joint TTI significantly.

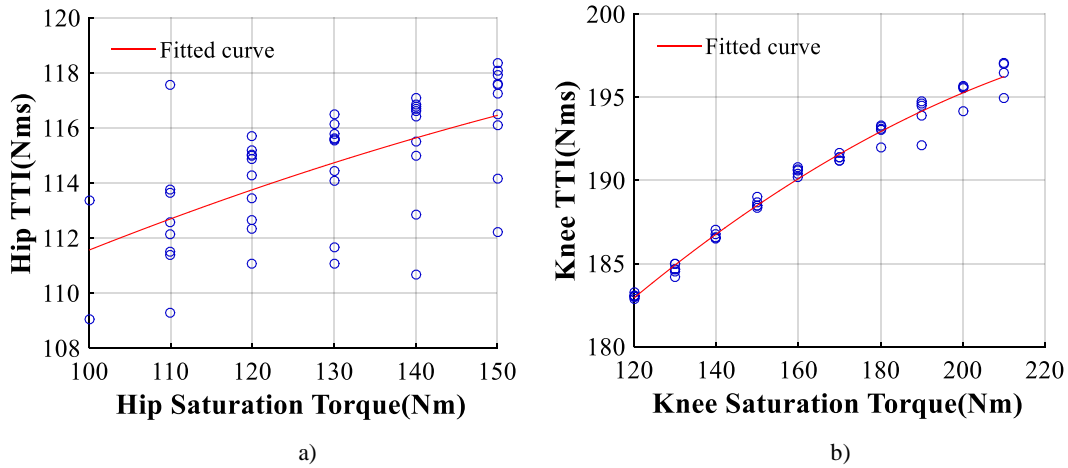


Figure 4.13 Relation between TTI and saturation torque for a) hip and b) knee joints

Finally, it was found that, as expected, there is an inversely proportional relation between the RMSE and TTI for both joints as shown in Figure 4.14 a) and b). However, for hip joint there are some points that do not follow this relation, as seen at the right section of Figure 4.14 a). These correspond to low hip saturation torques which have higher oscillations since they are barely able to supply the necessary torque to maintain the system stable.

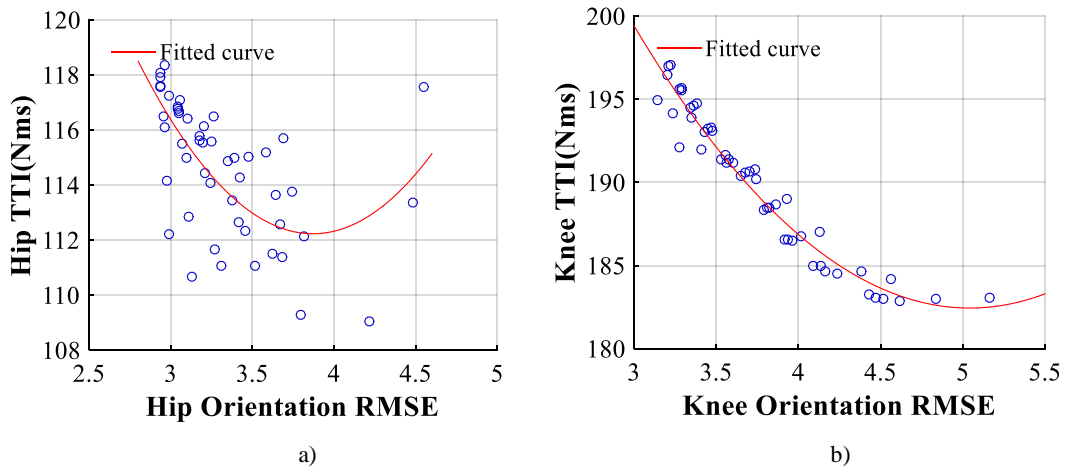


Figure 4.14 Relation between TTI and RMSE for a) hip and b) knee joints

Although it was demonstrated that saturation blocks of 100 Nm for hip joints and 120 for knee joints still produce good enough results in terms of RMSE and have low TTI, meaning that less energy would be required to control them, caution should be taken when minimising saturation torque to ensure stability of the system.

### 4.5.5 Tests with different velocities

In order to test the variation of torque needed to follow hip and knee trajectories while changing the velocity of the motion, a number of simulations were run considering only the standing up phase to decrease computation time. To simplify the task, hip revolute motor was set to be actuated by torque while ankle and knee trajectories were directly connected to revolute motors actuated by orientation at the plant. RMSE between the hip orientation reference and the actual value was calculated as before. TTI was also calculated to assess the amount of torque required for the whole movement.

Three different velocities were selected for this test:

- middle or average velocity of 43 degrees per seconds, where the total duration of the trajectory is 1.89 s. This is the average time that healthy people take to complete the motion.
- high velocity of 87 degrees per second, for a total duration of 0.94 s. Twice as fast as the average velocity.
- low velocity of 29 degrees per second for a total duration of 2.83 s. Half of the average velocity.

PID controller gains of  $K_p=14$ ,  $K_i=2$  and  $K_d=1.5$  for hip joints controller, were taken as an initial proposal. Saturation blocks were set to 160 Nm.

For high speed, the RMSE was 4.54, relatively high, although still beneath acceptable limits, while TTI was lower, 63 Nms. For average speed, RMSE was 3.22 and TTI 81 Nms, similar to the results of the previous section. However, for low velocity, the system became unstable as shown in Figure 4.15, with RMSE of 49.63 and TTI of 364 Nms.

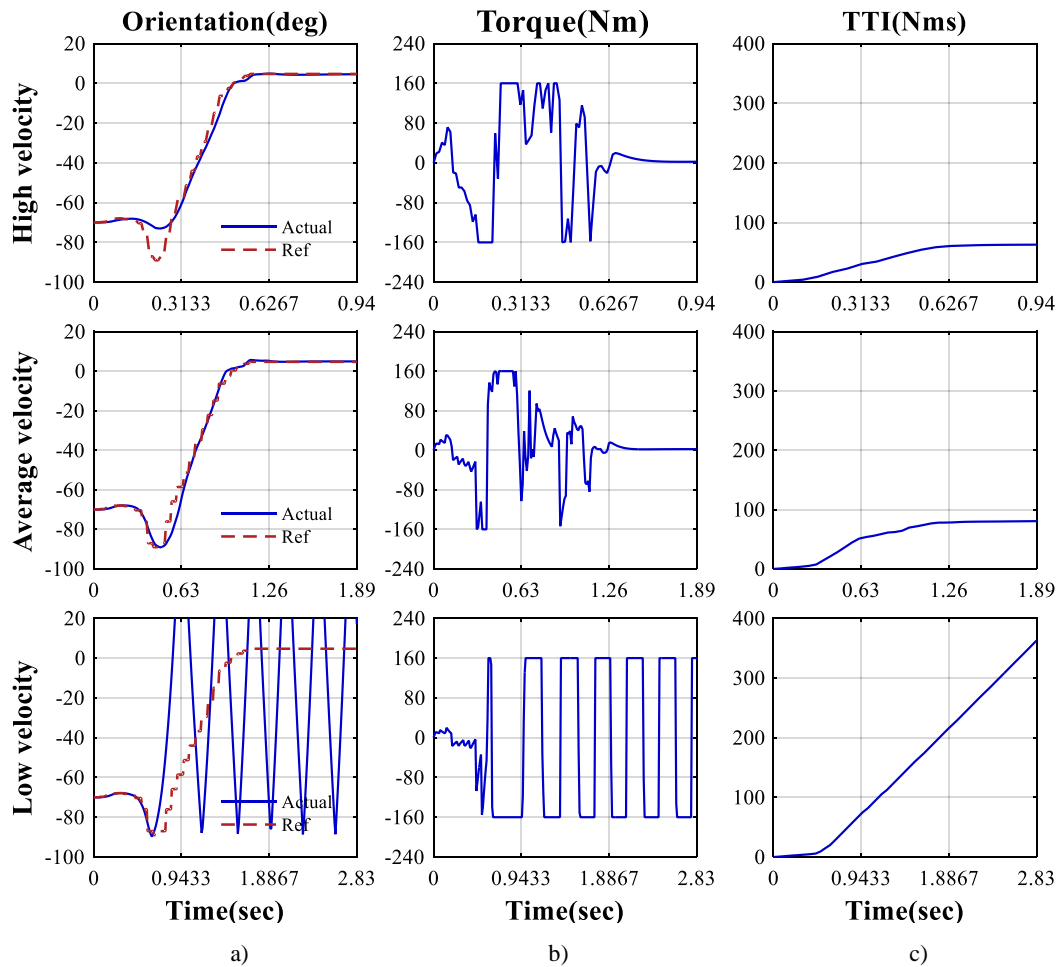


Figure 4.15 a)Orientation, b)torque and c)TTI of hip joints for three different velocities

Simulations were run with varying combinations of  $K_d$  and  $K_i$  gains, it was noted that all were successful in controlling standing-up motion at the three different velocities defined above. Those which were successful with high and average velocity, were not capable of controlling the system while performing motions with duration of more than 2.5 seconds. It was possible to observe that higher  $K_d$  gains provided better results, nevertheless, no further tests were done in this stage.

For the knee joint, the best PID controller gains from the previous section,  $K_p = 14$ ,  $K_i = 7$  and  $K_d = 2.8$ , were considered. Saturation blocks were set to 210 Nm. Results shown in Figure 4.16 correspond to a RMSE of 4.15 and a TTI of 71 Nms for high velocity, a RMSE of 4.08 and TTI of 143 Nms using average velocity, and RMSE of 3.65 and TTI of 210 Nms for low velocity. In this case, the error was very similar with the 3 different velocities and TTI was proportional to the duration of the movement.

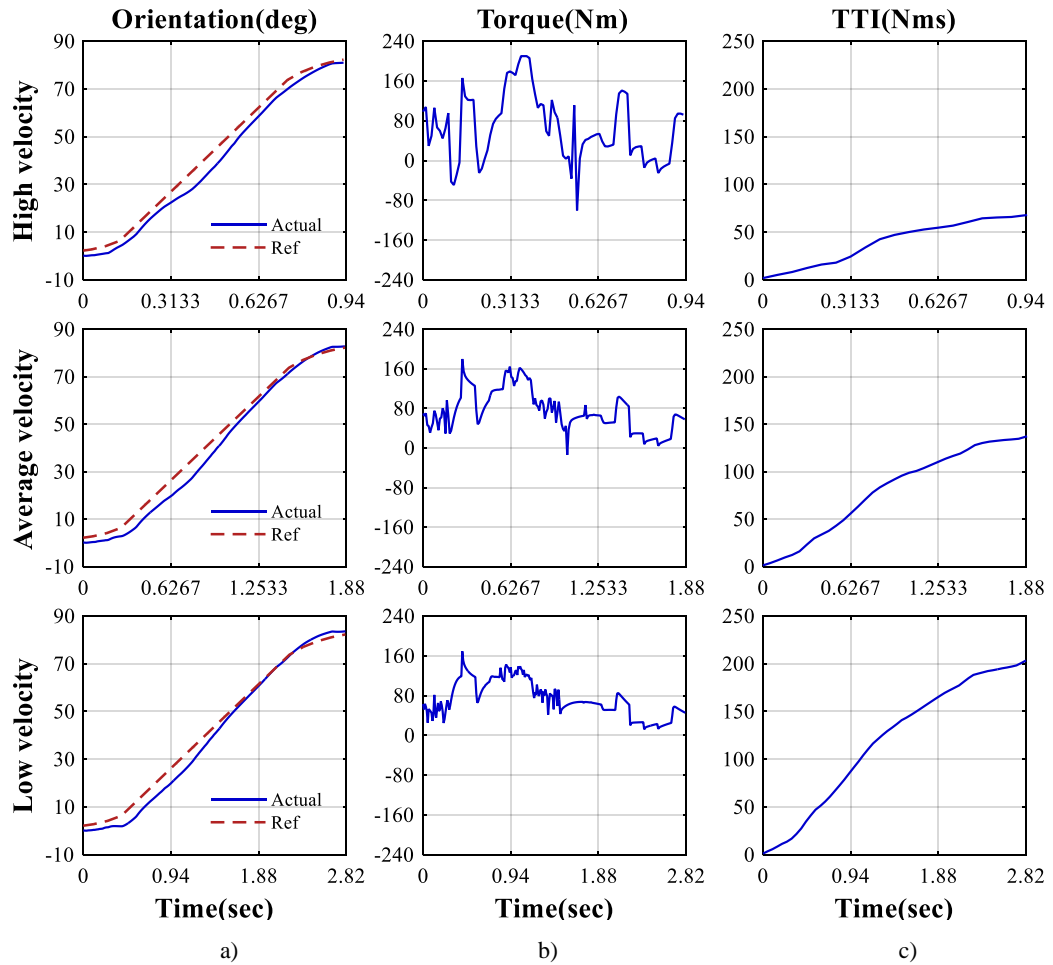


Figure 4.16 a)Orientation, b)torque and c)TTI of knee joints for three different velocities

Tendencies obtained in the present work, shown in Figure 4.15 and Figure 4.16, are in line with previous studies (Sveistrup et al., 1999). While the magnitude of peak forces at joints decrease when rising slowly, there is also a loss of momentum and increase in the duration of maximum hip and knee forces. This increases the strength requirements for the motion when performed slowly; therefore it is perceived as requiring more effort (Sveistrup et al., 1999)

## 4.6 PID control of exoskeleton for standing-up assistance

### 4.6.1 Standing-up with unactuated exoskeleton

A deeper understanding of the system was obtained through the analysis of the behaviour of the humanoid model during standing-up and sitting-down motions, with different combinations of gains, speeds and torque saturation values, as described in the previous section. Investigations were then carried out by incorporating the exoskeleton with the humanoid model. One of the reason for including it until this stage, is that the computational time increases proportionally to the complexity of the model.

As described in Chapter 2, the exoskeleton model is comprised of 3 revolute joints at hip, 1 at knee and 2 at ankle, as well as prismatic joints at thigh and leg supports to adjust the length according to the user's dimensions. In total, there are 16 joints from which, only 6, hip, knee and ankle joints in the sagittal plane, can be actuated, and the rest are blocked. These are better illustrated in Figure 4.17

Initial tests with the exoskeleton were done with the humanoid carrying the exoskeleton which means that only the humanoid joints were actuated by torque while the exoskeleton joints in sagittal plane were set as revolute joints. Therefore, the exoskeleton follows the motion of the humanoid. Hip and knee joints were actuated to assess their independent behaviour for three different standing-up velocities. A similar PID control as that shown in Figure 4.5 was set up in Simulink.

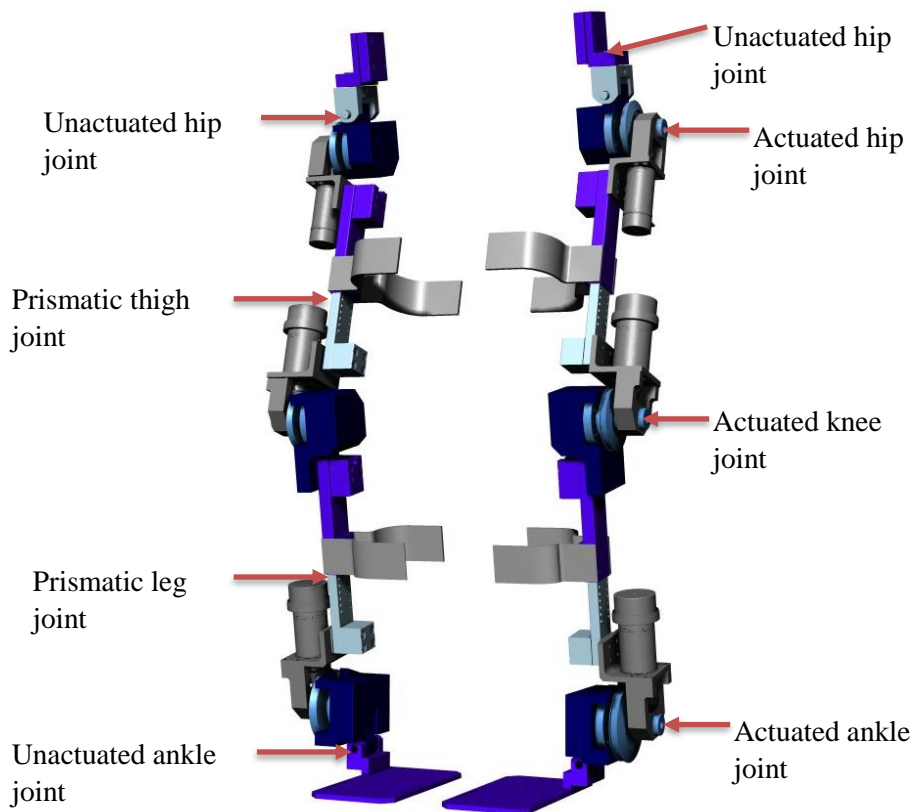


Figure 4.17 Exoskeleton joints

The three velocities for standing-up motion were assessed. For hip joints, gains used were,  $K_p = 14$ ,  $K_i = 1$ , and  $K_d = 1.4$  for high velocity,  $K_d = 4.2$  for average velocity, and  $K_d = 7.7$  for low velocity. The reason for varying  $K_d$  is that in the last section, it was noted that the same combination of gains was not capable of controlling hip motion at the three different speeds. Further, it was observed that increasing derivative gain enabled the control of low velocity motions.

As shown in Figure 4.18, using the gain values mentioned, and saturation torques of 160 Nm, the system could be controlled even at low velocities. RMSE of 8 and a TTI of 92 Nms was obtained at high velocity, RMSE of 2.9 and a TTI of 157 Nms at average velocity and RMSE of 2.58 and a TTI of 242 Nms at low velocity.

As it is possible to observe, the effect of increasing  $K_d$  is higher sensibility, allowing the system to reduce the error using all the available torque to keep the system under control. However, in addition to generating undesirable oscillations, this is a costly alternative since TTI is much higher, meaning that energy expenditure is larger and damage to the actuators a possibility.

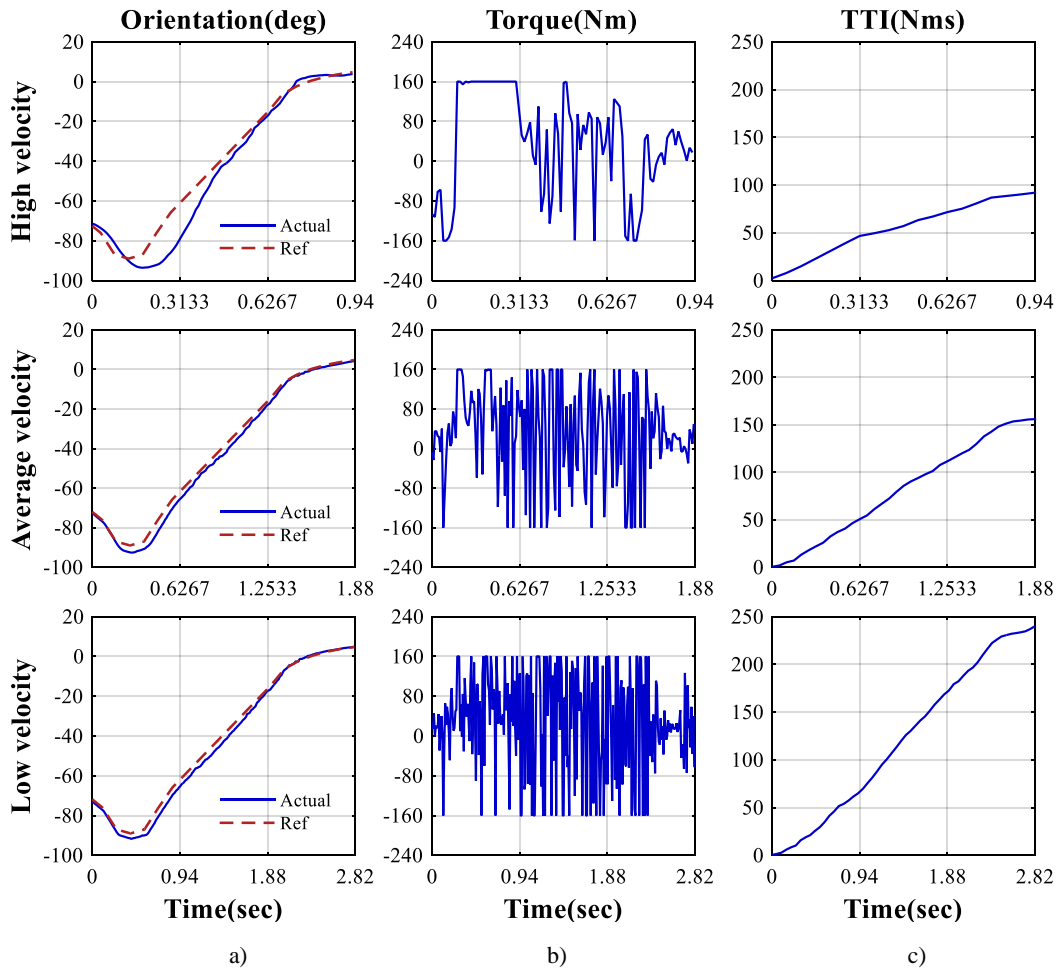


Figure 4.18 a)Orientation, b)torque and c)TTI of hip joints with unactuated exoskeleton for different velocities

For the knee joints,  $K_p = 14$ ,  $K_i = 7$  and  $K_d = 1.9$  were used for the three different velocities. Results in Figure 4.19 show that this combination of gains is successful in controlling the system. RMSE was 5.08 and TTI 85 Nms for high velocity while for average velocity RMSE was 4.77 and TTI 142 Nms, and for low velocity, RMSE was 4.28 and TTI 207 Nms.

Although  $K_d$  was decreased as compared with previous section, the additional weight of the exoskeleton seems to add instability to the system, therefore, more oscillations are present and TTI was increased, similarly as with hip joints.

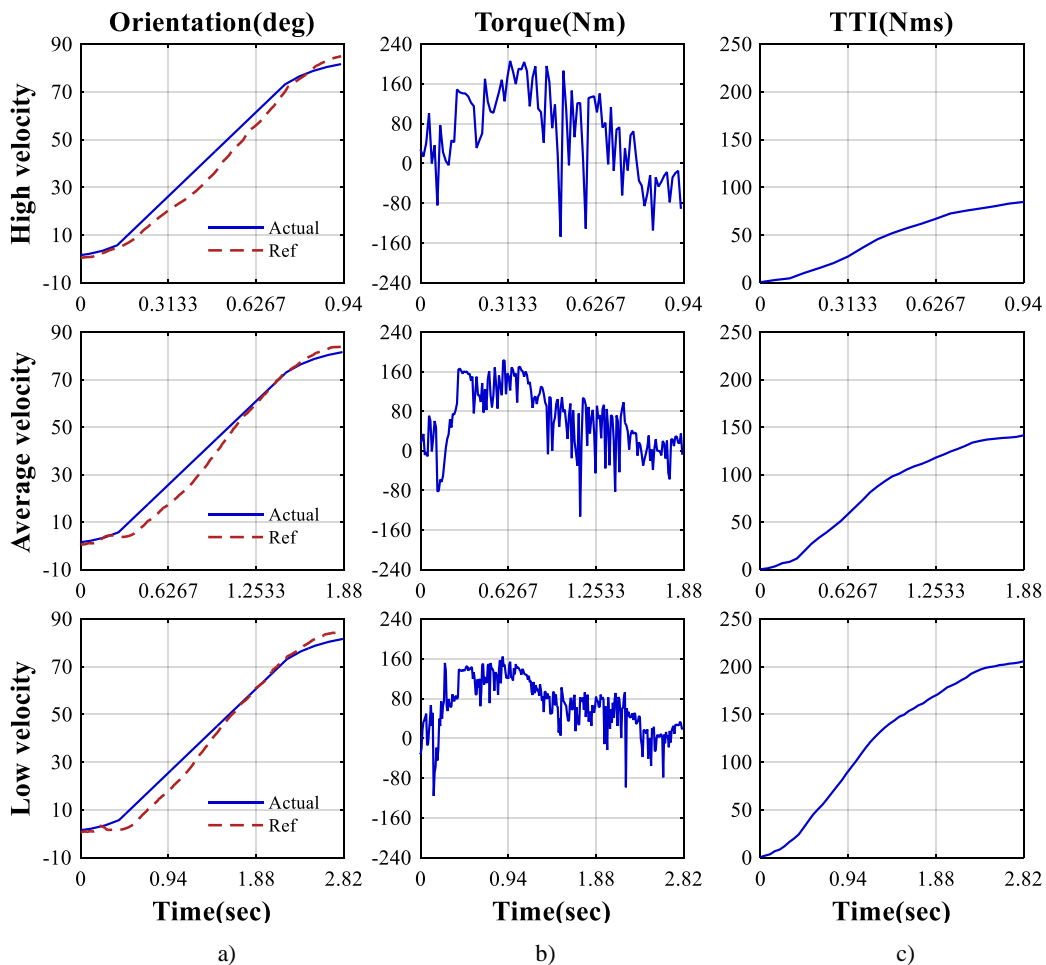


Figure 4.19 a)Orientation, b)torque and c)TTI of knee joints with unactuated exoskeleton for different velocities

## 4.6.2 Exoskeleton assistance

The focus in previous sections had been on obtaining an estimate of the amount of torque required for the complete system to perform the standing-up and sitting down motions. In this section, the Simulink model was modified to send 70% of the torque supplied by the PID control to the humanoid joints, and only a 30% to the exoskeleton hip and knee joints. This represents a user that is only capable of supplying 70% of the torque required to perform the standing-up and sitting-down motions and therefore, needs assistance to complete the task. Additionally, slight modifications had to be done to hip reference orientation profile.

These tests assume that both humanoid and exoskeleton follow the same trajectory although they are only “coupled” using a collision setting between exoskeleton supports at thigh, calf, and humanoids legs, and through rigid joints at belt and shoes. This assumes that

the high-level control in charge of the intention estimation is capable of sending the exoskeleton the exact same trajectory that the person intends to follow.

The resulting Simulink model is shown in Figure 4.20. It can be observed that it now has four control loops, the first for exoskeleton's hip joints, the next for humanoid's hip joints, the third for exoskeleton's knee joints and the last one for humanoid's knee joints.

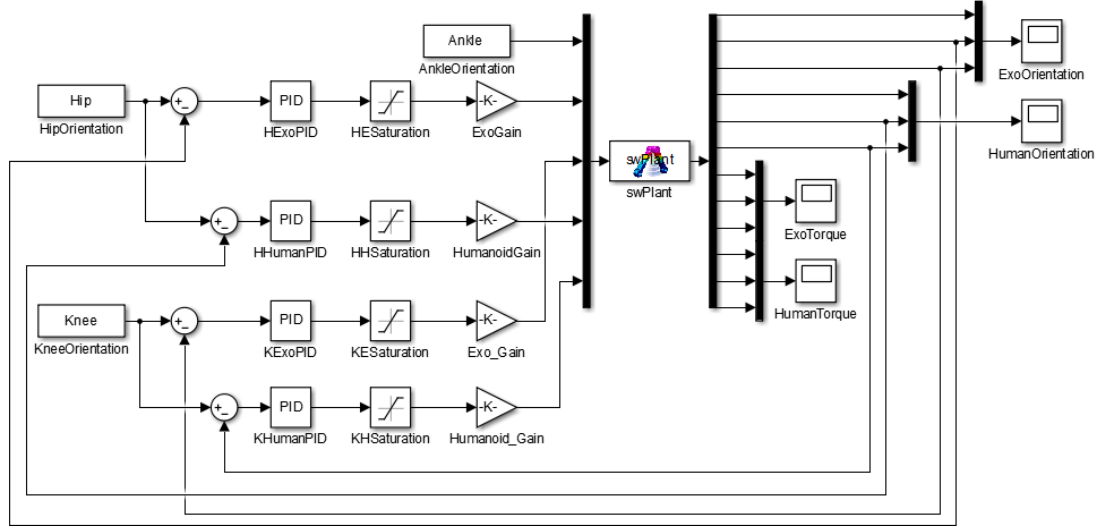


Figure 4.20 Simulink control diagram of hip and knee joints of humanoid and exoskeleton

Figure 4.21 shows the behaviour of the hip joint with feet unfixed from ground, while standing-up and sitting down, with exoskeleton assistance of 30% and a saturation torque of 160 Nm. Three different velocities were tested, high velocity of 57 degrees per second, average velocity of 28.5 degrees per second and low velocity of 19 degrees per second. PID gains used were  $K_p = 14$ ,  $K_i = 1$ , and  $K_d = 1.4$  for high velocity,  $K_d = 4.2$  for average velocity, and  $K_d = 7.7$  for low velocity.

An RMSE of 6.95 and humanoid TTI of 37 Nms were obtained for high velocity, RMSE of 2.69 and TTI of 46 Nms for average velocity, and RMSE of 1.83 and TTI of 125 Nms for low velocity. Moreover, it is possible to observe that high and normal velocity behaviours are acceptable, though that of the system at low velocity must be improved.

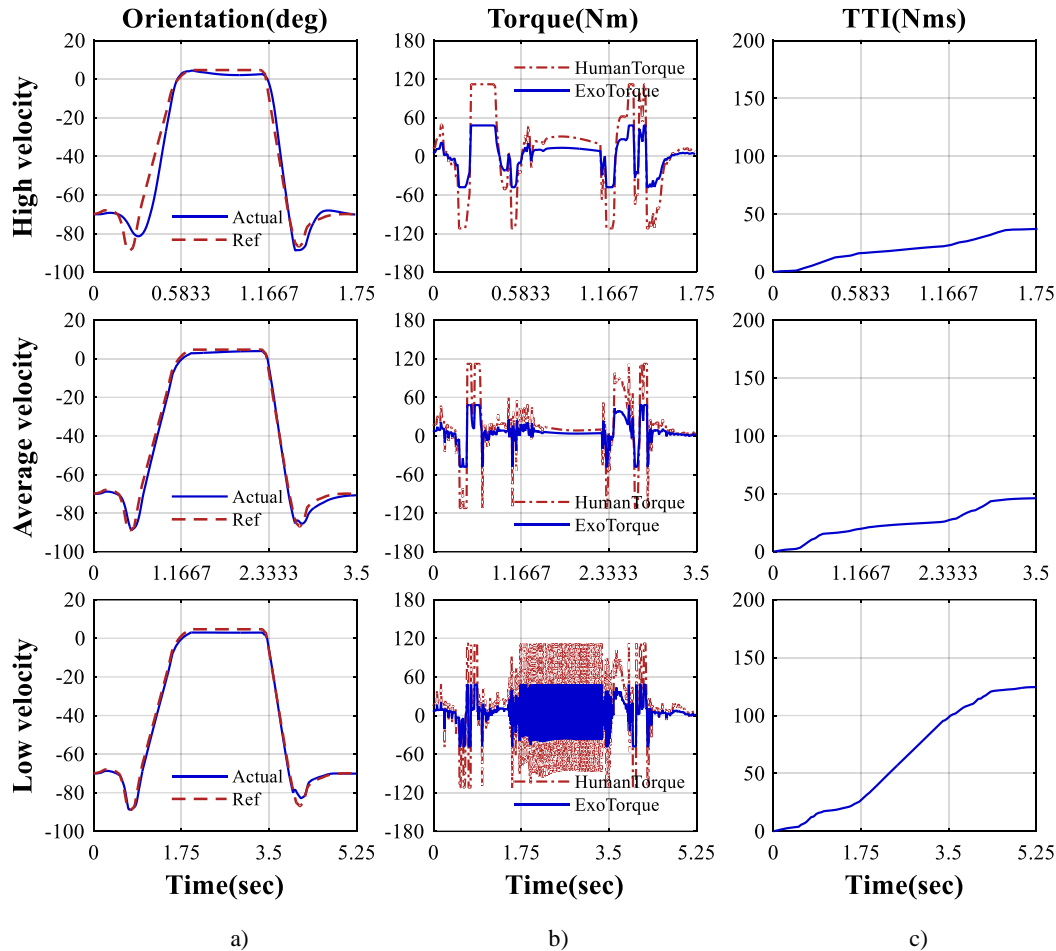


Figure 4.21a)Orientation, b)torque and c)TTI of hip joints with actuated exoskeleton for different velocities

Figure 4.22 shows the behaviour of knee joints under the previous conditions, a saturation torque of 210 Nm and PID gains  $K_p = 14$ ,  $K_i = 7$ , and  $K_d = 1.9$ , for the three velocities. For high velocity, a RMSE of 8.82 and humanoid TTI of 37 Nms were achieved, while RMSE of 3.74 and 3.4, and TTI of 51 Nms and 71 Nms, were obtained for average and low velocities, respectively. Unlike at hip joints, TTI was reasonable for knee joint, even for low velocity. Some oscillations observed in the standing period could be eliminated through further optimisation of the controller gains.

Comparing RMSE and TTI of the three different speeds, it was found that, RMSE increases at high speed, and decreases at low speeds. The TTI has the opposite relation, due to the oscillations in the system while trying to control it. Figure 4.23 shows the resulting standing-up and sitting-down sequence at average velocity while the exoskeleton provides assistance to the humanoid.

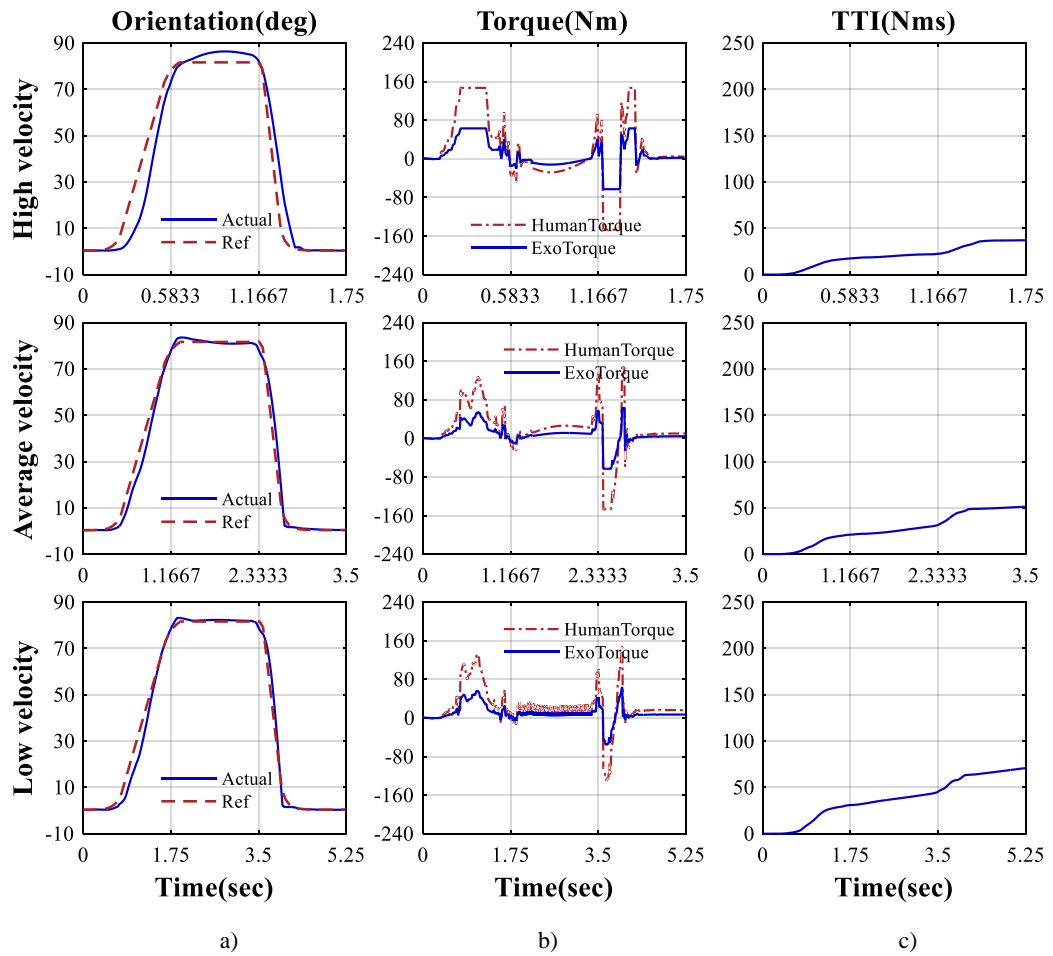


Figure 4.22 a)Orientation, b)torque and c)TTI of knee joints with actuated exoskeleton for different velocities

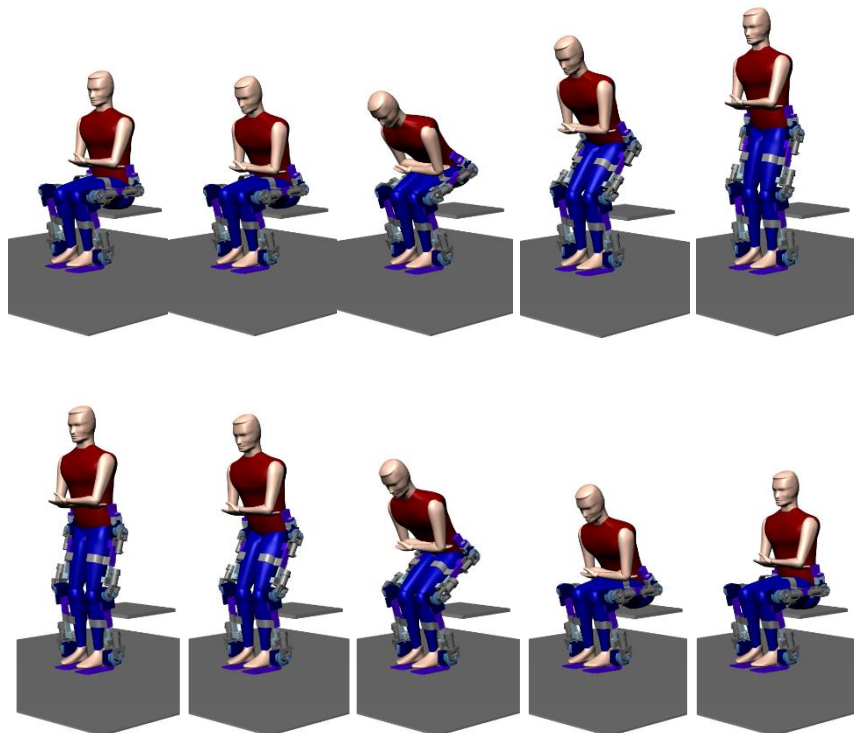


Figure 4.23 Standing-up and sitting-down motion with exoskeleton assistance

Two additional tests were performed. One where the exoskeleton was unactuated or passive, and the user can only supply 70% of the required torque. This represents a scenario where the exoskeleton runs out of battery power, for example. Therefore, it is important to assess if the user could still execute the standing-up and sitting-down motions while carrying the exoskeleton.

Hip joints results for high velocity were, RMSE of 14.1 and humanoid TTI of 110 Nms, RMSE of 4.58 and TTI of 137 Nms for average velocity and RMSE of 2.39 and TTI of 176 Nms for low velocity. While for knee joints, RMSE was 21.04 and humanoid TTI 155 Nms at high velocity, RMSE was 5.83 and TTI 160 Nms at average velocity and RMSE was 6.36 and TTI 252 Nms at low velocity.

RMSE and TTI were additionally compared with those of a humanoid that can only supply 70% of the required torque without wearing the exoskeleton since it is also relevant to establish a baseline to assess the real assistance that the exoskeleton provides. In this case, hip joint results at high, average and low velocity were, RMSE of 11.01 and humanoid TTI of 108 Nms, RMSE of 4.36 and TTI of 132 Nms and RMSE of 2.4 and TTI of 176 Nms, respectively. While for knee joints, RMSE was 13.66 and humanoid TTI 105 Nms at high velocity, RMSE was 4.16 and TTI 61 Nms at average velocity and RMSE was 4.01 and TTI 85 Nms at low velocity.

Figure 4.24 shows the results of the motion while not wearing exoskeleton versus wearing an actuated exoskeleton. RMSE decreased 35% for hip joints and 27% for knee joints as shown in Figure 4.24 a), and TTI was 50% smaller for hip joints and 36% smaller for knee joints, as shown in Figure 4.24 b). Therefore, it is demonstrated that when actuated, the exoskeleton helps users to sharpen their standing-up and sitting-down manoeuvres, while decreasing their energy expenditure.

However, it is also shown that when the exoskeleton is passive, humanoid joints RMSE and TTI are increased between 80% and 255%, compared to results when the exoskeleton is actuated. It is possible to conclude that the system is too heavy and not transparent to the user when unactuated, therefore, efforts must be done to reduce the exoskeleton weight.

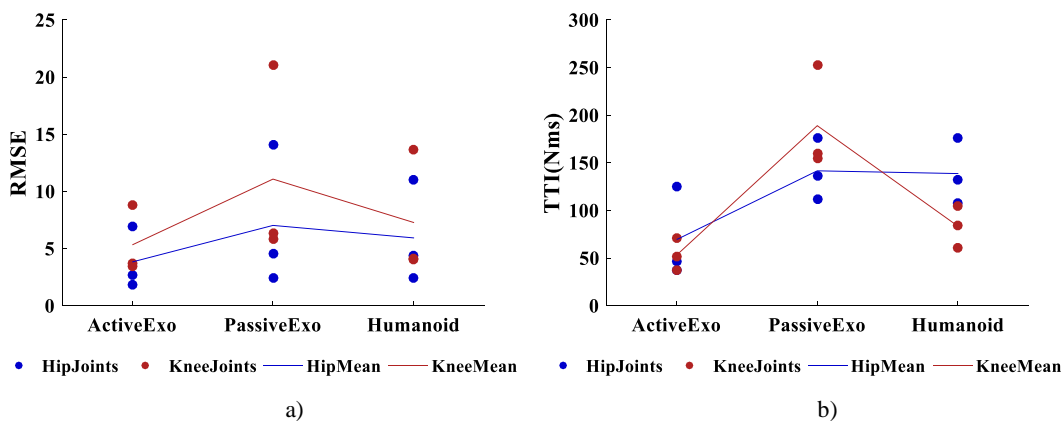


Figure 4.24 a) RMSE and b) TTI of with actuated exoskeleton, unactuated exoskeleton and humanoid alone

### 4.6.3 Reaction force with seat and ground

Once humanoid and exoskeleton were integrated, and feet unfixed from ground, reaction forces with both, seat and ground were measured during the standing-up and sitting-down motions at average velocity. In order to get realistic measurements of reaction with the ground, balance had to be guaranteed during the whole motion. Therefore, slight adjustments had to be made to hip trajectory to guarantee a balanced motion. Additionally, the duration of the upright standing position, between the two motions was decreased to save computation time.

Figure 4.25 shows resulting reaction forces with ground and seat in the vertical axis. The knee trajectory is shown as a guide to match the force peaks within the motion. Behaviour is similar to previous studies by Kralj and Badj, (1989), although the magnitude of some peaks is higher than expected considering the weight of the human and exoskeleton.

It is important to mention that during this project, it has been noticed that SimWise has issues to manage collisions between bodies, especially between flat surfaces as is the case of feet and ground. Although friction and restitution values can be setup, it has been found that behaviour in some cases varies in unexpected ways. Additionally, it was found that the reaction force with the seat depended on the orientation of pelvis at the moment of contact with the seat.

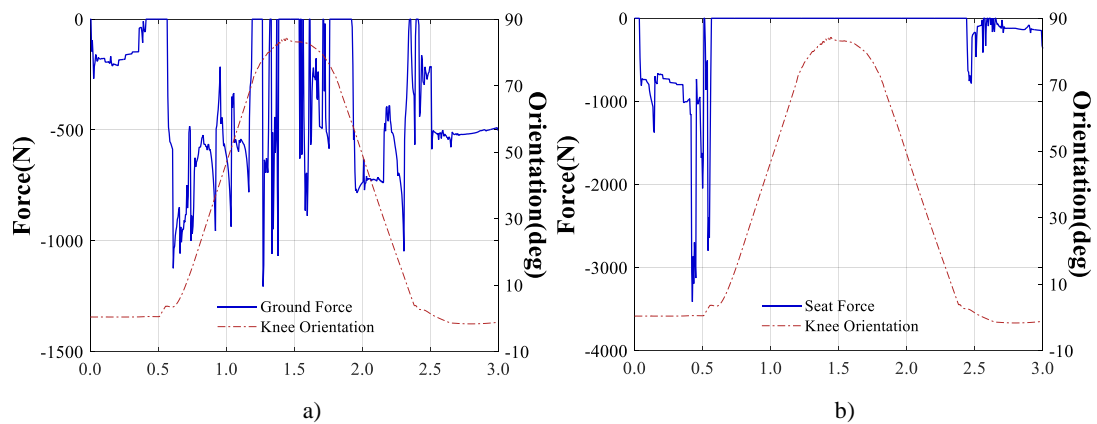


Figure 4.25 Reaction force with a) ground and b) seat with knee orientation as reference

Though SimWise is suitable for dynamic calculations, it uses only solid bodies which are different to human's body tissues. Therefore, due to the limitations aforementioned, reaction forces are an estimate only. In order to get more reliable results for this test, other software would need to be used, although it is not under the scope of this research.

## 4.7 Summary

Humanoid and exoskeleton models have been simulated within SimWise virtual environment, for theoretical investigations of standing-up and sitting-down mobility towards assistance for the elderly. Investigations of feasibility of the required torque profiles for actuating the various joint motors, to achieve normal joint displacement, have been carried out with the implementation of PID controllers.

It has been demonstrated that hip and knee joint torques can be contained within allowable limits with suitable control actions at different velocities of standing-up and sitting-down motions, although at low velocities, more energy is required. The latter is a result of the increase in oscillations and the loss of momentum which forces the system to provide high torques over a longer period.

Adequate  $K_p$ ,  $K_d$  and  $K_i$  gains were identified which minimise RMSE and TTI, to decrease energy consumption in addition to properly tracking the desired reference. Moreover, it was demonstrated that torque can be limited to 100 Nm for hip joints and 120 for knee joints, to further decrease TTI, and motions can still be performed with acceptable error.

A comparison of the torque requirements while wearing the actuated exoskeleton versus not wearing it, in addition to wearing it in passive or unactuated state was carried out. In the case when the exoskeleton was passive, humanoid joint RMSE and TTI were much higher than when the exoskeleton is actuated. This is one of the main issues with exoskeletons nowadays, where, should the device fail or run out of power, the user would need to carry it, becoming a burden to the user. In order to avoid this issue, the only feasible solution is to reduce the exoskeleton weight.

Comparing the results while wearing the actuated exoskeleton versus not wearing it, it was found that the exoskeleton decreases RMSE and TTI in around 30%, showing that it can help the users sharpen standing-up and sitting-down manoeuvres while decreasing their energy expenditure.

Finally, initial estimations of ground and seat reaction forces have been obtained. These can be used as input parameters for the exoskeleton upper level control in future research to be able to identify user intention to stand or step. However, more accurate simulations need to be performed in future research to obtain more significant results.

# CHAPTER 5

## Online trajectory tracking control of exoskeleton for paraplegic assistance on standing-up and sitting-down tasks

### 5.1 Introduction

In this chapter, a control system able to generate reference trajectories for standing-up and sitting-down motions, at variable velocities, is developed. It was also designed to include equilibrium control, and ensure that torque requirements and energy consumption are within the admissible limits.

A middle level controller is described and coupled to the low level PID controllers developed in Chapter 4 for standing-up and sitting-down with an exoskeleton, and trajectories are automatically adjusted online according to the state of the system. This controller is suitable for use in an exoskeleton for paraplegic patients, since it is capable of independently generating motions considering the current orientation of lower limbs, as well as the position of feet and upper body.

The control scheme includes a finite state controller developed considering the biomechanics of standing-up and sitting-down motions. It requires joints orientation, position of the ground projection of centre of mass, and upper body centroid position to transition between states, and maintain proper hip and knee orientations during the upright standing state.

Torque and torque time integral are assessed during the simulation of controlled standing-up and sitting-down motions at three different velocities. RMSE is measured to ensure that the PID controllers manage to adequately follow the trajectories generated by the middle level control. Finally, zero moment point is calculated offline to assess whether the reference trajectories generated by the system enable its dynamic equilibrium.

## 5.2 Equilibrium of mobile systems

One of the most important purposes of a locomotion mechanism during tasks such as walking, standing-up, climbing stairs, among others, is to maintain balance. There are different strategies to achieve this goal, an example is the restriction of the centre of mass (CoM) ground projection to the support base. This technique takes into consideration the forces generated due to mass, acting upon the base of the system. Although it is useful to assess the equilibrium of static objects, it does not account for the dynamic forces affecting the system (Azevedo et al., 2004).

When a system moves on its base or when its base displaces, all the forces that act upon it must be in equilibrium; only then, can the system be considered in dynamic equilibrium. The position of the zero moment point (ZMP) is similar to the CoM in the sense that dynamic equilibrium is guaranteed when the ZMP is inside the support area. However, this property is only valid in cases where all the contact points are in the same plane, and when the whole area of foot sole is in contact with the ground (Azevedo et al., 2004; Vukobratovic and Borovac, 2004).

### 5.2.1 Static equilibrium and-centre of mass

When all the resultant forces and moments acting on a system are equal to zero, it is considered to be in equilibrium (Kell and Everett, 2010). In the case of a standing human or robot submitted to an external force, it has to compensate for the displacement induced by the force. Therefore, in order to maintain its static equilibrium, it has to use contact ground forces. If the disturbance is greater, contacts may be insufficient to compensate the displacement and static equilibrium is lost.

Static equilibrium can be evaluated with the distance between the CoM/ centre of gravity (CoG) projection, and the support base contour (Azevedo et al., 2004). Thus, a feasible solution to avoid a fall is to increase the size of the support base as this is what occurs when a human places one foot in front of the other when a pushing force is applied to his back.

The support base of a body is the surface area of the part or parts in contact with the ground that are involved in the support of the object itself. It corresponds to the surface of the convex hull linking the contact points together (Azevedo et al., 2004). In case of humans, the support area can include arms against armrests, hands in contact with a wall, a crutch against the ground when standing, or even full body when lying on a bed.

When standing, the support base is the area between, and including, the foot soles; when sitting, it includes buttocks in contact with the seat. During the walking motion, there are two types of support base, single support and double support. The former refers to the swing phase in which only one foot is in contact with the ground, and double support refers to the stance phase in which both feet or at least a section of both feet are supporting the body (Dekker, 2009)

Formally, the CoM is defined as the point about which the total mass of an object is evenly distributed, is often referred to as CoG. The latter is defined as the point at which the gravity force acts. The CoM and the CoG of an object are in the same position when the gravitational field in which the object exists is uniform, therefore, although these terms by definition, are not equal, in the current research project, they can be used as synonymous (Vukobratovic and Borovac, 2004)

For multibody systems, centre of mass can be calculated as:

$$CoM(t) = \sum_{i=1}^n \frac{c_i(t) \cdot m_i}{m_T} \quad (5.1)$$

Where  $n$  is the total number of links,  $c_i$  is the position of the centroid of the  $i$ -th link at every sample time,  $m_T$  is the summation of the mass  $m_i$  of the  $i$ -th link, of the  $n$  segments that make up the humanoid and exoskeleton, given by:

$$m_T = \sum_{i=1}^n m_i$$

If the position  $c_i$  is a vector with centroid positions in  $x$ ,  $y$  and  $z$  axis, the location of the three components of the CoM can easily be obtained (Kell and Everett, 2010).

During human standing, the CoM is at the level of the second sacral vertebra, inside the pelvis, however, when the person starts moving upper or lower limbs, or executes even a small change of inclination, the CoM starts shifting. The projection of the CoM on the ground is particularly important when compared against the support area to assess if the system is statically stable (Kell and Everett, 2010).

In this research, the centroids were obtained directly from SimWise. Since each segment of the humanoid and exoskeleton is a separate part, SimWise is able to calculate centroids according to the mass, material and dimensions of each segment. As mentioned in Chapter 2, these two parameters were set as close as possible to human characteristics according to Winter, (2009). Centroids could also be calculated or estimated through geometrical approximation.

Afterwards, the position of the centroid of each segment with respect to the world origin has to be obtained. In simulation, these are easily acquired as a meter can be set in SimWise

to monitor the position of a location of interest within the geometry, relative to the three axes. Finally, through the connection block with Simulink, it is possible to get all the centroids' positions, and using a matrix that contains all the masses of the different segments, perform the CoM calculation according to equation (5.1).

For this research, the CoM is calculated in the three-axis. However, it is assumed that both legs move synchronously and therefore, a leg cannot significantly shift the CoM sideways, that is, in the frontal or  $y$  axis. Thus  $CoM_y$  is always zero. CoM position in the vertical or  $z$  axis,  $CoM_z$ , is used to assess the extension of the body in the standing posture. Most importantly, CoM position in the lateral or  $x$  axis and  $CoM_x$ , is compared against the support area for balance control. Figure 5.1a) illustrates humanoid and exoskeleton models and CoM during walking with wheel walker, and Figure 5.1c) shows humanoid and exoskeleton models along with the calculated CoM during the standing-up motion.

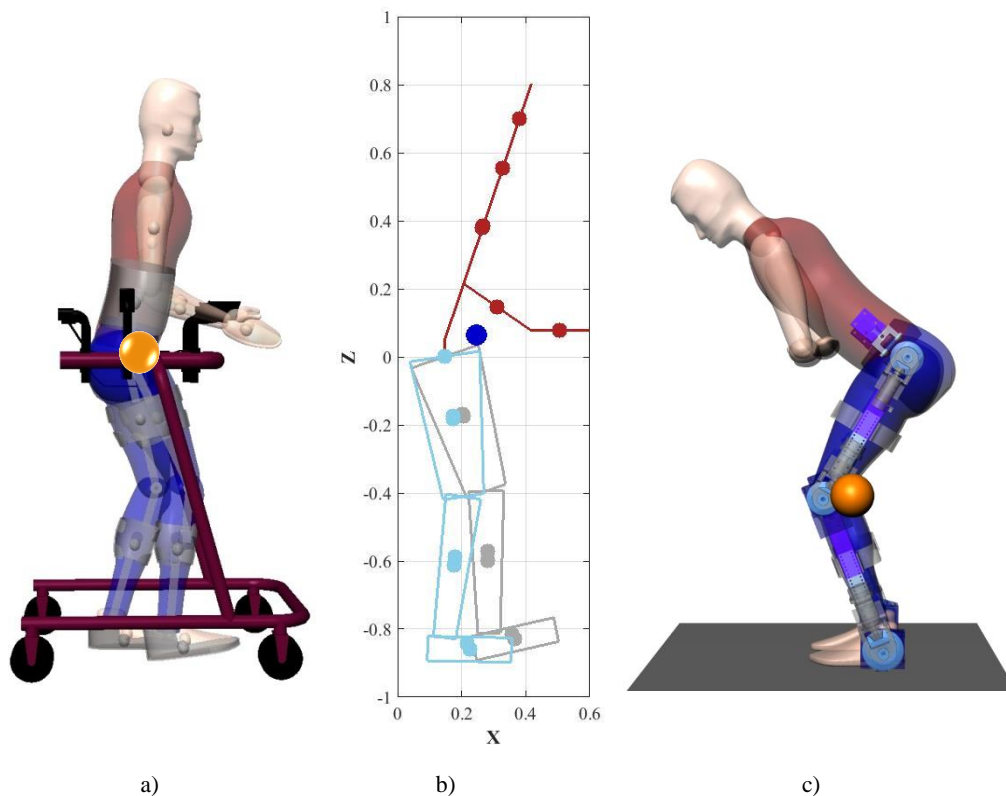


Figure 5.1 a) Humanoid and wheel walker CoM b) CoM and centroids diagram c) CoM during standing-up motion

In practice, CoM calculation could be achieved through gyroscope readings, which are the most precise alternative, when sensors are properly placed, however it is not the most feasible nor cost effective way. Another strategy is to calculate positions of each segment using kinematics, however, goniometers would still be needed at joints, and the resulting position would not be as accurate. A combination of information from gyroscopes and goniometers is

commonly used to calculate CoM. Estimation of the centre of pressure has also been selected as a more feasible alternative (Azevedo et al., 2004).

### 5.2.2 Dynamic equilibrium and zero moment point

Zero-Moment Point was introduced by Vukobratovic between 1968 and 1973, and is defined as a transitory point at the contact surface between the extremity and the ground, where the resultant of the reaction forces is zero (Vukobratovic et al., 1970; Vukobratovic and Stepanenko, 1972; Vukobratovic, 1973). These forces include the moment of gravity, inertial forces of the human or manipulator, and external forces (Sugano, 1993).

ZMP is often used interchangeably with Centre of Pressure (CoP). CoP is the point of application of the ground reaction force (GRF), where the latter is the reaction to the human weight exerted to the ground. It can also be understood knowing that the pressure between the foot and the ground can always be replaced by a force acting at the CoP (Kiela, 2015).

When all forces acting on the mechanism during the motion are in equilibrium, including inertia, gravitation, Coriolis, and centrifugal forces and moments, they can be represented by a force acting in the ZMP. Therefore, in the case of a dynamically balanced gait, CoP and ZMP are equal. However, when the motion is not dynamically balanced, the ZMP does not exist and the human or humanoid falls about the foot edge (Vukobratovic and Borovac, 2004).

During quiet standing, CoP, CoM and ZMP are in the same position, however once the person starts walking or sitting-down, CoM differs from CoP and ZMP (Kell and Everett, 2010; Vukobratovic and Borovac, 2004).

Although CoP is easier to obtain experimentally than ZMP, using sensors located in insoles, however, this can only be done online. It is not possible to make a prediction about the balance state of a motion profile using CoP since it relies only in measured forces. The computation of the ZMP can solve this problem (Kiela, 2015).

In order to calculate the ZMP for a multibody system, the reaction force and torque in the base of the system must be calculated, using information such as mass, position, velocity, acceleration and type of joint of every link. This is called the computed ZMP or cZMP (Kiela, 2015)

According to Kiela, (2015), the procedure to compute ZMP in a multibody system is as follows. Firstly, it is necessary to understand that a moving system exerts forces and moments onto its support base. Forces can be represented by a single resultant force  $F_R$ , and moments by a resultant moment  $M_R$  acting on point  $R$ . Therefore, a reaction force  $F_P$  and moment  $M_P$  can be calculated for any point  $P$ , so that all forces and moments sum zero to keep the robot in balance, thus:

$$F_P + F_R = 0 \quad (5.2)$$

$$M_P + M_R + r_P \times F_P + r_R \times F_R = 0 \quad (5.3)$$

Where  $r_P$  is the distance from the origin to point  $R$  and  $r_R$  the distance from the origin to point  $P$ .

When a mobile system is in equilibrium, the external forces  $F_E$  and external moments  $M_E$  that cause the movement of the system are in equilibrium with a resulting force  $F_R$  and resulting moment  $M_R$ , therefore:

$$\sum F = F_E + mg + F_R + mg = 0 \quad (5.4)$$

$$\sum M = M_E + r_c \times mg + M_R + r_c \times mg = 0 \quad (5.5)$$

Where  $r_c$  is the distance from the origin to the centroid. Equation (5.4) and (5.5) can be rewritten as:

$$F_E + mg = -F_R + mg \quad (5.6)$$

$$M_E + r_c \times mg = -M_R + r_c \times mg \quad (5.7)$$

Newton Euler equations state that the sum of external forces results in change of linear momenta, and the sum of external moments results in angular momenta:

$$\sum F = \dot{P} \quad (5.8)$$

$$\sum M = \dot{H} \quad (5.9)$$

Considering equations (5.6) and (5.8), the change in linear momentum can be rewritten as:

$$\dot{P} = -F_R + mg$$

or

$$F_R = -\dot{P} + mg \quad (5.10)$$

And considering equations (5.7) and (5.9), angular momentum can be rewritten as:

$$\dot{H} = -M_R + r_c \times mg$$

or

$$M_R = -\dot{H} + r_c \times mg \quad (5.11)$$

From equation (5.2), it is known that  $F_P = -F_R$ , therefore, substituting equation (5.10) in (5.2) it is possible to obtain:

$$F_P = \dot{P} - mg \quad (5.12)$$

Now, since all the forces are given with respect to the origin, point  $R$  coincides with origin, thus  $r_R = 0$ . Substituting equation (5.11) and (5.12) in equation (5.3), it is possible to see that:

$$M_P - \dot{H} + r_c \times mg + r_P \times (\dot{P} - mg) = 0$$

From where it is possible to obtain reaction moment  $M_P$ :

$$M_P = \dot{H} - r_c \times mg - r_P \times (\dot{P} - mg)$$

The  $x$  and  $y$  components of  $M_P$  are zero by definition, therefore:

$$\dot{H}_x - r_{c,y} \times mg_z + r_{c,z} \times mg_y - r_{P,y} \times (\dot{P}_z - mg_z) + r_{P,z} \times (\dot{P}_y - mg_y) = 0$$

$$\dot{H}_y - r_{c,z} \times mg_x + r_{c,x} \times mg_z - r_{P,z} \times (\dot{P}_x - mg_x) + r_{P,x} \times (\dot{P}_z - mg_z) = 0$$

Where  $\dot{P}_x$  and  $\dot{P}_y$  are the  $x$  and  $y$  components of change in linear momenta.  $\dot{H}_x$  and  $\dot{H}_y$  are the  $x$  and  $y$  components of change in angular momenta,  $r_{c,x}$ ,  $r_{c,y}$  and  $r_{c,z}$  are distances from the origin to the centroid in  $x$ ,  $y$  and  $z$  axes, respectively,  $r_{P,x}$ ,  $r_{P,y}$  and  $r_{P,z}$  are distances from the origin to point  $P$ , in  $x$ ,  $y$  and  $z$  axes, respectively,  $g_x$ ,  $g_y$  and  $g_z$  are gravity  $x$ ,  $y$  and  $z$  components, and  $m$  is the mass of the system.

Considering that the floor is in the horizontal or  $x$ - $y$  plane,  $r_{P,z} = 0$  and:

$$r_{P,x} = \frac{-\dot{H}_y + r_{c,z} \times mg_x - r_{c,x} \times mg_z}{\dot{P}_z - mg_z} \quad (5.13)$$

$$r_{P,y} = \frac{\dot{H}_x - r_{c,y} \times mg_z + r_{c,z} \times mg_y}{\dot{P}_z - mg_z} \quad (5.14)$$

Where the  $x$  and  $y$  components of point  $P$  refer to the location of the ZMP. To obtain these values, it is necessary to calculate the change in linear momenta  $\dot{P}$ , the change in angular momenta  $\dot{H}$ , as well as the three components of the distance from the origin to the centroid  $r_c$  of each segment.

Linear momenta is given by:

$$P = \sum_{i=1}^n m_i \dot{r}_{ci}$$

Where  $m_i$  is the mass of each link, and  $\dot{r}_{ci}$  is the linear velocity of the  $i$ -th link. Angular momenta is given by:

$$H = \sum_{i=1}^n r_{ci} \times m_i \dot{r}_{ci} + I_{Ri} \omega_i$$

Where  $r_{ci}$  is the distance from the origin to the centroid of the  $i$ -th link,  $\omega_i$  is angular velocity of the  $i$ -th link, and  $I_{Ri}$  is the inertia tensor of the  $i$ -th link with respect to the origin,  $I_{Ri}$  can be calculated as:

$$I_{Ri} = R_i I_i R_i^T$$

Where  $R_i$  is the rotation matrix from the origin to frame  $i$  and  $I_i$  is the body fixed inertia tensor defined previously for each link.

Change in linear momenta  $\dot{P}$  can be obtained through derivation of  $P$  as:

$$\dot{P} = \sum_{i=1}^n m_i \ddot{r}_{ci}$$

And for each link  $i$ :

$$\dot{P}_i = \dot{P}_{i-1} + m_i \ddot{r}_{ci} \quad (5.15)$$

Where  $\dot{P}_{i-1}$  is the change in linear momenta of frame  $i - 1$  and  $\ddot{r}_{ci}$  is linear acceleration of the  $i$ -th link.

Change in angular momenta  $\dot{H}$  can be obtained through derivation of  $H$  as:

$$\dot{H} = \sum_{i=1}^n r_{ci} \times m_i \ddot{r}_{ci} + I_{Ri} \dot{\omega}_i + \omega_i \times (I_{Ri} \omega_i)$$

And for each link  $i$ :

$$\dot{H}_i = \dot{H}_{i-1} + r_{ci} \times m_i \ddot{r}_{ci} + I_{Ri} \dot{\omega}_i + \omega_i \times (I_{Ri} \omega_i) \quad (5.16)$$

Where  $\dot{H}_{i-1}$  is the change in angular momenta of frame  $i - 1$ , and  $\dot{\omega}_i$  is angular acceleration of the  $i$ -th link.

Linear acceleration  $\ddot{r}_{ci}$  at the centroid of each link and linear acceleration  $\ddot{r}_i$  at the end of each link with respect to the origin can be calculated as:

$$\ddot{r}_{ci} = \ddot{r}_{i-1} + \dot{\omega}_i \times r_{i-1,ci} + \omega_i \times (\omega_i \times r_{i-1,ci}) \quad (5.17)$$

$$\ddot{r}_i = \ddot{r}_{i-1} + \dot{\omega}_i \times r_{i-1,i} + \omega_i \times (\omega_i \times r_{i-1,i}) \quad (5.18)$$

Where  $\ddot{r}_{i-1}$  is the linear acceleration at the end of the previous link,  $r_{i-1,ci}$  is the distance from frame  $i-1$  to the centre of mass of the  $i$ -th link, and  $r_{i-1,i}$  is the distance from frame  $i - 1$  to  $i$ .

It is possible to calculate angular velocities and accelerations at the end of each link  $i$  with respect to the origin using:

$$\omega_i = \omega_{i-1} + \dot{\theta}_i z_{i-1}$$

(5.19)

$$\dot{\omega}_i = \dot{\omega}_{i-1} + \omega_i \times \dot{\theta}_i z_{i-1} + \ddot{\theta}_i z_{i-1}$$

(5.20)

where  $\dot{\theta}_i$  is angular velocity of the  $i$ -th link,  $\ddot{\theta}_i$  is angular acceleration of link  $i$  and  $\omega_{i-1}$  is angular velocity of frame  $i - 1$  with respect to the origin, and vector  $z_{i-1}$  is the position in  $z$  axis of the link  $i - 1$ . Angular velocity  $\dot{\theta}_i$  and angular acceleration  $\ddot{\theta}_i$  are obtained through derivation of  $\theta_i$  with respect to time.

It is evident that the kinematics and dynamics of the system are required to complete the ZMP calculation. For a multibody robot, the homogeneous transformation matrix  $T_i^0$  between the origin and frame  $i$  can be calculated as:

$$T_i^0 = T_{i-1}^0 * A_i \quad (5.21)$$

Where  $T_{i-1}^0$  is the transformation matrix between the origin and frame  $i - 1$ , which is the frame at the joint that attaches link  $i$  and link  $i - 1$ , and  $A_i$  is the homogeneous transformation matrix for each link, and is obtained according to the Denavit-Hartenberg parameters of the system.  $A_i$  is given by:

$$A_i = \begin{bmatrix} \cos \theta_i & -\sin \theta_i \cos \alpha_i & \sin \theta_i \sin \alpha_i & a_i \cos \theta_i \\ \sin \theta_i & \cos \theta_i \cos \alpha_i & -\cos \theta_i \sin \alpha_i & a_i \sin \theta_i \\ 0 & \sin \alpha_i & \cos \alpha_i & d_i \\ 0 & 0 & 0 & 1 \end{bmatrix}$$

It is possible to extract vector  $z_{i-1}$ , which is the position in  $z$  axis of the link  $i - 1$ , from the first three elements of the third column of  $T_{i-1}^0$ .

The vector  $r_{ci}$ , the distance from the origin to the centroid of each link  $i$  is given by:

$$\begin{bmatrix} r_{ci} \\ 1 \end{bmatrix} = T_i^0 \begin{bmatrix} r_{i,ci}^i \\ 1 \end{bmatrix}$$

Where  $r_{i,ci}^i$  is the centroid position of each link  $i$ .

The vector  $r_{i-1,ci}$ , which indicates the distance from frame  $i - 1$  to the centre of mass of link  $i$  can be calculated as:

$$r_{i-1,ci} = r_{ci} - o_{i-1}$$

Where  $o_{i-1}$  is the distance from the origin to frame  $i - 1$ , and can be obtained from the first three elements of the fourth column of  $T_{i-1}^0$ .

Similarly, it is possible to obtain  $r_{i-1,i}$ , the distance from frame  $i - 1$  to  $i$  as:

$$r_{i-1,i} = o_i - o_{i-1}$$

Where  $o_i$  is the distance from the origin to frame  $i$ , and can be obtained from the first three elements of the fourth column of  $T_i^0$ .

With the aforementioned vectors, it is possible to calculate angular velocities and accelerations at the end of the  $i$ -th link with respect to the origin through equations (5.19) and

(5.20), respectively, and linear acceleration at the centroid and at the end of each link with equations (5.17) and (5.18).

Once the dynamics of the system are available, it is possible to obtain the change of linear momenta  $\dot{P}$  for each link using equation (5.15), and change in angular momenta  $\dot{H}$  for each link using equation (5.16). Finally, it is possible to compute the position in  $x$  and  $y$  of the ZMP,  $r_{P,x}$  and  $r_{P,y}$  respectively, with equations (5.13) and (5.14).

A more detailed explanation on the theory behind the calculation of the ZMP can be found in the lecture by Henk Kiela, (2015)

## 5.3 Methodology for online trajectory tracking control

### 5.3.1 Control scheme

Low and middle level controllers were coupled in this chapter to simulate the system behaviour in SimWise and MATLAB to assess its functionality. For the low level control, closed-loop, set-point tracking PID controllers, for hip and knee joints, were used to follow the standing-up and sitting-down motion references. Inputs to the PIDs are the orientation errors between the current orientation and the reference, while outputs are torques required by each joint to follow the desired reference. Saturation blocks were added at the output to avoid excessive torque that could be harmful for the user. More details of the low level control are described in Chapter 4.

For the middle level control, a system capable of generating reference trajectories for standing-up and sitting-down motions at variable velocities was required for the exoskeleton to better adapt to the user. It was also desirable to include equilibrium control and to ensure that torque requirements were within human body admissible limits according to Low, (2011).

A finite state machine whose states are based on the biomechanics of standing-up and sitting-down motions was proposed. It takes into consideration the position of the centre of mass to transition between states, and to generate proper hip and knee orientation references during standing position. It also requires hip joint and feet orientations.

Depending on the state from the FSC, a different function is selected by the reference generator. Functions can be as simple as constant slopes, or more complex such as those generated by inverse kinematics. A moving average filter is also included at the input of each PID controller, to smoothen the orientation trajectories in order to avoid sudden changes that could add unnecessary torque requirements. The full control scheme of the system designed in the current research, is shown in Figure 5.2. The blue area shows the low-level control described in Chapter 4, whilst the yellow area shows the middle-level control described in this chapter.

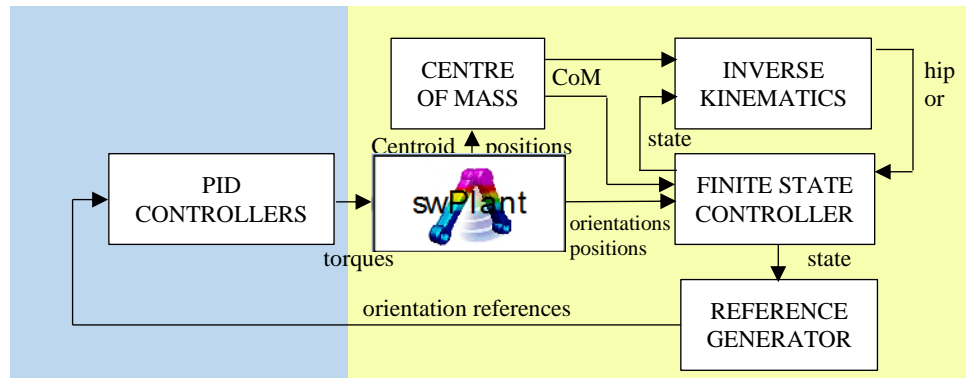


Figure 5.2 Middle and low level control scheme

### 5.3.2 Finite state controller for standing-up and sitting-down

For the middle level control, a finite state machine was designed according to biomechanical analyses of standing-up and sitting-down motions. States were defined based on the work of Kralj, Jaeger, and Munih, (1990). They classified the standing-up motion in normal subjects into four phases: initiation, seat uploading, ascending and stabilisation, all lasting approximately 1.5 s.

Research by Kerr (1994), which identified the different stages of the standing up motion, such as initial and final forward lean, knee extension, vertical displacement and backward lean, was also considered. In this study, specific conditions were identified as triggers for the changes between stages. These conditions are hip joint and feet orientations in  $y$  axis, and Center of Mass (CoM) position in  $x$  and  $z$  axis (Kerr, 1994)

Table 5.1 presents a summary of the biomechanics of the standing-up motion. It is divided into seated and stance phases, and in sub-phases such as preparation, momentum/transfer, extension and stabilisation. The most characteristic actions or postures during these phases of the upper limbs and feet, as well as hip, knee and ankle joints, are summarised. Position of CoM and a comparison with the support area, is also included due to its importance in the standing-up motion. A description of velocities of the main motions, as well as momenta are included for reference along with the approximate duration of each phase– (Kralj, et al., 1990; Kerr, et al., 1994, Sveistrup et al., 1999)

The finite state controller developed in this research can be described by the sextuplet  $\{S, I, O, n(s, i), o(s, i), s_0\}$ . Where  $S$  is the set of states it contains,  $I$  is the set of inputs or input vocabulary,  $O$  is the set of outputs or output vocabulary,  $n(s, i)$  is the next-state function that maps the current state and inputs to the following state  $s(t + 1)$ ,  $o(s, i)$  is the current output function which depends on the current state and input, and  $s_0$ , is the set of initial states. A diagram of the FSC developed to control standing-up and sitting-down motions of each exoskeleton leg for paraplegic assistance is shown in Figure 5.3.

Table 5.1 Standing-up motion biomechanics including phases and characteristic actions/postures

	<b>Seated</b>			<b>Stance</b>							
<b>%</b>	0	10	20	30	40	50	60	70	80	90	100
	<b>Preparation</b>			<b>Momentum/Transfer</b>		<b>Extension</b>				<b>Stabilisation</b>	
<b>Upper body</b>	Forward motion			Forward momentum peaks and transfers into upward momentum		Backwards motion				Practically static	
<b>Hip Joint</b>	Flexion initiated by concentric hip flexor muscles, continued by gravity and restrained by eccentric hip extensors muscles			Flexion velocity decreases and extension velocity increases. Extension moment reaches maximums at or shortly after lift-off. Hip moments during standing-up are higher than level walking		Decrease in extension velocity. Concentric hip extensor activity provides additional control and rotates the upper body backwards to realign the CoM and CoP				This phase begins after hips cease to extend and the upright position has been attained.	
<b>Knee Joint</b>	Practically static			Extension velocity increases and extension moments reach large maximums at or shortly after lift-off. Knee moments are comparable to level walking		Decrease in extension velocity				Practically static	
<b>Ankle Joint</b>	Practically static			Body rotates with ankle as pivot, therefore, moves forward. Major propulsive forces are provided by ankle dorsiflexors		This phase starts when maximum ankle dorsiflexion is reached. Ankle eccentric plantarflexion provides braking impulse and control of forward motion				Practically static	
<b>Feet</b>	Sharing weight with buttocks, creating a large three-point support area			Weight moves to a smaller two-point support base		Support base is formed by feet only				Support base is formed by feet only	
<b>CoM</b>	Moves horizontally and slightly downwards, until it is above feet			Vertical upwards velocity increases. Posture is stable when on top of support base, between heel and toe, anterior to the ankle and close to seat		This phase starts when forward position of COM is attained				Standing balance continues to be a primary concern	

Its twelve states are represented by the set

$$S = \{0,1,2,3,4,5,6,7,8,9,10,11\}$$

Additional intermediate states were necessary to save specific orientations and time offsets in memory, used in the output functions, and to calculate orientation offsets. These are needed to avoid discontinuities in the generated reference, when transitions between states occur. However, these states are not included in the diagram, transition function, nor states set, for simplification purposes.

In order to trigger transitions and to calculate some of the output functions, nine inputs are required as shown in the input set:

$$I = \{heel_{pos}, toe_{pos}, thorax_{pos}, ankle_{pos}, hip_{or}, knee_{or}, ankle_{or}, height, a_x, a_z, leg, thigh, thorax, v\}$$

Where heel, toe and thorax positions as well as hip, knee and ankle orientations need to be measured through sensors. The ankle position can be measured or calculated, while height, distance from heel to ankle in the  $x$  axis,  $a_x$ , and in the  $z$  axis,  $a_z$ , leg, thigh and thorax dimensions, as well as desired velocity  $v$ , would need to be input manually before the simulation, according the user characteristics. Other inputs are used for the calculation of outputs, however, these are either calculated or obtained from memory.

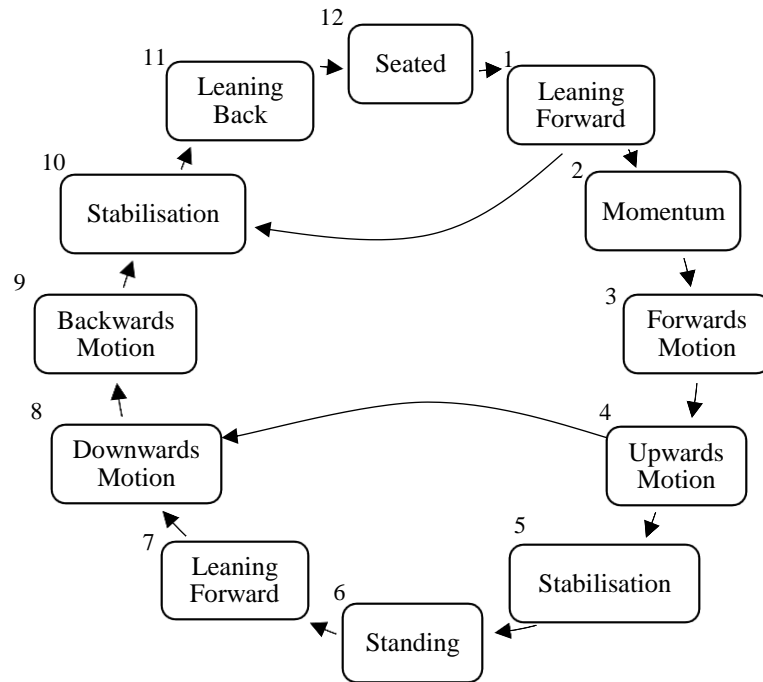


Figure 5.3 Finite state controller of standing-up and sitting-down motions

Three outputs, hip orientation,  $o_H$ , knee orientation,  $o_K$ , and ankle orientation,  $o_A$ , are generated for each leg, therefore the output set is

$$O = \{o_H, o_K, o_A\}$$

The next state or transitions function is

$$n(s, i) = \begin{cases} 1 & \text{if } s = 0, \quad heel_z = 0 \text{ mm and } toe_z = 0 \text{ mm} \\ 2 & \text{if } s = 1, \quad o_H \geq 28 \text{ deg} \\ 3 & \text{if } s = 2, \quad o_A \leq -24 \text{ deg} \\ 4 & \text{if } s = 3, \quad CoM_x \geq ankle_x + 7 \text{ cm} \\ 5 & \text{if } s = 4, \quad o_K \geq 50 \text{ deg} \\ 6 & \text{if } s = 5, \quad thorax_x = ankle_x + 8 \text{ cm and} \\ & \quad thorax_z \geq height_z * 0.67 \\ 7 & \text{if } s = 6, \quad t > t_{last\ s6} + 0.1 \\ 8 & \text{if } s = 4, \quad error \\ 8 & \text{if } s = 7, \quad o_H \geq -60 \text{ deg} \\ 9 & \text{if } s = 8, \quad o_H \geq 35 \text{ deg} \\ 10 & \text{if } s = 1, \quad error \\ 10 & \text{if } s = 9, \quad o_H \geq 39 \text{ deg} \\ 11 & \text{if } s = 10, \quad CoM_x \geq ankle_x + 2 \text{ cm} \\ 0 & \text{if } s = 11, \quad o_H \geq or_{H\ initial} \text{ and } o_A \geq or_{A\ initial} \text{ and} \\ & \quad t > t_{last\ s11} + 0.1 \end{cases}$$

States are generally connected to two others states only, forming a cycle of standing-up and sitting-down motions, as shown in Figure 5.3. This FSC, can start from state 0, sitting state, or 6, standing state, as indicated by the set

$$s_0 = \{0,6\}$$

Each state with its input sets and output functions are described below:

**0 SEATED:** This is the initial state in which the humanoid is in a seated position. The system takes measurements of the initial orientations of hip, knee and ankle joints and saves them in memory. Outputs remain constant with those initial values until both feet are touching the ground. This could be detected in a practical manner with the use of simple contact sensors or force sensors. Corresponding input set and output functions for this state are:

$$i_0 = \{ heel_x, toe_x, hip_{or\ initial}, knee_{or\ initial}, ankle_{or\ initial} \}$$

$$o_{H0}(t) = hip_{or\ initial}$$

$$o_{K0}(t) = knee_{or\ initial}$$

$$o_{A0}(t) = ankle_{or\ initial}$$

**1 LEANING FORWARD:** In this state, ankle and hip start to flex, and knee to extend, moving the CoM forwards. During this and other states, predetermined trajectories in the form of polynomial functions are used as reference for hip, knee and ankle joints.

These functions were adjusted from the data sets in Figure 4.3. Although the functions in every state are the same for different velocities, trajectories differ slightly at higher or lower velocities not only in the horizontal axis, but also in the vertical axis since duration of some states might be longer due to the dynamics of the system. This is better illustrated in Figure 5.10 in section 5.5

In order to have a smooth transition, an intermediate state between 1 and 2 was added. The output functions  $o(t)$ , for state 1, and  $o(t + 1)$ , for state 2 are calculated. The differences between them are saved in memory as  $or_{H1\ offset}$  for hip joint,  $or_{K1\ offset}$  for knee joint, and,  $or_{A1\ offset}$  for ankle joint. Intermediate states are only active during one sample time. When state 2 is activated, offsets are subtracted from the new reference, ensuring that no discontinuities are created and that transitions are smoother. The same procedure is applied for every state whose output functions require offset.

State 1 ends once the hip has reached a specific level of flexion. Input set and output functions for this state are:

$$i_1 = \{or_{H1\ offset}, or_{K1\ offset}, or_{A1\ offset}\}$$

$$o_{H1}(t) = 210118 t^6 + 311664 t^5 - 167019 t^4 + 37612 t^3 - 2909.8 t^2 + 58.223 t + 18.8 - or_{H1\ offset}$$

$$o_{K1}(t) = 166.43 t^2 - 14.391 t - 23.1 - or_{K1\ offset}$$

$$o_{A1}(t) = 345.77 t^3 - 219.7 t^2 + 4.1764 t - 14 - or_{A1\ offset}$$

**2 MOMENTUM:** During this state, the hip joint reference remains constant at the maximum flexion, this is represented by  $o_{Hs1}(t_{last})$ , the output of the hip reference in the last moment of the previous state. CoM is moved forwards through ankle flexion and knee extension. Although ankle and knee joint references are still based on predefined trajectories, for knee joint, the function used changes to a constant slope. A new offset is calculated and stored for the knee joint. However, for the ankle joint, the same offset as in the previous state is used. It is during this state that the momentum is enough for seat lift-off to occur. This state ends when ankle has reached the maximum flexion. Input set and output functions used for this state are:

$$i_2 = \{o_{Hs1}(t_{last}), or_{K2\ offset}, or_{A1\ offset}\}$$

$$o_{H2}(t) = o_{Hs1}(t_{last})$$

$$o_{K2}(t) = 130 t - or_{K2\ offset}$$

$$o_{A2}(t) = 345.77 t^3 - 219.7 t^2 + 4.1764 t - 14 - or_{A1\ offset}$$

**3 FORWARDS MOTION:** In this state, ankle reaches maximum flexion and is kept constant. Hip slowly starts extending, following a polynomial function, however, the maximum contributor to keep the CoM moving forwards is the knee extension. This state ends when CoM is 7 centimetres in front of ankle, CoM is calculated through equation (5.1). Corresponding input set and output functions for this state are:

$$i_3 = \{or_{H3\ offset}, or_{K2\ offset}, o_{As2}(t_{last})\}$$

$$o_{H3}(t) = -19529 t^6 + 35152 t^5 - 24609 t^4 + 8421.6 t^3 - 1446.9 t^2 - 76.443 t + 40.868 - o_{r_{H3} offset}$$

$$o_{K3}(t) = 130 t - o_{r_{K2} offset}$$

$$o_{A3}(t) = o_{As2}(t_{last})$$

4 UPWARDS MOTION: During this state, hip extension velocity is higher and therefore the forward motion of CoM converts into upwards motion. Hip trajectory changes to a constant slope, while the knee keeps extending as in previous state, the ankle joint starts to extend. All the trajectories have a constant slope as seen in the output functions. This state ends when knee joint has reached a specific extension. Input set and output functions for this state are:

$$i_4 = \{o_{r_{H4} offset}, o_{r_{K2} offset}, o_{r_{A4} offset}\}$$

$$o_{H4}(t) = -190t - o_{r_{H4} offset}$$

$$o_{K4}(t) = 130 t - o_{r_{K2} offset}$$

$$o_{A4}(t) = 40 t - o_{r_{K4} offset}$$

5 STABILISATION: In this state, hip and knee joints start to decelerate to stabilise the system in the upright position and to avoid tipping backwards. Functions were chosen to decrease its value through time, considering only the current orientation and target. Desired velocity  $v$  was added to the function to modify the rate at which the functions decrease their values. Ankle joints keeps extending with a constant slope until the maximum extension is reached.

The next state is triggered when the thorax centroid reaches a horizontal position of 8 centimetres in front of ankle joint, and a vertical position of 67% of the total height. Position of the thorax centroid is used instead of the CoM because, since the exoskeleton adds weight in the lower body, CoM is shifted downwards. Therefore, the position of upper body is not properly represented by this measurement. Corresponding input set and output functions for this state are:

$$i_5 = \{o_{H5}(t-1), o_{K5}(t-1), o_{r_{A4} offset}\}$$

$$o_{H5}(t) = o_{H5}(t-1) - \frac{o_{H5}(t-1) + 95) * v}{202.3}$$

$$o_{K5}(t) = o_{K5}(t-1) + \frac{(85 - o_{K5}(t-1)) * v}{350}$$

$$o_{A5}(t) = 40 t - o_{r_{A4} offset}$$

6 STANDING: In this state, the knee joint reference is constant while the ankle and hip joint references are calculated according to the position of thorax. Input set and knee output function for this state are:

$$i_6 = \{o_{K5}(t_{last}), o_{A6}(t-1), thorax_{x6}(t), thorax_{x5}(t_{last}), v, foot_{or}(t), \\ toe_z(t), heel_z(t), toe_x(t), heel_x(t)\}$$

$$o_{K6}(t) = o_{K5}(t_{last})$$

The ankle joint reference is calculated according to:

$$o_{A6}(t) = o_{A6}(t-1) - \frac{thorax_{x6}(t) - thorax_{x5}(t_{last}) * v}{thorax_{x5}(t_{last}) * 11.4}$$

Where  $thorax_{x6}(t)$  is the current position of thorax centroid, and  $thorax_{x5}(t_{last})$  is the desired position of thorax centroid, which corresponds to that in the last moment of the previous state.

For hip joint reference, inverse kinematics are calculated to obtain the adequate change of hip joint orientation  $\Delta\theta_{H\text{ calc}}(t)$  to compensate the difference between the current thorax centroid position, and its position in the last moment of the previous state. The first step is to calculate foot orientation using:

$$foot_{or}(t) = -\frac{\pi}{2} + \text{acos} \frac{toe_z(t) - heel_z(t)}{\sqrt{(toe_z(t) - heel_z(t))^2 + (toe_x(t) - heel_x(t))^2}}$$

Foot orientation could alternatively be measured. The next step is to calculate the position of the hip in the x axis using direct kinematics:

$$hip_x(t) = heel_x(t) + a_x * \sin\left(\frac{\pi}{2} - foot_{or}(t)\right) + a_z * \sin(foot_{or}(t)) \\ + leg * \sin(foot_{or}(t) + o_{A6}(t)) \\ - thigh * \sin\left(\frac{\pi}{2} - foot_{or}(t) - o_{A6}(t) - o_{K6}(t)\right)$$

Where  $heel_x(t)$  is the heel position in the horizontal axis,  $a_x$  and  $a_z$  are distances from heel to ankle in the x axis and z axis respectively,  $leg$  is the length between ankle and knee joints and  $thigh$ , is the length between knee and hip joints. Calculated knee and ankle joints as well as foot orientations are also needed. These orientations and distances can be observed in Figure 5.4.

The next step is to calculate the desired change in thorax centroid position depending on its current position, the previously calculated hip position, and a target position of thorax centroid. In this case, the target is the position in the last moment of the previous state, in order to keep the upright position. This function was selected to move the system towards the target in a slow manner if the difference is small, or faster, if the difference is large.

$$\Delta thorax_x(t) = thorax_x(t) - hip_x - \frac{(thorax_x(t) - thorax_{x5}(t_{last})) * v}{thorax_{x5}(t_{last}) * 7}$$

Alternatively,  $\Delta thorax_x(t)$  could be calculated depending on the measured position of thorax and the hip joints orientation.

Afterwards, inverse kinematics enable the calculation of change in hip orientation needed to take the thorax centroid to the desired position in x axis by

$$\Delta o_{H\text{ calc}}(t) = \text{asin}\left(\frac{\Delta \text{thorax}_x(t)}{\text{thorax}_c}\right)$$

Inverse kinematics are used as an alternative of estimating since, to do so, it would be necessary to measure the position of each segment.

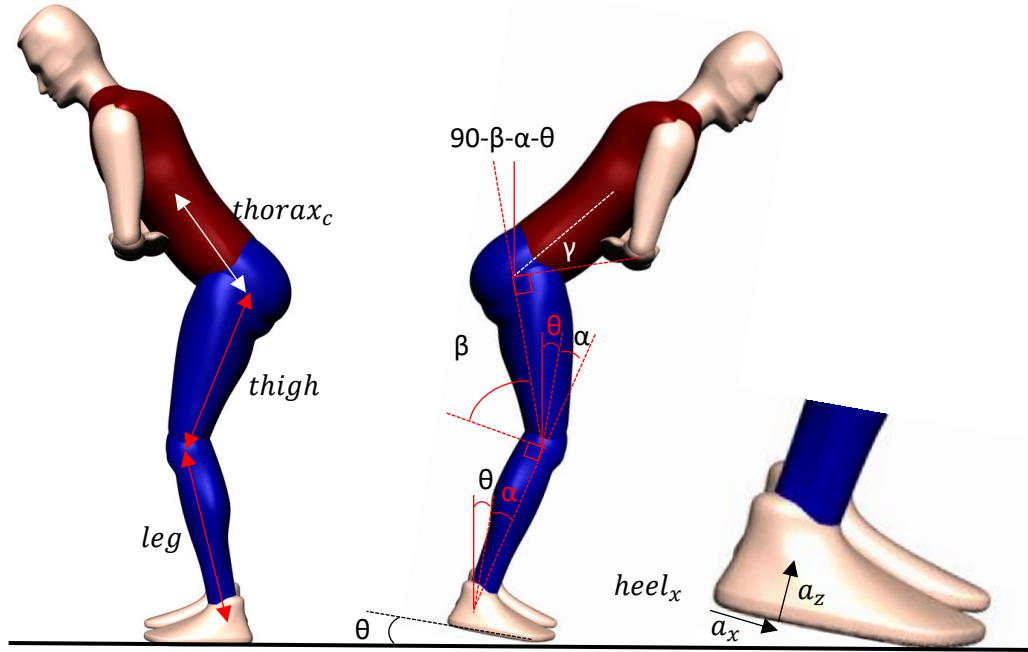


Figure 5.4 Feet and joints angles and distances between joints

Finally, hip orientation output is calculated considering the change in hip orientation and orientations of the other segments using

$$o_{H6}(t) = \Delta o_{H\text{ calc}}(t) - \text{foot}_{or}(t) - o_{A6}(t) - o_{K6}(t) - o_{r_{H6\text{ offset}}}$$

To decrease simulation time, the start of the sitting down process, which is the next state, is triggered 0.1 seconds after the current state is activated. However, experimentally, it could be manually started by the user or by a high level controller which would detect user's intention to sit down.

7 LEANING FORWARD: During this state, the hip and knee start flexing slowly following polynomial functions to initiate downwards motion, while the ankle joint is kept constant. Next state is triggered when hip is flexed beyond a specific orientation. Corresponding input set and output functions for this state are:

$$i_7 = \{o_{r_{H7\text{ offset}}}, o_{r_{K7\text{ offset}}}, o_{A6}(t_{last})\}$$

$$o_{H7}(t) = 2484.4t^4 - 3216.9t^3 + 1518.9t^2 - 24.096t - 86.169 - o_{r_{H7\text{ offset}}}$$

$$o_{K7}(t) = 190.52t^3 - 209.66t^2 - 79.803t + 80.526 - o_{r_{K7\text{ offset}}}$$

$$o_{A7}(t) = o_{A6}(t_{last})$$

8 DOWNWARDS MOTION : This is the state in which most of the vertical motion is achieved, hip and knee joint references are still polynomial functions while ankle starts flexing with a constant slope. The following state is activated when hip is near the maximum flexion. Input set and output functions for this state are:

$$i_8 = \{or_{H7\ offset}, or_{K7\ offset}, or_{A8\ offset}\}$$

$$o_{H8}(t) = 2484.4t^4 - 3216.9t^3 + 1518.9t^2 - 24.096t - 86.169 - or_{H7\ offset}$$

$$o_{K8}(t) = 190.52t^3 - 209.66t^2 - 79.803t + 80.526 - or_{K7\ offset}$$

$$o_{A8}(t) = -40t - 8 - or_{A8\ offset}$$

9 BACKWARDS MOTION: During this state hip and knee joints decelerate to slowly approach their target orientation, and vertical motion converts into backwards motion. The ankle joint keeps flexing in order to maintain CoM on top of the support area.

The next state is activated when hip joint reaches its maximum flexion. Corresponding input set and output functions for this state are:

$$i_9 = \{o_{H9}(t-1), o_{K9}(t-1), or_{A8\ offset}\}$$

$$o_{H9}(t) = o_{H9}(t-1) + \frac{(45 - o_{H9}(t-1)) * v}{60}$$

$$o_{K9}(t) = o_{K9}(t-1) - \frac{(o_{K9}(t-1) + 13.1) * v}{140}$$

$$o_{A9}(t) = -40t - 8 - or_{A8\ offset}$$

10 STABILISATION: In this state, the hip and knee joints keep flexing slowly but ankle joint is kept constant at its value at the last moment of the previous state. It is during this state that contact with seat is produced. This state ends once the CoM in the horizontal axis is 2 centimetres in front of ankle joint. Input set and output functions for this state are represented by:

$$i_{10} = \{o_{H10}(t-1), o_{K10}(t-1), o_{A9}(t_{last})\}$$

$$o_{H10}(t) = o_{H10}(t-1) + \frac{(45 - o_{H10}(t-1)) * v}{60}$$

$$o_{K10}(t) = o_{K10}(t-1) - \frac{(o_{K10}(t-1) + 13.1) * v}{140}$$

$$o_{A10}(t) = o_{A9}(t_{last})$$

11 LEANING BACK During this state, the hip joint leans back following a predefined polynomial function, the knee continues flexing if this is still possible. The ankle extends

according to a polynomial function until the initial positions saved in memory are reached. In that moment, the seated state is activated and the system awaits an indication to start a standing-up state. Corresponding input set and output functions for this state are:

$$i_{11} = \{or_{H11\ offset}, o_{K11}(t - 1), or_{A11\ offset}\}$$

$$o_{H11}(t) = -24604t^4 + 15335t^3 - 2615t^2 - 1.0113t + 39.547 - or_{H11\ offset}$$

$$o_{K11}(t) = o_{K11}(t - 1) - \frac{(o_{K11}(t - 1) + 13.1) * v}{140}$$

$$o_{A11}(t) = 345.77t^3 + 215.94t^2 - 2.6099t - 25.384 - or_{A11\ offset}$$

Transition conditions selected for all the states were based on the biomechanical analysis of the motion and different inequalities were tested in order to generate the best possible reference. However, these conditions could be further optimised or adapted depending on the user’s capabilities and needs.

Two additional states were added and are depicted as transitions between states in Figure 5.3. These states would be activated in case of error during the standing-up motion, connecting standing-up to sitting-down states to allow the system to recover. These states are active during a single sample time and are used to generate new offsets considering the orientation of joints in the last time step of the previous state, and the orientation of joints for the following state.

As an initial trial, only the states with longer time duration were connected to sitting-down states. However, in the future it would be desirable to add error transitions to every state to increase safety and robustness.

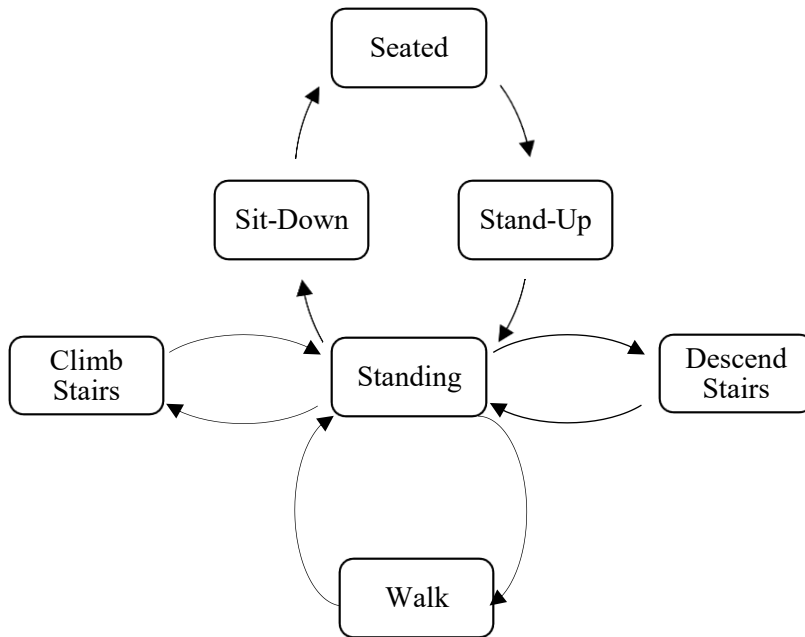


Figure 5.5 Finite State Machine of fundamental mobility tasks

A benefit of using FSCs for controlling human motions is that, when states are properly defined, their connection to other states or even other motions is practically seamless. An example is the transition of standing-up to sitting-down states even when the motion has not finished, as explained above. This FSC could be integrated with a walking motion or a climbing and descending stairs FSC to form a more complete controller as shown in Figure 5.5.

## 5.4 Offline verification of dynamic stability

The Robotics Toolbox for MATLAB, was developed by Peter Corke throughout 20 years and is used in this research to ease the offline calculation of the ZMP during the standing-up and sitting-down motions. Among the toolbox capabilities, it is possible to simulate arm-type robots. The toolbox is based on a general method of representing kinematics and dynamics of serial-link manipulators through MATLAB objects. Therefore, robot objects can be created for any serial-link manipulator by the user, and its kinematics and dynamics can be obtained (Corke, 2011).

This toolbox has been used in several studies, and is a point of comparison for the development of other algorithms (Dekker, 2009). Since in this research, the plant is a model in SimWise, and the mathematical model of the system is not available, it was decided to take advantage of the Robotic toolbox to approximate the kinematics and dynamics of the system in MATLAB, and, in that manner, obtain an estimation of the ZMP using a modification of the upper limb work by Kiela, (2015).

The first step was to create a robotic arm with a prismatic base that represents the left foot, and 11 cylindrical links that simulate the segments of the lower limbs; 2 links for calves, 2 for thighs, 1 which joins both legs and at the same time represents the upper body, 1 link for the right foot or final effector, and 5 mass-less auxiliary links with no rotation used to properly connect and orient the aforementioned links.

For each link, parameters such as mass, centroid, inertia tensor, kinematic parameters and type of joint, were defined. Mass, centroid and inertia parameters were selected according to the model in SimWise described in Chapter 2, to get a realistic ZMP approximation.

The kinematic model used was represented according to Denavit-Hartenberg (D-H) convention. Table 5.2 shows the complete list of D-H parameters obtained using same notation as Dekker, (2009). Necessary modifications are included to allow for its use in the robotics toolbox, while being compatible with the SimWise humanoid and exoskeleton model. Active rotations are  $\theta_2, \theta_3, \theta_4, \theta_9, \theta_{10}$  and  $\theta_{11}$ , which correspond to left and right ankle, knee, and hip

joints rotations in the sagittal plane. The corresponding kinematic model can be found in Appendix C.

Once the definition of each link was performed, a robotic arm was created as a chain of links. The next step was to provide orientation, angular velocity and angular acceleration trajectories for each of the 6 actuated joints. It was assumed that both legs move synchronously, therefore the same trajectories were sent to both ankle joints, knee joints and hip joints.

Table 5.2 Denavit Hartenberg parameters

Link	$a_i$	$d_i$	$\alpha_i$	$\theta_i$
1	0	0	$\pi/2$	$\theta_1$
2	$a_1$	0	0	$\theta_2$
3	$a_2$	0	0	$\theta_3$
4	$a_3$	$d_3$	$-\pi/2$	$\theta_4$
5	0	0	$-\pi/2$	$\theta_5$
6	$-a_5$	$-d_5$	0	$\theta_6$
7	0	$d_6$	$-\pi/2$	$\theta_7$
8	$-a_3$	0	$\pi/2$	$\theta_8$
9	$-a_2$	$-d_8$	0	$\theta_9$
10	$-a_1$	0	0	$\theta_{10}$
11	$a_{10}$	0	0	$\theta_{11}$

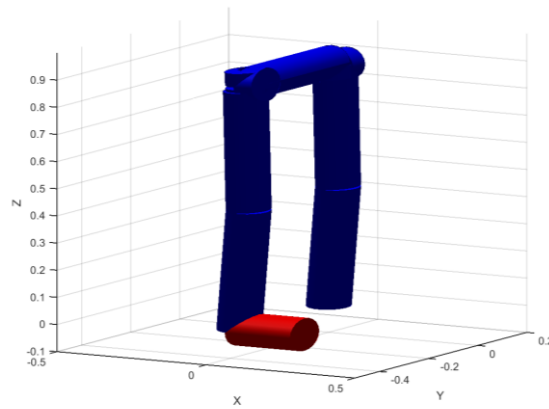


Figure 5.6 Robotic arm representing lower limbs

Angular velocity  $\omega$  and angular acceleration  $\dot{\omega}$  were obtained through derivation of the orientation profile from the FSC using the *diff*( $\cdot$ ) MATLAB function:

$$\omega(t) = \frac{\text{diff}(\theta(t))}{\Delta t}$$

$$\dot{\omega}(t) = \frac{\text{diff}\left(\frac{\text{diff}(\theta(t))}{\Delta t}\right)}{\Delta t}$$

Figure 5.7 and Figure 5.8 show orientation, angular velocity and angular acceleration trajectories of the standing-up and sitting-down motions at average speed. Motions are shown separately, since the ZMP calculation and analyses was done in this manner. Once the trajectories were ready, the gravity vector was defined as:

$$g = \begin{bmatrix} g_x \\ g_y \\ g_z \end{bmatrix} = \begin{bmatrix} 0 \\ 0 \\ -9.81 \end{bmatrix}$$

and all the information was loaded into the robotic arm. The robot can be visualised in the Robotics toolbox, as shown in Figure 5.6 with the proper orientations for the standing position.

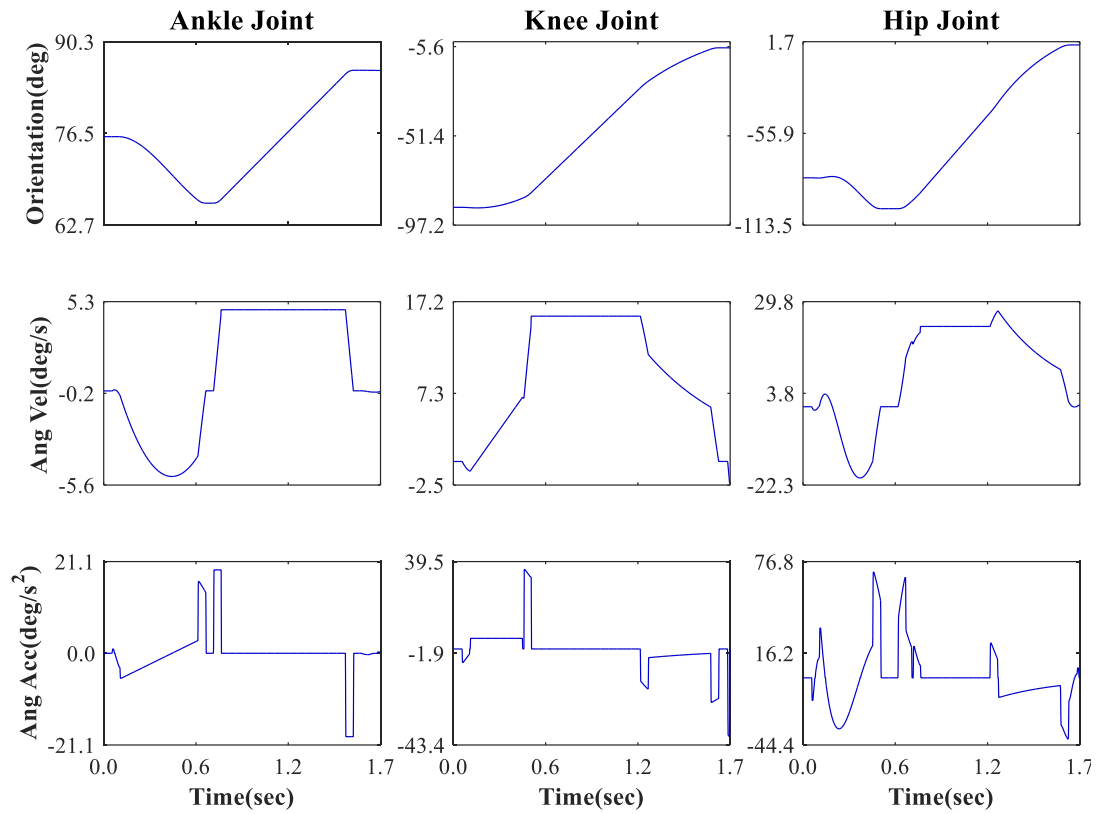


Figure 5.7 Orientation, angular velocity and angular acceleration during standing-up motion

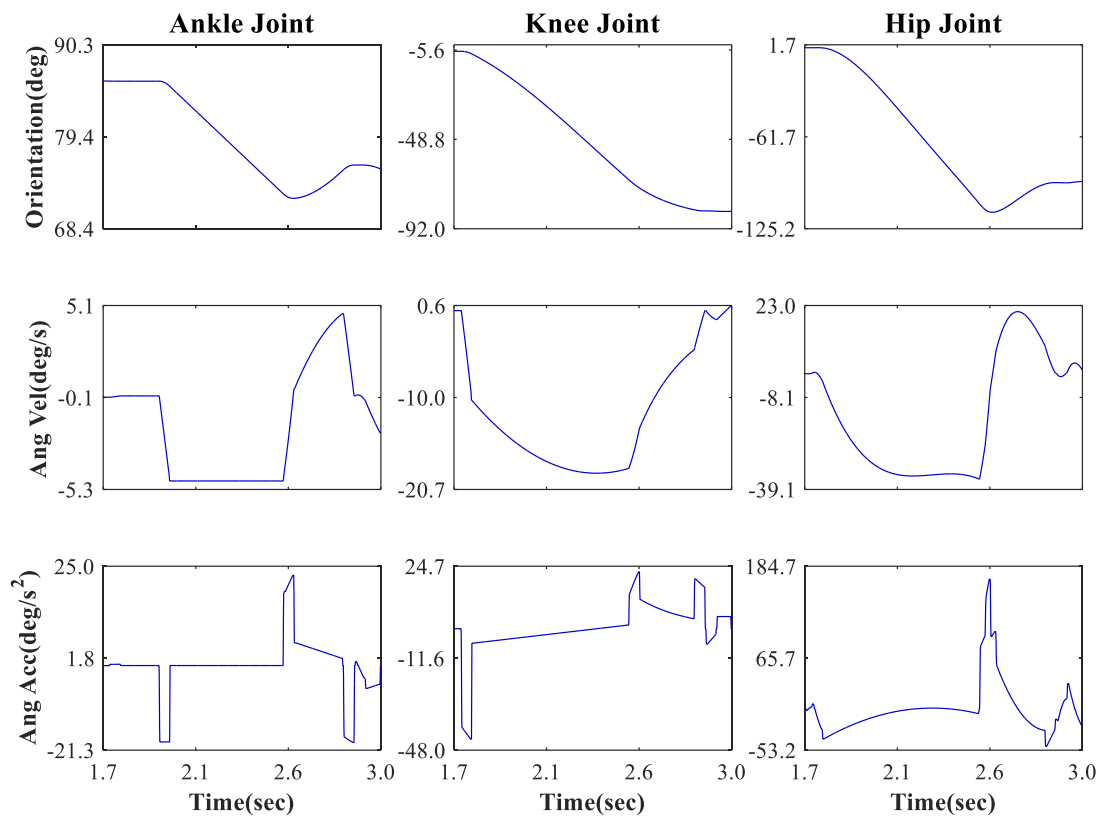


Figure 5.8 Orientation, angular velocity and angular acceleration during sitting-down motion

The next step was to calculate transformation matrices for all the links using the D-H parameters and equation (5.21). Vectors  $r_{ci}$ , from the origin to the centre of mass of each link,  $o_i$ , from the origin to the end of each link, and  $o_{i-1}$ , from the origin to the end of the previous link were obtained for each sample time. Using this information, it was possible to calculate angular velocity, angular acceleration, and linear acceleration at the end of each link at every sample time with equations, (5.19), (5.20), and (5.17), and angular acceleration at each link's centroid with equation (5.17).

Once the dynamics of the system had been calculated, change in linear momenta was obtained for each link using equation (5.15) and change in angular momenta using equation (5.16). Finally, ZMP in  $x$  and  $y$  axis, lateral and frontal axis, respectively, was calculated for each sample time using equations (5.13) and (5.14). CoM was also calculated for comparison purposes using equation (5.1)

## 5.5 Implementation of online trajectory tracking control with FSC

Standing-up and sitting-down manoeuvres were simulated and controlled using the loop shown in Figure 5.2, which is mainly coordinated by the finite state controller developed for this purpose. Figure 5.9 shows the results obtained for hip, knee and ankle trajectories. States and their duration are indicated by the gridlines.

The biomechanics of human standing-up and sitting-down motions were considered in order to program the FSC, therefore the duration of the states corresponds approximately, to the duration of each stage in Table 5.1. Around 30% of the standing-up time is spent in the preparation and moment generation phases while approximately 60% of the time is spent in the extension phase, and 10% in stabilisation phase. And for the sitting-down motion, around 60% of the time is spent at flexion phase, and 40% at seat loading and stabilisation. A sequence of equally time-spaced images showing the standing-up and sitting-down motions performed by the humanoid and exoskeleton are shown in Appendix D.

PID controllers developed in Chapter 4 were used to follow hip and knee joint references generated by the FSC described in the present Chapter. PID gains of  $K_p = 14$ ,  $K_i = 1$ , and  $K_d = 1.4$ , were selected for hip joints controller and PID gains of  $K_p = 14$ ,  $K_i = 7$  and  $K_d = 2.8$  were selected for knee joints. These were the combinations of gains that generated the lowest root mean squared error (RMSE) and torque time integral (TTI).

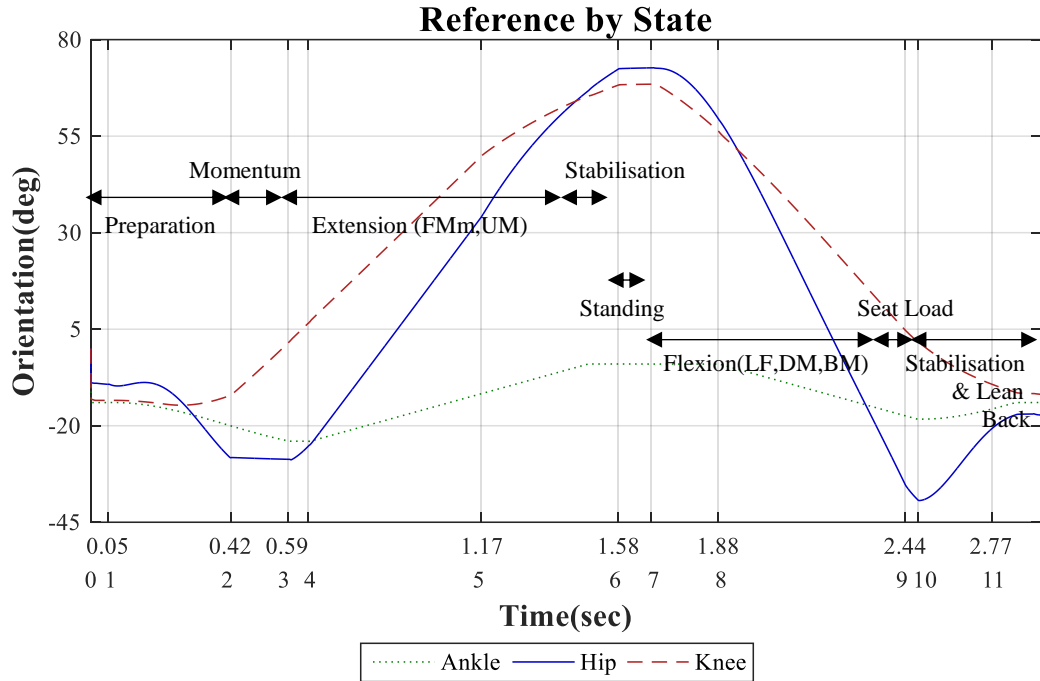


Figure 5.9 Standing-up and sitting-down joints trajectories divided by state

Three different velocities were studied in this test:

- average velocity of 60 degrees per second, in which the duration of the complete standing-up and sitting-down motions is 3 seconds
- high velocity of 113 degrees per second for a total duration of 1.6 seconds
- low velocity of 32 degrees per second for a duration of 5.7 seconds.

For the three velocities, the same FSC and PID gains were used, as the FSC state transitions are either position or orientation based, not time based. Figure 5.10 shows that the orientation trajectories do not differ significantly at different velocities. This coincides with the analysis made by Sveistrup et al., (1999), they concluded that forces vary more significantly than orientations when standing-up at different velocities.

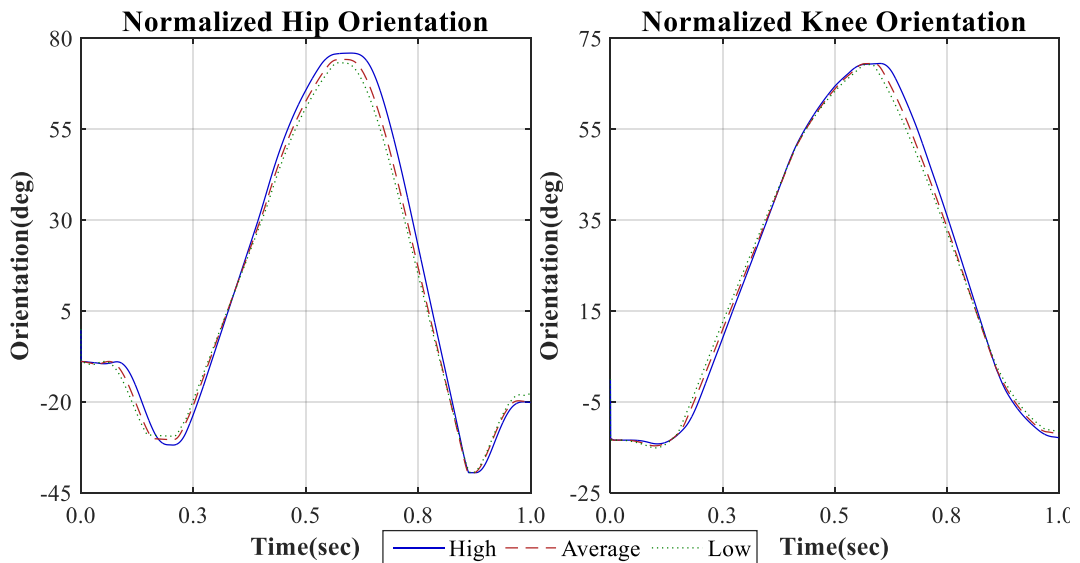


Figure 5.10 Normalised orientation of a) hip joint and b) knee joint at different velocities

Saturation blocks were initially set to 160 Nm for hip joint and 210 for knee joint as in the previous chapter. With the FSC developed and the incorporation of the moving average filter to the orientation reference, it was observed that torque remained within 60 and -60 Nm for hip joint, and 105 and -105 Nm for the knee joint, therefore, the saturation limits were updated and the system shown to be capable of performing the standing-up and sitting-down motions successfully.

Figure 5.11 shows the results obtained for hip joint. In the first column, a comparison of the orientation against the reference generated by the FSC at the three different velocities is shown. For high velocity, RMSE was 5.50, for average velocity 3.22, and for low velocity 2.17. Therefore, the RMSE was found to be proportional to the motion velocity, however, even at high velocity, error is below admissible limits.

In the second column, the torque sent to the exoskeleton to perform the motion is presented. It is possible to observe that torque trajectories present less, or no oscillations between the saturation values, as compared with results in Chapter 4. With the FSC proposed and the moving average filter, torque is smoother even at high velocity.

Finally, in the third column, it is possible to observe the TTI, which represents the amount of energy required by the exoskeleton to perform the motion. For high velocity, exoskeleton TTI was 37 Nms, for average velocity 70 Nms, and for low velocity 135 Nms. This confirms that, as expected, TTI is directly proportional to motion duration, as shown in previous results with the humanoid TTI.

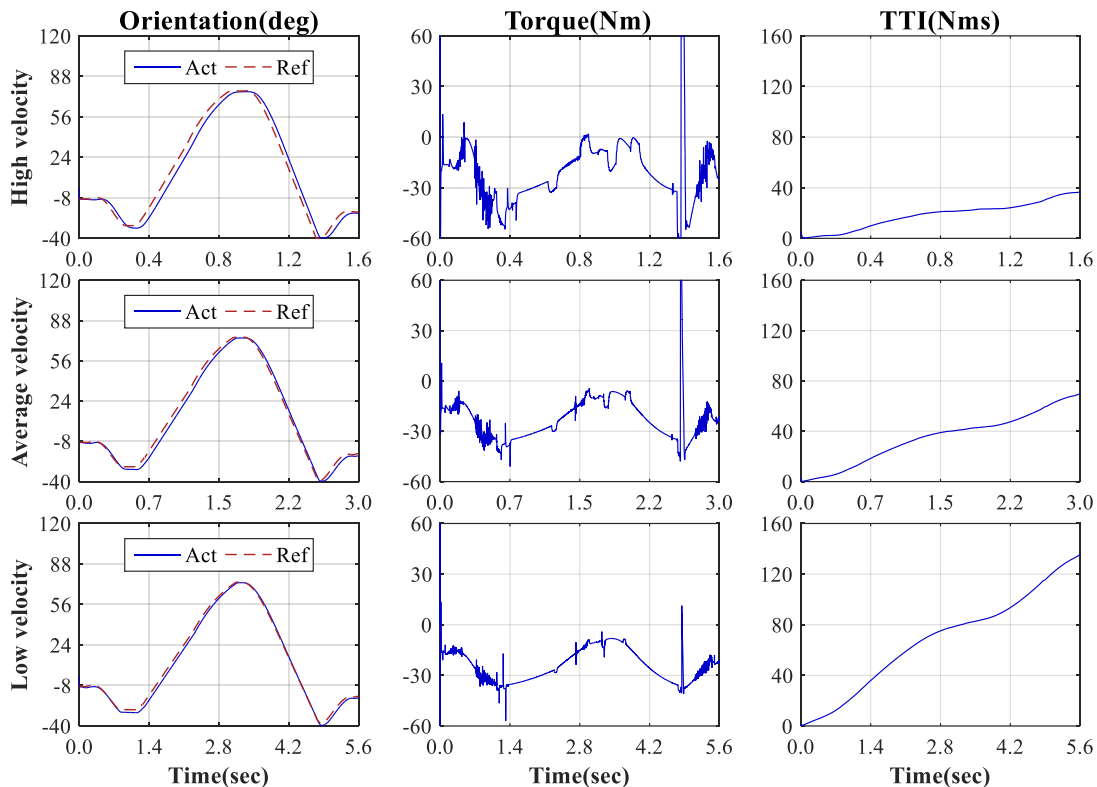


Figure 5.11 Hip joint orientation, torque and torque time integral at different velocities

Figure 5.12 shows results obtained for the knee joint. For high velocity, RMSE was 3.92, for average velocity 2.77, and for low velocity 2.08, thus RMSE is also proportional to the motion velocity and within acceptable limits. Knee joint torque trajectory is also smoother, even at high velocity as shown in the second column. Peaks are observed in the transition between states. Finally, for high velocity, exoskeleton TTI was 62 Nms, for average velocity 108 Nms, and for low velocity 199 Nms. Thus, for knee joint, TTI is also directly proportional to motion duration.

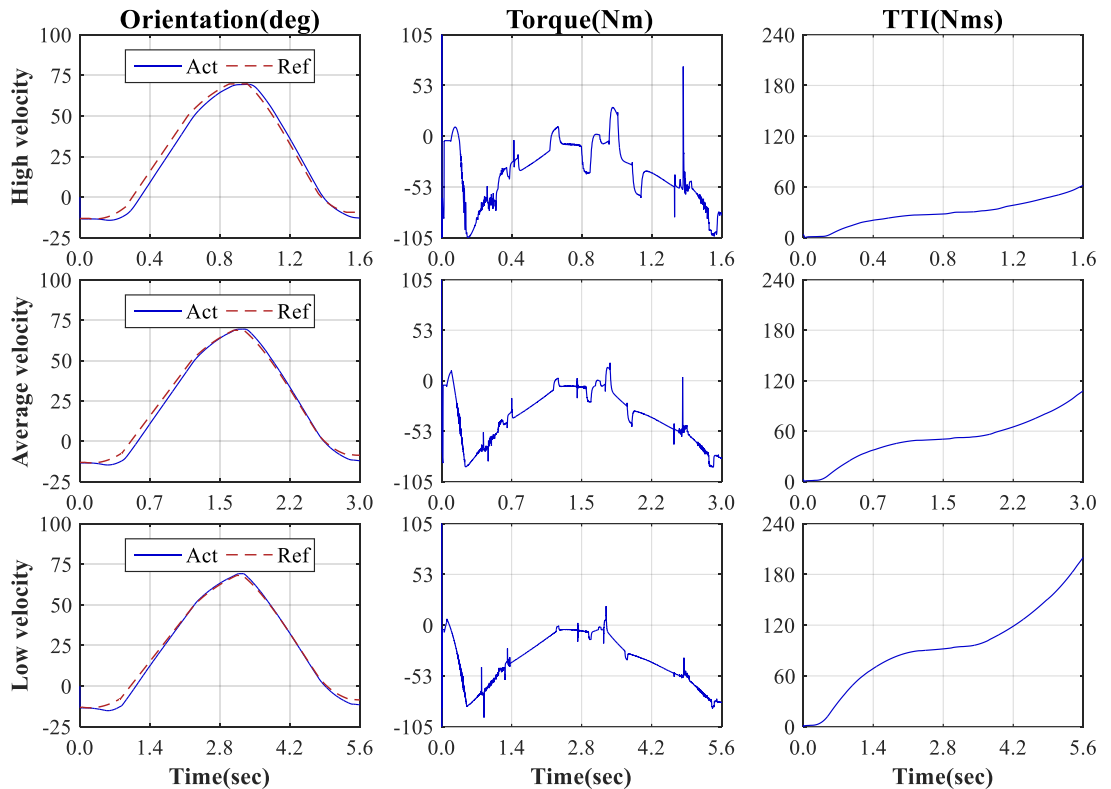


Figure 5.12 Knee joint orientation, torque and torque time integral at different velocities

Simulation of errors to interrupt the standing-up motion were applied to the system during state 1 and 4 to evaluate the performance of the transitions between intermediate standing-up and the sitting-down states. Results in Figure 5.13 and Figure 5.14 show the system response for hip joint and knee joint respectively, during the transition from the incomplete standing-up motion to the sitting-down motion. In both figures, the instant in which the error was detected is shown with a red dotted line. It is possible to observe in Figure 5.13 and Figure 5.14 that the transitions were performed without discontinuities or excessive torque peaks. Therefore, the sequence progressed through the states to recover, and then, to perform the standing-up motion.

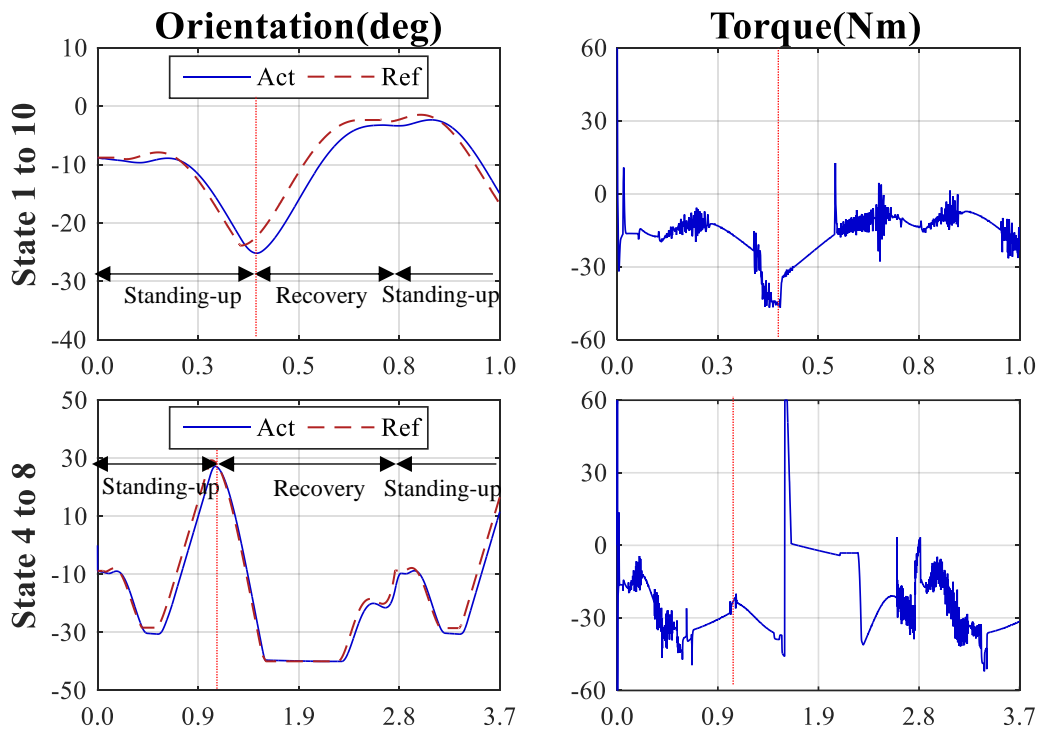


Figure 5.13 Hip joint orientation and torque after error

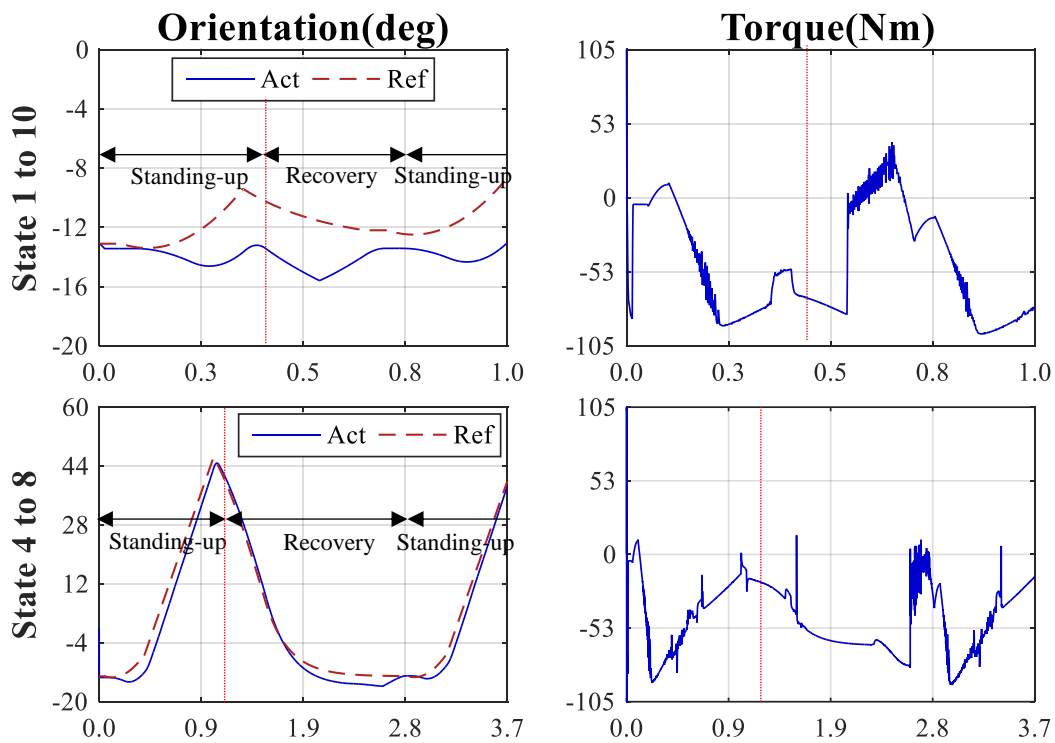


Figure 5.14 Knee joint orientation and torque after error

Calculation of the first and second derivatives was performed to assess equilibrium of the system. Ankle, knee and hip orientation trajectories measured from the simulation of the standing-up motion at average velocity were used to obtain the angular velocity and angular acceleration shown in Figure 5.7.

The previously described robotic arm, used to simulate the lower limbs, was generated using the robotic toolbox. The orientation, angular velocity and angular acceleration were set as inputs to the system. An offset was added to the orientations to ensure that the robotic arm coincides with the humanoid and exoskeleton in SimWise. Additionally, information including dimensions, mass, inertia tensor and centroid were set according to the model in SimWise to obtain a good approximation of ZMP.

Using this information in addition to the robotic toolbox, it was possible to obtain the kinematics and dynamics of the complete system. Then, the change in linear momenta  $\dot{P}$  is calculated using equation (5.15), and change in angular momenta  $\dot{H}$  using equation (5.16). Afterwards, it is possible to calculate the position in  $x$  and  $y$  of the ZMP, with equations (5.13) and (5.14).

Figure 5.15 shows a stick diagram of the lower limbs during the standing-up motion, specifically thighs, calves and feet which are shown in blue. Centroids of each segment are represented by black circles. As mentioned, the upper body was considered as a single prism whose centroid is also shown in this figure. The trajectory of the CoM is represented by red crosses and its projection is the ground as green crosses. A sequence of images of the standing-up and sitting-down motions performed by the robotic arm are shown in Appendix E.

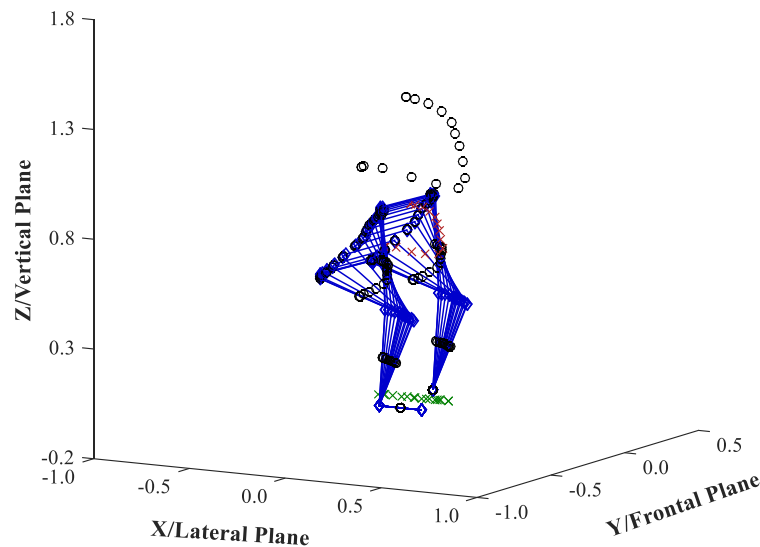


Figure 5.15 Stick diagram of standing-up motion

In Figure 5.16 and Figure 5.17 the ZMP trajectory is shown in blue and CoM as the red dashed line, while green crosses mark the start and end points of the ZMP and red dots indicate the start and end points of the CoM trajectory. Figure 5.17 is a zoomed in image of Figure 5.16, where it is possible to observe the motion of the ZMP trajectory in greater detail. It additionally shows that the ZMP does not vary significantly in the  $y$  axis, which is expected since both legs follow the exact same trajectory.

It is known that the system is in equilibrium while the CoM and ZMP stays within the support area. Figure 5.16 shows that while standing-up, the support area transforms from a bigger area, shown in blue, formed by the seat and feet, to a smaller area made up of feet only, shown in grey. From the simulation of standing-up motion at average velocity, it is possible to affirm that the system is in dynamic equilibrium throughout the motion, however there is a moment when the ZMP is at 0.22 meters, which is just below the limit. To further understand this point, the state in which it occurs was found to be Momentum state, which according to the literature, is the phase in which the major propulsive forces are needed, therefore torque requirements are higher (Laporte et al., 1999). Although it is an expected behaviour, further issues could be avoided by modifying the conditions for ankle controller to take in consideration the ZMP instead of the CoM.

The same issue but in higher magnitude occurs while standing-up at high velocity since the ZMP moves to 0.29 meters in the Momentum state. This position is out of the support area, hence, the system is not in equilibrium. For low velocity, maximum ZMP in the x axis is 0.19 meters, which is well within the support area. This behaviour also coincides with the literature which mentions that at higher velocities, dynamic equilibrium is more difficult to achieve (Kell and Everett, 2010).

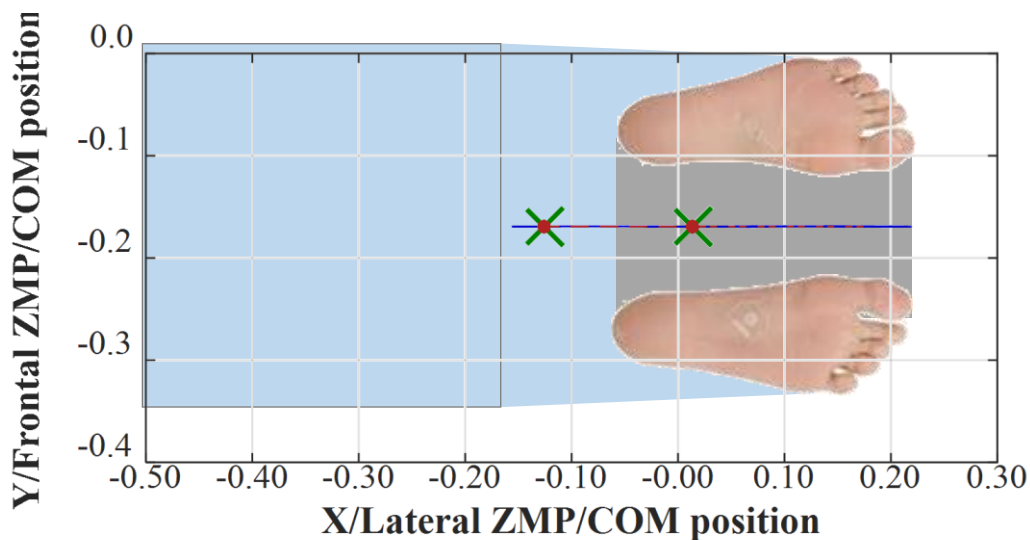


Figure 5.16 ZMP and CoM during standing-up motion at average velocity compared to the support area

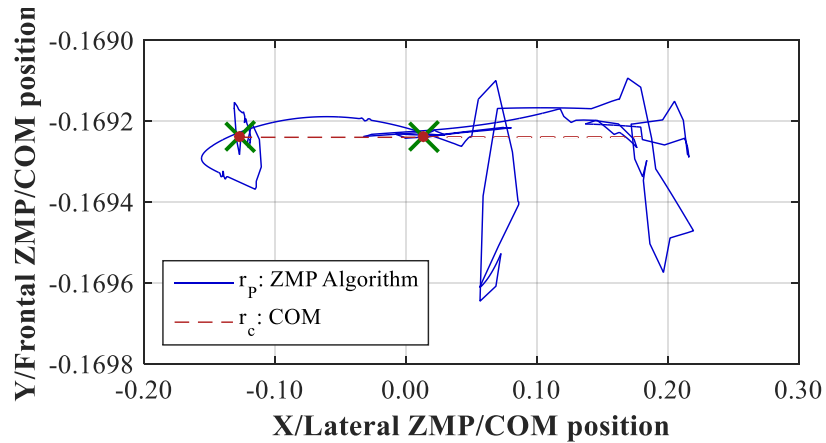


Figure 5.17 Zoom in view of ZMP and CoM during standing-up motion at average velocity

For sitting-down motion, joints orientations, along with angular velocity and acceleration are shown in Figure 5.8. Using this information and the same methodology described above, kinematics and dynamics were calculated, enabling the computation of the CoM and ZMP. Figure 5.18 a) and b) show the initial and final position of both CoM and ZMP for the sitting-down motion. For average velocity, both stayed below 0.2 meters, and for low velocity, below 0.13 meters, however, for high velocity ZMP moved to 0.3 meters, outside the support area.

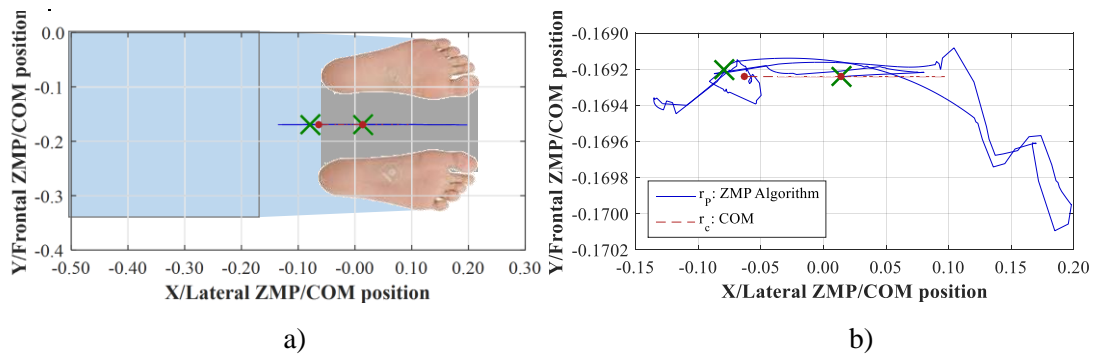


Figure 5.18 ZMP and CoM during sitting-down motion at average velocity a) compared to the support area b) zoom in view

It is important to mention that although balance parameters were incorporated in the development of the FSC in order to always maintain the CoM on top of the support area, results shown above were obtained with feet fixed to ground. Some tests were done with feet unfixed, however they were not successful and it was found that a further controller is needed to maintain feet in contact with the ground due to the sliding issues between flat surfaces in SimWise.

Additionally, ankle joints are still not controlled through torque as hip and knee joints are. Although a combination of PID gains was found to properly follow the reference generated through the FSC, the torque oscillates at a high frequency between the saturation values during

specific stages of the standing-up and sitting-down motions, therefore, the integral of torque was much higher than desired.

Optimisation of ankle PID gains to decrease torque oscillations, and therefore energy consumption, is described in Chapter 6, along with the implementation of a controller for torque compensation at ankles that keep the feet in contact with the ground.

## 5.6 Summary

In this chapter, a thorough analysis of the standing-up and sitting-down motions was performed to better comprehend the actions that occur during every stage, as well as the triggers required to move to the succeeding stages. Through the understanding of how humans perform these motions, a controller was programmed, using such information as a basis to create states and transitions of a finite state controller. This was found to be able to properly guide the lower level controllers and produce the desired standing-up and sitting-down motions.

By having a specially selected function for each state, which in some cases is a constant slope, while for others is as complex as inverse kinematics of the upper body; the system behaved in the desired way at every phase of the motion. Additionally, by means of connections between the states of the standing-up and the sitting-down motions, the system proved to be capable of recovering from incomplete transitions, and unexpected errors, preventing the exposure of the user to falls. Moreover, by making sure that the transitions between states are smooth, the equilibrium of the system and the decrease of energy consumption are easier to accomplish.

Through the offline calculation of ZMP, it was possible to evaluate the effect of dynamics of the system on its equilibrium. Effects of velocity in the performance of the motion were also assessed and some issues were identified through the calculation of ZMP, which additionally opened a window to the possibility of including these calculations into the online loop, to make the system more robust.

# CHAPTER 6

## **Particle swarm optimisation of ankle joint control parameters for dynamic equilibrium during standing-up and sitting-down tasks**

### **6.1 Introduction**

In Chapter 4, selection of control parameters for knee and hip exoskeleton joints was performed through several simulations. The effect of different combinations of such parameters was assessed, and the best performing in terms of RMSE, TTI, and torque profiles were selected. Although solutions found were not optimal, the trade-off between the time used to obtain them, and the system performance achieved was positive.

For the ankle joint however, acceptable results were not obtained when the same methodology was followed, and feet were fixed to ground. Therefore, it was found that alternative strategies were needed to complete the control system. Firstly, the use of an optimisation algorithm was considered to systematically look for the best combination of gains for the ankle joint controller.

Secondly, an additional control loop was considered when unfixing feet from ground, to compensate for the sliding of the feet due to lack of friction between them and the ground, in the SimWise model. The controller is designed to generate minimum torque when foot orientation error against a zero reference is small. In practical experiments, sliding would be almost null, and this controller might be unnecessary. However, for SimWise, this additional controller is necessary to compensate for the software shortcomings.

Thirdly, the incorporation of the ZMP calculation as input for a fuzzy controller was considered to enhance the equilibrium of the system, especially when generating motions at high velocity.

## 6.2 Particle Swarm Optimisation algorithm

Optimisation is a methodology with two main elements, adaptation and purpose. It is defined by Mikki and Kishk (2008) as a systematic change, modification or adaptation of a process that aims to achieve a previously specified purpose; which can be the maximum or minimum of a numerical function defined by the user. Therefore, optimisation involves the establishment of the purpose, and the ignorance of how to achieve it. Although some knowledge of the problem is necessary when selecting the relevant algorithm parameters.

The purpose is usually measured by an objective function. It can be of any form, and is integrated by several parameters leading into a single result. There is an enormous variety of properties that these functions can have (Bell and Oommen, 2015). In particle swarm optimisation (PSO), the objective function is called a fitness function, and is one of the main components of optimisation algorithms. It is responsible for indicating which solutions from a population, are better at solving a particular problem (Nelson et al., 2009).

Although, optimisation algorithms commonly fail to achieve the exact goal, a satisfactory approximation is usually found. For that reason, acceptable margins of error must be established considering the resources employed, including time (Mikki and Kishk, 2008). Particle swarm optimisation is a simple algorithm, effective for optimising a wide range of functions, including non-linear ones. The proper selection of fitness function is essential to obtain good results in an acceptable convergence time (Mikki and Kishk, 2008).

PSO originated when simulations of a simplified social model in animals, such as flocks of birds or schools of fish, was performed by Kennedy and Eberhart (1995). PSO has roots in artificial life, specifically in swarming theory, and is also related to evolutionary computation, i.e. genetic algorithms and evolutionary programming. It comprises a simple concept, which can be implemented in a few lines of code and requires primitive mathematical operators, making it computationally inexpensive (Kennedy and Eberhart, 1995).

In PSO, each particle represents a potential solution, a set of particles is called swarm. The algorithm updates the position and velocity of each particle in the swarm at every iteration, considering the “knowledge” of each particle, and the communal “experience” of the swarm. To update the velocity, a comparison is made between the current position of the particles and the position which generated the best fitness (Kennedy and Eberhart, 1995).

Although performance of PSO depends on the number of particles in the swarm, and the defined search space, in general, its main advantages compared to other optimisation algorithms are: faster convergence towards the global optimum, easy to implement, no complex computations, and the use of a low number of parameters. The main research goals of PSO are to avoid local optima and accelerate convergence speed, however, it has been

shown that it is difficult to accomplish both goals with the same algorithm (Amoshahy et al. 2016)

Several modifications to the original PSO algorithm have been proposed since its creation. One of the most prominent was introduced by Shi and Eberhart (1998). They presented the concept of inertia weight, by incorporating a constant that multiplied the first component of the velocity computation as shown in equation (6.2). A large inertia weight facilitates global search, while a small inertia weight enables local search.

Therefore, inertia weight is used to balance local and global search, as well as to control the “explosion” of particles. The value of the inertia weight has taken various forms in previous studies, examples are random, linearly decreasing, adaptive, oscillating, simulated annealing, chaotic, sigmoid increasing, logarithmic, and exponential values, among others; all of them trying to achieve better PSO performance (Abd Latiff and Tokhi, 2009; Bansal et al., 2011).

In this research, a strategy called spread factor by Abd Latiff and Tokhi (2009) is used for faster convergence. This is an expansion of the inertia weight PS optimiser introduced by Shi and Eberhart (1998). Apart from varying inertia weight, modification through time of cognition and social factors, also called acceleration coefficients, was proposed by Ratnaweera et al. (2004). This seeks a good balance between exploration and exploitation. Positive results were obtained when linearly decreasing coefficients, although they were not favourable in terms of convergence time.

The spread factor algorithm was conceived to continuously modify the value of the inertia weight, but not in a linear manner as done before. It measures the distribution of the particles in the search space, as well as the precision and accuracy of the particles against the global optimum. Therefore, particles should not only know their position, but also their distance from the others.

Spread factor is influenced by the *spread*, which is the maximum distance between particles in the swarm at each iteration, and *deviation*, the average distance from the particles in the swarm to the position of the global best. It is also normalised by the magnitude of the search space for each variable. A PSO algorithm with spread factor is shown in Figure 6.1, where the original PSO blocks are shown in white and computations added or affected in the spread factor variation are shown in yellow. Each block is explained below.

**Initialise population:** The size of the swarm, number of variables to optimise, maximum number of iterations and error goal, as well as position and velocity minimum and maximum values are defined. For the spread factor variation used in this research, acceleration coefficients and inertia weight vary through time, therefore their minimum and maximum values are also selected and spread factor is initialised as:

$$sf_i(n) = x_{max\ i} - x_{min\ i}$$

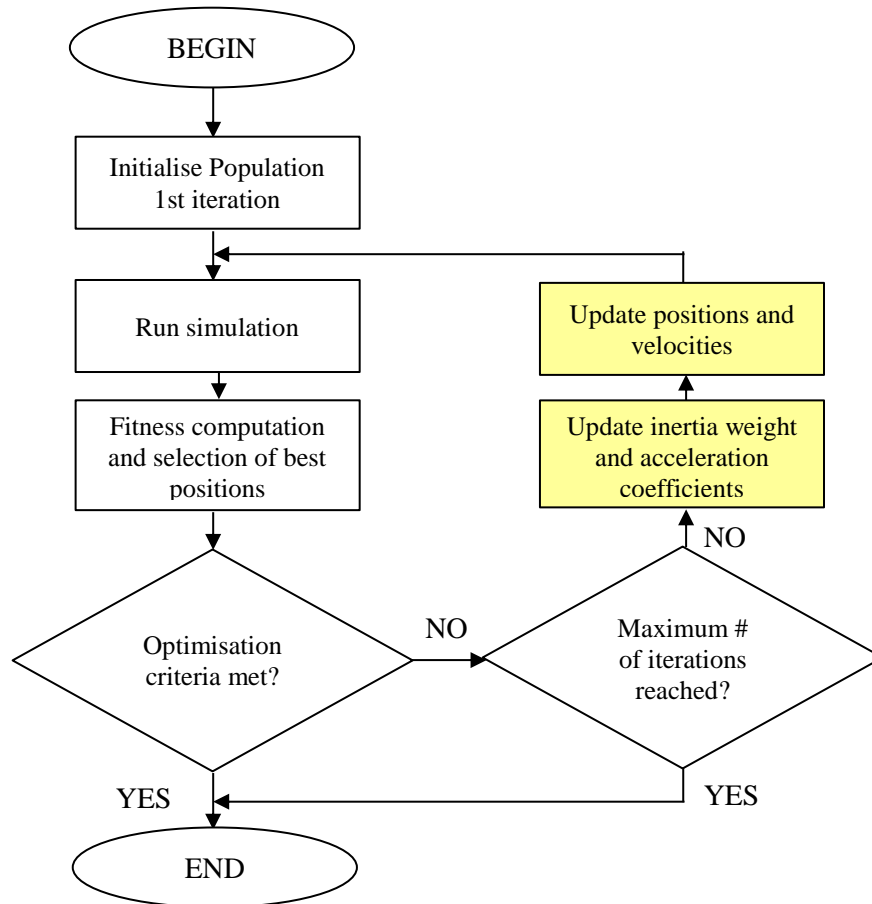


Figure 6.1 Particle swarm optimisation algorithm

A random selection of positions and velocities of each particle of the swarm, within the limits stated, is performed according to:

$$x_{ij}(n) = x_{min\ i} + (x_{max\ i} - x_{min\ i}) * a_{ij} \quad (6.1)$$

$$v_{ij}(n) = v_{max\ i} * b_{ij}$$

Where  $x_{ij}$  are positions of the  $i$ -th variable and  $j$ -th particle,  $x_{min}$  and  $x_{max}$  are position lower and upper limits, respectively.  $v_{ij}$  is the velocity of each variable,  $v_{min}$  and  $v_{max}$  are velocity lower and upper limits, respectively.  $a_{ij}$  is a matrix of random numbers  $a_{ij} \in [0,1]$  of size  $i \cdot j$ ,  $b_{ij}$  is a matrix of random numbers  $b_{ij} \in [-1,1]$  of size  $i \cdot j$ , and  $n$  is the current iteration. If the calculated  $x_{ij}(n)$  is greater than  $x_{max}$ , then  $x_{ij}(n)$  is set to  $x_{max}$ . Similarly, if the calculated  $v_{ij}(n)$  is greater than  $v_{max}$ , then  $v_{ij}(n)$  is set to  $v_{max}$ , and if the calculated  $v_{ij}(n)$  is less than  $v_{min}$ , then  $v_{ij}(n)$  is equal to  $v_{min}$ .

**Run simulation:** Set position values  $x_i$  as gains or control parameters and run the stand to sit and sit to stand simulation according to the control schemes in section 6.3 for each particle  $j$ . Inputs to Simwise are joints torques for ankle, knee and hip joints, and outputs are

root mean squared errors and integrals of torque of the three joints. Controller gains for hip and knee joints were selected as in Chapter 5.

**Fitness computation:** The type of fitness function used in this algorithm is behavioural fitness function, which is a task-specific hand-formulated function that measures various aspects of what the system does, and how it is done. Behavioural types of functions include several sub-functions or terms that are combined into a weighted sum or product, (Nelson et al, 2009).

In the first iteration, the value of the fitness function for each position is saved in a matrix of size 1 by  $j$ . In each iteration, every particle is assessed to determine if it produces a higher fitness than that stored in the best fitness matrix. When this is the case, the position of the particle is saved as the new personal best,  $p_{best\ ij}$  and the fitness value for that specific particle is updated in the fitness matrix. Otherwise, the stored position of the particle remains as the best personal best and the fitness matrix remains intact. Thus, matrix  $p_{best}$  contains the best position, which can also be referred to the best combination of variables  $i$ , of each particle  $j$  in the swarm, with respect to the fitness function. In this case, the highest fitness corresponds to the lowest value of the selected fitness function. In the first iteration,  $p_{best\ ij}$  is equal to  $x_{ij}$ , however, after the second iteration, matrix  $p_{best}$  starts to “evolve” combining the best positions from different iterations.

Afterwards, the position of the particle  $j$  with the highest fitness in the  $p_{best}$  matrix is saved as global best,  $g_{best\ i}$ . If the  $p_{best}$  matrix was updated in the previous step, there might be a better global best than the stored one, thus the global best is updated. Otherwise, the global best remains the same. For practical purposes and to be able to operate with the global best, it is formed as a matrix  $g_{best\ ij}$ , of  $i$  rows which correspond to the number of variables, and  $j$  columns according to the number of particles in the swarm, however, all the columns contain the same best global position.

**Update velocities and positions:** If the optimisation criteria have not been met, nor the maximum number of iterations reached, the position and velocity of each particle is updated according to equations (6.2) and (6.3), where  $c_1$  and  $c_2$  are cognition and social factors, respectively, and  $r_{1ij}$  and  $r_{2ij}$  are uniformly distributed random numbers  $r_{(\cdot)ij} \in [0,1]$ .

$$v_{ij}(n+1) = w_i v_{ij}(n) + c_1 r_{1ij} [p_{best\ ij}(n) - x_{ij}(n)] + c_2 r_{2ij} [g_{best\ ij}(n) - x_{ij}(n)] \quad (6.2)$$

$$x_{ij}(n+1) = x_{ij}(n) + v_{ij}(n+1) \quad (6.3)$$

The first component of equation (6.2) is the inertia weight  $w$  multiplying current velocity. The inertia weight varies through time, and is computed as shown in equation (6.4).

The second component of equation (6.2) is called the cognitive contribution, and represents particles' learning from their own experience while the third component, called social contribution, represents the cooperation with other particles in order to find the optima, (Latiff and Tokhi, 2009).

**Update inertia weight and acceleration coefficients:** This is an additional block necessary for the spread factor variation used in this research, and must be computed before the calculation of velocity and position. The first step is to compute the spread factor for each variable according to:

$$sf_i(n) = \frac{0.5(\text{spread}_i(n) + \text{deviation}_i(n))}{x_{\max i} - x_{\min i}}$$

where spread is the maximum distance between particles

$$\text{spread}_i(n) = x_{\max i} - x_{\min i}$$

and deviation is the average distance from the particles in the swarm to the position of the global best for that specific variable.

$$\text{deviation}_i(n) = \sum_{j=1}^j \frac{[x_i - g_{\text{best } i}]}{j}$$

Having computed the spread factor, the inertia weight can be calculated as in equation 6.4. The purpose of having an inertia weight of this form, is that, while the spread factor remains high, the inertia weight maintains its value within the range of 0.95 to 1, allowing particles to keep exploring the search space until convergence to the global optimum is almost in sight. Once all the particles are in the vicinity of the global optimum, the spread factor and inertia weight, drop drastically, forcing all the particles to converge and allowing the algorithm to achieve high precision, (Latiff and Tokhi, 2009).

$$w_i(n) = e^{-\frac{n}{sf_i(n) n_{\max}}} + 0.25 \quad (6.4)$$

where  $n$  is the current iteration,  $n_{\max}$  is the maximum number of iterations and  $sf_i$  is the spread factor for each variable in the iteration  $n$ . If the calculated  $w_i(n)$  is greater than  $w_{\max}$ , then  $w_i(n)$  is equal to  $w_{\max}$ . and if  $w_i(n)$  is less than  $w_{\min}$ , then  $w_i(n)$  is equal to  $w_{\min}$ .

Acceleration coefficients are linearly decreased at each iteration according to

$$c_{1i}(n) = c_{1\max} + (c_{1\min} - c_{1\max}) \frac{n}{n_{\max}}$$

$$c_{2i}(n) = c_{2\max} + (c_{2\min} - c_{2\max}) \frac{n}{n_{\max}}$$

There are usually two stopping criteria for PSO, the first is minimum error, which is set according to system requirements. However, as it is possible that the target error is never met, a maximum number of iterations is also selected to stop the optimisation. For the standard

PSO algorithm, a low or high number of iterations could be selected, and the result would be the same, however, for the inertia weight with spread factor method and other variations, the number of maximum iterations is relevant since it is included in the calculation of the inertia weight and acceleration coefficients (Abd Latiff and Tokhi, 2009).

Regarding PSO parameters selection, the typical range of swarm size is between 20 and 40, although according to Hu (2010), for most problems 10 particles is enough to get good results. The number of variables, the search space  $x_{min}$  and  $x_{max}$ , and the stop conditions, maximum number of iterations and minimum error, depend specifically on the problem to be solved. However, the maximum velocity  $v_{max}$  is often set as the range of positions  $[x_{min} \ x_{max}]$  and the acceleration coefficients  $c_1$  and  $c_2$  are generally equal and selected from the range  $[0 \ 4]$  (Hu, 2010).

### 6.3 Particle swarm optimisation of ankle joint control parameters

Although the same procedure used to find controller gains for hip and knee joints described in Chapter 4 was applied for ankle joints, it was insufficient to find a combination of gains that generate low RMSE and integral of torque. Therefore, an optimisation algorithm was implemented to find adequate gains in a more automatic manner. Two additional controllers, a PID controller and a fuzzy logic controller (FLC), were tested to control feet orientation to avoid sliding of feet.

PSO with spread factor method was utilised, since the simulation time of the standing-up and sitting-down motions with SimWise is high, and therefore, an algorithm with fast convergence was required. PSO with spread factor meets this criterion, thus, it was used in this research to optimise  $K_p$ ,  $K_i$  and  $K_d$  gains for PID controllers and  $K_{in}$ ,  $K_{in2}$ ,  $K_{out}$  scaling factors for the fuzzy controller. A torque saturation value for ankle joint was also included in the optimisation variables for some schemes. PID controller gains, as well as saturation values for hip and knee joints were selected according to Chapter 5.

#### 6.3.1 Optimisation of ankle joint PID controller gains

Optimisation of ankle PID gains was performed with the following settings: Size of swarm was set to 10 to speed up the convergence of the algorithm. A maximum of 50 iterations was selected, along with an error target of 0.01. Acceleration coefficients  $c_{1\ min} = c_{2\ min} = 0.5$ , while  $c_{1\ max} = c_{2\ max} = 2$ . Finally, inertia weight  $w_{min} = 0$  and  $w_{max} = 1$ .

Figure 6.2 shows a diagram of the control for ankle joints, including the finite state controller, reference generator, and moving average filter in the yellow shaded area. Although

not shown in the diagram, an identical loop was used for knee and hip joints. The PSO algorithm implemented in MATLAB is shown in blue. This algorithm generates the position of particles in the swarm that correspond to the ankle joint PID controller gains. Positions of the particles are calculated according to equations (6.1) and (6.3), then, simulations are run for each set of positions. After each simulation, results including RMSE and TTI of all the joints are stored.

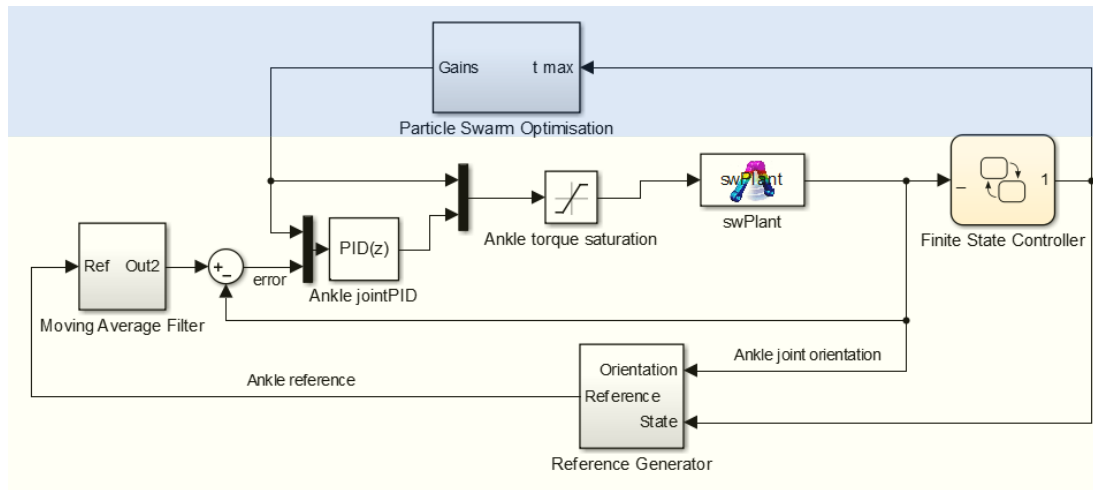


Figure 6.2 PID low level control scheme for ankle joint

Maximum simulation time of each run was not constant. This due to additional stopping conditions that were included in the Simulink model, to save time by interrupting simulations that were likely to become unstable, or that had surpassed the error limits.

Stopping conditions were:

- $ARMSE > 3$ , where  $ARMSE$  is ankle joint root mean square error. The limit was set to 3 degrees since more than 10% of error between the reference and the actual ankle orientation would be unacceptable.
- $COM_x - ankle_x > 0.15$  where  $COM_x$  is the ground projection of the centre of mass in the  $x$  axis, and  $ankle_x$  is the position of ankle in the  $x$  axis. The limit was set to 0.15 meters to ensure that the CoM was always within the support area, therefore, this condition prevents the humanoid from tipping over. If the limit is reached, it can be assumed that the combinations of gains selected by the PSO algorithm were not good enough to make the system properly follow the reference trajectory considering that the middle level controller was previously tested and proved to generate appropriate trajectories.
- $ankle_x - CoM_x > .05$  The limit was set to 0.05 meters to ensure that the CoM is always within the support area, therefore, this condition prevents the humanoid to slip backwards.

- $thorax_x - ankle_x > 0.15$  where  $thorax_x$  is the position of thorax centroid in the  $x$  axis. Similar to  $CoM_x$ , the limit was set to 0.15 meters to ensure that thorax centroid is always within the support area. As mentioned in Chapter 5, position of thorax is included since, although CoM calculation considers the position of upper body,  $CoM_z$  is shifted downwards due to the weight of exoskeleton. Therefore, it does not provide an accurate approximation of the position of upper body. This condition helps to discard gain combinations that would cause the humanoid to tip over.
- $ankle_x - thorax_x > 0.05$  In a similar way to previous stopping conditions, this limit was set to 0.05 meters to discard gain combinations that could cause the humanoid to slip backwards.

It is important to note that these conditions were used to help the system find combinations of gains for the ankle joints of low level PID controllers, in a quicker manner. If the reference trajectories originated by the FSC were followed with minimum error, and the system was in equilibrium, none of these conditions would be met.

Therefore, each one of these conditions, when activated, shows that the humanoid and exoskeleton are in a position or orientation that would eventually generate a fall. Moreover, when activated, they generate an error code that enables analysis of relations between controller gains and behaviour of the system.

Although it would be ideal to have a controller capable of managing and solving these unstable conditions, this would require additional states and controllers. Balancing tasks such as stepping forwards or backwards would be required to counteract the instabilities, this however is out of the scope of the current project.

Considering that simulations are stopped when any of the conditions above are met, simulations time is different for every combination, therefore, it was necessary to normalise the results to be able to compare them. A fitness function for this strategy was defined as:

$$Fitness Function_j(n) = \frac{1}{t_{\max}} + \frac{ARMSE}{a * t_{\max}} + \frac{ATTI}{b * t_{\max}} \quad (6.5)$$

Where  $t_{\max}$  is the duration of the current simulation,  $ARMSE$  is ankle root mean squared error, and  $ATTI$  is ankle torque time integral. This fitness function was used to select the gains that enable the system to complete the motion with the lowest error and torque. The inverse of time is used since this algorithm is set to minimise the fitness function.

ARMSE and TTI were included since it was also relevant to minimise these, however, more importance was given to the duration of the motion. Considering that target  $t_{\max}$  was around 1.5 seconds, the first term would be optimally 0.67. Since ARMSE was usually around 1 and 10,  $a$  was selected to 30 to add from 0.022 to 0.22 to the fitness function when  $t_{\max}$  was

1.5 seconds. ATTI was in the range of 10 and 100, therefore,  $b$  was selected to 3000 to add from 0.002 and 0.022 to the fitness function when  $t_{max}$  was 1.5 seconds. It is possible to see that more importance was given to maximising the duration of the motion, then to minimise ARMSE and finally to minimise ATTI.

Once fitness is calculated, it is possible for the PSO algorithm to look for the combination of gains with the best fitness. Afterwards, spread factor, inertia weight and acceleration coefficients are updated, before calculating the new positions which are assigned as the next set of gains and sent to the PID controller. With the new set of gains, simulations are run again and the cycle continues until a stopping criteria is met.

It is important to mention that during the optimisations, the feet were still fixed to ground, therefore it was assumed that there was no sliding with the ground. Optimised gains were assigned to the ankle joint and feet unfixed to test the controller in a more realistic manner. Nevertheless, as shown in the results section, the combination of FSC and PID controllers was not enough to generate a proper standing-up and sitting-down motion for paraplegic patients.

### 6.3.2 Optimisation of feet orientation PID controller gains

The addition of a controller whose input is the error between the current orientation of the feet, and a constant value of zero was proposed. The output is the torque of the ankle joint, which is added to the output torque of PID controller of ankle joint. The proposed scheme is shown in Figure 6.3.

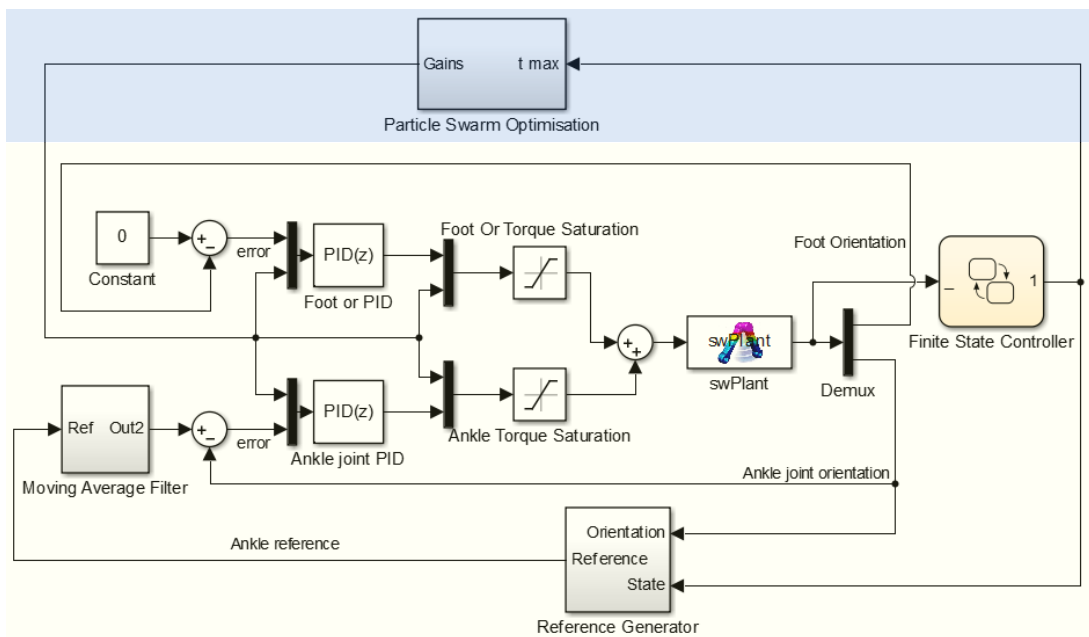


Figure 6.3 Control scheme with feet orientation PID controller

This controller was added to compensate for the sliding of feet and ground. PSO with spread factor was used again to find proper gains for feet orientation and ankle joint PID controllers. The same stopping conditions mentioned in section 6.3.1, were used. Additional conditions were added to stop simulations that were near, or already out of equilibrium, considering the orientation of feet and the difference between the left and right hip joints.

- $foot_{or} > 5$  where  $foot_{or}$  is orientation of foot in the sagittal axis. The limit was set to 5 degrees as an initial trial, however, the orientation in which the system becomes unstable needs to be explored through the calculation of ZMP. This stopping condition discards the gain combinations in which feet are not well positioned on the ground, and cause the humanoid to tip over.
- $foot_{or} < -5$  Like the previous stopping condition, this one discards the gain combinations in which feet are not well positioned on the ground and causes the humanoid to slide backwards.
- $abs(knee_{Lor} - knee_{Ror}) < 5$  where  $knee_{Lor}$  and  $knee_{Ror}$  are left and right knee joint orientations respectively. This limit was set since the sliding of the feet occasionally results in undesired or unbalanced postures. It was noted that when this occurs, the system is not able to recover.
- $abs(hip_{Lor} - hip_{Ror}) < 5$  where  $hip_{Lor}$  and  $hip_{Ror}$  are left and right hip joint orientations. Similarly, to the knee joints, this limit was set to discard gains combinations that caused sliding of feet, and therefore, falls.

Optimisation of feet orientation and ankle joint PID controller gains was performed with the same parameters and fitness function as in section 6.3.1, and stopping conditions were complemented with those described in this section.

### 6.3.3 Optimisation of feet orientation fuzzy control parameters

A control scheme that uses feet orientation fuzzy logic controllers (FLC) instead of PID controllers was also implemented. Thus, a FLC with two inputs, these being the error and rate of change of error between foot orientation and the zero reference, and one output, the ankle torque, was set up.

The fuzzy controllers have five Gaussian type membership functions for each input and output, they are normalised from 0 to 1. Linguistic variables used are NB: Negative Big, NS: Negative Small, Z: Zero, PS: Positive Small, and PB: Positive Big. In order to control both inputs, 25 rules were determined and are shown in Table 6.1. This set of rules allow for the activation of a single rule with any combination of inputs, they are consistent, continuous and

with no contradictions. The centroid of gravity method was used for defuzzification to obtain the crisp torque values.

Table 6.1 Fuzzy rules for knee joint flexion and extension

$\Delta e$ e	NB	NS	Z	PS	PB
NB	PB	PB	PS	PS	Z
NS	PB	PS	PS	Z	NS
Z	PS	PS	Z	NS	NS
PS	PS	Z	NS	NS	NB
PB	Z	NS	NS	NB	NB

Due to the normalisation of inputs and output membership functions, scaling factors  $K_{in}$ , and  $K_{in2}$  were also added at the two inputs, and  $K_{out}$ , at the output of the fuzzy controller to adapt them to the system. Figure 6.4 shows the control scheme with a foot orientation fuzzy controller and ankle joint PID controller. Optimisation of the six control parameters was performed with the same parameters, stopping conditions and fitness function as in section 6.3.2.

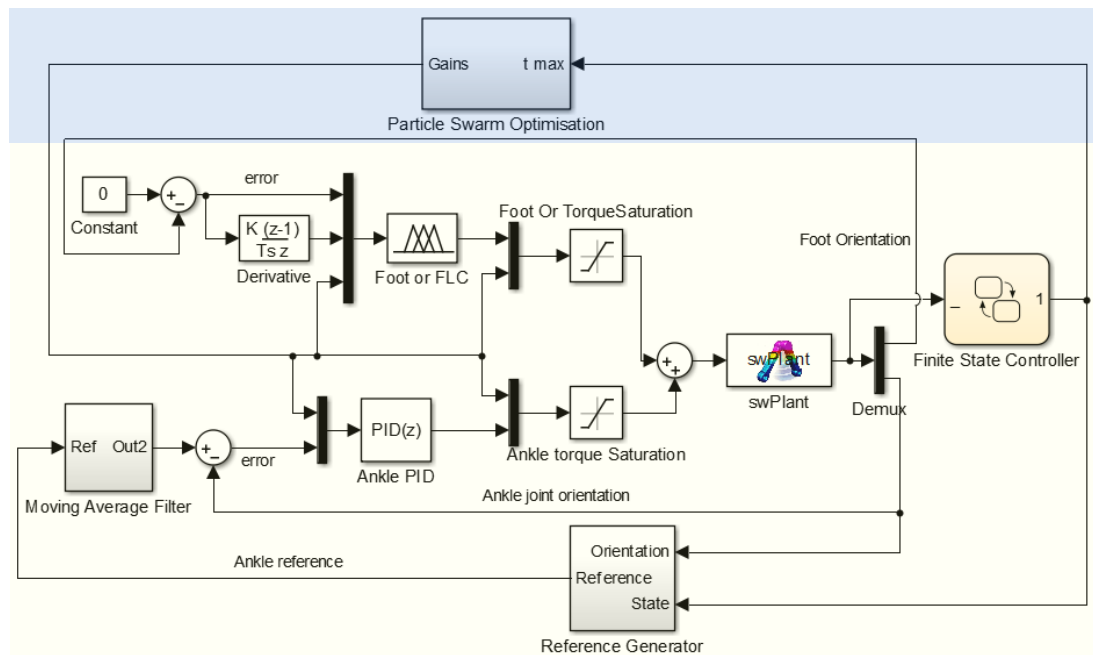


Figure 6.4 Control scheme with feet orientation fuzzy controller

## 6.4 Online tracking of ZMP

The ZMP was calculated offline in Chapter 5 to validate if the trajectories generated by the FSC could produce standing-up and sitting-down motions while maintaining equilibrium.

However, it was found that for high velocities, ZMP was out of the support area. To be able to produce a balanced motion with feet unlocked from ground, the calculation of ZMP would need to be carried out online, and incorporated as a transition condition and/or as an output function in the FSC.

To calculate ZMP online, the Simulink model was modified to stop the simulation every 10 sample times. Once the simulation was stopped, joints orientations were obtained, and ZMP was calculated considering only the last 2 orientations, which correspond to those in  $t$  and  $(t - 10)$ . Therefore, instead of using the complete joints trajectories to calculate ZMP at the end of the simulation, as it was done in Chapter 5, ZMP can be fed back into the system once the simulation is restarted, and can be used to maintain the equilibrium of the system.

Figure 6.5 shows a diagram of the Simulink model for obtaining joint orientations from the SimWise plant to calculate ZMP, and feed it back to the reference generator, to be used as control parameter. The same PSO algorithm with the configuration described in previous sections was also connected offline to the controller to be able to optimise gains.

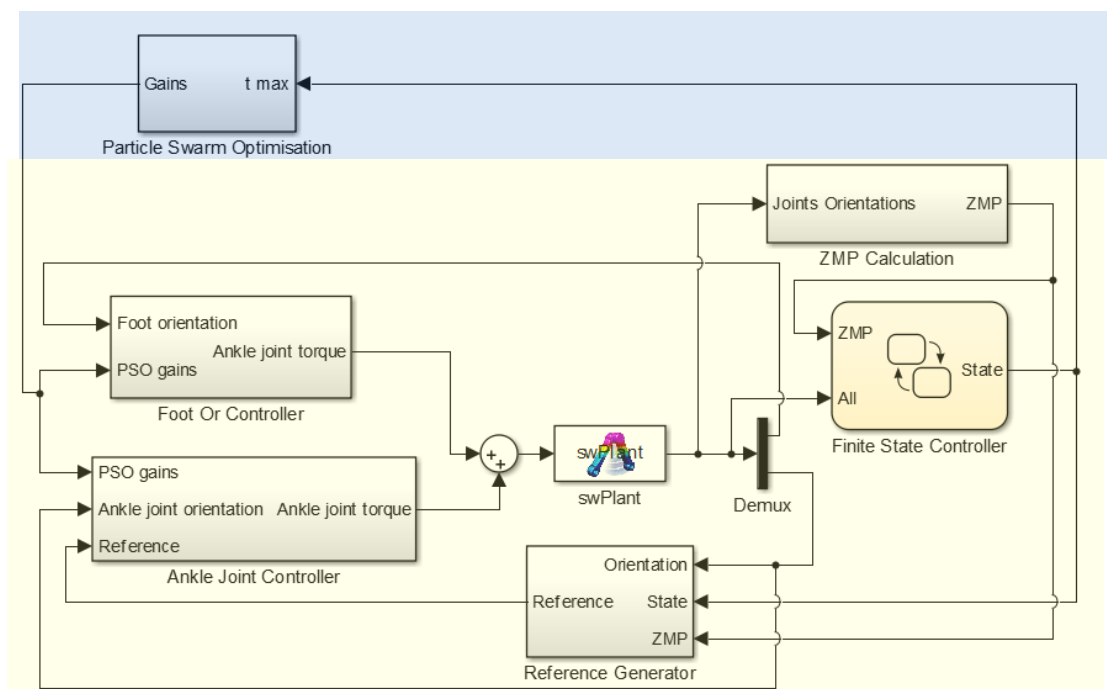


Figure 6.5 Middle and low level control scheme with ZMP calculation and PSO optimisation

A fuzzy controller with the same characteristics as that described in section 6.3.3 was also incorporated into the system. However, the input was the error and change of error between a reference and the position of the ZMP. The selected reference was 0.37 meters, which is 4 centimetres in front of ankle joint.

This controller was only active in states after the transfer phase, to avoid interference with the ankle joint controller. The output of the fuzzy controller was an orientation value added to the ankle joint reference.

## 6.5 Implementation of ankle joint control

Optimisation of the ankle joint PID gains was performed to find the combination of gains that produced the best performance of the control scheme in Figure 6.2. As mentioned in section 6.3.1, several stopping conditions were established to discard simulations that were prone to become unstable, or had reached an unacceptable level of error. Therefore, the best performance was selected mainly according to the duration of the standing-up and sitting-down motions.

An ankle PID controller, with gains  $K_p = 27.18$ ,  $K_i = 17.58$  and  $K_d = 0.35$  was found to be the best performing. Torque saturation was set to 60 Nm and simulations were ran at average velocity, which means that the complete motion lasts around 2.7 seconds.

Together with PID controllers for hip and knee joints, described in Chapter 4, and references provided by the middle level control described in Chapter 5, the exoskeleton produced acceptable standing-up and sitting-down motions as shown in Figure 6.6.

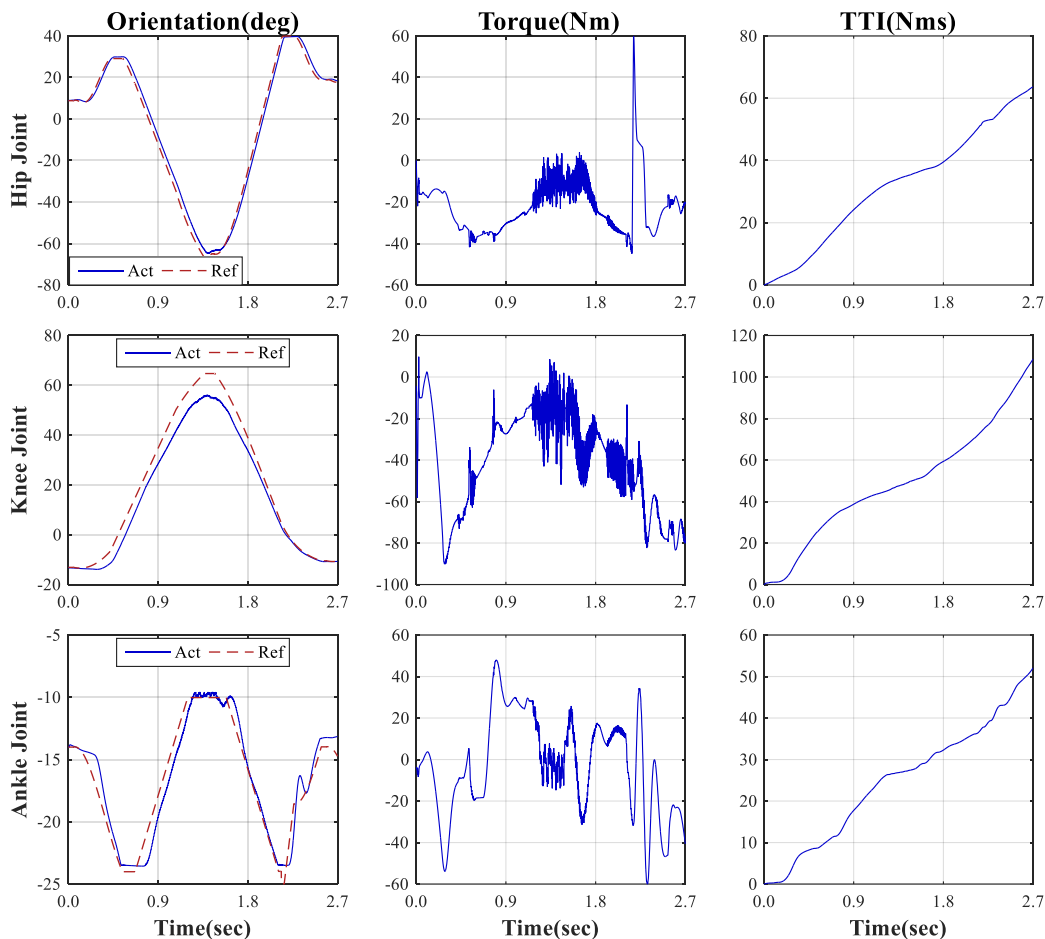


Figure 6.6 Hip, knee and ankle joints orientation, torque and TTI, with feet fixed to ground

For hip joints,  $RMSE = 2.87$  and  $TTI = 64 Nms$ , for knee joints  $RMSE = 5.12$ , and  $TTI = 109 Nms$ , and for ankle joints  $RMSE = 1.22$ , and  $TTI = 52 Nms$ . Hip and knee

joints results are in line with those in Chapter 5, even though ankle joint control was included. It is important to note that in previous chapters, the ankle joint was forced to follow the trajectory with unlimited amount of torque, a situation that was useful to select gains for hip and knee joints and parameters for the FSC.

Errors of the three joints are below admissible limits and TTI is reasonable. However, as shown in Figure 6.6., torque profiles presented undesirable oscillations that need to be reduced. This could be done through further optimisation of PID gains, though, it was not possible during the current research due to time constrains.

Control parameters of the scheme shown in Figure 6.3, composed of an ankle and a feet orientation PID control, were optimised through PSO. However, selected parameters were not enough to find a proper combination of gains to complete the motion.

The best gains for ankle control were  $K_p = 5.64$ ,  $K_i = 19.84$  and  $K_d = 0.01$ . while for feet orientation, the combination of gains with better fitness were  $K_p = 0.0705$ ,  $K_i = 0.3617$  and  $K_d = 0.01$ . Torque saturation was set to 60 Nm for ankle and 40 Nm for feet control. As depicted in Figure 6.3, the outputs of both controllers are summed, therefore, the total saturation value was set to 100 Nm. Simulations were performed at average velocity.

In Figure 6.7, it is possible to see that the controller of ankle joints struggled to track the reference, since the feet orientation control was trying to overcome the sliding of feet and ground. Although the motion was not completed, these results were useful to demonstrate that the controllers could guide the exoskeleton through the momentum phase. This is the most complicated part of the standing-up motion, due to the high torque requirements. Moreover, it was proved that middle-level control is capable of generating the required references, and that the selection of low-level controllers is appropriate. Although control parameters must be further optimised.

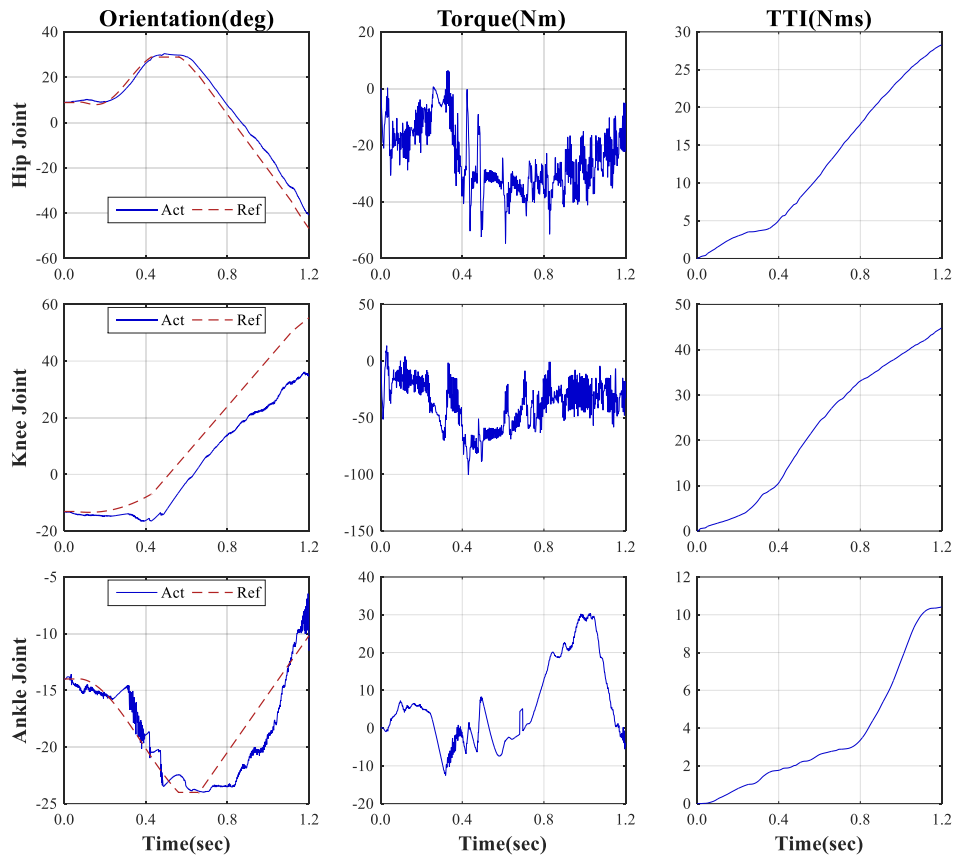


Figure 6.7 Hip, knee and ankle joints orientation, torque and TTI, of control scheme with feet orientation PID and feet unfixed from ground,

For hip joints,  $RMSE = 3.89$  and  $TTI = 28.28 Nms$ , for knee joints  $RMSE = 10.84$ , and  $TTI = 44.81 Nms$ , and for ankle joints  $RMSE = 1.99$ , and  $TTI = 10.42 Nms$ . These results show that knee joint control parameters which had been capable of tracking the motion in previous chapters, are not enough in the present control scheme. Optimisation of knee joint PID gains is recommended for future work.

The control parameters of the scheme depicted in Figure 6.4, which incorporated an ankle PID controller and a feet orientation fuzzy controller, were also optimised through PSO and the best gains for ankle control were  $K_p = 6.65$ ,  $K_i = 0.1$  and  $K_d = 0.01$ . And for feet orientation, the combination of gains with better fitness were  $K_{in} = 68.24$ ,  $K_{in2} = -100$  and  $K_{out} = 31.97$ . Torque saturation was set to 60 Nm for ankle and 40 Nm for feet control.

For hip joints,  $RMSE = 1.42$  and  $TTI = 22.96 Nms$ , for knee joints  $RMSE = 7.82$ , and  $TTI = 41.11 Nms$ , and for ankle joints  $RMSE = 1.81$ , and  $TTI = 61.4 Nms$ . Even though hip and ankle joint errors are within acceptable limits, and knee error is just above them, the balance of the system could not be achieved since the feet orientation controller was not enough to prevent the system to slide backwards. Online tracking and control of ZMP position should help to reduce this issue.

However, as shown in Figure 6.8, torque profiles present fewer oscillations than the PID control, which results in lower TTI. Therefore, fuzzy control should be further explored as a

solution for reducing the sliding of feet and ground. A similar issue with knee joint control is observed, therefore optimisation of PID control parameters for this joint should also be considered in the future.

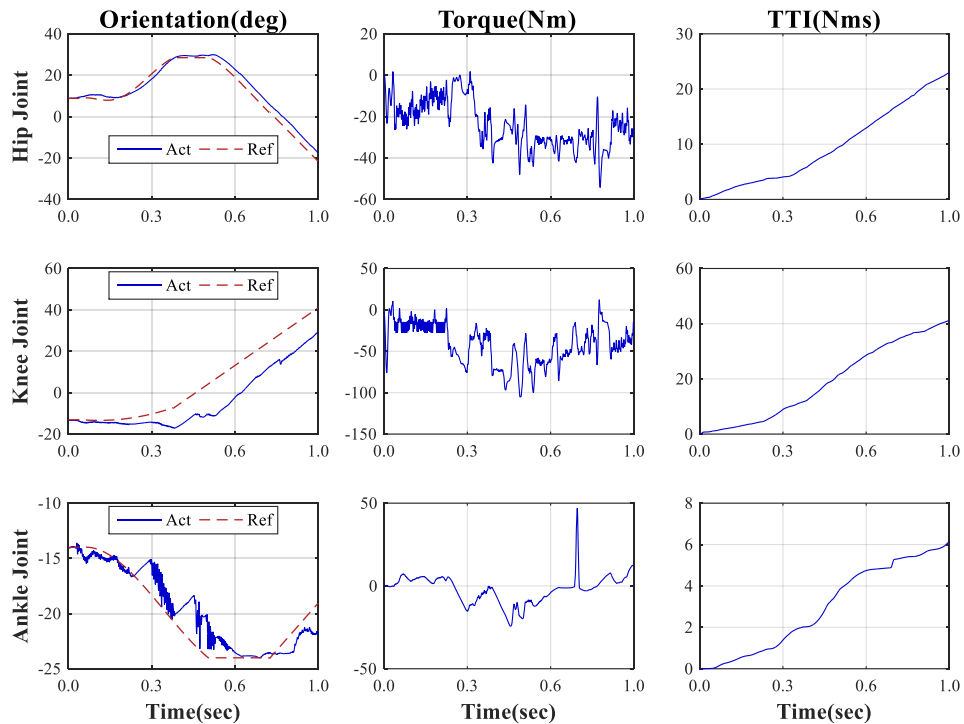


Figure 6.8 Hip, knee and ankle joints orientation, torque and TTI, of control scheme with feet orientation FLC and feet unfixed from ground,

ZMP was calculated online and incorporated into the control loop as described in section 6.4. PSO was used to find the best combination of ankle joint PID gains and fuzzy control parameters to complete the standing-up motion. The gains which produced the highest fitness were  $K_p = 39.74$ ,  $K_i = 11.33$  and  $K_d = 0.14$ . While for the ZMP position fuzzy controller, the best parameters were  $K_{in} = 17.89$ ,  $K_{in2} = 25.36$  and  $K_{out} = 0.5238$ . Torque saturation was set to 60 Nm for ankle and 40 Nm for feet control.

This test was done with feet fixed to ground to assess the performance of the controller without the interference of the feet orientation controller. For hip joints,  $RMSE = 3.24$  and  $TTI = 38.55 Nms$ , for knee joints  $RMSE = 3.47$ , and  $TTI = 44.07 Nms$ , and for ankle joints  $RMSE = 1.56$ , and  $TTI = 47.39 Nms$ . It is possible to observe in Figure 6.9 that the controller attempted to maintain the system in balance, generating oscillations of the ankle joint. This helped to keep ZMP within a limited portion of the support area during part of the motion. However, near the end of the extension phase, the controller became unstable.

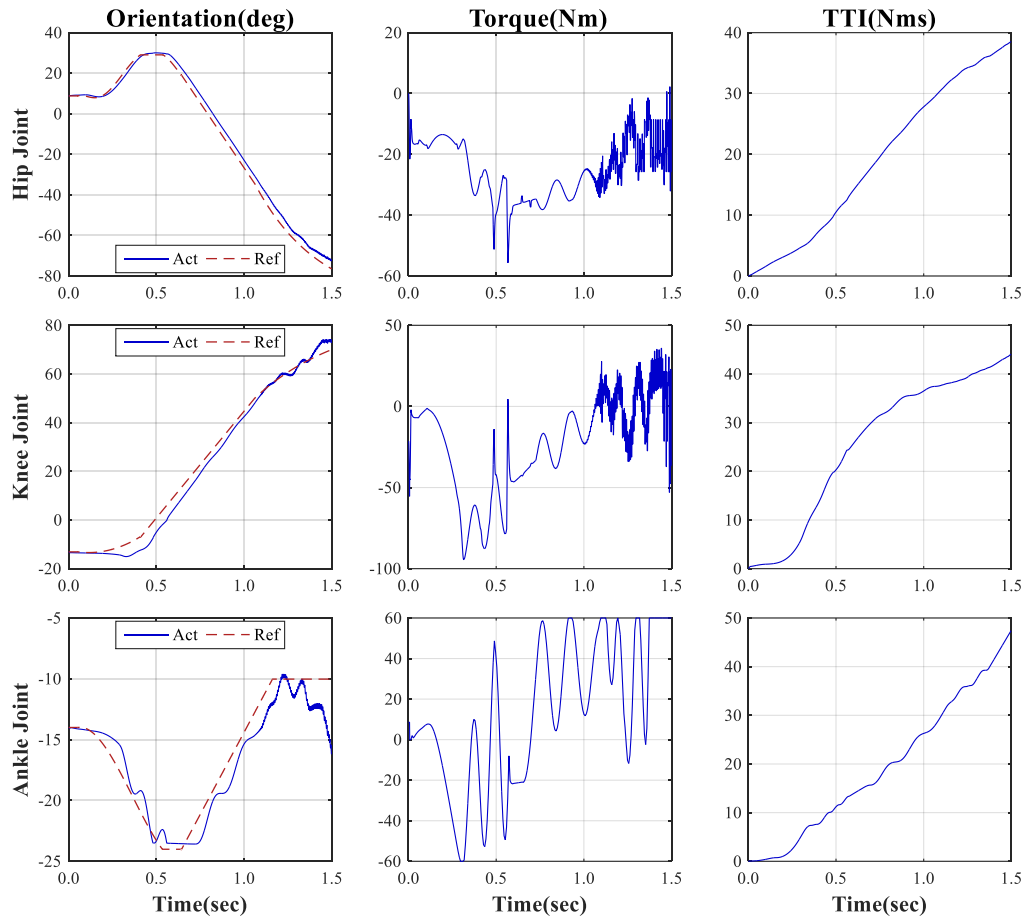


Figure 6.9 Hip, knee and ankle joints orientation, torque and TTI, of control scheme with ZMP fuzzy controller.

Although, in this case, the optimisation was also not enough to find the proper control parameters to complete the motion, it is clear that ZMP should be kept in the control loop. Activating the controller once the weight of the exoskeleton and user is on top of feet, eases the definition of the reference position of ZMP.

Optimisation was a useful tool to automate the search for proper control parameters, however, the high time cost of simulations, with the resources and software available, greatly limited the potential of this tool. Moreover, it was noticed that the selection of optimisation parameters, such as the search space and velocity, greatly influences the speed and accuracy of convergence. Additionally, the fitness function employed, in which more than one objective was relevant, would need to be rethought, and the parameters used, modified. Therefore, a deeper understanding of this optimisation tool would benefit this research.

Due to time constraints, it was not possible to test alternative strategies to overcome the sliding issues with the ground. Although the proposed control techniques could eventually lead to a solution to that problem, it has been concluded that it might be more beneficial to test the control system in a software platform in which the interaction between surfaces is more accurate than in SimWise.

## 6.6 Summary

This chapter explored options for controlling the exoskeleton's ankle joints during standing-up and sitting-down motions. Although results were acceptable when feet were fixed to ground, alternative strategies were required for the case when feet were detached from the ground.

The first challenge was to overcome the contact issues between feet and ground. Although this is a software related problem, a solution had to be investigated to be able to test the performance of the controller in a more realistic scenario, in which the interaction between the exoskeleton and the environment is not limited. Two control techniques were used to control feet orientation using ankle joint torque.

The second challenge was to propose a control technique to maintain the system in dynamic equilibrium, therefore ZMP was calculated online and incorporated into the control loop. A fuzzy controller was used to maintain the ZMP on top of the support area, however the selection of gains should be further optimised to achieve this objective.

Although results were not acceptable, and further tuning of control parameters is needed, a feasible control scheme has been presented and should be tested in another virtual environment to truly evaluate its capabilities.



# CHAPTER 7

## Conclusions and recommendations for future work

This chapter presents a summary of the main contributions of this research followed by the conclusions of the project. It also describes issues which had to be faced during the development of the models and controllers, and finally, a list of recommendations for future work in the research area explored throughout this work.

### 7.1. Summary of contributions

A literature review of the causes and effects of mobility issues, including SCI and elderly muscle weakening, muscles operation, functional electrical stimulation, biomechanics of fundamental mobility tasks, orthoses and exoskeleton components, including control techniques employed was carried out. Gaps have been identified regarding software facilities for early design assessments. Additionally, there is a low quantity of publications regarding middle and low level exoskeleton control strategies, for standing-up and sitting-down motions, especially for elderly assistance.

It was found that most of the publications on developments of lower limb exoskeleton devices described the construction of the prototype or upper level control strategies. Only a few described the use of virtual environments to assess the design in early stages; therefore, it is possible that these have not been implemented. Existing computational tools allow for the integration of complex simulations of physical and mathematical systems to be carried out. Therefore, it was decided to take advantage of available software facilities to design and study control strategies using a virtual representation of the human and exoskeletons. Additionally, it was decided to focus on the development of middle and low level controllers for

exoskeletons, since as mentioned, a limited number of publications have been found in this area.

Secondly, it was found that most of the publications on exoskeletons developments were focused on paraplegic and alike patients. Therefore, an effort was made to consider exoskeletons for the elderly, where a review of applications was performed, and a controller proposed for this goal.

Finally, it was found that there are few assessments of exoskeleton devices to perform standing-up and sitting-down tasks. Although some commercial exoskeletons can perform these, they do so with the aid of crutches, and there are few publications that describe the methodology used. Moreover, exoskeletons developed in recent years are mainly focused on assisting or restoring walking. For that reason, the study of sit to stand assistance for the elderly and paraplegic patients was included in this research.

This research is aimed at the development and evaluation of control approaches for robotic assisted mobility, for disabled and elderly people. More specifically, to develop lower-extremity exoskeletons, in addition to low and middle level controllers to help individuals perform fundamental mobility tasks such as standing-up, sitting-down and walking. Furthermore, to perform the validation of the system through simulation in a virtual environment.

The content of this thesis can be summarised in two main applications, the first is the development of a controller for a hybrid exoskeleton device for paraplegic patients. Functional electrical stimulation is considered for actuation, the frame supports the lower limbs by means of brakes, activated through a finite state middle level controller and fuzzy low level controllers. The user is guided to walk in a straight line with the aid of a wheel walker. For this device, the only actuated joint through FES is the knee joint, whereas the motions of hip and ankle joints are only controlled through the activation of brakes.

The second application is the control of an actuated exoskeleton frame adopted from the EXO-LEGS project for the elderly. The humanoid torque requirements were assessed through the use of PID controllers, to perform standing-up and sitting-down tasks, with the lowest root mean squared error and torque time integral at three different velocities. Once the system and relationship between error, torque saturation and velocity of the motions were understood, the exoskeleton was coupled to the system. Low level PID controllers were combined with a middle-level finite state controller for online tracking of the system, enabling the use of dynamic and static stability calculations as control parameters. This allowed system to adapt according to the desired behaviour. Initially only hip and knee joints were actuated and analysed. However, in the last part of the research, the control of ankle joints was included, together with an equilibrium compensation strategy through the calculation of ZMP.

The modelling of a humanoid, two exoskeletons and a wheel walker were necessary to enable the implementation and validation of the controllers. Models were designed in SOLID WORKS, assembled and configured in SimWise to behave realistically. Joint controls and meters were incorporated into the system to represent actuators and sensors. The communication channel with MATLAB Simulink was set up to enable the closed-loop control of the models. Thus, this research was also useful to assess the capabilities of SimWise and Simulink as a platform for the initial validation of assistive robots, their controllers and interaction with humanoid models.

## 7.2. Conclusions

The modelling of humanoid has been performed in such a way that the kinematics and dynamics of the system are as close as possible to those of the human body, without considering its musculoskeletal characteristics. Although the development of a more realistic humanoid would enhance the accuracy of results, its development would have deviated the goal of this research. Moreover, taking into account the available resources, a higher complexity on the model would have led to a considerable increase of computation time.

In a similar way, exoskeletons have been modelled in a simplified manner to include the necessary parts for joint generation, and interaction with the humanoid. The physical characteristics such as mass, dimensions, friction and restitution coefficients have been included. Prior to an experimental verification of the system, more accurate models could be tested to have more reliable results. However, the exoskeleton models presented in this research were sufficient to provide a platform in which controllers can be tested with confidence, and no severe changes are likely to be needed.

Simulation of the finite state and fuzzy controllers for the middle and low control levels, of a hybrid exoskeleton for paraplegic walking in straight line have been conducted. These have enabled the testing of the full system, which has proved to be capable of generating a continuous walking motion in the absence of obstacles, at an average velocity of 0.3 meters per second. This is within the range of similar devices whose velocity is between 0.14 and 0.44 meters per second.(Fuente) Moreover, the system has been able to withstand external disturbances, between 500N and 1000N, applied at different instants of the walking cycle in the frontal and lateral directions. Additionally, it has been capable of starting the motion from different initial conditions.

Torque profiles of the system have been assessed and considered acceptable since FES application has been minimised, due to its activation during knee flexion only, which

represents around 20% of a walking cycle. Brakes and a wheel walker have been used to support the user in the remaining time. These characteristics have helped to minimise the energy requirements of the system, where it was estimated that a  $TTI=4$  Nms is needed on average, for knee flexion during a walking cycle. Wheel walker motors also need to be considered, however, energy requirements of the proposed system would still be lower compared to a fully actuated exoskeleton.

Although other hybrid systems have been tested in the past, the one presented in this research can serve as an assistive or a rehabilitation technology. It offers a safe and semi-autonomous alternative to patients that want to maximise their lower limbs locomotion, with the additional advantage of enabling them to stand and move to perform daily tasks such as cooking. Thus, providing them a sense of independence and self-sufficiency. Moreover, the use of FES as actuation increases muscle contraction, enhancing blood circulation and overall health.

The analysis of the torque requirements while performing standing-up and sitting-down tasks with the use of PID controllers, has provided essential information regarding relationships between gains, maximum torque, error and velocity of the motion. It has been found that by increasing the torque saturation value, it is possible to decrease RMSE, however TTI would also be increased. These relationships have been useful to assess if motions could be performed with less torque, additionally, the analysis has been useful to highlight the importance of considering the trade-off between RMSE and TTI to define the priorities of the system.

From the simulations, it has also been found that the RMSE varies inversely with the proportional gain, the derivative gain is directly proportional to TTI, and velocity is indirectly proportional to TTI. These relationships are useful to know the limits of the system in terms of velocity, and to enable manual adjustment of the exoskeleton PID controllers when required.

The coupling of exoskeleton and humanoid after this analysis has enabled the evaluation of the system, in addition to the real level of assistance that the exoskeleton provides. The controller has been set up in a way that the humanoid provided 70% of the required torque while performing the motions, and the exoskeleton contributed the remaining 30%. It has been found that when the exoskeleton is passive, humanoid joints RMSE and TTI increased between 80% and 255%, compared to the results when the exoskeleton is actuated. This means that the motion was hardly completed, even when using a significantly larger amount of torque. It is possible to conclude that, considering exoskeleton's weight, when not actuated, the device can represent a load for the user, therefore, efforts must be made to make the system lighter.

It has also been found that while wearing an actuated exoskeleton, RMSE decreased around 30%, and TTI around 40% compared to results when not wearing it. Therefore, it has

been demonstrated, that an actuated exoskeleton controlled through the proposed techniques, is capable of helping users sharpen their standing-up and sitting-down manoeuvres while decreasing energy expenditure.

With the incorporation of a finite state machine as a middle level controller, based on the biomechanics of standing-up and sitting-down motions, it has been possible to control the system to perform these using the same PID gains for three different motion velocities. It has also been confirmed that velocity of the motion does not cause an important variation in joint orientation, but greatly affects torque profiles.

Additionally, the FSC has enabled the inclusion of transitions which can be activated when a motion is not completed, specifically, from standing-up states to sitting-down states. It has been demonstrated that these transitions were done in a smooth manner without exposing the user to falls.

Moreover, the FSC as middle level control has allowed the connection of different controllers. Additionally, since the FSC transition conditions are based on specific events, it would be possible for trainers or physiotherapists to manually fine tune these parameters, depending on the performance of the system. This is a key achievement since it is often necessary for this kind of products to be tuned as they are intended for users of different dimensions and capacities.

Once the FSC was created, and due to the fact that feet were fixed with ground to be able to avoid balance issues while evaluating the performance of the controller, an offline evaluation of the dynamic equilibrium of the system was done through the calculation of the zero moment point. The evaluation showed that, for high velocity, the ZMP was not within the support area, therefore, the exoskeleton and humanoid were at risk of falling, although for average and low velocity the system was in equilibrium. These results have confirmed that the online calculation of ZMP is necessary to ensure the dynamic equilibrium of the system under any circumstance.

The inclusion of ZMP in the control loop has been easier to implement due to the nature of the finite state controller, however, to evaluate the real dynamic behaviour of the system, the feet had to be unfixed from ground. Therefore, the ankle joint was included in the control loop and three strategies were implemented to generate the standing-up motion with feet unfixed from ground.

An optimisation algorithm was used to find the best combination of control parameters, however due to time constraints it was not possible to produce a complete standing-up motion. However, the proposed control strategies were capable of guiding the exoskeleton through the momentum phase, which is the most challenging during this motion due to the high torque requirements needed to accomplish it.

Finally, after all the aforementioned simulations, it is possible to conclude that Simwise offers a user-friendly interface for creating coordinates, constraints, meters and controls; as well as a simplified communication channel with MATLAB Simulink through its predefined block. In addition, accurate calculation of the kinematics and dynamics of the system are performed. However, it must be noted that an issue regarding contact between objects, especially between flat surfaces, is present within this software. Additionally, the fact that non-solid parts cannot be implemented, coupled with the low computational speed and stability of the software, confirms that it may not be the best suited for the analysis of interactions between humans, exoskeletons, and the environment.

SimWise has been a useful platform to simulate, control and test humanoid and assistive devices presented in this thesis. However, the interest in this research area has been so important in recent years, that new packages are now available which may be capable of performing better than SimWise.

### **7.3. Challenges**

It is important to consider that unlike other assistive technologies such as wheel-chairs, standers, and wheel walkers, exoskeletons need to be closely attached to the user's body in order to be effective. This closeness is itself a challenge since it can restrict the range of motion of joints, originate clashes with other parts of the body or even cause injuries due to over load of joints or inadequate interface components.

Although some exoskeleton designs avoid the overloading of the frame by locating actuators in backpacks, and transmitting power through cables or belts, interface components will always be in contact with the body and structural and articulating components close to it. This closeness generates challenges in the design of the system but is also an important issue in the simulation of the motions. In this research, it was desired to have two separate bodies that represented the humanoid and exoskeleton, but connected in such a way that they could interact in a realistic manner. Several strategies were tested, and a solution was proposed in which the legs were set to collide with interface components, while straps at belt and shoes were represented by rigid joints. This solution assumes that there was no sliding between shoes and feet and belt and waist, and that interface components were close and tightly attached to the legs.

Additional challenges were the lack of motion capture and force plate equipment, required for the physical analysis of fundamental mobility tasks and exoskeleton prototypes. Although it would be desired to have access to these technologies, their construction would have deviated the scope of the project. Moreover, the exploration of the gap in the literature,

regarding the lack of simulation environments for the initial validation of exoskeleton designs, was considered a more interesting research direction, which replaced the need of a physical prototype. Regarding the analysis of mobility tasks, a review of the extensive literature on these fundamental motions was performed as an alternative to experimental motion capture.

As mentioned, although the selected software, Simwise, has several advantages from which this project benefited from, it also presents challenges which had to be overcome to accomplish the aim of this research. One of these is the fact that even though it is possible to select friction and restitution parameters for each part, the behaviour of these forces is not totally realistic within the virtual environment. Especially the contact between flat surfaces, as is the case of feet and ground. It was found that these forces varied with the dimensions of the parts in contact but not according to the physical laws that govern them.

Another related challenge is that SimWise, like many current software packages, can only handle solid objects. Although some human segments, such as bones, can be considered solids, there are other segments that contain muscle and adipose tissues, whose behaviour is very different from solid segments, especially when evaluating their contact forces with other bodies. This was relevant in the case of the sitting posture where humanoid buttocks were modelled as a solid that does not adopt the shape of the seat, as does in real scenarios.

Further, although SimWise was used to simulate all the results in the present thesis, this research initially utilised Visual Nastran 4D (VN4D), the previous version of SimWise. VN4D could only be connected to an older MATLAB release. The computational speed was not acceptable, therefore, it was decided to migrate the models to SimWise, which seemed to have the same capabilities than VN 4D, with the advantage of being able to communicate with recent MATLAB releases. However, when trying to run simulations with previously created models, it was discovered that the communication between the packages was not always successful. Many alternatives were tested trying to overcome this issue, however, the only solution found was to include an interface block per input. Although the computational speed of SimWise and recent versions of MATLAB Simulink together was much better than VN4D, the need to add interface blocks slowed down the performance considerably.

The inappropriate behaviour of contact between feet and ground increased equilibrium issues at critical moments especially of the standing-up motion, but also in all the other mobility tasks. This complicated the simulations and development of controllers, therefore, for an important part of this research, the feet had to be attached to ground, thus assuming that the system was in equilibrium. However, in later stages it was necessary to evaluate the behaviour of the system in a more realistic manner for the simulations to be valid, therefore, research on static and dynamic equilibrium techniques had to be performed.

Even after the incorporation of equilibrium algorithms, simulations still showed some sliding of feet with ground. However, the behaviour of the system was accurate excluding that

issue and it was demonstrated that the exoskeleton controllers developed in this research were adequate for producing stable fundamental mobility tasks.

#### **7.4. Recommendations for future work**

This research has embarked on the evaluation of control techniques for exoskeleton devices with the purpose of assisting paraplegic and elderly people on fundamental mobility tasks. A novel combination of control techniques were employed to propose devices which perform with low error and smooth torque profiles, additionally minimising energy consumption and being easily adaptable to the user. The scope of this project was wide and thus analyses, simulation and evaluation of the proposed controllers were done in a general manner. Therefore, deeper and more specific tests should be done to the devices before experimental implementation, to strengthen the results of the simulation validation presented in this thesis.

Regarding the hybrid orthosis for paraplegic walking in straight line, it must be noted that the design proposal was made in a conceptual manner rather than in a detailed form. Since the interest of the research was mainly oriented on the control area, the models used were simple to provide the platform for testing. Therefore, to move to a detailed design, some recommendations are: the use of lightweight and resistant materials for the frame to maintain the system portable, use of prefabricated orthoses as interface components since ergonomics have already been considered. It would also be useful to consider the size and form of encoders to incorporate these in the articulation component design. Although no spring or damping mechanism was attached to the joints and results were positive, it would be desirable to consider the inclusion of these components to minimise the impact on the users' joints.

Concerning the application of FES, electrodes could be attached or incorporated into the interface components so that the positioning is similar every time the device is worn. However, an analysis of the optimal location of electrodes to maximise the effects of FES, while minimising muscle fatigue, should be considered. The FES generator as well as power supply should be integrated into the wheel walker.

Regarding the expansion of the control validation through simulations, it would be recommendable to test other combinations of initial conditions as well as disturbances applied in different positions and durations to improve the controller as much as possible prior to practical implementation. Moreover, reference trajectories and controllers' parameters could be further enhanced to obtain better results including higher velocity, a wider range of motion of the joints, smoother torque profiles and lower energy consumption.

For the actuated exoskeleton for assistance on standing-up and sitting-down motions, as mentioned before, the design was adopted from the EXO-LEGS project. Therefore, the only

recommendations would be to keep weight as low as possible, to add adjustable mechanisms and interface components not only for the vertical axis but for the horizontal one as well to better fit the device to the user, and to properly align the exoskeleton joints with the corresponding anatomic position.

Considering that a more thorough analysis of the behaviour and parameters of the system was done, and the proposed control scheme is more complex than that of the hybrid orthosis; the time constraints did not allow for the implementation of sufficient validation test of the FSC middle level controller. Therefore, a complete set of tests to assess the limits of the system in terms of repeatability, stability and range should be carried out.

Additionally, different combinations of assistance percentage should be explored, along with a literature review to find out the real level of assistance needed by the elderly. Moreover, further optimisation of parameters of the proposed strategies for ankle joint and balance control should be carried out in order to improve the performance of the system.

For both devices, the upper level controller still needs to be developed. As the hybrid orthosis could be considered a rehabilitation device, suitable for controlled environments, user intention could be manually selected, whereas for the actuated exoskeleton, its development was intended for assisting more complex tasks, therefore user intention algorithms should be incorporated into the system. These would be of particular importance in the case of elderly assistance since also the middle level control would be based on the motion of the user. This is different from the case of the application for paraplegic patients, in which the upper control level could be manually selected and the middle level controller is in charge of generating the motion, thus guiding the motion of the patient's legs.

In terms of the software facilities, a comparison of the results obtained throughout this thesis with those of a second software would be desirable to assess and validate the conclusions made. An alternative could be AnyBody, which offers kinematic and dynamic calculation for both humanoid and exoskeleton models. This software comprises a full model of the musculoskeletal system that allows the calculation of metabolic costs of motions, more realistic contact forces estimation, and the capability to calculate reaction forces with ground while considering equilibrium of the system (AnyBodyTechnology, 2016). Finally, but not less importantly, experimental validation of the system in a controlled environment should be performed as this is the only way to observe the real behaviour of any proposed mechanism.



## References

- A.B. Zoss, A. B. Z., H. Kazerooni, H. K., and A. Chu, A. C. (2006). Biomechanical design of the Berkeley lower extremity exoskeleton (BLEEX). *IEEE/ASME Transactions on Mechatronics*, 11(2), 128-138. doi: 10.1109/TMECH.2006.871087
- Abd Latiff, I., & Tokhi, M. (2009). Fast convergence strategy for Particle Swarm Optimization using spread factor. *Evolutionary Computation*, 2009. CEC '09. IEEE Congress on, 2693-2700.
- Alexander, N., Schultz, A., and Warwick, D. (1991). Rising from a chair: Effects of age and functional ability on performance biomechanics. *Journal of Gerontology*, 46(3), M91-8.
- Amoshahy, M., Shamsi, M., & Sedaaghi, M. (2016). A Novel Flexible Inertia Weight Particle Swarm Optimization Algorithm. *PloS One*, 11(8), E0161558
- An, Q., Matsuoka, H., Ikemoto, Y., and Asama, H. (2009). Extraction of Behavior Primitives for Understanding Human Standing-up Motion. 2009 Ieee International Conference on Mechatronics and Automation, Vols 1-7, Conference Proceedings.
- Anam, K., and Al-Jumaily, A. A. (2012). Active Exoskeleton Control Systems: State of the Art. *Procedia Engineering*, 41(0), 988-994. doi: 10.1016/j.proeng.2012.07.273
- Anybody Technology (2016). AnyBody newsletter: Subject-specific models, AnyGait, SolidWorks2AnyBody, Publications, Kinect, and much more. [http://www.anybodytech.com/index.php?id=116&tx\\_ttnews\[tt\\_news\]=70&cHash=15b7c765f632896ab60f9ca09541dd92#d](http://www.anybodytech.com/index.php?id=116&tx_ttnews[tt_news]=70&cHash=15b7c765f632896ab60f9ca09541dd92#d) Accessed 15 October 2016
- AnyBodyTechnology (2016) <http://www.anybodytech.com/> Accesed 08 November, 2016.
- Argo Medical Technologies. (2012). ReWalk <http://rewalk.com/> Accessed 26 January2013
- Armytechnology.com (2016) Raytheon XOS 2 Exoskeleton, Second-Generation Robotics Suit, United States of America <http://www.army-technology.com/projects/raytheon-xos-2-exoskeleton-us/> Accessed 17 June 2016

Asbeck, A., De Rossi, S., Holt, K., and Walsh, C. (2015). A biologically inspired soft exosuit for walking assistance. *The International Journal of Robotics Research*, 34(6), 744-762.

Azevedo, Poignet, and Espiau. (2004). Artificial locomotion control: From human to robots. *Robotics and Autonomous Systems*, 47(4), 203-223.

Bansal, J., Singh, P., Saraswat, M., Verma, A., Jadon, S., & Abraham, A. (2011). Inertia Weight strategies in Particle Swarm Optimization. *Nature and Biologically Inspired Computing (NaBIC)*, 2011 Third World Congress on, 633-640.

Barr, M. L. (1979). *The human nervous system : an anatomic viewpoint*. Hagerstown, Md: Hagerstown, Md : Medical Dept., Harper and Row, c1979.

Basmajian, J. V. (1978). *Muscles alive : their functions revealed by electromyography*. Baltimore: Baltimore : Williams and Wilkins, 1978.

Bell, N. J., & Oommen, B. (2015). Particle field optimization: A new paradigm for swarm intelligence. *Proceedings of the International Joint Conference on Autonomous Agents and Multiagent Systems, AAMAS*, 1, 257-265.

Belohlavek, R., and Klir, George J. (2011). *Concepts and Fuzzy Logic [electronic resource]*. Cambridge: MIT Press.

Boundless. "Types of Muscle Contractions: Isotonic and Isometric." *Boundless Anatomy and Physiology*. Boundless, 27 Sep. 2016. <https://www.boundless.com/physiology/textbooks/boundless-anatomy-and-physiology-textbook/muscular-system-10/control-of-muscle-tension-97/types-of-muscle-contractions-isotonic-and-isometric-546-8434/> Accessed 15 november 2016.

Brown, C., and Flood, K. (2013). Mobility Limitation in the Older Patient A Clinical Review. *Jama-Journal Of The American Medical Association* , 310(11), 1168-1177.

Buesing, C., Fisch, G., O'Donnell, M., Shahidi, I., Thomas, L., Mummidisetty, C., . . . Jayaraman, A. (2015). Effects of a wearable exoskeleton stride management assist system (SMA®) on spatiotemporal gait characteristics in individuals after stroke: A randomized controlled trial. *Journal of Neuroengineering and Rehabilitation*, 12, 69.

Cordero, C. (2012) *Articulated human body*. Grabcad <https://grabcad.com/library/articulated-human-body--2>. Accessed 01 February 2014.

Cyberdyne (2015) HAL for living support (lower limb type). Accessed 01 March 2013

DailyTech(2014) *From HULC to FORTIS: the Evolution of Lockheed Martin's Incredible Exosuit*  
<http://www.dailytech.com/From+HULC+to+FORTIS+the+Evolution+of+Lockheed+Martin+s+Incredible+Exosuit/article36421.htm>. Accessed 17 June 2016

Dar Aziz, A., Cackler, J., and Yung, R. (2004) "The Intellectual Excitement of Computer Science". Eric Roberts' Sophomore College Class at Stanford University.

<https://cs.stanford.edu/people/eroberts/courses/soco/projects/2004-05/automata-theory/basics.html> Accessed 01 June 2016.

Dassault Systemes (2016) SOLIDWORKS standard. <http://www.solidworks.co.uk/sw/products/3d-cad/solidworks-standard.htm>. Accessed 01 June 2016.

Dekker, M.H.P. (2009). Zero-Moment point method for stable biped walking

Department of Work and Pensions (2015) Family Resources Survey. Chapter 4: Disability data tables. <https://www.gov.uk/government/statistics/family-resources-survey-financial-year-201314>. Accessed 01 June 2016.

Design Simulation Technologies (2016) SimWise 4D Integrated motion, stress analysis and optimization. MSC Software Corporation. <https://www.design-simulation.com/documents/simwise/simwisebrochure.pdf>. Accessed 01 June 2016.

Dictionary, M. (2009). Motor Unit <http://medical-dictionary.thefreedictionary.com/motor+unit> Accessed 05 February 2013

Disabled World (2016) Assistive Technology: Devices Products & Information <http://www.disabled-world.com/assistivedevices/> Accessed 20 August 2016.

Disabled World. (2015). Physical and Mobility Impairments: Information and News. <http://www.disabled-world.com/disability/types/mobility/> Accessed 03 June 2016.

Dollar, A., and Herr, H. (2007). Active Orthoses for the Lower-Limbs: Challenges and State of the Art. Rehabilitation Robotics, 2007. ICORR 2007. IEEE 10th International Conference on, 968-977.

Dutta, A., Kobetic, R., and Triolo, R. J. (2008). Ambulation after incomplete spinal cord injury with EMG-triggered functional electrical stimulation. [Article]. Ieee Transactions on Biomedical Engineering, 55(2), 791-794. doi: 10.1109/tbme.2007.902225

Eberhart, & Yuhui Shi. (2001). Tracking and optimizing dynamic systems with particle swarms. Evolutionary Computation, 2001. Proceedings of the 2001 Congress on, 1, 94-100

EFDS: English federation of disability sport (2016) Facts and statistics [http://www.efds.co.uk/resources/facts\\_and\\_statistics](http://www.efds.co.uk/resources/facts_and_statistics). Accessed 03 June 2016.

EksoBionics. (2012). Ekso Bionics. <http://www.eksobionics.com/ekso> Accessed 26 January 2013

elearnSCI.org, I. (2012). Introduction to SCI <http://www.elearnsoci.org/module.aspx?id=221&category=Overview+for+the+Whole+Team&module=Introduction+to+SCI&lesson=Overview> Accessed 29 January 2013.

Faulkner, J. (1997). Physical dimensions of aging - Spirduso, WW. Gerontologist, 37(3), 423-426.

G.S.Virk, U. Haider, I. Nyoman, R.Krishnan and N. Masaud (2013). EXO-LEGS for elderly persons. CLAWAR 2014 conference.

Garcia, P, Dias, Jmd, Dias, R, Santos, P, and Zampa, C. (2011). A study on the relationship between muscle function, functional mobility and level of physical activity in community-dwelling elderly. *Revista Brasileira De Fisioterapia*, 15(1), 15-22.

Gharooni, S., Heller, B., and Tokhi, M. O. (2001). A new hybrid spring brake orthosis for controlling hip and knee flexion in the swing phase. *IEEE Transactions on Neural Systems and Rehabilitation Engineering*, 9(1), 106-107. doi: 10.1109/7333.918283

Gofeer, A., and Zilberstein, C. (2013). United States Patent No. US20130123672.

Goldfarb, M., and Durfee, W. K. (1996). Design of a controlled- brake orthosis for FES- aided gait. *IEEE Transactions on Rehabilitation Engineering*, 4(1), 13-24. doi: 10.1109/86.486053

Harrison, P. (2006). *Managing spinal cord injury : continuing care : managing the long-term health and care needs of people with SCI in the community : information for general practitioners and community healthcare professionals*. Milton Keynes: Milton Keynes : Spinal Injuries Association, 2006.

He, H., and Kiguchi, K. (2007). A Study on EMG-Based Control of Exoskeleton Robots for Human Lower-limb Motion Assist. *Information Technology Applications in Biomedicine, 2007. ITAB 2007. 6th International Special Topic Conference on*, 292-295.

Hellendoorn, H., and Thomas, C. (1993). Defuzzification in fuzzy controllers. *Journal of Intelligent and Fuzzy Systems*, 1(2), 109-123.

Hernandez, D (2015) Fusion How soft robots will help sick kids walk and make the elderly stronger <http://fusion.net/story/232380/soft-robotics-revolution/>. Accessed 17 June 2016

Honda (2015) Walking assist device with stride management system. Accessed 01 March, 2015

Hoogers, G., and NetLibrary, Inc. (2003). *Fuel cell technology handbook* [electronic resource]. Boca Raton, Fla.: CRC Press.

Hopcroft, J., Motwani, Rajeev, and Ullman, Jeffrey D. (2007). *Introduction to automata theory, languages and computation*. (3rd ed.) Boston: Pearson, Addison-Wesley.

Hsu, J. D., Michael, J., and Fisk, J. (2008). *AAOS Atlas of Orthoses and Assistive Devices* J. D. Hsu, J. Michael and J. Fisk (Eds.)

Hu, X. (2010 ) *Particle Swarm Otimization*, <http://www.swarmintelligence.org/tutorials.php> Accessed 15 August 2016.

Ikehara, T., Nagamura, K., Ushida, T., Kojima, S., Tanaka, E., Saegusa, S., and Yuge, L. (2011). Development of closed-fitting-type walking assistance device for legs and

evaluation of muscle activity. IEEE International Conference on Rehabilitation Robotics, IEEE International Conference on Rehabilitation Robotics, 2011.

International Data Base (2016) World Population by Age and Sex <http://www.census.gov/population/international/data/idb/worldpop.php>. Accessed 01 June 2016.

Irving, R. A., and Little, R. (2009). European Patent No. EP2231096B1.

Jailani, R. (2011). Analysis and control of FES-assisted paraplegic walking with wheel walker. 2011.

Jailani, R., Tokhi, M. O., Gharooni, S. C. and Jogtaei, M. (2011). Finite state control of FES- Assisted walking with spring brake orthosis. Proceedings of UKSIM2011: 13th International Conference on Modelling and Simulation, Cambridge, UK, 30 March - 1 April 2011, pp. 183–188.

Jansen, J., Richardson, B., Pin F., Lind R., Bridwell J., Oak Ridge National Laboratory (2000) Exoskeleton for Soldier Enhancement Systems Feasibility Study

Kawamoto, H., Taal, S., Niniss, H., Hayashi, T., Kamibayashi, K., Eguchi, K., and Sankai, Y. (2010). Voluntary motion support control of Robot Suit HAL triggered by bioelectrical signal for hemiplegia. Conference Proceedings : Annual International Conference of the IEEE Engineering in Medicine and Biology Society. IEEE Engineering in Medicine and Biology Society. Conference, 462-466.

Kazerooni, H. (2008). Exoskeletons for human performance augmentation Springer Handbook of Robotics (pp. 773-793).

Kazerooni, H., Racine, J. L., Huang, L., & Steger, R. (2005). On the control of the Berkeley Lower Extremity Exoskeleton ( BLEEX) (Vol. 2005, pp. 4353-4360).

Kazerooni, H., Tung, W. Y., Reid, J. I., and Mckinley, M. G. (2013). United States Patent No. US20130158445 A1

Kell, C., and Everett, Tony. (2010). Human movement : An introductory text. (6th ed. / edited by Tony Everett and Clare Kell. ed., Physiotherapy essentials). Edinburgh: Churchill Livingstone.

Keller, R. M. (2001) Computer Science: Abstraction to Implementation. Finite-State machines. <https://www.cs.hmc.edu/~keller/cs60book/%20%20%20All.pdf> Accessed 01 June 2016.

Kennedy, J., & Eberhart, R. (1995). Particle swarm optimization. Neural Networks, 1995. Proceedings., IEEE International Conference on, 4, 1942-1948.

Kerr, White, Barr, & Mollan. (1994). Standardization and definitions of the sit-stand-sit movement cycle. Gait & Posture, 2(3), 182-190.

Kerr, White, Barr, and Mollan. (1997). Analysis of the sit-stand-sit movement cycle in normal subjects. Clinical Biomechanics, 12(4), 236-245.

Kiela, H. (2015) Mobile Robot Balance, the zero Momento Point <https://lectoraatmechatronica.wikispaces.com/Mobile+Robot+Balance%2C+the+zero+mome nt+point>

Kiguchi K., Imada Y. (2009) EMG-based control for lower-limb power-assist exoskeletons. IEEE Workshop on Robotic Intelligence in Informationally Structured Space. pp. 19-24

Kilicarslan, A., Prasad, S., Grossman, R., and Contreras-Vidal, J. (2013). High accuracy decoding of user intentions using EEG to control a lower-body exoskeleton. Engineering in Medicine and Biology Society (EMBC), 2013 35th Annual International Conference of the IEEE, 5606-5609.

Kim, Kyung, Kim, Jae-Jun, Kang, Seung-Rok, Jeong, Gu-Young, and Kwon, Tae-Kyu. (2010). Analysis of the assistance characteristics for the plantarflexion torque in elderly adults wearing the powered ankle exoskeleton. ICCAS 2010 - International Conference on Control, Automation and Systems, 576-579.

Koller, J., Jacobs, D., Ferris, D., and Remy, C. (2015). Learning to walk with an adaptive gain proportional myoelectric controller for a robotic ankle exoskeleton. Journal of Neuroengineering and Rehabilitation, 12, 97.

Kong, K. C., and Jeon, D. (2006). Design and control of an exoskeleton for the elderly and patients. IEEE-ASME Trans. Mechatron., 11(4), 428-432. doi: 10.1109/TMECH.2006.878550

Kopp, C (2011) DefenceToday Exoskeletons for warriors of the future September 2011. pp 38-40

Kosko, B. (1992). Neural networks and fuzzy systems : a dynamical systems approach to machine intelligence. Englewood Cliffs, NJ : London: Englewood Cliffs, NJ : Prentice Hall ; London : Prentice Hall International, 1992.

Kotake, Dohi, Kajiwara, Sumi, Koyama, and Miura. (1993). An analysis of sit-to-stand movements. Archives of Physical Medicine and Rehabilitation, 74(10), 1095-9.

Kralj, A. R., and Bajd, T. (1989). Functional electrical stimulation : standing and walking after spinal cord injury. Boca Raton, Fla.: Boca Raton, Fla. : CRC Press, c1989.

Kralj, Jaeger, and Munih. (1990). Analysis of standing up and sitting down in humans: Definitions and normative data presentation. Journal of Biomechanics, 23(11), 1123-1138.

Kwak, N., Müller, K., and Lee, S. (2015). A lower limb exoskeleton control system based on steady state visual evoked potentials. Journal of Neural Engineering, 12(5), 14.

Low, K. H. (2011). Robot-assisted gait rehabilitation: From exoskeletons to gait systems. Paper presented at the Defense Science Research Conference and Expo (DSR), 2011.

Low, K. H. (2011, 3-5 Aug. 2011). Robot-assisted gait rehabilitation: From exoskeletons to gait systems. Paper presented at the Defense Science Research Conference and Expo (DSR), 2011.

Mahfouf, M. (2013). Intelligent Systems: ACS6112-A Course in Fuzzy Systems. Department of Automatic Control and Systems Engineering, the University of Sheffield, MSc Control Systems Course Notes.

Makinson, and General Electric CO Schenectady Ny Specialty Materials Handling Products Operation. (1971). Research and Development Prototype for Machine Augmentation of Human Strength and Endurance. Hardiman I Project.

Marinov, B (2015) Reducing the cost of exoskeleton devices, <http://exoskeletonreport.com/2015/09/reducing-the-cost-of-exoskeleton-devices/>. Accessed 12 November 2015

Maxon Motors (2016) Program 2016/2017 High Precision Drives and Systems. <http://epaper.maxonmotor.com/>. Accessed 01 June 2016

Merletti, R., and Parker, P. (2004). Electromyography: physiology, engineering, and noninvasive applications IEEE Press series in biomedical engineering (pp. 1 online resource (xxii, 494 p.)).

Mikki, S., & Kishk, Ahmed A. (2008). Particle swarm optimization [electronic resource] : A physics-based approach (Synthesis lectures on computational electromagnetics (Online), #20). San Rafael, Calif. (1537 Fourth Street, San Rafael, CA 94901 USA): Morgan & Claypool.

Miranda-Linares, D. and Tokhi, M.O. (2015). Modelling and simulation of assistive exoskeleton for elderly mobility. CLAWAR 2015 conference.

MIT (2011) [https://ocw.mit.edu/courses/electrical-engineering-and-computer-science/6-01sc-introduction-to-electrical-engineering-and-computer-science-i-spring-2011/unit-1-software-engineering/state-machines/MIT6\\_01SCS11\\_chap04.pdf](https://ocw.mit.edu/courses/electrical-engineering-and-computer-science/6-01sc-introduction-to-electrical-engineering-and-computer-science-i-spring-2011/unit-1-software-engineering/state-machines/MIT6_01SCS11_chap04.pdf) Accessed 29 August 2016

Miyamoto, S., Shimada, Y., Sato, K., Kagaya, H., Matsunaga, T., and Obinata, G. (1999). Hybrid functional electrical stimulation for energy-efficient restoration of standing-up motion. Archives of Physical Medicine and Rehabilitation, 80(1), 40-47. doi: 10.1016/s0003-9993(99)90305-2

Mizen, and Cornell Aeronautical Lab Inc Buffalo Ny. (1964). Design and Test of a Full-Scale Wearable Exoskeletal Structure.

Multiple Sclerosis Trust (2016) Functional Electrical Stimulation Factsheet <https://support.mstrust.org.uk/shop?prodid=211> Accessed 15 May 2016

Mundermann, L., Corazza, S., and Andriacchi, T. (2006). The evolution of methods for the capture of human movement leading to markerless motion capture for biomechanical applications. Journal Of Neuroengineering And Rehabilitation, 3, Journal Of Neuroengineering And Rehabilitation, 2006 Mar 15, Vol.3.

Munton, J., Ellis, M., and Wright, V. (1984). Use of electromyography to study leg muscle activity in patients with arthritis and in normal subjects during rising from a chair. *Annals of the Rheumatic Diseases*, 43(1), 63.

National Spinal Cord Injury Statistical Center, Facts and Figures at a Glance. Birmingham, AL: University of Alabama at Birmingham, 2016.

Nelson, Barlow, & Doitsidis. (2009). Fitness functions in evolutionary robotics: A survey and analysis. *Robotics and Autonomous Systems*, 57(4), 345-370.

Next big future (2016). Affordable, lightweight, low power walking assistance and strength enhancement for the soldier and the elderly with the Superflex exosuit <http://nextbigfuture.com/2016/06/affordable-lightweight-low-power.html>. Accessed 17 June 2016

Nuzik, S., Lamb, R., VanSant, A., and Hirt. (1986). Sit-to-stand movement pattern. A kinematic study. *Physical Therapy*, 66(11), 1708-1713.

Odstock Medical Limited (2011) Equipment, Clinical Services and Education [.http://www.odstockmedical.com/sites/default/files/oml\\_fes\\_products\\_and\\_services\\_2011\\_1.pdf](http://www.odstockmedical.com/sites/default/files/oml_fes_products_and_services_2011_1.pdf) Accessed 20 august 2016.

Office of disability issues (2014). Disability prevalence estimates 2011/12. [https://www.gov.uk/government/uploads/system/uploads/attachment\\_data/file/321594/disability-prevalence.pdf](https://www.gov.uk/government/uploads/system/uploads/attachment_data/file/321594/disability-prevalence.pdf). Accessed 01 June 2016.

Ogata, K. (2010). *Modern control engineering* (5th ed., International ed.). Boston, [Mass.] ; London: Pearson.

Okamoto, T., and Okamoto, K. (2007). *Development of gait by electromyography : application of gait analysis and evaluation*. Osaka: Osaka : Walking Development Group, 2007.

P.I. Corke, "Robotics, Vision & Control", Springer 2011, ISBN 978-3-642-20143-1.

Papworth Trust (2016). Disability in the United Kingdom 2013 Facts and Figures <http://www.papworthtrust.org.uk/sites/default/files/Facts%20and%20Figures%202013%20web.pdf>. Accessed 01 June 2016.

Physiopedia (2016) Gait. <http://www.physio-pedia.com/Gait> Accessed 29 July 2016

Pons, J. L. (2008). *Wearable robots : biomechatronic exoskeletons*. Chichester: Chichester : John Wiley and Sons, Ltd., c2008.

Pratt, J. E., Krupp, B. T., Morse, C. J., and Collins, S. H. (2004). The RoboKnee: an exoskeleton for enhancing strength and endurance during walking (Vol. 3, pp. 2430-2435).

Quintero, H. A., Farris, R. J., and Goldfarb, M. (2012). A Method for the Autonomous Control of Lower Limb Exoskeletons for Persons With Paraplegia. *Journal of Medical*

Devices, Transactions of the ASME, 6(4), Journal of Medical Devices, Transactions of the ASME, 11 October 2012, Vol.6(4).

Ratnaweera, A., Halgamuge, S., & Watson, H. (2004). Self-organizing hierarchical particle swarm optimizer with time-varying acceleration coefficients. *Evolutionary Computation*, IEEE Transactions on, 8(3), 240-255.

RexBionics. (2011). Rex Bionics <http://www.rexbionics.com/index.php> Accessed 26 January 2013

Riener, R. and Edrich, T. (1999). "Identification of passive elastic joint moments in the lower extremities." *Journal of Biomechanics*: 539-544.

Rifton (2014) Rifton Pacer Gait Trainers <http://www.rifton.com/products/gait-trainers/pacer-gait-trainers>. Accessed 01 February 2014.

Rogers, M. A. (1986). *Living with paraplegia*. London: London : Faber, 1986.

Ross, T. (2010). *Fuzzy logic with engineering applications* (3rd ed.). Oxford: Wiley.

Rushton, D. N. (1997). Functional electrical stimulation. *Physiological Measurement*, 18, pp. 241-275.

Salzman, B. (2010). Gait and balance disorders in older adults. *American Family Physician*, 82(1), 61-8.

Schenkman, M., Berger, R., Riley, P., Mann, W., and Hodge. (1990). Whole-body movements during rising to standing from sitting. *Physical Therapy*, 70(10), 638-651.

Schultz, A. (1995). Muscle function and mobility biomechanics in the elderly: An overview of some recent research. *The Journals of Gerontology. Series A, Biological Sciences and Medical Sciences*, 50 Spec No, 60-3.

Schultz, Alexander, and Ashton-Miller. (1992). Biomechanical analyses of rising from a chair. *Journal of Biomechanics*, 25(12), 1383-1391.

Schütz, A (2012) Robotic exoskeleton: For more quality of life [http://www.maxonmotor.co.uk/medias/sys\\_master/8809291317278/2013-01-enUK-exoskeleton.pdf](http://www.maxonmotor.co.uk/medias/sys_master/8809291317278/2013-01-enUK-exoskeleton.pdf) . Accessed 18 June 2016

Seireg, A. and Grundmann, J.G. (1981). *Design of a Multitask Exoskeletal Walking Device for Paraplegics*. Biomechanics of medical devices, marcel dekker, Inc., New York. Pp 569-644.

Shi, Y., & Eberhart, R. (1998). A modified particle swarm optimizer. *Evolutionary Computation Proceedings, 1998. IEEE World Congress on Computational Intelligence., The 1998 IEEE International Conference on*, 69-73.

Siciliano, B., and Khatib, O. (2008). *Springer handbook of robotics*. Berlin ; London: Berlin ; London : Springer, 2008.

Spinal Research (2011) Facts and figures <http://www.spinal-research.org/research-matters/spinal-cord-injury/facts-and-figures/>. Accessed 01 June 2016.

Sugano, S., Huang, Q., and Kato, I. (1993). Stability criteria in controlling mobile robotic systems. 1993 International Conference on Intelligent Robots and Systems. Part 2 (of 3), Yokohama, Jap, 07/26-30/93, 1993 International Conference on Intelligent Robots and Systems. Part 2 (of 3), Yokohama, Jap, 07/26-30/93, 1993.

Sung, S., Lee, Jietae, and Lee, In-Beum. (2009). Process Identification and PID Control [electronic resource]. Chichester: Wiley.

Sveistrup, H. M., Laporte, D., and Chan, D. (1999). Rising from sitting in elderly people, part 1: Implications of biomechanics and physiology. *British Journal of Occupational Therapy*, 62(1), 36-42.

Sweeney, P. C., Lyons, G. M., and Veltink, P. H. (2000). Finite state control of functional electrical stimulation for the rehabilitation of gait *Med. Biol. Eng. Comput.* (Vol. 38, pp. 121-126).

Sylos-Labini, F., La Scaleia, V., D'Avella, A., Pisotta, I., Tamburella, F., Scivoletto, G., . . . Ivanenko, Y.P. (2014). EMG patterns during assisted walking in the exoskeleton. *Frontiers in Human Neuroscience*, 8(JUNE), <xocs:firstpage xmlns:xocs=""/>

Tan, F. C. (2004). *EMG secrets*. Philadelphia, Pa.: Philadelphia, Pa. : Hanley and Belfus, c2004.

The MathWorks, Inc (2016a) Fuzzy Logic Toolbox Design and simulate fuzzy logic systems <http://uk.mathworks.com/products/fuzzy-logic/>. Accessed 01 June 2016.

The MathWorks, Inc (2016b) Simulink Simulation and Model-Based Design [http://uk.mathworks.com/products/simulink/?s\\_tid=srchtitle](http://uk.mathworks.com/products/simulink/?s_tid=srchtitle). Accessed 01 June 2016.

The MathWorks, Inc (2016c) Stateflow Model and simulate decision logic using state machines and flow charts. [http://uk.mathworks.com/products/stateflow/?s\\_tid=srchtitle](http://uk.mathworks.com/products/stateflow/?s_tid=srchtitle). Accessed 01 June 2016.

Tsukahara, A., Kawanishi, R., Hasegawa, Y., and Sankai, Y. (2010). Sit-to- Stand and Stand-to- Sit Transfer Support for Complete Paraplegic Patients with Robot Suit HAL. *Advanced Robotics*, 24(11), 1615-1638. doi: 10.1163/016918610X512622

Tucker, M., Olivier, J., Pagel, A., Bleuler, H., Bouri, M., Lambercy, O., . . . Gassert, R. (2015). Control strategies for active lower extremity prosthetics and orthotics: A review. *Journal Of Neuroengineering And Rehabilitation*, 12, *Journal Of Neuroengineering And Rehabilitation*, 2015 Jan 5, Vol.12.

United Nations (2013). *World Population Ageing 2013*. Department of Economics and Social Affairs, Population Division. ST/ESA/SER.A/348

United Nations, Department of Economics and Social Affairs, Population Division (2013). *World Population Ageing 2013*. ST/ESA/SER.A/348

United States Census Bureau (2012). Americans with disabilities:2010. <http://www.census.gov/people/disability/publications/sipp2010.html>. Accessed 03 June 2016

Virk, G.S., Haider, U., Nyoman, I., Krishnan, R., and Masaud, N. (2014). EXO-LEGS for elderly persons. CLAWAR 2014 conference.

Vukobratovic (2007) When were active exoskeletons actually born? *Int. J. Human. Robot.*, 04, 459 DOI: 10.1142/S0219843607001163

Vukobratović, and Stepanenko. (1972). On the stability of anthropomorphic systems. *Mathematical Biosciences*, 15(1), 1-37.

Vukobratovic, M. (1973). How to Control Artificial Anthropomorphic Systems. *Systems, Man and Cybernetics, IEEE Transactions on*, 3(5), 497-507.

Vukobratovic, M., and Borovac, B. (2004 ). Zero Moment Point-Thirty five years of its life. *International Journal of humanoid Robotics*. World Scientific. Vol. 1, No 1 157-173.

Vukobratovic, M., Frank, A., and Juricic, D. (1970). On the Stability of Biped Locomotion. *Biomedical Engineering, IEEE Transactions on*, BME-17(1), 25-36.

Walsh, J. J. (1964). *Understanding paraplegia*. London: London : Tavistock Publications, 1964.

Warwick, K., and NetLibrary, Inc. (1996). *An introduction to control systems [electronic resource] (2nd ed., Advanced series in electrical and computer engineering ; vol. 8)*. Singapore ; River Edge, NJ: World Scientific.

Webber, S. C., Porter, M. M., and Menec, V. H. (2010). Mobility in older adults: A comprehensive framework. *Gerontologist*, 50, 443-450. doi:10.1093/geront/gnq013

Wheeler, Woodward, Ucovich, Perry, & Walker. (1985). Rising from a chair. Influence of age and chair design. *Physical Therapy*, 65(1), 22-6.

Winter, D. A. (2009). *Biomechanics and motor control of human movement*. Hoboken, N.J. : Chichester: Hoboken, N.J. : Wiley ; Chichester : John Wiley distributor, c2009.

Winter, D. A. (2009). *Biomechanics and motor control of human movement*. Wiley, New Jersey, USA.

World Health Organisation (2011). *World report on disability 2011*. ISBN 978 92 4 068521 5

World Health Organisation (2013) *Spinal Cord Injury Fact sheet No. 348* <http://www.who.int/mediacentre/factsheets/fs384/en/>. Accessed 01 June 2016.

World Health Organisation, (2015a). *International Classification of Functioning, Disability and Health*. <http://apps.who.int/classifications/icfbrowser/> Accessed 01 June 2016

World Health Organization (2015b) . *Media centre, Ageing and health factsheet No. 404*. <http://www.who.int/mediacentre/factsheets/fs404/en/> Accessed 20 august 2016.

World Health Organization (2016). Media Centre, Assistive Technology factsheet. <http://www.who.int/mediacentre/factsheets/assistive-technology/en/> Accessed 20 august 2016.

Yamamoto, K., Ishii, M., Hyodo, K., Yoshimitsu, T., and Matsuo, T. (2003). Development of power assisting suit - (Miniaturization of supply system to realize wearable suit). *JSME Int. J. Ser. C-Mech. Syst. Mach. Elem. Manuf.*, 46(3), 923-930.

Yan, Cempini, Oddo, and Vitiello. (2015). Review of assistive strategies in powered lower-limb orthoses and exoskeletons. *Robotics and Autonomous Systems*, 64, 120-136.

Yuan, K., Zhu, J., Wang, Q., and Wang, L. (2011). Finite-state control of powered below-knee prosthesis with ankle and toe. *IFAC Proceedings Volumes (IFAC-PapersOnline)*, 18(1), 2865-2870.

# Appendices

## Appendix A

Winter's human proportions used for the development of the humanoid model in SimWise

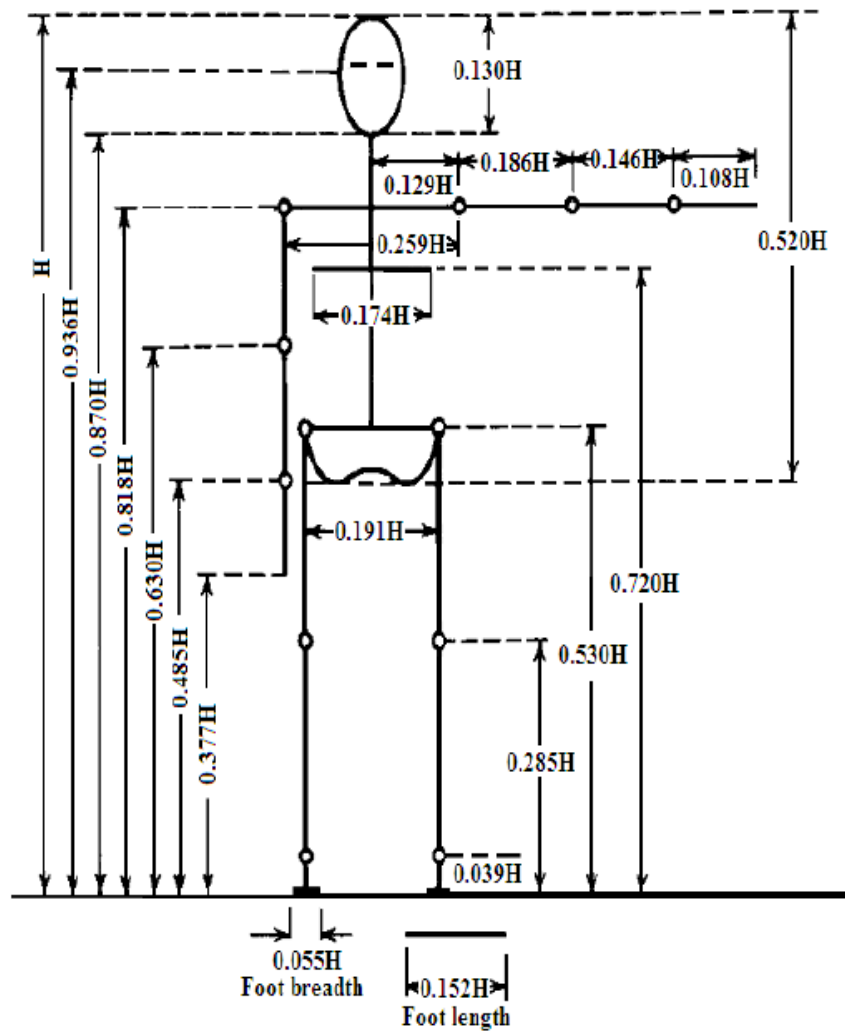


Figure A.1 Winter's human proportions

## Appendix B

Hip knee and ankle joint orientations during the walking cycle generated by the exoskeleton and wheel walker under different initial conditions and for humanoids of different dimensions

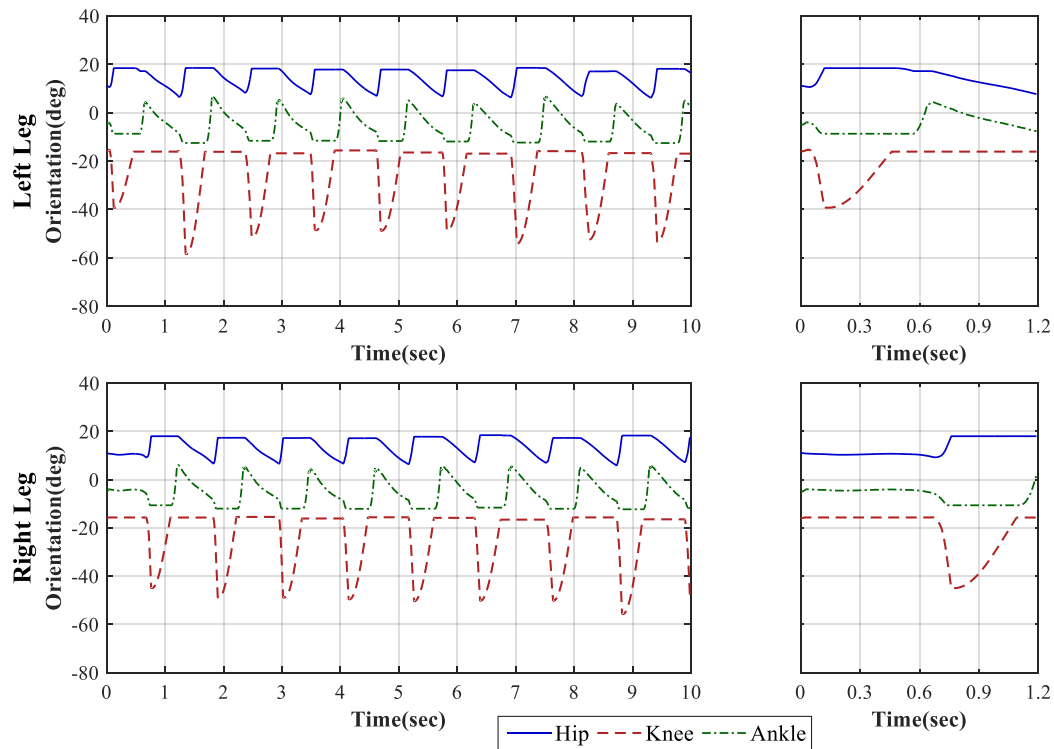


Figure B.1 Same orientations, starting with left step

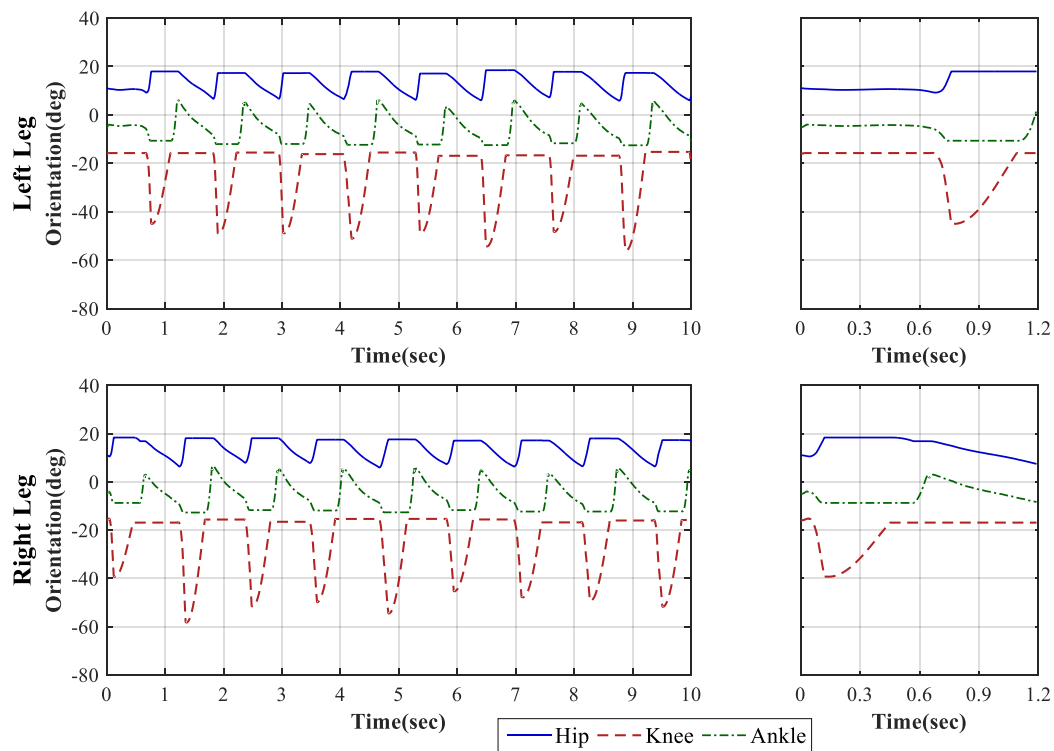


Figure B.2 Same orientations, starting with right step

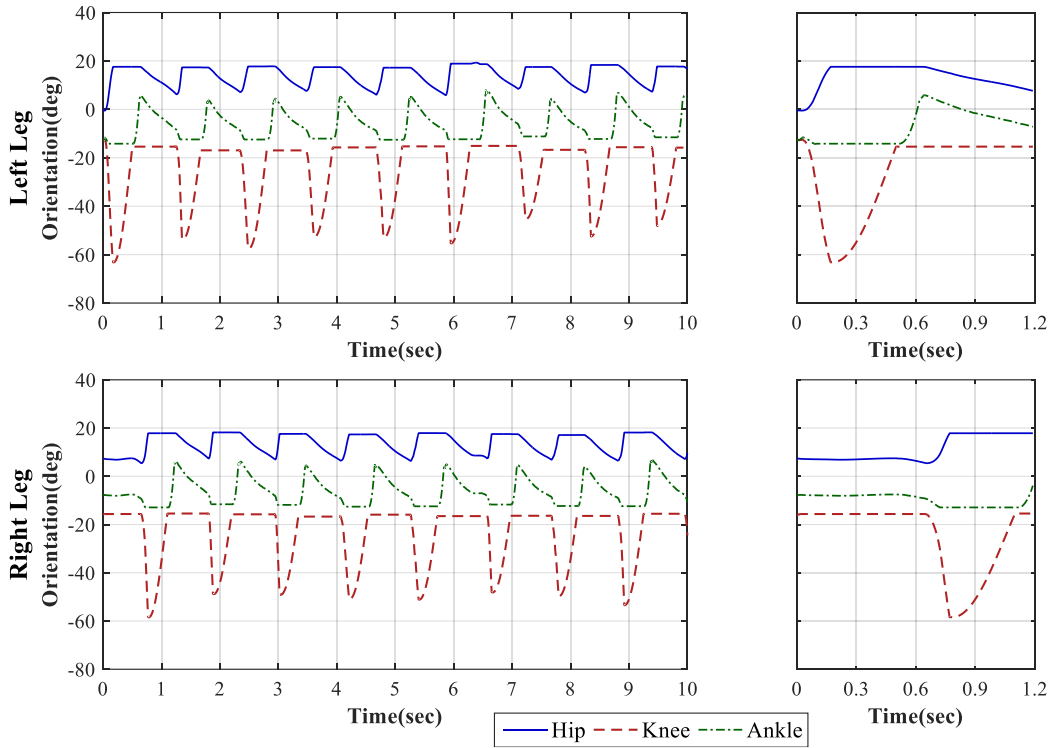


Figure B.3 Different Orientation, starting with left step

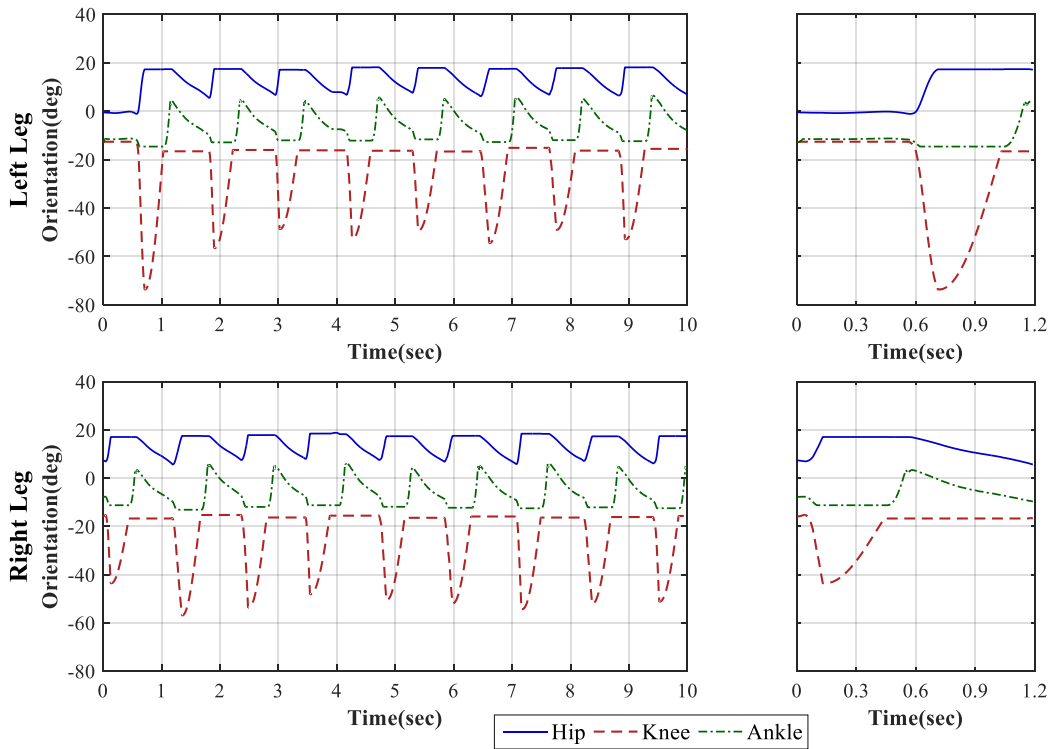


Figure B.4 Different Orientation, starting with right step

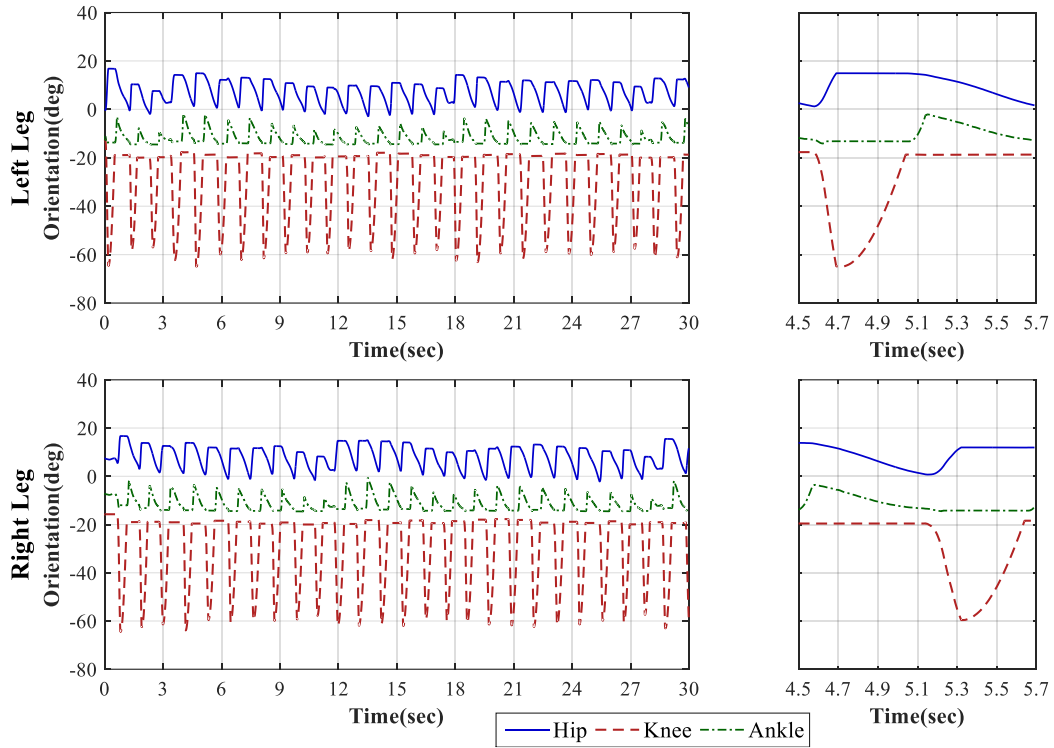


Figure B.5 Tall humanoid

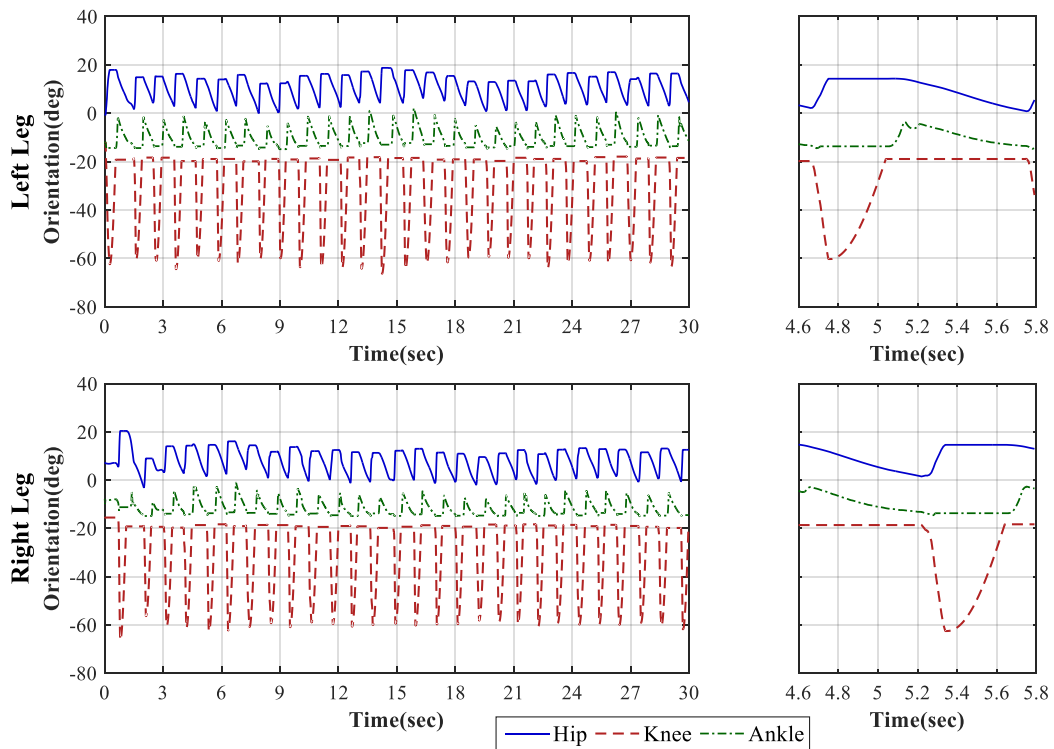


Figure B.6 Short humanoid

## Appendix C

Kinematic diagram for Denavit Hartenberg parameters used for the simulation of lower limbs and the calculation of zero moment point, using the Robotics Toolbox for MATLAB.

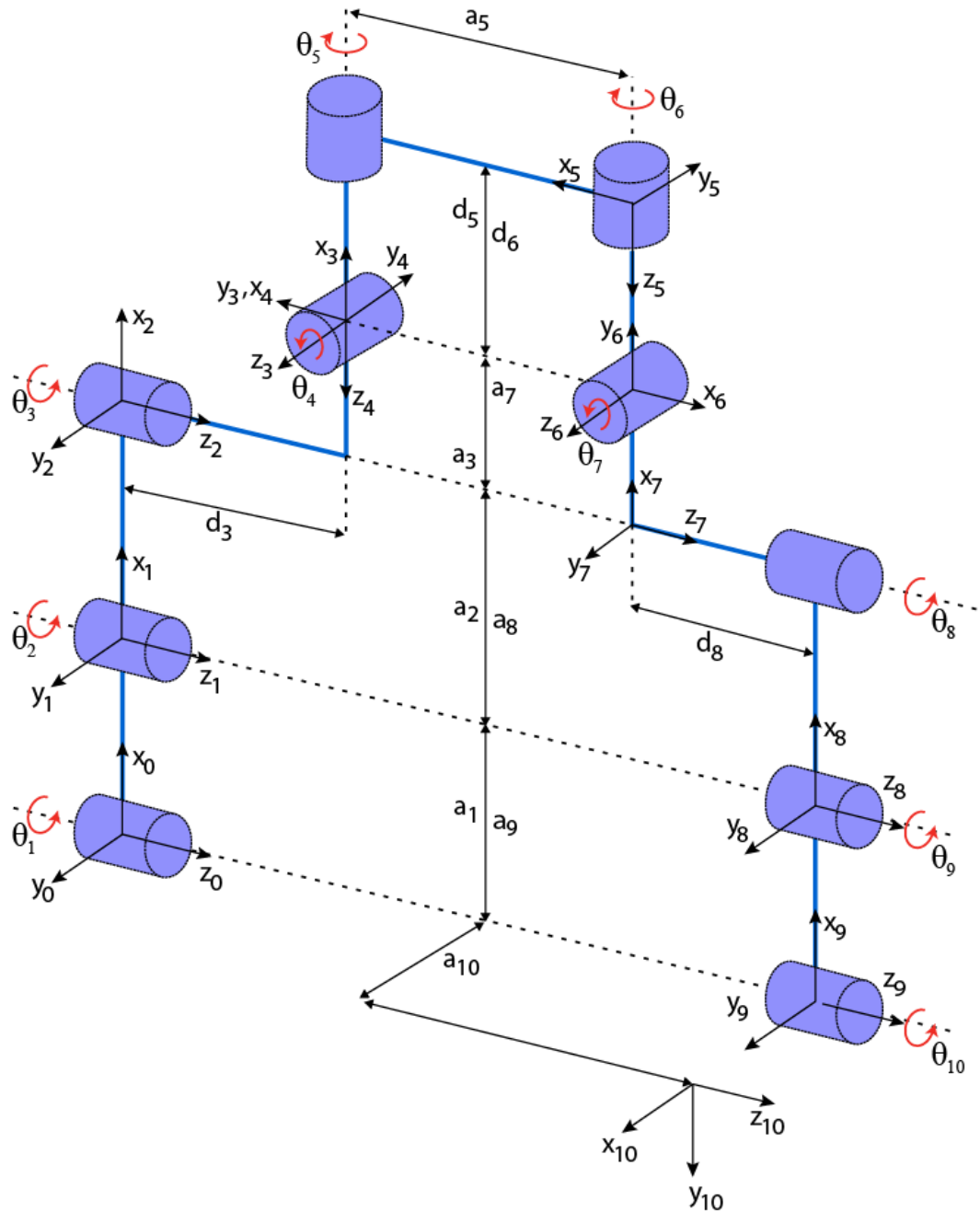


Figure C.1 Kinematic diagram for Denavit Hartenberg parameters

## Appendix D

Equally time-spaced snapshots of humanoid performing standing-up and sitting-down motions with exoskeleton assistance.

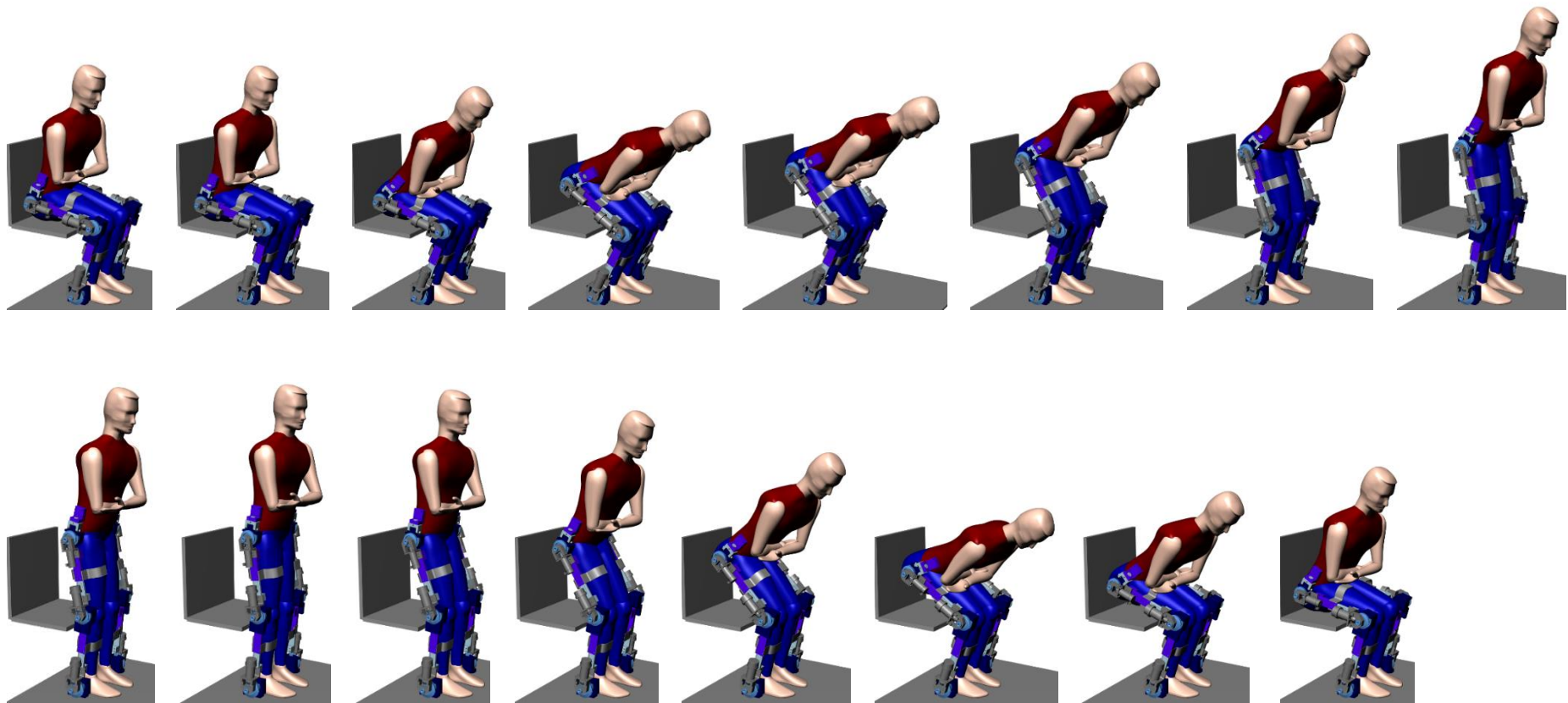


Figure D.1 Humanoid and exoskeleton during standing-up and sitting-down motions

## Appendix E

Equally time-spaced snapshots of robotic arm performing standing-up and sitting-down motions used for the calculation of zero moment point.

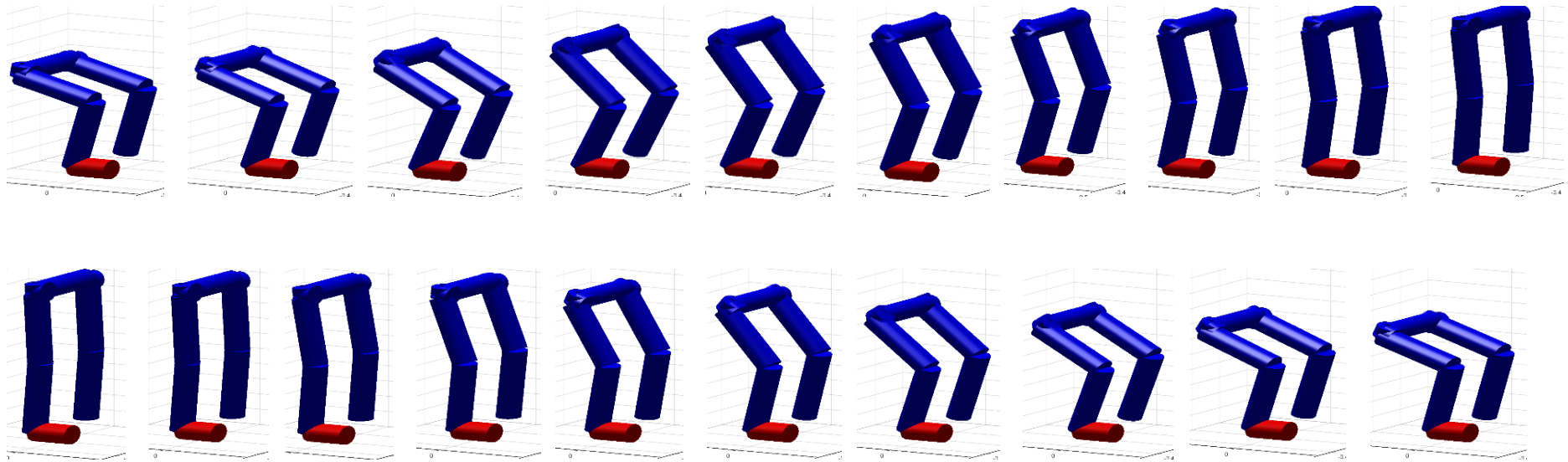


Figure E.1 Robotic arm during standing-up and sitting-down motions

